THE
PHYSICAL REVIEW
A Journal of Experimental and Theoretical Physics Established by E. L. Nichols in 1893
VOL. 51, NO. 6 MARCH 15, 1937 SECOND SERIES

Geiger-Müller Counter Measurements of Cosmic-Ray Intensities in the Stratosphere

W. F. G. SWANN, G. L. LOCHER AND W. E. DANFORTH
Bartol Research Foundation of the Franklin Institute, Swarthmore, Pennsylvania
(Received January 13, 1937)

WE are here reporting data concerning cosmic-ray intensities in the stratosphere, as measured during the three following manned balloon flights: (1) that of Professor and Mrs. Jean Piccard from Detroit, September, 1934, (2) that sponsored by the National Geographic Society and the U. S. Army Air Corps (Explorer I) from Rapid City, South Dakota, in July, 1934, and (3) the Second National Geographic flight (Explorer II) in November, 1935. These results were reported at the symposium held in connection with the April, 1936, meeting of the American Physical Society in Washington; and a complete description of the apparatus and experiments will be found elsewhere.[1]

Relative intensities as a function of distance below the top of the homogeneous water equivalent atmosphere are given, for several zenith angles, in Fig. 1. These were obtained in Explorer II by a triple coincidence counter telescope system provided with a suitably designed wall of shielding counters to eliminate spurious coincidences resulting from showers.

The intensity maximum, occurring at about 82 cm of water for the vertical component, is probably the most important feature of these data.[2] The initial rise of the curve with increase of distance below the top of the atmosphere can, we believe, be ascribed to the production of secondaries, whose number increases with thickness of atmosphere available to produce them. A suggestion of a secondary hump is indicated between 100 and 200 cm depth.

If one plots the data for different zenith angles (θ) as a function of $h \sec \theta$, where h is the vertical depth, the curves for 0°, 30°, and 60°, fall

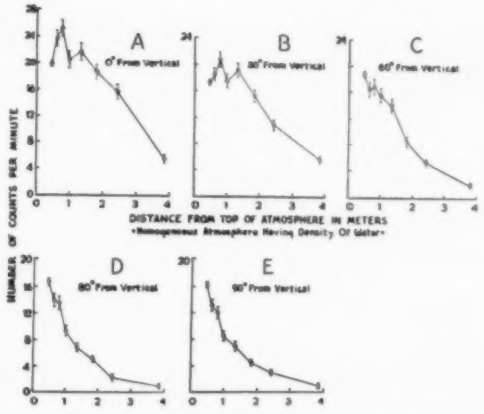

FIG. 1.

[1] W. F. G. Swann and G. L. Locher, J. Frank. Inst. **221**, 275 (1936); W. F. G. Swann, J. Frank. Inst. **222**, 23–58 (1936); W. F. G. Swann, J. Frank. Inst. **222**, 669–680 (1936); also W. F. G. Swann, G. L. Locher and W. E. Danforth, Nat. Geog. Soc. Contributed Tech. Papers, Stratosphere Series, No. 2 (1936).

[2] Our apparatus was installed and tested ready for flight, and the inflation was proceeding on July 11, 1935, when the top of the balloon blew off. The successful flight with the same apparatus was made on Nov. 11, 1935. In the interval, the intensity maximum was also discovered and reported by Regener (Nature **136**, 718 (1935)).

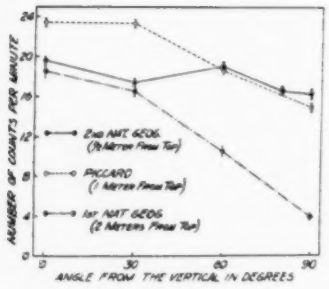

FIG. 2.

together when $h \sec \theta$ is greater than 200 cm, a result to be expected if the intensity depends only upon distance traveled in a straight line through the atmosphere. However, the intensities found at 80° and 90° are much greater than the values necessary to harmonize with the above laws. It is believed that such failure results from the influence of the earth's magnetic field in relation to the paths of the secondaries.

Curves showing the angular distribution at different altitudes are given in Fig. 2. Noteworthy here is a progressive flattening of the distribution as the altitude is increased, and a remarkably high horizontal intensity at the highest altitude. Care must be exercised in the interpretation of these curves, however, for, at high altitudes (particularly for large zenith angles) a countertelescope receives rays from both ends under conditions such as those prevailing, conditions in which the path lengths of the secondaries traveling in the rarified atmosphere can suffer appreciable bending by the earth's magnetic field.

Data from the different flights as to the relative increase of the radiation with altitude (referred to sea level) are as follows. At 40,000 ft. the Explorer I gave us a factor of 38; the Explorer II, 36. At 53,000 ft. our equipment in Dr. Piccard's gondola showed a factor of 44, while that in the Explorer II gave 42. At 57,000 ft, the Explorer II gave 51 (the maximum), and decreased from that point on to a ratio of 41 at 72,400 ft.

To compare these data with those obtained with ionization chambers we integrated the intensity, graphically, over all angles concerned. The large relative increase in the oblique (high-zenith angle) radiation serves to make the integrated intensity increase more rapidly with altitude than does the vertical component.[3] But still the counter detected increase with altitude falls short of that found with the ionization chamber. Whereas we find a 100-fold increase in the integrated counter radiation at 57,000 ft., the ionization measurements of I. S. Bowen, R. A. Millikan and H. V. Neher[4] in the Settle-Fordney stratosphere flight give a factor of about 200. That this should represent a real difference in cosmic-ray intensity seems unlikely since the latitudes of the two flights were so nearly equal.

A possible explanation of this counter-*vs.*-ionization-chamber discrepancy might be secondary rays arising from the wall of the chamber, the rate of production thereof increasing with altitude in proportion to the soft component of the general radiation.

Other matters whose altitude variation may be involved in this disagreement are: specific ionization, and relative number of multiple rays.

[3] The uncertainty in the number of counter impulses received from the two ends of the counter telescope becomes eliminated by the integration in its effect upon the calculated ionization.

[4] I. S. Bowen, R. A. Millikan and H. V. Neher, Phys. Rev. **46**, 641 (1934).

Energy and Absorption of the Gamma-Radiation from Li^7+H^1

L. A. DELSASSO, W. A. FOWLER AND C. C. LAURITSEN
California Institute of Technology, Pasadena, California

(Received December 29, 1936)

It is shown that a study of the pairs ejected from foils in a Wilson cloud chamber gives more reliable and useful information regarding gamma-radiation of very high energy than can be obtained from the recoil electrons. By this method the gamma-radiation from Li^7+H^1 is found to consist of a line at 17.1 ± 0.5 Mev of relative intensity 0.75 and probably one or more lines at about 14 Mev of relative intensity 0.25. No radiation is found between 2 and 10 Mev. The spectrum below 2 Mev has not been investigated. The distribution of recoil electrons is consistent with this and with the Klein-Nishina formula. The division of energy between members of pairs is in agreement with the predictions of Bethe and Heitler. It is shown that the usual method of measuring absorption coefficients leads to erroneous results for radiation much above 3 Mev and a method is described which depends on counting the number of high energy pairs observed in cloud chamber pictures taken alternately with and without 1 cm of lead in the beam. The results agree with theory within the experimental errors. The origin of the radiation is discussed and it is shown that the data can be accounted for if we assume that the proton is captured by the Li^7 nucleus producing a Be^8 nucleus in an odd state. According to Breit this should be a P state and the nucleus may drop to the ground state (^1S) with emission of 17 Mev radiation or to an even state at 3 Mev (^1D) and subsequently break up into two alpha-particles.

INTRODUCTION

IN an earlier attempt to investigate the gamma-ray spectrum from lithium bombarded with protons by means of the Wilson cloud chamber we[1] measured the tracks due to 1576 single electrons and 57 pairs. The single electrons were thought to be mostly recoil electrons from the chamber wall and seemed to suggest a line spectrum distributed more or less uniformly from 3 to 17 Mev. On the other hand, the 57 pairs were distributed mostly in the energy interval from 10 to 17 Mev, thus suggesting that most of the radiation was concentrated near the high energy end of the spectrum and giving no evidence for any radiation below 10 Mev.

Nevertheless, because the number of pairs observed was comparatively small we placed more emphasis on the single electrons. This we now realize was an unfortunate error, for subsequent work with better geometrical arrangement and improved technique has convinced us that most of the single electrons observed were of uncertain origin coming mainly from the field coils and from the top and bottom of the cloud chamber. On the other hand the origin of the pairs is in general unmistakable and they suffered in this early work only from the large energy loss in the thick wall of the chamber or the lead lining which served as scatterer.

For this and other reasons we decided to continue the work and to obtain a much greater number of pairs and at the same time learn more about the origin of the single tracks. To facilitate this a scatterer of low stopping power was placed within the cloud chamber and stereoscopic pic-

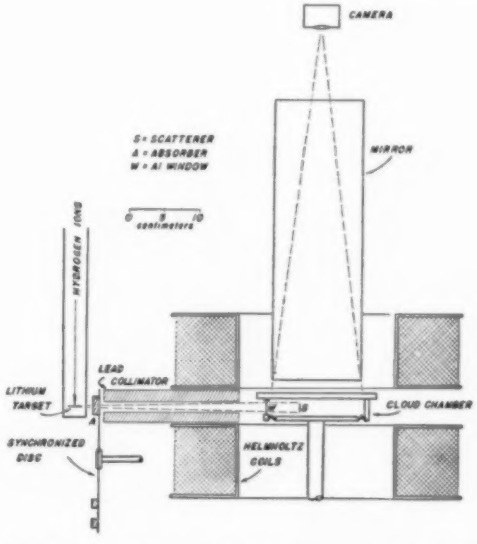

FIG. 1. Schematic diagram of the apparatus used in the determination of the energy and absorption of the gamma-radiation from Li^7+H^1.

[1] H. R. Crane, L. A. Delsasso, W. A. Fowler and C. C. Lauritsen, Phys. Rev. **48**, 125 (1935).

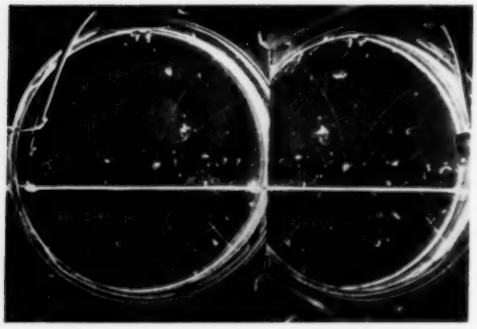

FIG. 2. Stereoscopic views of a 17.0 Mev pair ejected from a 0.012 cm lead scatterer by the gamma-radiation from Li^7+H^1. Magnetic field = 2580 gauss.

FIG. 3. Stereoscopic views of two pairs produced in a 0.012 cm lead scattered by the gamma-radiation from Li^7+H^1. In both pairs the greater portion of the energy has been given to the electrons. The total energies are 16.5 and 16.0 Mev. Magnetic field = 2580 gauss.

tures were taken. The results of a large series of exposures were reported at the Seattle meeting of the Physical Society in June, 1936. The principal conclusion reached was that most of the radiation is concentrated in a band or line at approximately 17 Mev.

When projected onto a model of the chamber and scatterer these stereoscopic pictures revealed the fact that most of the single tracks originated outside the cloud chamber and in the top and bottom of the chamber. In order to eliminate as many of these unwanted tracks as possible we have recently increased the distance between the target and the chamber and have interposed a lead collimator 18 cm thick with an aperture just large enough to illuminate the scatterer. A 1 mm aluminum window is provided in the wall of the chamber where the radiation enters, thus decreasing the number of electrons from the wall. In addition scatterers of lower stopping power were used in order to obtain better resolution. All of these improvements led to a considerable sacrifice in intensity but this was more than compensated for by certain improvements in operation and by the fact that the ratio of useful to unwanted tracks was very much increased.

The uniformity of photography has been much improved by replacing the carbon arc with four 300 watt lamps, two on each side. These lamps are standard 110 volt lamps flashed to about 190 volts. The magnetic field was 2580 gauss. The tube was operated continuously at 750 kv peak while the proton current was about 20 microamperes during the expansion. Metallic lithium

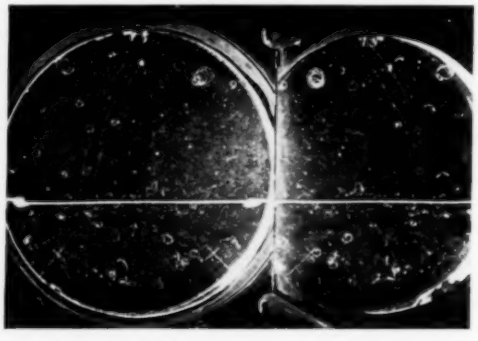

FIG. 4. Stereoscopic views of a single electron (9 Mev) ejected from a 0.012 cm lead scatterer and of an electron (11 Mev) traversing the scatterer. An electron of lower energy ejected from the bottom of the chamber is seen between the two. Magnetic field = 2580 gauss.

was used for the target. The general experimental arrangement is indicated in Fig. 1 and sample pictures are shown in Figs. 2, 3 and 4.

We propose to present all of our measurements on pairs, but in addition we shall present separately our data on single tracks and pairs obtained most recently and with the thinnest scatterer because we consider them more reliable. In addition we shall present some data on the absorption of this radiation in 1 cm of lead.

RESULTS

Pairs

Fig. 5 shows the distribution in energy of a total of 770 pairs obtained from stereoscopic

pictures. 513 of these were obtained with 0.032 cm lead scatterer and 257 with 0.012 cm. Fig. 6 represents the 257 pairs plotted separately. These were obtained most recently and under the best conditions. It is seen that the two curves are in good agreement as far as the distribution in energy is concerned but the width at half-maximum is considerably greater in Fig. 5. This is to be attributed mostly to greater experimental errors as indicated by the displacement of the high energy side of the curve. The still greater displacement of the low energy side is presumably due to the somewhat greater energy loss in the thicker scatterer used in most of the pictures.

These curves indicate clearly a gamma-radiation with a strong maximum near 17 Mev. To account for the observed distribution of pairs we must consider the following possibilities for the gamma-ray spectrum:

(1) a continuous spectrum beginning at about 10 Mev and ending above 17 Mev and having a strong maximum at or near the upper limit,
(2) a single line at about 17 Mev,
(3) a line at 17 and one or more weaker lines between 10 and 17 Mev.

Of these the first seems the least likely for no mechanism is known which might produce such a continuous spectrum and there is no evidence for such a spectrum in any nuclear reaction so far observed. Nevertheless, it cannot be ruled out from our data and since the final product of the reaction is unknown there is no direct experimental evidence against it.

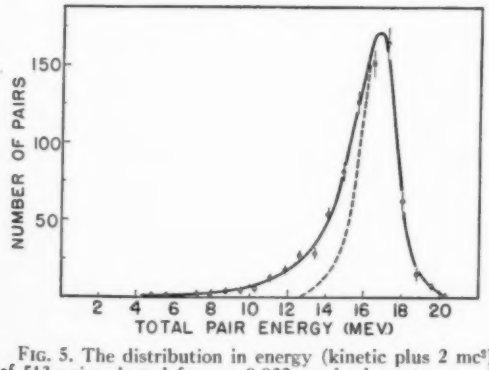

FIG. 5. The distribution in energy (kinetic plus 2 mc^2) of 513 pairs ejected from a 0.032 cm lead scatterer and 257 pairs ejected from a 0.012 cm lead scatterer. The dotted line is symmetrical about 16.7 Mev with the front portion of the curve.

It does not seem possible to account for the observed distribution of pairs as being due to a single line. The observed width of the distribution in energy of the pairs produced by such a line would be due to the following causes:

(1) natural line breadth,
(2) ionization losses in the scatterer,
(3) radiation losses in the scatterer,
(4) fluctuations in the magnetic field,
(5) scattering of the electrons in the gas,
(6) errors in reprojection and measurement of curvature of the tracks.

According to Crane, Delsasso, Fowler and Lauritsen[1] the radiation in question is produced by resonance. The best measurements on the excitation as function of energy are those by Hafstad, Heydenberg and Tuve[2] who find strong resonance at 0.440 Mev with a half-width of 0.011 Mev. From this we conclude that the half-width of the gamma-ray line is not much more than 0.011 Mev.

The scatterer used for obtaining most of the data in Fig. 5 was 0.032 cm of lead and the ionization losses for 17 Mev pairs are therefore uniformly distributed between zero and 0.800 Mev. The effect of this is to broaden the line uniformly toward lower energy by this amount. The radiation losses for electrons in this energy range are, according to Bethe and Heitler,[3] approximately

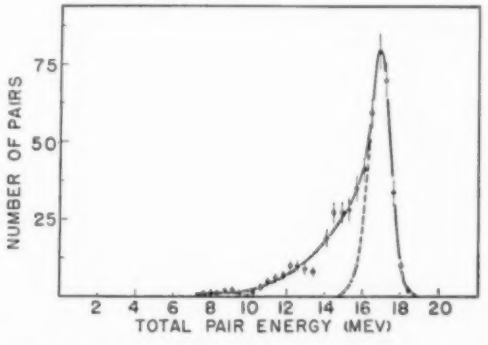

FIG. 6. The distribution in energy (kinetic plus 2 mc^2) of 257 pairs ejected from a 0.012 cm lead scatterer. Although no definite resolution of radiation between 10 and 17 Mev has been obtained the asymmetry of the curve is even more pronounced than in Fig. 5.

[2] L. R. Hafstad, M. T. Heydenberg and M. A. Tuve, Phys. Rev. **50**, 504 (1936).
[3] H. A. Bethe and W. Heitler, Proc. Roy. Soc. **146**, 83 (1934).

equal to the losses by ionization but the number of electrons which would suffer a radiative collision in 0.032 cm of lead comes out to be rather small. Radiation losses will not produce a uniform broadening of the line but only a tailing off toward lower energy. The number of pairs contained in this tail may be calculated from data given by Bethe and Heitler and is about 10 percent.

Fluctuations in the magnetic field amount to less than 2 percent, causing a symmetrical broadening of not more than 0.340 Mev.

The scattering of these high energy electrons in air at a pressure of one atmosphere is extremely small and we prefer to include this in the errors of measurement of curvature.

The measurement of curvature is usually reproducible to 1 Mev for any pair and we consider the probable error due to scattering, reprojection and measurement less than this amount.

The total effect of all these factors would be a nearly symmetrical broadening of the line but with a shift of the center of gravity amounting to about half of the ionization loss in the scatterer. We have indicated such a symmetrical distribution in Fig. 5 and it is seen that most of the pairs observed lie within this distribution and may be attributed to a line at 17.1 ± 0.5 Mev but it is clear that a considerable fraction of the pairs of lower energy cannot be attributed to this line directly.

Analyzing the data in this manner we obtain the following results. The average energy of 580 pairs lying within the symmetrical high energy region is 16.7 ± 0.5 Mev. To this must be added 0.4 Mev for the mean loss due to ionization in the scatterer, giving as the most probable value of the energy of the high energy gamma-ray 17.1 ± 0.5 Mev. The number of pairs lying below the symmetrical distribution in Fig. 5 is 190 or about 25 percent of the total. It seems likely that approximately one-fourth of these pairs, that is 10 percent of 580, can be accounted for as being pairs which have lost from 1 to 10 Mev in escaping from the scatterer. The remaining pairs, amounting to some 15 to 20 percent of the total, can apparently not be accounted for in this manner and must then be due to radiation of energy less than 17 Mev falling on the scatterer. This radiation may be due to one or more of the following causes:

(1) one or more lines or bands of gamma-radiation from Li^7+H^1 in addition to the 17 Mev radiation,
(2) secondary radiation produced by the 17 Mev line in the material surrounding the cloud chamber and scattered into the chamber,
(3) radiation due to contamination in the beam or target, or both.

From the work of Bethe and Heitler we can calculate the number of quanta produced by the secondaries of a 17 Mev quantum and having energies between 10 and 17 Mev. This comes out to be less than 2 percent even for lead and can therefore not account for the low energy pairs observed.

The only reaction known which might give radiation of sufficient energy to account for the observed pairs is $B^{11}+H^1$ but it has an excitation efficiency of the same order as Li^7+H^1 and hence the contamination would have to amount to some 20 to 30 percent which is obviously out of the question.

Thus we seem forced to the conclusion that Li^7+H^1 emits some radiation between 10 and 17 Mev in addition to the radiation at 17 Mev.

It seems highly probable that this radiation consists of a line in the neighborhood of 14 Mev and that the intensity amounts to some 20 percent of the total but it is possible that it is distributed among two or more lines between 10 and 17 Mev. From our measurements we may further conclude that there is no radiation between 2 and 10 Mev amounting to more than 5 percent of the total. We find no evidence for softer radiation but our present data do not definitely exclude radiation much below 2 Mev.

Recoil Electrons

It is much more difficult to obtain reliable data on the recoil electrons for clearly not all of the

Table I. *Reduction produced by collimation in relative number of single tracks.*

	Scatterer	Pairs	Electrons	Positrons	Electrons minus Positrons (Recoil Electrons)
No collimation	Pb	513	381	155	
Collimation	Pb	257	101	49	52
	Al	71	105	12	93

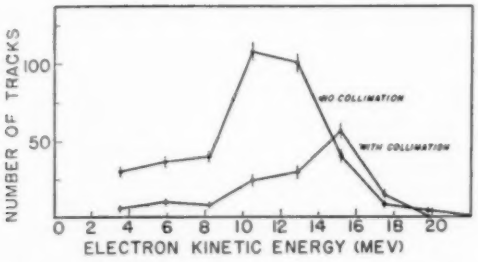

FIG. 7. The distribution in kinetic energy of the recoil electrons (observed electrons minus observed positrons) ejected from lead and aluminum scatterers with and without collimation of the gamma-ray beam. The curves are normalized to the same number of pairs. The large number of spurious tracks without collimation is apparent.

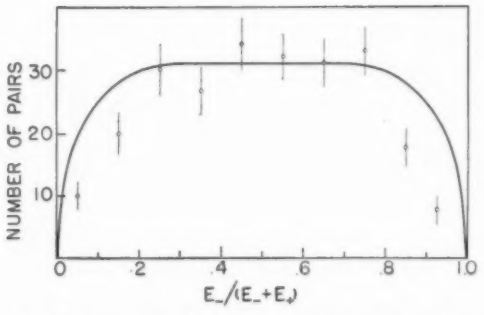

FIG. 8. Energy distribution of negative members of pairs with total energy between 15 and 18 Mev. The theoretical distribution (normalized to the average number within the central six intervals) is shown in the heavy line. The experimental points are shown.

single tracks observed belong to this category. This is particularly true in the pictures taken without collimation. The reduction due to collimation in the relative numbers of single tracks is best seen from Table I.

It seems most reasonable to assume that the single positrons observed when collimation is used are in reality members of pairs originating in the scatterer and that an equal number of the single electrons are of the same origin. Presumably the corresponding pair members have escaped detection either due to large energy loss and scattering or to imperfect photography. To obtain the approximate number of recoil electrons we have therefore subtracted the number of single positrons observed from the number of single electrons.

The effect of collimation is also apparent from Table II in which we have shown the average energies of the several groups with and without collimation. The average energy of recoil electrons obtained with collimation and determined as indicated above is 12.7 ± 0.7 Mev which is in satisfactory agreement with the value 12.2 Mev predicted by the Klein-Nishina formula for 17.1 Mev radiation.

TABLE II. *Average energy of various particle groups, with and without collimation.*

	WITH COLLIMATION	WITHOUT COLLIMATION
Average energy of pairs	15.7 ± 0.7	15.7 ± 0.5
Average energy of electrons	12.2 ± 0.6	10.7 ± 0.3
Average energy of positrons	11.1 ± 1.0	10.8 ± 0.6
Average energy of recoil electrons	12.7 ± 0.7	10.7 ± 0.4

Fig. 7 shows the distribution in energy of apparent recoil electrons with and without collimation. The distribution obtained with collimation probably represents quite accurately the true recoil electrons and is in satisfactory agreement with expectations based on the Klein-Nishina theory and the radiation indicated by the pairs.

ENERGY DIVISION BETWEEN PAIR MEMBERS

Bethe and Heitler have calculated the probability for the energy division between the two members of pairs of various energies. The curve in Fig. 8 shows this probability for 17 Mev pairs and the points represent the number of electrons observed having a given fraction of the total energy of the pairs. The deviation at the low and high end are to be expected because of the great probability that a pair is not measured as such if the energy division is very unequal. This systematic error is not included in the probable errors indicated. The agreement with the theory is entirely satisfactory.

ABSORPTION IN 1 CM OF LEAD

Up to the present time the only measurements of absorption coefficients for radiation in this energy range have been made in the usual way by means of ionization chambers.[4, 5] Unfortunately, such measurements are not reliable and cannot be taken as valid tests of the theory developed by

[4] E. McMillan, Phys. Rev. **46**, 868 (1934).
[5] H. R. Crane, L. A. Delsasso, W. A. Fowler and C. C. Lauritsen, Phys. Rev. **46**, 531 (1934).

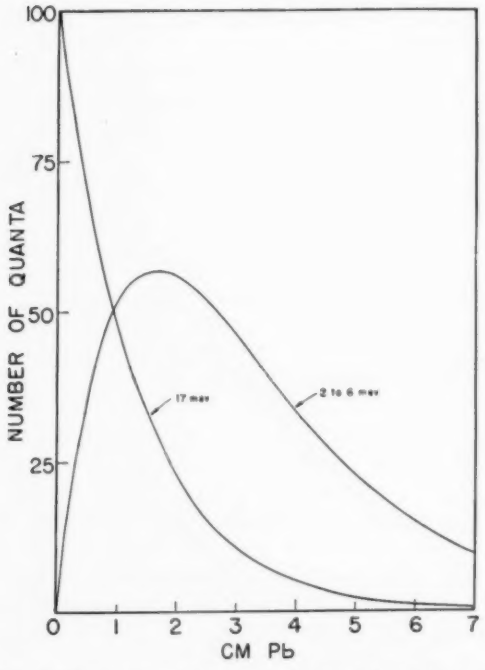

FIG. 9. The number of primary and penetrating secondary quanta as a function of absorber thickness.

Oppenheimer and Plesset[6] and by Bethe and Heitler.[3] This is evident from an examination of cloud chamber pictures taken under similar conditions for they show that most of the ionization is produced by electrons which cannot be attributed to the direct beam. With the low intensity available the geometrical arrangement is necessarily such that stray and scattered radiation contributes a large part of the ionization and because the absorption coefficient for much of this radiation is lower than that for the primary radiation this part becomes relatively greater with increasing absorber thickness. With such an arrangement we should therefore expect to obtain a value of the absorption coefficient which lies below the true value and approaches the minimum of the absorption curve as the thickness of absorber is increased. For lead this minimum occurs at about 3 Mev and the measured absorption coefficient may therefore correspond to any value of the gamma-ray energy between 3 and 17 Mev, depending on how the measurement is made.

That this is so can be seen from a simple calculation. Let us consider an arrangement in which the target is comparatively close to the ionization chamber and the absorbers are interposed directly in front of the ionization chamber. Such an arrangement is far from ideal but is usually necessitated by the low intensity available.

We wish to determine approximately the composition of the radiation as a function of absorber thickness and from this the ionization to be expected. This gives the apparent absorption coefficient.

Let us assume that the primary radiation initially consists of N_0 quanta of 17 Mev. Then the number of primary quanta present at any depth x in the absorber is

$$N = N_0 e^{-\mu x},$$

μ being the total absorption coefficient for the material. The high energy quanta removed from the beam produce pairs and recoil electrons which in turn produce a continuous x-ray spectrum extending from zero to 17 Mev. If the absorber consists of a heavy element, say lead, a part of this continuous spectrum will have an average absorption coefficient μ' which is lower than μ. Let α be the number of such quanta produced for each primary quantum removed from the beam, then the change in the number N' of such quanta occurring in a layer Δx in the absorber is, if we neglect the range of the electrons in lead,

$$\Delta N' = \alpha \Delta N - N' \mu' \Delta x; \qquad \text{or}$$

$$\Delta N' = \alpha N_0 \mu e^{-\mu x} \Delta x - N' \mu' \Delta x;$$

and hence the number of these secondary quanta present at any depth x in the absorber

is $$N' = \alpha N_0 (\mu/(\mu' - \mu))(e^{-\mu x} - e^{-\mu' x}).$$

From the data given by Bethe and Heitler we can calculate α for any desired energy interval. We are particularly interested in the secondary quanta in the energy interval for which the absorption coefficient is near the minimum, that is roughly the interval from 2 to 6 Mev for which the average absorption coefficient is $\mu' = 0.50$ cm^{-1} in lead. For this interval α is equal to 1.3 and we can therefore calculate N' for any value

[6] J. R. Oppenheimer and M. S. Plesset, Phys. Rev. **44**, 53 (1933).

of x if we assume that the secondary quantum is produced at the point where the primary quantum is absorbed. This is of course not quite true but permissible in the approximation which we are attempting. Fig. 9 shows N and N' plotted against absorber thickness. It is seen that already at a depth of 1 cm the number of penetrating secondary quanta equals the number of primary quanta and they predominate more and more with increasing thickness of the absorber. In addition to these quanta there will be produced a considerable number of quanta of lower energy, partly belonging to the continuous x-ray spectrum just discussed and partly due to anihilation of pairs but these are comparatively rapidly absorbed and we shall neglect them.

The ionization to be expected in the ionization chamber is

$$I \sim N + \beta\gamma N',$$

where β is a factor smaller than 1 due to the fact that not all of the N' quanta are directed toward the chamber. They are, however, directed mostly in the forward direction and $\beta = 0.8$ seems a reasonable value. The factor γ is the ionization function which in this energy region is approximately proportional to the energy, hence $\gamma = 0.3$.

The calculated value of the logarithm of I is plotted in Fig. 10 giving an almost straight line with a constant slope corresponding to $\mu = 0.50$ cm^{-1} for all thicknesses of absorber. If the calculations were carried out exactly for still greater thicknesses the slope would gradually decrease, ultimately approaching the value $\mu = 0.46$ cm^{-1} which is the minimum absorption coefficient in lead and corresponds to radiation of approximately 3 Mev. For comparison the line $\mu = 0.73$ cm^{-1} is shown. This is the theoretical value of the absorption coefficient for 17 Mev radiation and it is worthy of note that the penetrating secondary radiation builds up so rapidly that the absorption

TABLE III. *Numbers of pairs in three energy intervals, with and without absorber.*

	Number of Pairs in Symmetrical High Energy Region	Remainder above 10 Mev	Pairs below 10 Mev	Total
No absorber	260±11	66±6	2	328
With 1 cm lead absorber	135± 8	51±5	8	194

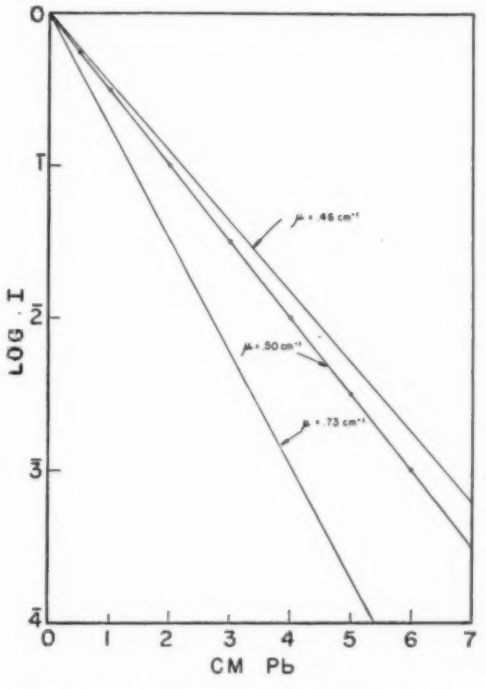

FIG. 10. The points on the curve marked $\mu = 0.50$ cm^{-1} are calculated neglecting the range of electrons in lead. This approximation is satisfactory except for the transition layer which is a few millimeters of lead.

curve as here calculated is straight, even for very thin absorbers, and at no point is the absorption coefficient for 17 Mev radiation approached. This is in agreement with the results of the experiments referred to above. It is clear, therefore, that this method is unsuited for determining the true absorption coefficient for radiation much in excess of 3 Mev.

To circumvent this difficulty we have taken cloud chamber pictures alternately with and without 1 cm of lead interposed between the target and the cloud chamber. By comparing the number of pairs obtained with lead in the beam with the number obtained without lead we have a true measure of the total attenuation in 1 cm of lead of the radiation which produces these pairs.

It seems likely that some pairs of low energy are produced by radiation which is scattered into the chamber from the lead absorber hence it would be reasonable to consider only pairs having energies near the maximum, say within the sym-

metrical distribution indicated in Fig. 5. In Table III we have listed the number of pairs observed in three energy intervals with and without absorber. The attenuation in 1 cm of lead of the radiation producing the high energy pairs is seen to be

$$(135\pm8)/(260\pm11)=0.52\pm0.04,$$

which gives a total absorption coefficient for this radiation of

$$\mu=-\log 0.52=0.66\pm0.07\ \text{cm}^{-1}.$$

The Klein-Nishina formula gives for 17.1 Mev radiation

$$\sigma=0.09\ \text{cm}^{-1},$$

while Bethe and Heitler give for the absorption due to pair formation

$$\pi=0.64\ \text{cm}^{-1}.$$

Hence $$\mu=\sigma+\pi=0.73\ \text{cm}^{-1}$$

which is in fair agreement with the observed value.

The data given in Table I permit us to determine the ratio σ/π for lead and for aluminum if we assume that the observed positrons as well as an equal number of electrons are members of pairs originating in the scatterer. The number of recoil electrons is then equal to the number of electrons minus the number of positrons and the true number of pairs is equal to the observed number of pairs plus the number of positrons plus an equal number of electrons. This gives for lead

$$(\sigma/\pi)_{\text{Pb}}=52/(257+98)=0.15$$

compared to the theoretical value of 0.142 and for aluminum

$$(\sigma/\pi)_{\text{Al}}=93/(71+24)=1.0,$$

for which the theory gives 0.90. The accuracy is not high and it is difficult to estimate the probable errors due to the uncertainty in the origin of some of the tracks.

Origin of the Gamma-Radiation

That the gamma-radiation here discussed is due to the Li^7 isotope is clear from energy considerations and this has recently been verified by Rumbaugh and Hafstad[7] who, using the separated isotopes of lithium, observed gamma-radiation from Li^7 and confirmed the resonance at 0.44 Mev but found no gamma-radiation from Li^6. The energy available may be calculated from the masses and is

$$7.0182+1.0081-8.0080=0.0183$$

or 17.0 Mev. To this must be added 7/8 of the kinetic energy of the bombarding proton. Hence the total energy available is 17.4 Mev.

Several suggestions regarding the possible mechanism of the radiation from Li^7+H^1 have been made but the discussions have usually been complicated or unsatisfactory owing to the uncertainty regarding the facts to be accounted for. In the article referred to above as (2) Breit gives a most excellent discussion of the several possibilities and the facts which we have just presented appear to fit well with certain of these and should prove helpful in excluding others. We enumerate our conclusions regarding the radiation to be accounted for:

(1) a line at 17 Mev of relative intensity 0.75,
(2) one or more lines between 10 and 17 Mev of total relative intensity 0.25,
(3) little or no radiation between 2 and 10 Mev. Relative intensity less than 0.05,
(4) radiation below 2 Mev not excluded by these experiments.

In particular it should be noted that we failed to find any radiation in the neighborhood of 8 Mev. If such radiation is emitted it is probably less than 2 percent of the total observed.

We have previously[1] discussed the following two possibilities for the mechanism responsible for the radiation.

(1) After capture of the proton by the Li^7 nucleus the resulting unstable (Be^8) nucleus breaks up into two alpha-particles, one or both of which may be in an excited state and subsequently drop to the normal state with emission of radiation.

(2) The (Be^8) nucleus is formed in a quasi stable state with a life time for alpha-particle disintegration which is long compared with the radiation time. It subsequently drops to the ground state in one or more jumps.

[7] L. H. Rumbaugh and L. R. Hafstad, Phys. Rev. **50**, 681 (1936).

The experimental data available at the time did not allow of a decision between these two alternatives but it seemed difficult to account for the long life time of the excited (Be^8) nucleus. This difficulty may, however, be resolved as Breit has pointed out and hence the second alternative now seems the more attractive, particularly since it is in complete analogy with the mechanism known to be responsible for the production of the gamma-radiation from Be^9 and B^{11} bombarded by protons.[1] In these two cases a mechanism analogous to (1) is ruled out by energy considerations. The mechanism which appears to account best for our observations is one of the several possibilities suggested by Breit and fully discussed by him. It is based on the assumption that the proton is captured on a virtual level forming a Be^8 nucleus in an excited state which is supposed to be odd in order to exclude disintegration into two alpha-particles. This was independently suggested to us by Dr. Elsasser, his assumption being that only protons having the correct combination of angular momentum and spin could be captured on this level. The model of the Be^8 nucleus used by Breit is based on unpublished calculations by Feenberg and Wigner.[8] The ground state of Be^8 is a ^1S level which is even and there is an even ^1D level at approximately 3 Mev. The next even level would be a ^1G at about 8 Mev. The virtual level at 17 Mev is supposed to be an odd P level.

This gives the following three possibilities for transition with gamma-ray emission.

$$Li^7+H^1\rightarrow(Be^8)\rightarrow Be^8+17 \text{ Mev } \gamma\text{-ray} \quad (1)$$

$$\rightarrow {}^*Be^8+14 \text{ Mev } \gamma\text{-ray} \quad (2)$$

$$\rightarrow {}^*Be^8+8 \text{ Mev } \gamma\text{-ray}. \quad (3)$$

[8] Now published, E. Feenberg and E. Wigner, Phys. Rev. **51**, 95 (1937). They give 3.8 mc^2 and 12.6 mc^2, respectively, for the ^1D and the ^1G level values. See also P. I. Dee and C. W. Gilbert, Proc. Roy. Soc. **154**, 279 (1936).

Our observations indicate that reactions (1) and (2) occur with a relative probability of at least 3 to 1, and (3) occurs rarely if at all. It is to be expected that the probability for reaction (3) would be very low since a transition between P G levels would be strongly forbidden. Since we find no radiation at 3 Mev it is most reasonable to suppose that $^*Be^8$ in reaction (2) breaks up into two alpha-particles each having an energy of approximately 1.5 Mev. This is consistent with an even ^1D level at 3 Mev. In reaction (1) Be^8 is presumably formed in the ground state which is even and it may or may not break up into two low energy alpha-particles depending on whether Be^8 is stable or not. The ^1D level here discussed may also be involved in the reactions

$$Li^7+H^2\rightarrow Li^8+H^1, \quad (4)$$

$$Li^8\rightarrow Be^8+\epsilon^-. \quad (5)$$

Rumbaugh and Hafstad[7] have shown that the protons from reaction (4) have a range of less than 8 cm which leaves some 3 or 4 Mev to be accounted for. It is not unlikely that Be^8 in reaction (5) is formed in the excited state ^1D and subsequently breaks up into two alpha-particles with approximately 1.5 Mev each.*

In conclusion we wish to express our appreciation to the Seeley W. Mudd Fund for financial support.

* *Note added in proof.* W. B. Lewis, W. E. Burcham and W. Y. Chang, Nature **139**, 24 (1937) have observed radioactive alpha-particles after bombarding lithium with 500 kv deuterons. The half-life of the alpha-particles as well as the beta-particles from (5) is given as 0.88 ± 0.1 seconds. This is probably a more reliable value than the value 0.5 ± 0.1 seconds observed for the beta-particles in this laboratory as the probable error was calculated only from the number of tracks observed and did not include possible systematic errors arising from the timing of the cloud chamber. We have confirmed the existence of these alpha-particles by cloud chamber observations and find a distribution extending from 5 cm range down to at least 0.5 cm with a maximum probability at 0.7 cm range or 1.5 Mev. Whether or not the spectrum is continuous or complex is as yet uncertain. Attempts to detect an instantaneous alpha-emission of similar distribution in the case of Li^7+H^1 are now in progress.

A Determination of h/e from the Short Wave-Length Limit of the Continuous X-Ray Spectrum

JESSE DUMOND AND VERNON BOLLMAN
California Institute of Technology and Occidental College

(Received November 30, 1936)

Two precision determinations of the short wave-length limits of the continuous x-ray spectrum have been made, one in the region of 10,000 volts, the other in the region of 20,000 volts by the method of isochromats under very steady applied voltage. The two crystal spectrometer was used as a monochromator. The $K\beta_2$ line of molybdenum and the $L\beta_1$ line of tungsten were used for setting the monochromator. The experimental technique is fully described. A thin window tube with a nickel target coated with tungsten by evaporation was used as the x-ray source. The effect of the finite resolution of the two crystal spectrometer, its behavior as a function of wave-length, and the pitfalls resulting from the "tails" of the spectral window as defined by the selective bicrystalline reflection are carefully considered. The advantage of using a thin layer target of high atomic number on a back support of lower atomic number in order to minimize the danger from these pitfalls is explained. Arguments for the applicability of a correction to the measured voltage for the work function of the cathode are presented. All effects such as the finite resolution of the spectrometer tending to render the voltage threshold for a given wave-length setting less well defined are here called for brevity "smearing effects" and five different new methods of "desmearing" the isochromats or of locating the thresholds are considered. The presence of a hitherto unsuspected knee in the isochromat within a few volts of the quantum limit is shown to render inapplicable the only method so far in use for locating the threshold voltage, the "method of the projected tangent," which is also shown to contain other objectionable pitfalls. The experiment permits of determining either h/e or $e/h^{3/4}$ according to whether we assume the ruled grating wave-lengths of x-rays to be correct or make no such assumption but include the data from selective x-ray crystal reflection, crystal density, molecular weight and the Faraday constant as part of the computation. By these respective methods we obtain $h/e=1.3762 \pm 0.0003\times10^{-17}$; $e/h^{3/4}=2.0720\pm0.0004\times10^{10}$. These results agree with those of Kirkpatrick and Ross and those of Schaitberger on the same experiment with deviations which are small compared to the disagreement with two other entirely different experiments for determining functions of e and h. This discrepancy on the Birge-Bond diagram already emphasized by Birge is carefully discussed and possible causes for it are considered. Two possible objections to the present experiment are raised and we believe successfully disposed of. The practical impossibility of blaming this discrepancy on the short wave-length limit experiment is, we believe, convincingly proven by our results.

I. PRESENT IMPORTANCE OF THE PROBLEM

AS Birge[1] has recently and repeatedly pointed out there still exists a stubborn and baffling discrepancy between the results of different types of experiment in the determination of the important natural constants e and h. So much emphasis has been placed on the discrepancy between the directly measured values of e obtained on the one hand from x-ray measurements and on the other hand from the oil drop experiment that now when the oil drop value of e seems in the opinion of many competent workers about to be rendered concordant with the x-ray value by more recent redeterminations of the viscosity of air[2] it is well worth while to re-emphasize the discrepancies in other quarters which are still as great a mystery as ever.

The diagram of Fig. 1 shows at a glance the present status of the problem. The reader is referred to the caption for an explanation of the diagram. We will not concern ourselves with the point marked "oil drop" since its proper position depends on the viscosity of air now in process of being redetermined. The discrepancy which we here wish to emphasize concerns the three points: I, the x-ray crystal value of e; II, the determination of $e/h^{3/5}$ from a combination of the measured values of the Rydberg constant and e/m; and, III, the determination of $e/h^{3/4}$ from the short wave-length limit of the continuous x-ray spectrum. These three points do not lie in the same straight line on the diagram. Any pair selected from the three experiments above yields values of e and h which are discordant with values obtained from any other pair by a much larger error than one would reasonably expect from internal consistency of the measurements and a

[1] Raymond Birge, Nature **137**, 187 (1936); Phys. Rev. **48**, 918 (1935).
[2] G. Kellström, Nature **136**, 682 (1935); Phys. Rev. **50**, 190 (1936).

careful consideration of all the sources of systematic error.

The order of accuracy attainable in measurements of e/m and R renders the point II by far the most accurate and reliable one of the three mentioned on the Birge-Bond diagram. It seems out of the question to expect any significant yielding here sufficient to explain even a small fraction of the discrepancy.

The authors have recently[3] answered by an experimental test what they believe constituted the one remaining objection which it seemed possible to raise to the x-ray crystal method used in determining point I. The powdered calcite method discriminates definitely in favor of the x-ray crystal values of e as against values computed from points II and III, all three determinations by Bäcklin, Bearden and Söderman lying inside the probable error of the first mentioned method. We attach no important significance to the slightly lower value obtained by the powder method which by its nature involves greater accidental errors and believe it safe now from these indications to assume the mean value of Bäcklin, Bearden, and Söderman as probably best, always conditional, of course, upon the correctness of the ruled grating values of x-ray wave-lengths.

As regards point III the experiment here described was performed in the hope that new light might be thrown on this discrepancy situation but it must be frankly admitted that the result has served simply to reemphasize the difficulty. The apparent impossibility of bringing point III into line with points I and II by any stretching of the short wave limit data will be made manifest in the following pages.

[3] DuMond and Bollman, Phys. Rev. **50**, 524 (1936).

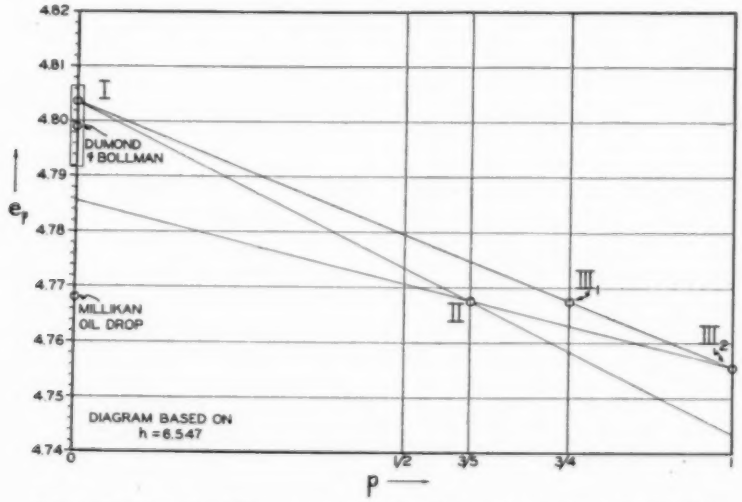

FIG. 1. The Birge-Bond diagram as applied by Birge to the problem of determining e. To each point on the diagram there correspond one or more experiments which determine in general some function of the constants e and h so that the results of each experiment or set of experiments can be written in the form $e=h^p\times$ (a measured constant). The Birge-Bond diagram above is plotted by assigning to h the arbitrary value $h=6.547$, a value known to differ but little from the true one and computing nominal values of e from such equations. The nominal value of e called e_p is plotted as ordinate against the power p which represents the degree to which h was involved in its computation. Direct determinations of e which do not involve h at all thus appear at the extreme left. Since two unknowns e and h are involved, any three points may be consistent or inconsistent as to their evidence on the values of e and h. If three points are consistent, it is easily shown that they must lie in the same straight line and if otherwise, they are inconsistent. The experimental data leading to the establishment of points I, II and III are outlined in the last section near the end of this paper. If points lie in the same horizontal straight line, they indicate a value of h equal to that assumed in computing the diagram, $h=6.547$. Any two points determine a value of e which is given by the intercept on the y axis (at $p=0$) of a straight line through the points.

II. Experimental Procedure

Our present experiment, like nearly all precision determinations of $e/h^{3/4}$ by observations on the short wave-length limit of the continuous x-ray spectrum, has been done by the method of isochromats. An x-ray spectrometer, in the present case a two-crystal ionization spectrometer, is set to select from the continuous spectrum a narrow band with its center coincident in wave-length with the center of a conveniently chosen standardizing line from the characteristic x-ray spectrum. Since the wave-lengths of these lines have been previously determined on the Siegbahn relative scale with high precision this part of the work need not be repeated. With the spectrometer thus set, an x-ray tube (not necessarily the one used to excite the standardizing line) is excited with gradually increasing applied voltage and the intensity of any of the radiation from it admitted through the spectrometer, the latter, being held always at the above constant setting, is measured in an ion chamber. As the quantum limit of the continuous spectrum from the tube pushes toward shorter wave-lengths with increasing voltage, a point is reached where continuous radiation finds its way through the bicrystalline selective reflection of the spectrometer and is registered as ionization in the ionization chamber. With increasing voltage the ionization then rises more or less suddenly as the short wave limit pushes forward to wave-lengths distinctly shorter than that for which the spectrometer is set. The threshold so defined fails to be abrupt principally because of the finite resolving power of the spectrometer.

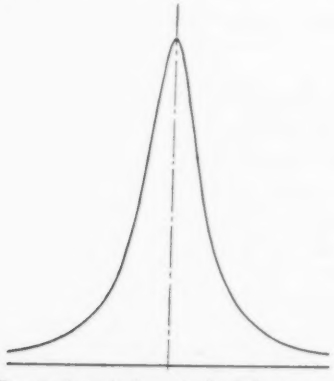

Fig. 2. A typical spectral window curve.

The slit curve of the spectrometer

We shall make frequent reference to what we shall call the "slit curve" or the "spectral window curve" of the spectrometer. The mechanism of selective x-ray diffraction at the crystal surfaces combined with the imperfection of the crystal lattice itself define a region or "window" which the spectrometer selects from a continuous spectrum. This region or window cannot be made to have sharp abrupt edges or limits for its long and short wave-length boundaries by any experimental device of slits or screens because it is primarily the result of a diffraction phenomenon. This spectral window can thus be best described by plotting a curve such as the one shown in Fig. 2. A fair idea of the shape of such a curve can be obtained experimentally if the procedure for exploring the shape of a characteristic x-ray line be followed, choosing a line *considerably narrower than the slit to be studied*. The observed "line shape" is thus in reality chiefly descriptive of the "slit curve." Such a procedure is of course only approximate. The window curve is a characteristic of the spectrometer and should not be confused with an x-ray emission line. Characteristic of such window curves are the gradually diminishing asymptotic "tails," "wings," or "fillets" which mar the sharp definition of their short and long wave-length boundaries. No definite point of termination can be set for these "tails" and unfortunately for the experiment in question it is probable that they diminish at large distances from the maximum more or less as the inverse square of the distance. Thus even though the resolution of a spectrometer is excellent as regards the width of its slit curve at half-maximum height there will always be a small amount of radiation admitted which may differ in wave-length by many times this half-maximum breadth from the central wave-length value. Furthermore if the continuous spectrum is such that at these remote wave-lengths the intensity is very considerably stronger than the intensity in the immediate neighborhood of the center of the slit curve it is evident that the intensity leaking through the tail of the slit may be very far from a negligible portion of the total and the center of gravity of the wave-lengths transmitted through the spectrometer may be quite different

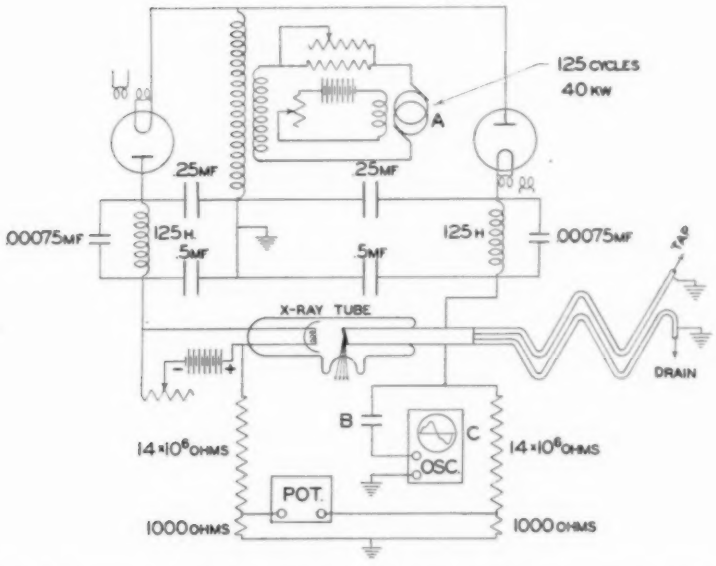

FIG. 3. Diagram of constant potential d.c. supply and high voltage measuring circuits.

from what it would be if the continuous spectrum were nearly "flat."

Object of the experiment

The object of the experiment is to determine the critical or threshold voltage at which x-rays of a given wave-length λ just begin to appear as the shortest wave-lengths emitted in the continuous spectrum. The frequency ν corresponding to this wave-length is believed to be related to the threshold voltage V at which it just begins to be excited by the well-known relation

$$eV = h\nu \tag{1}$$

or what is equivalent

$$\lambda V/c = h/e. \tag{2}$$

Photoelectric experiment and the method of increments

Thus a single measurement of V and λ would appear to furnish sufficient data to compute h/e. In the closely related inverse experiment first performed by Millikan[4] the critical stopping potential for photoelectrically emitted electrons *is measured for a large number of incident wave-lengths* and the resulting curve of frequency or wave number plotted against voltage turns out to be a straight line whose slope serves to compute h/e while the intercept of this line prolonged to the voltage axis gives in electron volts the "work function" of the photoelectrically emitting material. For brevity we shall call this the method of increments since it is a method of determining h/e from the increments of voltage and frequency $(V_1 - V_2)$ and $(\nu_1 - \nu_2)$ according to the equation

$$e(V_1 - V_2) = h(\nu_1 - \nu_2). \tag{3}$$

It is strange that in the x-ray experiment universally recognized as "the inverse photoelectric effect" the method of increments has never been applied at least according to any published report. The reason is probably to be found in the fact that while corrections for work function appear in the x-ray case just as surely as in the direct photoelectric effect these corrections are relatively so much smaller for the much higher voltages of the former than for the latter case that a resort to the method of voltage and frequency increments was not imperative. Nevertheless the present application of the method of increments has led us to some interesting conclusions.

[4] R. A. Millikan, Phys. Rev. **1**, 18 and 355 (1916).

The constant potential supply and high voltage measuring circuits

Ripple measurements.—Fig. 3 shows the diagram of electrical circuits used in this experiment. The 40 kw, 125 cycle alternator *A* is driven by a synchronous motor and is therefore very steady and free from fluctuations imposed by local variations in line voltage. Control of the high voltage applied to the x-ray tube is obtained by controlling the field of the alternator *A* supplied from batteries. A fine grained control of voltage was obtained by a small resistance paralleling a still lower fixed resistance in series with the current supplied to the transformer primary. This 125 cycle supply is stepped up and rectified by means of a valve tube rectified commercial set manufactured for medical use in deep therapy. The pulsating high potential output which is designed so that ground is midway between the potentials of the two terminals is filtered by two stages of condensers as shown with 125 henry inductances between stages. The filtering effect of this arrangement was greatly improved at very small extra expense by the addition of the two small 0.00075 microfarad condensers shunted around the inductances. These evidently need only have the dielectric strength sufficient to withstand safely the voltage drop across the inductance, that is to say, the ripple voltage prevailing at the first stage condensers. The capacity of 0.00075 microfarad is calculated to resonate with the inductance at 125 cycles or thereabouts. This tuning is, however, not very critical on account of the rather high resistance in the inductance.

So effective did this filter circuit prove to be that we found the ripple amplitude to ground to be less than 0.6 volt with the tube working at 10 milliamperes at which load it was operated. This ripple, as one would expect, was practically independent of the voltages of 20,000 or 10,000 volts used in the experiment. Without the 0.00075 mf condensers the ripple was three times as large.

The ripple amplitude was measured under operating conditions both near the tube and near the supply set (which are separated by two or three meters of transmission line) and found to be the same at both points. The ripple measurements were very easily made by means of an RCA cathode-ray oscilloscope C protected from the high voltage d.c. by a blocking condenser B made of two photographic plates from which the emulsion had been removed and which had been coated with thin sheet copper. The oscilloscope deflections obtained in series with this blocking condenser were calibrated by first applying by means of a resistance network a known small 125 cycle a.c. voltage to the oscilloscope with the same blocking condenser in series. The ripple from anode to ground was found to be slightly larger than the ripple from cathode to ground and this is to be expected because of the increased load on the anode side caused by the current flowing back through the cooling water supply, a long zigzag of glass tubing through which inlet and outlet water flows from the tap to the target and back to the drain.

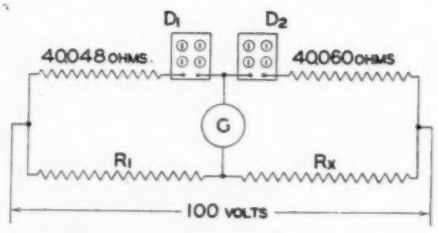

FIG. 4. Bridge for measuring megohm unit resistors.

E. O. Lawrence has suggested the possibility of very high radiofrequency ripple generated in the x-ray tube itself which would not be observed with the cathode-ray oscilloscope. We are indebted to G. Potapenko who has made an exploration in the vicinity of our x-ray tube with a very sensitive aperiodic thermocouple detector easily capable of detecting a source of 0.001 watt power and any radio wave-length down to a couple of centimeters. With nothing between this detector and the cathode and anode elements of the x-ray tube save the thin glass wall of the tube and a 1/16 inch enclosing tube of Bakelite and with the antenna of the detector at a distance of about 10 cms only, not the slightest indication of radiofrequency ripple could be observed with the tube in normal operation. Thus if such a ripple be present its energy is less than one part in two hundred thousand of the principal energy of the cathode-ray stream.

The high voltage measurements.—The high voltage measurements which are of highest importance in this experiment were made by means of a

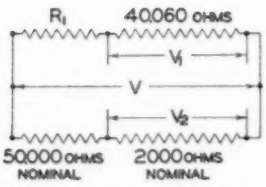

FIG. 5. Method of extending the range of the potentiometer to obtain the ratio of the megohm units to a 40,000 ohm unit.

pair of 14 megohm resistance columns consisting of Shallcross wire wound resistances each connected to ground through a 1000 ohm resistance unit of the same kind of wire. The potential drop across these two 1000 ohm units in series was measured with a Leeds & Northrup latest type K potentiometer recently returned from a check by the manufacturers. Careful comparisons of our standard cell were made against three other standard cells which have been kept in this laboratory under carefully controlled conditions as laboratory standards. A check of the three latter cells as well as our own against a fourth standard cell freshly received from the makers with a calibration from the National Bureau of Standards was also made.

Since there is very likely to be an appreciable current to ground on account of the above mentioned unbalanced load from the water-cooling system it is very essential that the ratio of each 14 megohm stack to its 1000 ohm resistor be *exactly* the *same*. If this equality of ratio is accurately satisfied it is then only necessary to multiply the potentiometer reading by this common ratio to get the potential at the tube no matter how much ground current may be present, whereas if the two ratios were different it would be necessary to take two potentiometer readings, one across each 1000 ohm resistor and add the results. This would have been very awkward for in practice the potentiometer was used as a continuous indicator to maintain the supply voltage constant at each chosen value during the ionization readings.

Calibration of the resistor ratios.—The high resistances consist of two stacks or columns of approximately 14 megohms each built up of Shallcross Super Akra-ohm units of one megohm each. These units, each of which is noninductively wound in 12 separate coils in a porcelain form are furnished by the manufacturers accurate to 0.1 percent. This means that the deviation of each megohm unit from one megohm will be of the order of 1000 ohms or less. We decided that the simplest way to obtain *equality* of the ratios of the 14 megohm stacks to their 1000 ohm resistors in the case of the two stacks would be to make the 1000 ohm resistors as nearly equal as possible first, then measure each of the megohm units accurately and distribute the twenty-eight units between the two stacks in such a way that their slight measured accidental excesses or defects over or under a megohm would balance out in the two stacks so as to make the two 14 megohm stacks as nearly identical as possible.

Throughout the work two instruments were used, one a Leeds & Northrup No. 4725 open dial Wheatstone bridge, the other a Leeds & Northrup type K potentiometer. The bridge had just been returned from the factory where it had been carefully checked and reconditioned. Its standard resistances were good in international ohms to 0.02 percent while the ratios of its ratio coils were good to 0.01 percent. The potentiometer also had been through a factory check not long before. It had a precision of about one part in forty thousand.

Equalization of the 1000 ohm (nominal) resistances was done with the L & N Wheatstone bridge and checked by means of the potentiometer (comparing the P.D.'s across the two resistors while carrying the same current). Wire was unwound from them until they were equalized to one part in 40,000. Their resistances as measured by the bridge were 999.18 and 999.17 international ohms.

For measurements of the megohm units the bridge shown in Fig. 4 was set up. Two 40,000 ohm (nominal) Shallcross resistors (good to about 0.1 percent) were used. With the L & N bridge these measured 40,048 and 40,060 ohms (international) (ratio, 1.00030). By putting them in series and measuring the P.D. across each one with the L & N potentiometer this ratio was very satisfactorily checked at the value 1.00029. One of the megohm units (not used in forming the stacks) was selected as a standard of reference and called R_1. The other megohm units were successively placed in the arm of the bridge marked R_x. The bridge was balanced by adjusting

the appropriate one of the two decade boxes to the nearest ohm and leaving the other one shorted out. From the reading of this decade box the excess or defect in the resistance of R_x as compared to R_1 could readily be computed. The final result after a judicious allocation of the megohm units so as to equalize the stacks gave the ratio of each stack to R_1 as follows:

Stack No. 1 $\Sigma R_x/R_1 = 14.00881$,
Stack No. 2 $\Sigma R_x/R_1 = 14.00877$.

It was now necessary to measure the ratio of each stack to its 1000 ohm resistor. The most direct method (but not the best) was to measure the arbitrary standard megohm unit R_1 with the L & N Wheatstone bridge. This gave $R_1 = 999{,}115$; 998,800 Av. = 998,960 international ohms. The ratio of R_1 to the resistor having 40,060 ohms was measured by passing current through both in series under a total P.D. of 1.5 volts and measuring the P.D. across each of them with the L & N potentiometer. This gave a check as good as the Wheatstone bridge measurements warranted (3 parts in 10,000). The currents in both methods are so small that a very sensitive galvanometer is required. To surmount this difficulty the device illustrated in Fig. 5 was used consisting of a divided circuit in one branch of which is placed R_1 and the 40,060 ohm resistance while in the other branch are two resistances one of about 50,000 ohms the other of about 2000 ohms. The applied voltage V was first made 1.5 volts and the ratio of the P.D.'s across the 50,000 and 2000 ohm resistances was measured with the potentiometer. Call this ratio N. The applied voltage V was then raised to 30 volts and the ratio of the P.D.'s marked v_1 and v_2 in the diagram was measured with the potentiometer. It is easy to see that the ratio of R to the 40,060 ohm resistance can now be computed by the formula

$$R_1/40{,}060 = (N+1)(v_2/v_1) - 1.$$

Finally, by the same identical method the ratio of the 1000 ohm resistors to the 40,060 ohm resistor was determined. As a sample of the satisfactory agreements obtained we give some of the results of these ratio determinations. Subscripts indicate Wheatstone bridge values of resistances (except for R_1).

$$\frac{R_{40,060}}{R_{999.18}} = 40.0777;$$

$$\frac{R_{40,060}}{R_{999.17}+R_{999.18}} = 20.0393; \quad 20.0396,$$

whence

$$\frac{R_{40,060}}{R_{999.18}} = \frac{R_{40,060}}{R_{999.17}} = 40.0785 \pm 0.0006.$$

Similarly three independent determinations with slightly different values of the intermediate resistance ratio N above mentioned gave

$$\frac{R_{1(\text{megohm})}}{R_{40,060}} = 24.9408,\ 24.9398,\ 24.9393,$$

whence $\dfrac{R_{1(\text{megohm})}}{R_{40,060}} = 24.9396 \pm 0.0006.$

We believe the ratios measured by means of the potentiometer are far more accurate than the ratios to be computed from the resistance values given by the Wheatstone bridge. In all cases the ratios computed by the bridge method checked the ratios as measured by the potentiometer to within the precision to be expected from the bridge (say 0.03 percent) but we believe the potentiometer ratios to be accurate to about one part in forty thousand. Many checks and cross checks which space does not permit us to describe also gave highly satisfactory agreement. From these results we conclude that the ratio of $R_1/R_{999.18}$ was

$$R_1/R_{1000} = 999.5418 \pm 0.039.$$

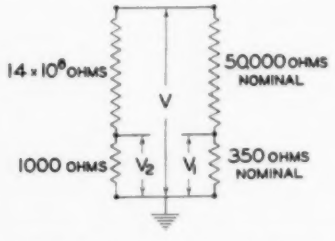

FIG. 6. Method of extending the range of the potentiometer for measuring the ratio of the fourteen megohm stack to the 1000 ohm units in a single step. The constancy of this ratio as a function of temperature was checked in this way.

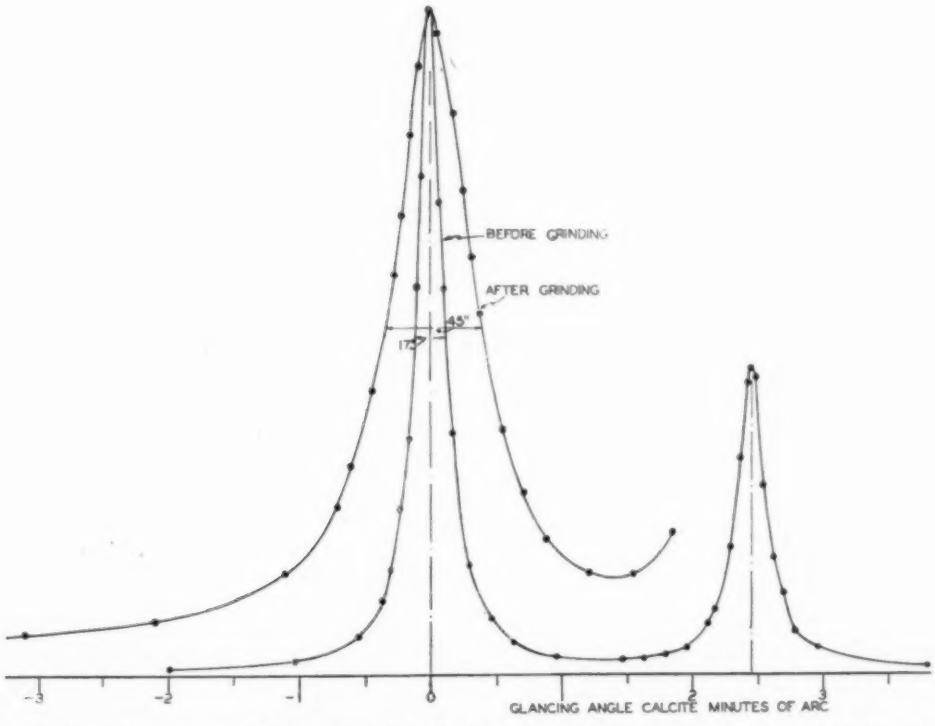

FIG. 7. Profiles of the α doublet of molybdenum K radiation before and after grinding the calcite reflecting surfaces.

Now multiplying this by the ratio of either 14 megohm stack to R_1 and adding unity we get the final ratio of the entire stack plus the thousand ohm resistor to the thousand ohm resistor, that is to say, the ratio by which the potentiometer readings in the hookup of Fig. 3 must be multiplied to give the actual high voltages applied to the resistance stacks. This was

$$14{,}003.38 \pm 0.55.$$

A check of this ratio in a single step measurement was made, good to about one part in 15,000, by extending the range of the potentiometer as before according to Fig. 6. The ratio of the 50,000 ohm resistor to the 350 ohm resistor was first measured with the potentiometer with 1.5 volts for V. Then the ratio of v_2 to v_1 was measured with 180 volts from B batteries applied across V. This afforded a very satisfactory check of the above measured ratio and also permitted us to check this ratio for both stacks as a function of their working temperature.

Resistance ratio as function of temperature. Elimination of thermal e.m.f.—The stacks were constructed by simply screwing the 14 megohm units together terminal to terminal in a chain with the thousand ohm resistors hanging at the bottom. The entire chain was hung in a glass tube large enough to permit ample air circulation. The two stacks were then connected to the high voltage d.c. generating plant of Fig. 3 and allowed to come up to this equilibrium temperature by long continued operation. They were then disconnected from the high voltage and the ratio was repeatedly measured at equal time intervals by the method of Fig. 6. To the precision of this method (1 part in 15,000) no change in ratio could be detected in one stack. The other stack showed a decided change however as the stack cooled off. By reversing the polarity of the B battery supplying the 180 volts it was easy to establish that this apparent change in resistance ratio was in fact due to a thermal e.m.f. at the junction where the lowest megohm coil connects

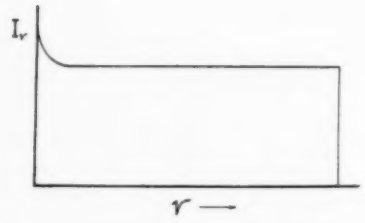

FIG. 8. Continuous spectrum from a thin target.

to the thousand ohm coil and where the potentiometer is connected. Since the voltages measured here are low a small thermal e.m.f. can readily vitiate the measurement considerably. This thermal e.m.f. was completely eliminated by resoldering the joints at this point with advance resistance wire at the tap. The final resistance ratio on both stacks showed no detectable change over the entire range of temperature from full load to no load and was independent of the polarity of the battery.

Study of the spectral window.—The two-crystal spectrometer, Hoffman electrometer and ionization chamber with internal grid for reducing background have been described in a previous paper.[5] The $K\beta_2$ line of molybdenum and the $L\beta_1$ line of tungsten were chosen as the lines for setting the crystals of the spectrometer. With the molybdenum tube in position the entire K spectrum of molybdenum was carefully explored. Fig. 7 shows a profile of the α_1, α_2 doublet. As these are the strongest K emission lines they were used for the study of the profile of the spectral window. After a little preliminary work on the isochromats of the continuous radiation near the short wave-length limit we reluctantly decided that in order to obtain the requisite ionization for precise measurements in a reasonable time it would be necessary to grind the surfaces of our calcite crystals. The limitation imposed by the random fluctuations of the natural ionization (cosmic rays and local radiation) was the chief factor necessitating this. Fig. 7 shows the α line profiles before and after grinding. The much greater breadth of the profile after grinding is the best justification for interpreting that profile as a good approximation to the spectral window curve. The curve before grinding, even, must be considerably broader than the natural emission line profile because it too is a composition of the spectral window curve of the cleaved crystal surfaces with the natural emission line breadth. The vitiation of the profile obtained after grinding by the structure of this same emission line used to explore it can therefore, we feel, be safely regarded as slight especially in the wings of the profile.

Variation of window width with wave-length setting.—These studies of the window profile made it apparent that on a frequency or voltage scale the width as defined by the same spectrometer with the same crystals is different for different wave-length or frequency settings. The reason for this is easily understood. With ground crystals most of the width of the spectral window defined by the bicrystalline selective reflection in the two crystal spectrometer is caused by the geometrical disturbance of the crystal surfaces. This disturbance can be characterized by a parameter $\Delta\theta$ describing say the width at half-maximum of the distribution curve of crystal disorientation. Whatever wave-length setting for which the crystals may be mutually orientated $\Delta\theta$ remains a constant and since $\sin\theta$ is nearly proportional to θ we have practically as a result that $\Delta\lambda$ is nearly a constant for any value of λ. Now, however, we have upon differentiating the equation

$$\lambda\nu = c,$$
$$\Delta\lambda/\lambda = -\Delta\nu/\nu,$$
$$\Delta\nu = -(\nu^2/c)\Delta\lambda,$$

whence multiplying by h

$$\Delta V = -(\Delta\lambda/hc)V^2, \qquad (4)$$

which means that with increasing voltage the

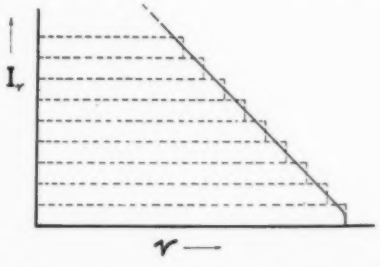

FIG. 9. Continuous spectrum from a thick target conceived as the summation of infinitesmal thin target contributions.

[5] DuMond and Hoyt, Phys. Rev. **36**, 1702 (1930).

width of the spectral window expressed in volts increases approximately as the *square* of the voltage.

We wish to state here that this behavior is a consequence of the use of *ground crystals*. If cleaved crystals or crystals that have been polished and etched according to the specifications worked out at Cornell[6] had been used the width $\Delta\lambda$ of the spectral window would then vary proportional to λ so as to maintain $\Delta\lambda/\lambda$ a constant. In consequence $\Delta\nu/\nu$ and $\Delta V/V$ would be constant for all settings ν, λ, or V. (To prove that $\Delta\lambda/\lambda$ should be a constant for crystals approximating perfection requires an appeal to the Darwin-Ewald-Prins dynamical theory of diffraction by a "perfect" crystal lattice which would occupy unjustified space here since it does not apply to the case in point.) This would be a far more desirable state of affairs for then the threshold voltage uncertainty introduced by the finite resolving power of the crystals would always represent the same percent error at all voltages and one could feasibly extend the present experiment to much higher voltages. The authors project doing exactly this with equipment whose construction has just been completed which permits of the use of a 30 kw x-ray tube. The large power will permit the use of polished and etched or freshly cleaved crystals.

Returning to the state of affairs with the ground crystals used in this experiment it is evident that since ΔV is proportional to V^2 a smaller percentage accuracy in the determination of the threshold voltage will be permitted by the effect of finite resolving power at higher voltages. For this reason the region of 20,000 volts was practically as high as it seemed worth while to go and the region of 10,000 volts promised the best precision attainable with workable intensities.

The x-ray tube.—A nickel target tube was chosen for the excitation of the continuous x-ray spectrum whose short wave-length limit was to be measured. This choice was governed by the fact that this particular tube was provided with an extremely thin glass window blown in the shape of a reentrant hemisphere in a projecting side tube and sufficiently thin to permit the exit of Ni K characteristic radiation in considerable quantities in a previous experiment. The importance of the determinations around 10,000 volts where the limited resolution of the spectrometer introduces so much less uncertainty in the voltage threshold than at higher voltages made this thin window especially desirable. It is of course highly desirable to have a target of the highest atomic number possible because as was shown by H. Kulenkampff[7] the slope of the isochromat plotted on a voltage scale is proportional to the atomic number of the target. In spite of the fact that the tube we used had a target of nickel when it was first assembled we have every reason to believe that the coating of tungsten deposited on the nickel surface by evaporation from the cathode filament was of sufficient thickness to give the continuous spectrum the slope and shape to be expected from tungsten over a voltage range extending back from the short wave-length limit several hundred volts. There are certain advantages to be gained by having a target such as this one which while it cannot be described as thin in the sense of percent retardation of the impinging cathode rays is nevertheless only a few hundred volts thick and is backed up with a supporting material of much lower atomic number. Let us recall the theory of the production of the continuous x-ray spectrum first in a "thin" target, then in a

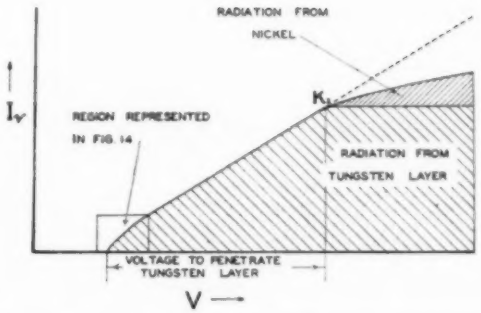

FIG. 10. Illustrating reduction in slope of continuous spectral distribution to be expected for a target consisting of a thin layer of tungsten laid upon a nickel backing. The knee K_3 should occur on the isochromat at voltages exceeding the threshold voltage by the amount required for an electron to penetrate the tungsten layer. The two slopes at K_3 should be about in proportion to the atomic numbers of nickel and tungsten.

[6] K. V. Manning, Rev. Sci. Inst. **5**, 316 (1934).

[7] H. Kulenkampff, Ann. d. Physik **69**, 548 (1922).

"thick" one. For the case of a target so thin that the impinging cathode rays lose a negligible fraction of their initial voltage in penetrating it, both theory[8] and experiment[9] indicate that the frequency spectrum excited by a homogeneous beam of electrons of voltage V will be, save at very low frequencies, a level plateau ending abruptly in a precipice at the short wave-length limit as indicated in Fig. 8. (The slight rise in this plateau at the low frequency end need not concern us here since this radiation would be absorbed before emerging from the window in the tube.) If we think now of the thick target as being divided into many successive thin layers each of these layers will emit a spectrum like that of Fig. 8 but only the first layer will be bombarded with cathode rays of the initial voltage. Successively deeper layers will receive electrons which have been retarded by passage through more and more layers above. Thus the triangular frequency spectrum from a thick target can be thought of as made up of infinitesimal contributions from these thin layers consisting of level plateaus with precipices at successively lower and lower frequencies as shown in Fig. 9. This rough first approximation to the mechanism of the production of the continuous spectrum in a thick target leaves out of account the effect of straggling of the electrons both in direction and speed and the effect of reemergence of some of the electrons from the target, but it seems clear that if a layer of tungsten sufficient to retard the impinging cathode rays by several hundred volts were present on top of the nickel target face then the continuous spectral distribution of x-ray intensity in the region from the quantum limit back a corresponding distance of several hundred volts would be characteristic of tungsten while the remainder of the spectrum would be characteristic of nickel bombarded by electrons retarded by the tungsten as indicated in Fig. 10.

The reduction in the intensity of the continuous spectrum in its longer wave-length regions starting at wave-lengths a few hundred "equivalent" volts back from the quantum limit caused by the low atomic number of the nickel support seems to us to be a highly desirable effect for the following reason. The spectral "window" defined by the diffraction patterns of the crystals in the two crystal spectrometer has as we have already stated no sharp boundaries. The effect of the slight transparency of the tail of this window on its long wave-length side at remote distances from the "center" of the window is exaggerated if the continuous spectral intensity available to penetrate the tail of the window increases rapidly with increasing wave-length. Regions of the spectral window curve remote from its "center" by amounts equivalent to several hundred volts cannot be studied at all with present technique. It therefore seems most desirable to prevent the rapid increase of continuous spectral intensity with increasing wave-length after a point a few hundred volts beyond the quantum limit so as to minimize this effect for which we are not in a position to calculate a correction.

It may seem at first that the transparency of the spectral window several hundred volts away from its center could safely be neglected but this is not so certain. If, for instance, the transparency of the window decreased at large distances from its center according to the inverse square of the spectral distance (as both theory and experiment on the less remote parts of the "wings" indicate) while the spectral intensity *increased* linearly with this distance on the long wave-length side there would be no point beyond which one could safely neglect the transparency of the tail of the window because the total transmitted intensity would increase logarithmically with the position of this arbitrary point all the way down to zero wave-length. One would certainly hesitate to make a correction for the window transparency curve based on either theory or experiment over any such huge spectral range.

Estimates of the thickness of the tungsten coat on the target.—We believe the coat of deposited tungsten on our nickel target was more than "three hundred volts thick" for 20 kv cathode rays so that in Fig. 14 the knees K_1 and K_2 in the isochromat over the range observed by us cannot be attributed to the composite nature of the target. The four following lines of argument

[8] A. Sommerfeld, Ann. d. Physik **11**, 257 (1931).
[9] W. W. Nicholas, National Bur. Stands. J. Research **2**, 837 (1929).

support this belief and serve to place rough limits on the thickness of the tungsten film.

I. The nickel target showed strong emission of the tungsten L spectrum characteristic lines. In fact with about 20,000 volts applied to the tube these lines gave ionization in the chamber of the same or slightly greater intensity than those from a thick tungsten target tube which we had used for the wave-length setting. The nickel target tube, however, had the considerable advantage over the tungsten target tube of possessing a thin window which would make a very considerable difference for tungsten L radiation. We cannot, therefore, conclude that the tungsten layer was 20,000 volts thick especially when we recall what a large fraction of the *characteristic* line radiation from a target is indirectly excited by fluorescence. This evidence, however, does make it highly improbable that the tungsten layer was only a few atoms thick as it would necessarily be if the first knee K_2 in our isochromat were caused by it. We shall discuss this knee at greater length in its proper place.

II. The tube was originally built for the study of powder diffraction with Ni K radiation. Many long exposures had been made in this previous work with the tube totaling considerably more than 500 hours before it was used in the present experiment. With increase in the hours of life there seemed to be a noticeable decrease in the intensity of the nickel lines (though this might have been only a decrease in contrast) and a marked increase in the background of the powder diffraction patterns. This was what first led us to suspect the building up of a tungsten deposit on the target. The thickness of tungsten which will absorb half the intensity of the Ni $K\alpha_1$ line is 1.7×10^{-4} cm.

III. An x-ray tube filament run at ordinary emission temperatures usually has a life around 1000 hours and may lose by evaporation roughly 10 percent of its weight. From the weight of an entirely similar filament and the solid angle subtended by the target we compute that if all of the vaporized tungsten which hit the target during its operating life remained there it would have built up a layer 224A thick. Williams'[10] formula for β-ray retardation gives for such a layer

$$d(\text{kv})/dx = 1060\rho\beta^{-1.4} \text{ or } 455 \text{ volts retardation,}$$

while the Thompson-Whiddington[11] formula which is probably better in this voltage range gives

$$V_0^2 - V_x^2 = 7.6\times10^{12}X \text{ or } 836 \text{ volts retardation.}$$

Estimating the first knee K_2 on our isochromat at 18 volts beyond the quantum limit the film of tungsten which would retard the cathode rays by this amount would be only about 9A thick. We therefore feel sure this knee is not ascribable to the composite nature of the target but is characteristic of the tungsten itself. In fact this knee, more or less pronounced, appears in previous work[12] with thick tungsten targets although it has heretofore been overlooked or interpreted as accidental, principally, we believe, because the limited resolving power of the spectrometer has more or less masked its presence.

IV. An effort was made to detect the effect of the L_{III} absorption discontinuity of tungsten in the continuous spectrum from the target. The height of the resulting discontinuity in the otherwise continuous spectrum if it could be measured would furnish information sufficient to compute the effective thickness of tungsten film traversed by the continuous radiation. This thickness would be given by the formula

$$x = (\log I_h/I_s)/(\mu_s - \mu_h). \tag{5}$$

Here I_h and I_s are, respectively, the continuous spectrum intensities on the hard and soft sides of the discontinuity and μ_s and μ_h are the linear absorption coefficients on the soft and hard sides of the absorption edge. Or for such small absorption to good approximation

$$x = r/(\mu_s - \mu_h) \tag{6}$$

where r is the relative change in intensity $(I_h - I_s)/I_s$. Unfortunately there is an L emission line β_{10} of tungsten only two X.U. longer in wave-

[10] E. J. Williams, Proc. Roy. Soc. London **A130**, 310 (1932).

[11] R. Whiddington, Proc. Roy. Soc. London **A86**, 360 (1912).

[12] Kirkpatrick and Ross, Phys. Rev. **45**, 457 (1934).

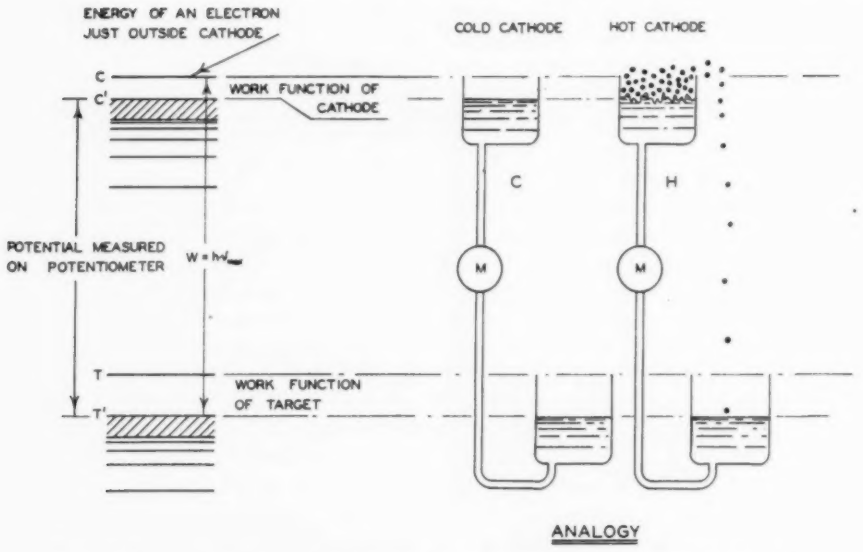

FIG. 11. Energy level diagram for electrons in an x-ray tube to illustrate the situation calling for a correction for the cathode work function. Hydraulic analog.

length than the position of the L_{III} absorption edge. This makes it necessary to extrapolate the continuous background from some considerable distance in order to ascertain whether a discontinuity is present and the discontinuity we were looking for was too small to measure with certainty for this reason although we believe it to have been just barely detected. A control in the form of a tungsten filter made of blotting paper impregnated with 2.21 mg/cm² of tungsten in the form of $Na_2WO_4+2(H_2O)$ could easily be not only detected but roughly measured. We concluded from this that the effective thickness of the tungsten on our target was probably less than 0.95 mg/cm² or 5.4×10^{-5} cm.

We believe the use of a coating of heavy atomic number on top of a support of much lower atomic number to be a real improvement in the technique of this experiment for reasons already discussed, to which we shall return.

This tube was maintained at a very hard vacuum by a glass charcoal trap connected to it through a one inch glass tube. The charcoal and the entire tube had been thoroughly outgassed by long continued pumping in a bake oven and was then sealed off. The charcoal was kept cool in liquid air.

III. INTERPRETATION OF DATA

Corrections to the measured voltage

Only two small corrections to the measured voltage are necessary: The correction for the P.D. of the filament and the correction for the work function of the filament.

Referring to the diagram of Fig. 3 it is evident that the correction for the 6 volt filament P.D. requires that half of this operating P.D. across the filament, that is to say, three volts must be *added* to the voltage measured with the potentiometer. The electrons starting from the filament will be nearly uniformly distributed over a range of energies 6 volts wide and the corrected voltage will then refer to the middle of this range.

The correction for the work function of the filament merits some discussion as it seems to be regarded in certain quarters as of doubtful applicability. In Fig. 11, an energy level diagram of the energies assumed by electrons at different points in the x-ray tube, c represents the energy level of an electron just outside the cathode, T the energy level of an electron just outside the target while C' and T' are the energy levels of the electrons of (algebraically) highest energy

inside the cathode and target, respectively. These are the electrons of highest energy in the continuous Fermi degenerate gas distribution. The difference in level between C' and T' is the quantity measured in volts by the potentiometer in connection with the high resistances. The difference in level between C and T' is the maximum energy available for thermally emitted electrons in the production of x-rays and should therefore be the energy to be equated to $h\nu_{max}$ or $(hc)/\lambda_{min}$. These electrons can fall no lower than T' because there are no empty energy levels in the target below this. (The relative population of ionized levels in the target can easily be shown on energy considerations to be many orders of magnitude too small to furnish any observable x-ray intensity.) Not 1 percent of the electrons emitted at 2300°K can have an initial level higher than C by more than 0.9 volt as is well known from studies of thermionics. Thus it is evident that to the measured voltage must be added the difference in energy level between C and C'. This is the work function of the tungsten cathode or 4.52 volts. It is a fortunate fact that it is the cathode work function which must be considered in this correction because the hot cathode is thoroughly outgassed at its working temperature and its work function is very unlikely to be changed by surface impurity. The authors can see no reason for considering this a "doubtful" correction.[13] The situation is simply that the electrons capable of transforming the greatest amount of energy into x-rays derive that energy from two sources; first, from the high tension d.c. generating equipment, second, from the electrically maintained thermal energy of the cathode. This work done on the electrons by the heat supplied to the cathode is well known and has been repeatedly measured directly[14] by observing the enhanced cooling effect on the cathode when voltage is applied to a two element vacuum tube sufficient to give the thermionic emission current its saturation value as compared to the ordinary cathode cooling without electronic emission. In fact it furnishes one of the reliable methods of determining the thermionic work function.

[13] But see Schaitberger's unsupported statement to the contrary. Schaitberger, Ann. d. Physik **24**, 84 (1935).

[14] Davisson and Germer, Phys. Rev. **20**, 300 (1922); **24**, 666 (1924).

To drive the argument home we have also shown in Fig. 11 an hydraulic analog of the situation requiring the correction for cathode work function. At C is the analog of the situation for a cold cathode while at H appears the analog for the hot cathode. Let us consider the cold cathode case first. Two vessels of water, one high above the other, are connected by a very fine narrow capillary tube in "series" with which is a water meter M calibrated so that its rate of flow reads directly the difference of "head" or level which is causing water to flow against viscous resistance in the capillary. This is the analog to the two 14 megohm stacks and the potentiometer connected across the two thousand ohm shunt. This device evidently measures the difference in level between the *free surfaces* of the water in the two vessels. As shown, each of these free surfaces is at a certain distance below the top of the vessel containing the water. Now let us examine the hot cathode case. We suppose that some device supplies energy to agitate the water in the upper vessel so that a very little bit of it occasionally escapes over the edge in droplets. These droplets will fall in the lower vessel and will dissipate there an energy equal to the difference in head measured by the meter, M, *plus* the work done on a droplet by the agitating mechanism to lift the droplet over the edge of the vessel. The meter M will still obviously measure only the *average* difference in head which will be essentially unchanged by the agitation.

The two corrections which we have just outlined thus require that about 7.5 volts in all be added to the voltage measured by the potentiometer.

Smearing effects and the fillet

The authors have decided to adopt on trial the homely verb "to smear" to meet a situation arising frequently in physics. To smear shall mean to render less sharply defined or determined. A smearing effect may be caused by the unsharpness of the exploring tool and may or may not be irreparable. Thus if a spectrum is examined with a finite slit of known character or with a spectrometer whose spectral "window" has a determinable shape it may be possible to "desmear" the observed spectrum to some extent

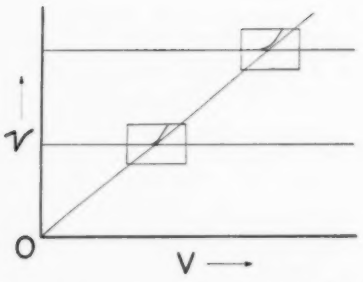

FIG. 12. Plot to rectangular coordinates of the threshold voltage (abscissae) against maximum emitted x-ray frequency (ordinates). At each "point" is shown a small view of the threshold region of the isochromat in its proper position on the voltage scale.

by the mathematical methods of integral equations and functionals. In this sense to "desmear" means to render more well defined or more homogeneous but not necessarily to completely purify observational data of every last vestige of inhomogeneity or indetermination.

A precise definition of the verb "to smear" is in order. We intend the verb to indicate an operation which in its simplest essential application may be thought of as acting on a single number or physical magnitude so as to transform it into a weighted complex of numbers. The weighted complex may be a continuous distribution or a discontinuous one. It may consist of an infinite set or a finite set of numbers. In what follows and more often than otherwise the single number is transformed into a continuous set of numbers grouped with symmetrical weighting around (above or below) the original number. The original number is then said to be smeared symmetrically. In order to definitely describe an operation of smearing it is obviously necessary to specify either by an analytic function or a plotted curve or a table of values or in some other way the characteristic distribution of weights to be attached to the set of numbers into which the original number is to be transformed. It is quite evident that this definition of smearing can be extended from that of an operation which acts on a single number to an operation which acts on a set of numbers, each number of the set suffering the same fate as all others and independently of them. It is a simple step from this to the concept of the smear of a smear. A word already common in mathematics closely related to smearing is "composition." One speaks of the composition of two curves or functions by integration. We find, however, that this word in many cases is much easier to misunderstand.

The smearing effects in the present experiment are three, namely: 1. The finite resolving power of the spectrometer which is by far the most important. 2. The filament P.D. which is relatively unimportant. 3. The high voltage ripple which is completely negligible.

The actions of smearing effects may be regarded as operators and they frequently follow the commutative and distributive laws of ordinary algebra. Thus, as far as the result is concerned, it is entirely indifferent in what order or with what types of aggregation the three above mentioned effects are thought of as operating to produce the observed isochromat from what may be thought of as the "ideal" isochromat which would be observed if the three above effects could be rendered negligible.

The threshold voltage at which radiation just begins to appear of wave-lengths corresponding to the "center" of the spectral window of the spectrometer is smeared by the three effects just mentioned so as to give a "fillet" in place of a sharp inset point. It is the correct location of this inset point in spite of the masking fillet which constitutes one of the important problems in the present experiment.

Method of plotting the isochromats

The two threshold voltages which we have determined and their corresponding x-ray frequencies or wave numbers can be conceived as points lying on a curve expressing the functional relation between voltage and maximum emitted frequency in the x-ray tube, a curve which we expect to find a straight line passing through the origin when all the requisite voltage corrections have been made. The equation of this curve we expect to be $eV=h\nu$. We shall plot this curve with corrected voltage as the horizontal coordinate and with frequency as the vertical coordinate. For the purpose of computing e/h the absolute value of this frequency is important and may be determined either from the ruled grating wave-lengths of x-rays or from the internal data of this experiment itself taken in conjunction with computations based on the density and

structure of crystals and the Faraday constant (in which case this experiment really determines $e/h^{3/4}$); but for our present purpose of representing the results it is merely important that the vertical coordinate shall be *proportional* to x-ray frequency or wave number. For the sake of definiteness we have plotted the vertical coordinate on a scale which represents the frequency (sec.$^{-1}$) computed from the ruled grating wavelengths of x-rays but we do not, of course, by so doing commit ourselves to the assumption that these are correct but only that they are proportional to the correct values. At the end of the paper we discuss the consequences of all possible assumptions and methods of computing both (e/h) based on the ruled grating x-ray wavelengths and $(e/h^{3/4})$ not so based.

Fig. 12 shows the normal way in which one might plot the above mentioned curve on rectangular coordinates. Since it is not really *a point* that we observe when we find the threshold voltage but rather a curve (the isochromat) in which the threshold point is somewhat masked by the fillet there is a real advantage in representing this curve with its fillet right in place on the voltage scale. Now to do this graphically in rectangular coordinates to a visible scale without sacrificing any of the precision of the voltage observations would require an impossibly large plot. We have therefore adopted the scheme of plotting in oblique coordinates. If one imagines the coordinate system of Fig. 12 subjected to a *uniform shear* so that the ν axis rotates about the origin O in a counterclockwise sense a new plot will be obtained like Fig. 13 in which the two isochromats in the neighborhood of the threshold points will be the one nearly vertically above the other while the zero points of their two voltage scales will be at very remote positions to the left far off the edge of the plot on an oblique straight line (the oblique ν axis) passing through the original O. This shearing of the plot can of course be endowed with *unlimited precision*. It is only necessary to plot the two voltage scales at vertical heights above the origin strictly proportional to the two x-ray frequencies at which the isochromats were observed and to locate these voltage scales horizontally in such a way that the voltages V_1' and V_2' which are situated exactly vertically over the origin strictly satisfy the

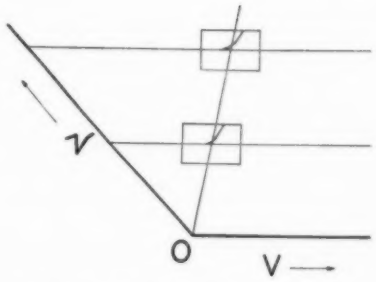

FIG. 13. Plot to oblique coordinates obtained by subjecting Fig. 12 to a uniform shear so as to bring the small views of the two isochromats into the same horizontal vicinity without sacrifice of scale.

relation $V_2'/V_1'=\nu_2/\nu_1$ with all the precision consistent with our knowledge of these quantities from the physical measurements that determine them. In this shearing distortion all lines that were originally straight remain straight and the graph of the equation $eV=h\nu$ is of course no exception. In the plot of our results, Fig. 14, we have shown a fan-shaped array of lines radiating from the origin whose inclinations correspond to those of graphs $eV=h\nu$ for various values of h/e on the assumption that the ruled grating values of x-ray wave-lengths are correct. The line for $h/e=0$ is obviously the skewed y axis and its very slight inclination to the horizontal indicates how very far to the left of the plot the zero points of the two voltage scales are.

Location of the threshold points

In the plot of Fig. 14 we have also shown *to correct voltage scale* a curve which we call the "g" curve and which is very nearly the spectral window curve of the spectrometer for the case of each isochromat. The vertical scale of these g curves is of course entirely arbitrary. Their horizontal position is also arbitrary. They are simply placed as shown for visual comparison with the fillet for which each is presumably responsible. The g curve is in fact a composite of the smearing effects of the spectral window curve and the 6 volt filament P.D. This latter influence changes the shape of the lower g curve in Fig. 14 slightly but makes no significant difference in the upper g curve. The 0.6 volt ripple has been therefore completely neglected. The composition of these two smearing effects is accomplished in the following way. Let $w(x)$

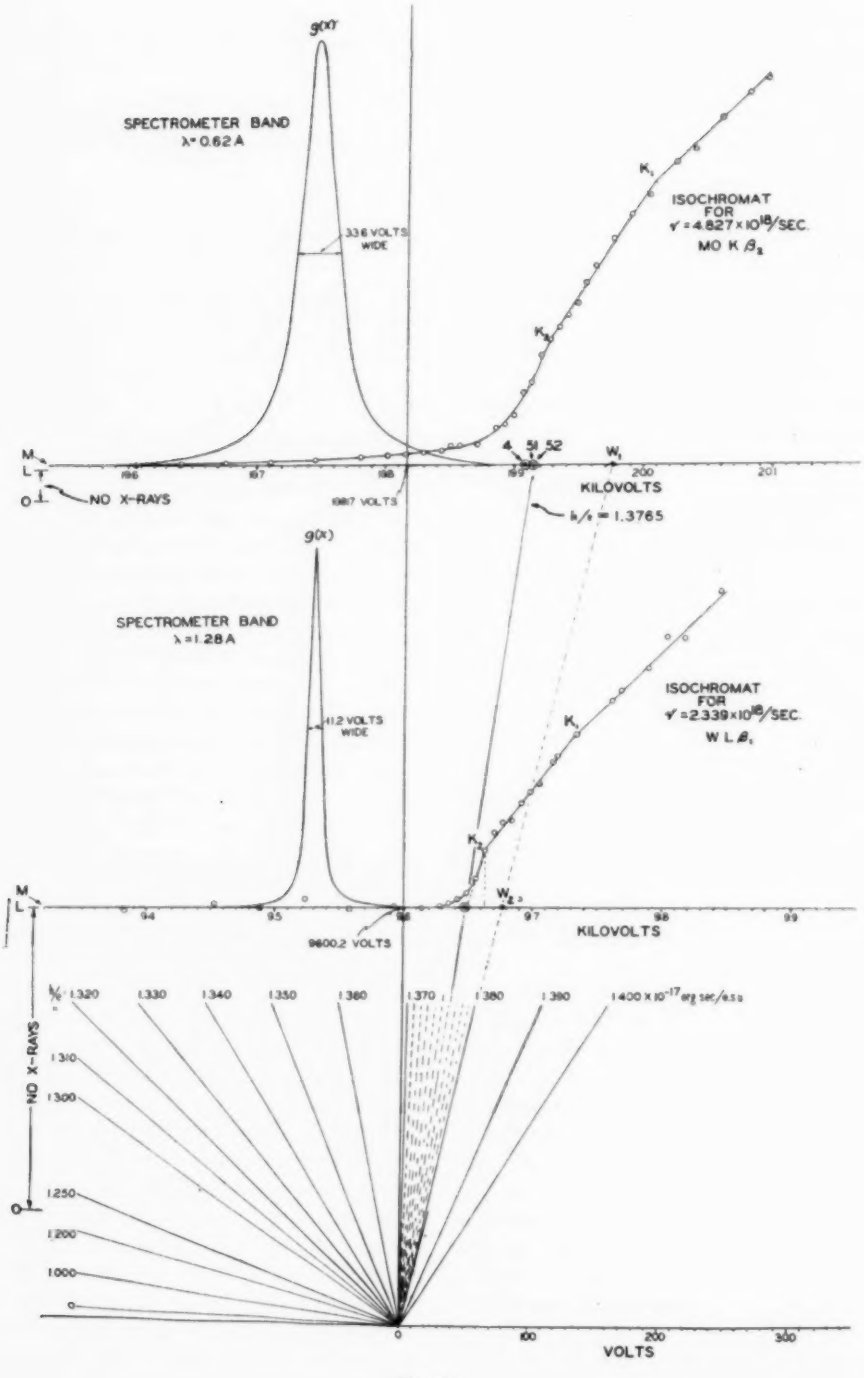
g(x)
SPECTROMETER BAND
λ=0.62 A
336 VOLTS WIDE
ISOCHROMAT FOR
ν = 4.827 × 10^18/SEC.
MO K β2
K1
K2
M
L
O
NO X-RAYS
196
197
198
199
200
201
KILOVOLTS
1987 VOLTS
λ/ν = 1.3765
SPECTROMETER BAND
λ=1.28A
41.2 VOLTS WIDE
ISOCHROMAT FOR
ν = 2.339 × 10^18/SEC.
W Lβ1
94
95
96
97
98
99
9600.2 VOLTS
1.320
1.330
1.340
1.350
1.360
1.370
1.380
1.390
1.400 × 10^-17 erg sec/cm²
1.310
1.300
1.250
1.200
1.000
0
100
200
300
VOLTS

FIG. 14.

FIG. 14. Our experimental results are here plotted as explained in Fig. 13. W_1 and W_2 are the points where the respective thresholds would have to be to make this experiment harmonize with points I and II of the Bond diagram. The finite resolution of the spectrometer, together with a slight contribution from filament P.D. are responsible for the "g" or "smearing" curves shown, which in turn satisfactorily explain the observed fillets on the isochromats. The widths of the g curves are to correct voltage scale but their positions on the voltage scale have no significance. At the left of this plot the level O corresponds to zero rate of drift of the electrometer which measures the ionization. The level L is proportional to the rate of drift with x-rays off while M is the rate of drift with x-rays on at voltages well below the threshold. L and M are indistinguishable on the lower voltage isochromat. The difference LM is principally diffuse scattering by the crystals of the spectrometer. The frequency for the upper isochromat should read 4.828×10^{18}/sec.

represent the spectral window curve expressed as a function of "equivalent voltage." Now we may assume with but little error that the filament emits over its six volt range as many electrons in one elementary voltage interval as in any other. Hence to get the curve g we smear the curve w by averaging it with uniformly distributed weight over a six volt range. The precise expression for this is

$$g(x) = \int_{-3}^{+3} w(x-z)du. \tag{7}$$

These g curves may be thought of in their turn as smearing the ideal isochromat f by a similar mechanism to give the observed isochromat $F(z)$; only in this case the range of smear has no sharp limits and the weighting over this range is not uniform but is distributed according to the ordinates of the g curve. The precise expression for this is

$$F(z) = \int_{-\infty}^{+\infty} g(x)f(x-z)dx. \tag{8}$$

Eq. (8) is a little more general than necessary to express the situation in the present experiment and there are distinct advantages in an expression which takes into account the fact that the ideal isochromat (or what is the same thing with reversed sign of the independent variable, the continuous spectral distribution near the quantum limit) has a finite positive value everywhere on one side of the threshold point and vanishes completely everywhere on the other side.

In Fig. 15 let the independent variable x be thought of as proportional to x-ray frequency. $g(x)$ is the window curve of the spectrometer (corrected for the slight smearing effect of filament P.D.). $f(z-x)$ is the curve expressing the true distribution of the continuous x-ray spectrum as a function of frequency and voltage in the neighborhood of the limit. z is that value of x where the curve $f(z-x)$ meets the x axis and for all points to the right of which f vanishes. z is directly proportional to the voltage applied to the x-ray tube. The fact that f is here postulated as a function of $(z-x)$ and not simply as $f(z, x)$ gives explicit expression to the assumption that for small changes in the applied voltage the *shape* of the continuous x-ray spectrum in the vicinity of the quantum limit does not change appreciably. We are to think of the $f(z-x)$ as a rigid foothill which simply slides uniformly to the right with increasing z. Now on the lower curve in Fig. 15 we plot the "isochromat" which is proportional at each point to the observed ionization produced by that portion of the spectrum f which can pass through the window g. This is

$$F(z) = \int_{0}^{z} g(x)f(z-x)dx. \tag{9}$$

To get each ordinate of F such as the one shown we integrate over x the product of the two overlapping curves f and g up to $x=z$ and plot the resulting value at the point z on the lower curve. Our problem is to find from the lower curve $F(z)$, which is all we have given us, at what precise value P of z the threshold point of the curve f was in contact with some known essential feature of the curve g such for example as the abscissa value at its peak or its center of gravity. The particular feature of the g curve chosen to define the wave-length whose threshold voltage is sought is important. The authors believe that the peak abscissa or, what amounts to very nearly the same thing, an abscissa midway between two nearby values having equal ordinates on either side of the peak is preferable to the center of gravity because the wave-length of the former can be determined with less uncertainty than the wave-length of the center of gravity.

The only method of locating the threshold point used up to the present may be described as

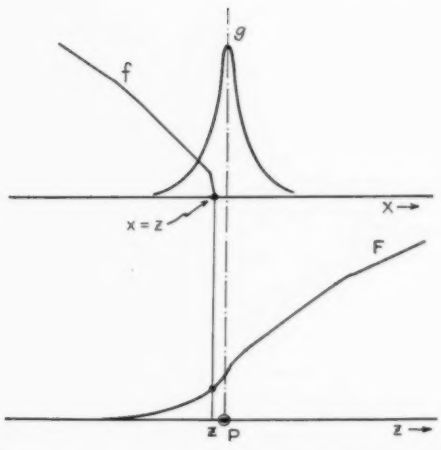

FIG. 15. Illustrating how the isochromat is a composition of the continuous spectrum as it slides across the spectral window curve of the spectrometer. For any position z of the foot of the continuous spectrum on the frequency scale, x, the ordinate of the isochromat is the product integral of f and g from $x=0$ up to $x=z$.

the method of the projected tangent. The method consists in drawing a tangent to the isochromat at a point sufficiently remote from the fillet in the region of the quantum limit so that one feels that the isochromat has become and will remain for some distance sensibly a straight line. This tangent is then projected until it intersects the axis of abscissa (after subtracting off the residual ionization from cosmic rays and local radiation, etc., of course) and this point of intersection is taken as the threshold without explicit proof or analysis of what particular feature of the spectral window or g curve it refers to. We shall now proceed to prove that this method of the projected tangent gives the threshold point corresponding to the *center of gravity* of the g curve *provided* one can assume that for a sufficient distance back starting from the quantum limit the continuous x-ray spectral distribution is simply a sloping straight line. On this assumption Eq. (9) becomes

$$F(z)=\int_0^z S\cdot(z-x)\cdot g(x)dx, \qquad (10)$$

where S is simply a constant of proportionality, the slope of the curve f. Differentiating the integral with respect to z according to Leibniz' rule we have

$$F'(z)=\frac{d}{dz}F(z)=\int_0^z S\cdot g(x)dx+S\cdot(z-z)\cdot g(z), \qquad (11)$$

the last term of which vanishes. Now, referring to Fig. 16, at some point $z=b$ sufficiently far to the right, the short wave-length limit of the continuous spectrum may, as we here suppose, be considered to have crossed over the whole of the significant region of the spectral window curve g and on our assumption of linearity for the continuous spectrum the isochromat $F(z)$ will remain a linearly increasing function indefinitely thereafter. To find the expression for the point P given by the intersection of the projected tangent at b we have only to evaluate the quantity $b-F(b)/F'(b)$

$$F(b)=\int_0^b S\cdot(b-x)g(x)dx; \quad F'(b)=\int_0^b S\cdot g(x)dx;$$

$$b-F(b)/F'(b)$$

$$=b-\frac{S\cdot b\int_0^b g(x)dx}{S\int_0^b g(x)dx}+\frac{S\int_0^b x\cdot g(x)dx}{S\int_0^b g(x)dx}. \qquad (12)$$

The first two terms in the right-hand member cancel leaving as the expression for the value of z at P the last term which we see is simply the formula for the center of gravity of the g curve.

It is appropriate here to point out that even if the linear assumption with regard to the f curve were applicable this method of the projected tangent contains a dangerous pitfall closely associated with the nature of the wings of the g curve. If these wings decrease in intensity no more rapidly than an inverse square law of distance from the center there will be no point b sufficiently far to the right to give a definite fixed position P. This is easily seen if we suppose the window curve given by the "witch" expression (with center at p)

$$g=[1+(x-p)^2/a^2]^{-1}. \qquad (13)$$

Then the expression for the center of gravity will be

$$\frac{\int_0^b \frac{x\,dx}{1+(x-p)^2/a^2}}{\int_0^b \frac{dx}{1+(x-p)^2/a^2}} = \frac{\frac{1}{2}a^2 \log\{[a^2+(b-p)^2]/[a^2+p^2]\}+\pi a p}{\pi a}. \quad (14)$$

With increase of b this expression obviously increases without limit. Physically this means that the curve $F(z)$, Fig. 16 in spite of the assumed linear nature of f never becomes and remains sufficiently straight to fix a point b where one can safely draw a tangent but is always concave upward so that though this concavity decreases toward the right tangents drawn at points b farther and farther to the right continue always to intersect the axis at points P farther and farther to the right. Briefly the center of gravity of the "witch" type of curve (13) is indefinite in the sense that even if the limits of integration are infinitely remote the position of the center of gravity still depends on those limits.

The preceding method and its proof as we have stated is only applicable if there is a point b on the isochromat beyond which the effect of the wings of the g curve can be neglected and if from the quantum limit up to well beyond this point the distribution of the continuous x-ray spectrum can be assumed to be a sloping straight line. That this last is unfortunately not the case can be seen at a glance from our two observed isochromats in Fig. 14 which show beside the rather well-known upper knee K_1 a new knee K_2, never before reported, much closer to the quantum limit. There is evidence for this second knee K_2 in the work of Kirkpatrick and Ross[12] (see their Fig. 2) but it was apparently treated by them as an accident of observation. We might easily have done the same thing had it not been for the evidence from the lower isochromat in the 10,000 volt region where the voltage resolution of the spectrometer is four times as good as at 20,000 volts. This is the first time to our knowledge that this experiment has ever been done at this voltage with the resolution available in the two crystal spectrometer.

The presence of the knee K_2 as well as the possible pitfall from the effect of the too slowly

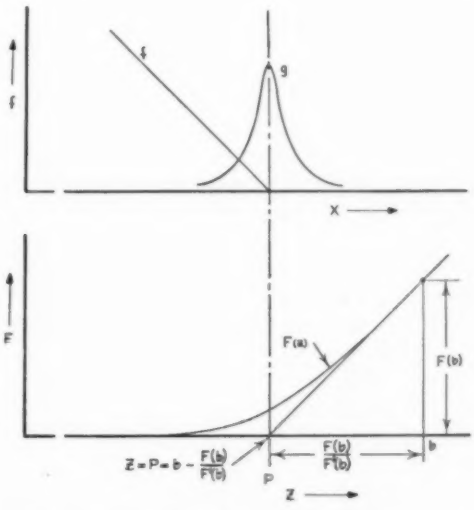

FIG. 16. Illustrating the projected tangent method of locating the threshold point on the assumption that the f curve is linear.

decreasing wings of the g curve makes it imperative to find a better method of locating the threshold point than the method of the projected tangent.

Returning to Fig. 15 and expression (9) we see that it would be sufficient for our purposes to find the solution of the integral Eq. (9) where g and F are given and f is to be found. This is called by Whittaker the generalized equation of Abel's type. Ordinary methods recommended in the texts for reducing this to an equation of the "second kind" unfortunately break down with the type of g curve we have to deal with. It would be interesting of course to devise a general method for finding f over a large range of the independent variable and out of the five methods we have tried the first three listed below aimed at this. For our present purpose, however, it is not necessary to do this and the last two methods listed aimed only at *locating the position* of the threshold point which is all we need. A list of the five principal methods we have tried follows:

1. Solution of integral equation by solving a large number of simultaneous linear equations whose unknowns are successive ordinates of the f curve. This was abandoned after many attempts at approximate solutions. Solution depends too

much on the too uncertain properties of the remote wings of the g curve.

2. Solution of integral equation by assuming analytical expressions for $g(x)$ and for $f(z-x)$, in the case of the latter with adjustable parameters which are adjusted to make a least squares fit to the given F curve. This may be regarded as merely a device for reducing the number of equations of method 1. It is the standard method usually recommended for the practical solution of an integral equation whose functions are defined by physical observations. It suffers from the same weakness as the first method.

3. Solution of integral equation by a symbolic operator method of our own invention using the operator E of the difference calculus. We were able by this method to find a solving kernel in the form of a symbolic operator for certain simple types of g curve but were unable to generalize it to a g curve of the type given in this experiment.

4. To locate the threshold point on the higher voltage isochromat of Fig. 14 the lower voltage isochromat is assumed to be, relative thereto, a good approximation to the ideal isochromat (because it is four times as well resolved on a voltage scale). The fillet on this lower isochromat is removed for simplicity by the simple expedient of cutting it off along the projected tangent to the fillet at the lower side of the lower knee K_2 as shown by the oblique dotted line. The resulting curve is then smeared or composed with the g curve belonging to the upper isochromat and the resulting smeared curve now has a fillet beneath which there is a determined threshold point. This curve after multiplication by an appropriate normalizing factor and plotting on transparent paper can be superposed upon the upper isochromat and fitted thereto and this at once locates the position of the threshold point. Fig. 17 shows how convincing this fit is. The point marked 4 in Fig. 14 was located in this way. Minor objections may, of course, be raised to cutting off the lower fillet with a projected tangent from K_2. It is difficult, however, to see how the ideal isochromat sought can help but fall somewhere between the two dotted lines from K_2 one of which is vertical, the other tangent to the fillet. There is nothing of an irregular nature in the *wings* of the g curve which could account for the knee K_2 and we feel confident that this knee must correspond to that voltage at which a similar break in the continuous x-ray spectral distribution close to its limit just passes over the peak of the g curve. Even if the continuous x-ray spectrum had a vertical precipice up to this first knee the threshold point could not be located at higher voltages than K_2. Furthermore if the oblique dotted cut-off line is assumed correct and smeared or composed with the *lower* g curve a fillet is obtained which fits the lower isochromat very satisfactorily.

In Fig. 17 whether the curve PK_2K_1R or the curve QK_2K_1R is smeared with g makes a wholly indistinguishable difference in the resultant curve SL and we therefore locate the threshold 4 midway between P and Q and regard the range PQ as defining approximately the uncertainty of method 4.

This method just outlined is obviously based on the assumption that in passing from the 10,000 volt region of the lower curve to the 20,000 volt region of the upper curve the shape of the continuous x-ray spectrum in the immediate vicinity of the quantum limit does not change. This assumption is purely a guess and one which we feel is not too well supported by the facts since the knees of the artificially constructed isochromat SL do not fit the knees of the observed isochromat perfectly. We were therefore very happy to discover method 5 which we consider by far the best and most convincing.

5. This method of locating the threshold point consists simply in examining the first or second derivative curves obtained by plotting the *slope* of the isochromat (or the slope of its slope curve) as a function of voltage. These derivative curves contain pronounced peaks whose interpretation is quite clear on the basis of very simple and acceptable qualitative hypotheses about the general nature of the shape of the continuous x-ray distribution. These peaks serve to locate with a high degree of certainty and inner consistency the position of the threshold point. The most welcome and superior feature of this method is that the location of the threshold is the one corresponding to the *peak* of the g curve rather than to some dangerous conditionally convergent quantity like a center of gravity. Furthermore it is the one method which depends not at all on the shape of the wings of the g curve nor indeed to

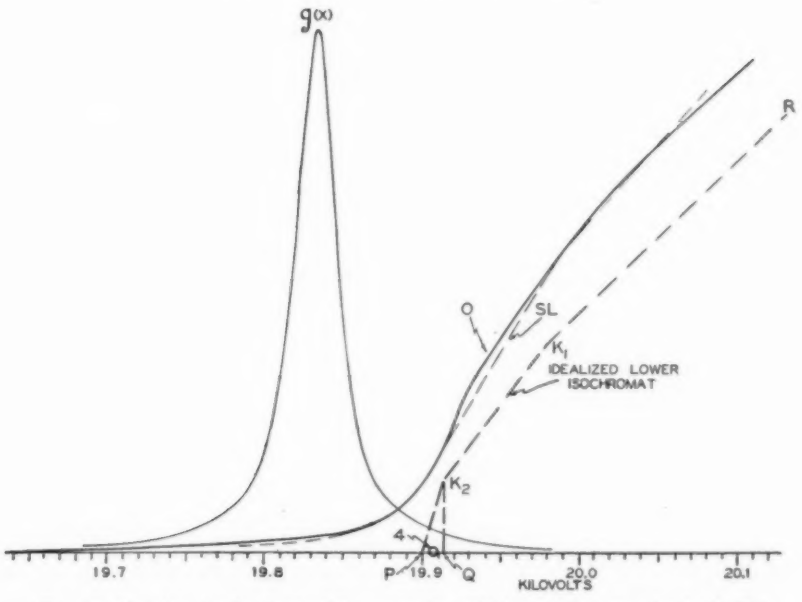

FIG. 17. Showing the fit obtained in our method IV for locating the threshold. The observed isochromat is marked *O* while the curve marked *SL* was obtained by "smearing" the lower voltage isochromat with the *g* curve of higher voltage as explained in text.

any important extent on any property of the *g* curve other than its feature of having a sharp peak. We have therefore great confidence in its reliability.

Fig. 18 illustrates the situation upon which method 5 depends. We have the choice of using either the first or second derivative methods. If the first derivative is used we assume as a sufficient approximation to the shape *f* of the continuous x-ray spectrum the curve having an abrupt vertical precipice at the quantum limit and a more or less pronounced break K_1 somewhat more remote from the limit. As stated in Eq. (9) we have

$$F(z)=\int_0^z f(z-x)g(x)dx. \tag{15}$$

Differentiating this integral according to Leibniz' rule

$$\frac{dF(z)}{dz}=F'(z)=\int_0^z\left[\frac{\partial}{\partial z}f(z-x)\right]g(x)dx+f(0)g(z). \tag{16}$$

Now $f(0)$ is simply the height of the curve *f* at the vertical precipice. There need be no fear of trouble from this discontinuity since the *function f* in an analytic sense can be thought of as having the continuous dotted prolongation. The *effect* of a discontinuity is reproduced by the presence of *z* as the upper limit of the integral 15. This assures that *z* shall be that value of *x* where the quantum limit is, for any given voltage applied to produce the x-rays.

What does Eq. (16) tell us? It says that the first derivative of the isochromat can be decomposed into two additive terms *one of which is a curve shaped exactly like the g curve and with its peak at the value of z corresponding to the value of x where the peak of the original g curve is indeed situated*. It is only necessary for us to understand the general nature of the other term. If it were not for the knee K_1 the factor in square brackets in the integrand which represents the slope of the *f* curve would be a constant. The integral would then be

$$(\text{a constant})\int_0^z g(x)dx$$

and since *g* is not very different from a "witch" $[1+x^2/a^2]^{-1}$ we know that this integral will

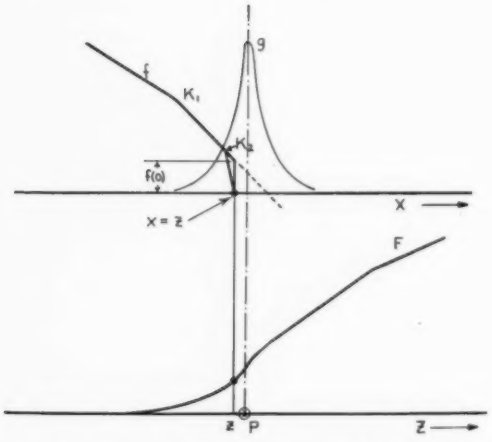

FIG. 18. Illustrating the first and second derivative methods of locating the threshold.

closely resemble an antitangent curve, $\tan^{-1} z$, similar to the sketch Fig. 19 at A. The presence of the knee K_1 or any similar tendency for the slope of the f curve to decline with increase in its independent variable will distort the right-hand part of the curve in Fig. 19 so as to produce a sag as at b. This will have little or no distorting effect, however, on the nearly straight region of this pseudo-antitangent curve near the point of inflection P. This is the region on which the peak of the term $f(0)g(z)$ is superposed. Such a superposition, if the peak is at all pronounced and sharp, has very little effect on the location of the peak and even this small effect can be estimated and corrected for. The truth of this statement can be best appreciated by examining Fig. 20 in which the derivative curve of the 20,000 volt isochromat obtained by carefully taking tangent slopes has been plotted on the voltage scale. The two terms predicted in Eq. (16) are beautifully apparent and the sharpness of the peak contributed by the term $f(0)\cdot g(z)$ leaves little doubt as to the correct position of the threshold to within a very few volts. The partition of the derivative curve into the two terms of (16) involves admittedly a little artistic guesswork but it is easily seen that the peak of the g curve is such a pronounced feature that its location could be changed by only a very few volts at most even by the most extreme assumptions as to the shape of the two curves.

If now the second derivative is to be used for locating the threshold point we assume as a slightly better approximation to the shape f of the continuous x-ray spectrum the curve of Fig. 18 having a finite slope at the quantum limit and two knees K_2 and K_1. On this assumption we can now strike out the second term of Eq. (16) since $f(0)=0$ and differentiating again we obtain

$$\frac{d^2}{dz^2}F(z)=F''(z)=\int_0^z\left[\frac{\partial^2}{\partial z^2}f(z-x)\right]g(x)dx + \left[\frac{\partial}{\partial z}f(z-x)\right]_{x=z}\cdot g(z). \quad (17)$$

Here again we have two additive terms composing the second derivative curve one of which is simply $g(z)$ with a coefficient proportional to the *slope* of the continuous spectrum at the quantum limit. It is simply necessary as before to inquire qualitatively what the other term, the integral, will resemble to be prepared to understand the result. The presence of the two more or less concentrated knees K_1 and K_2 correspond to finite sudden diminutions in slope with increase of the independent variable of f and give to the integral in 17 somewhat the nature of a Lebesgue integral, because the bracketed coefficient in the integrand may be regarded as assuming a value after the nature of a δ function (negative in sign) only at two concentrated points of $(z-x)$ namely K_1 and K_2. In consequence the integral terms of Eq. (17) will appear as two curves each shaped exactly like the principal g curve but with negative intensities and with displacements to the right of the principal g curve equal to the displacements in the continuous x-ray spectrum of K_2 and K_1 to the left of the quantum limit. The principal (positive) g curve and the two inverted g curves g_1 and g_2 just mentioned will

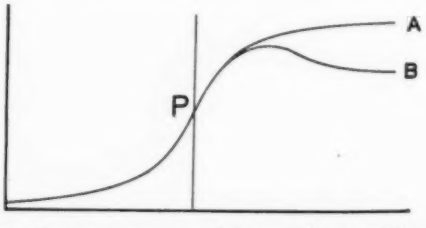

FIG. 19. General appearance of the contribution of the first term of the right-hand member of Eq. (16).

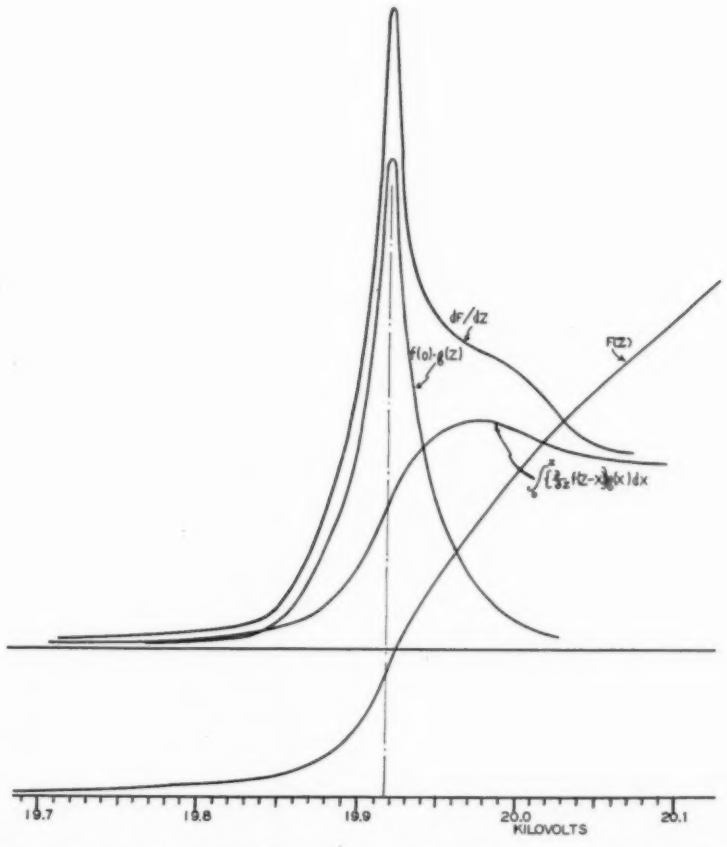

FIG. 20. Location of threshold of higher voltage isochromat with first derivative analysis. Note the contributions of the two terms of Eq. (16).

have relative intensities proportional respectively to the slope of the continuous spectrum at the quantum limit and to the two discrete changes in slope K_1 and K_2. An examination of Fig. 21 shows how beautifully all of these predicted features are brought out in the second derivative curve. Here again the partition of the second derivative into g, g_1 and g_2 involves a little guesswork but the position of the peak of g is very clearly fixed in spite of this.

The use of these two derivative methods gives the two points marked 51 and 52 as threshold points in Fig. 14, the point 51 referring to the first derivative method. An average between these two points gives us the voltage 19,915 for the threshold on the upper isochromat. The voltage scales in Figs. 14, 17, 20 and 21 are our potentiometer observations multiplied by the resistance ratio already mentioned, 14,003, with the 7.5 volt correction for filament P.D. and cathode work function added thereto. To get the true value in international volts, however, this must be diminished by 0.015 percent, a correction shown to be required by a very careful recheck of the voltages of our standard cells against a new cell just calibrated at the National Bureau of Standards.

IV. CRITICAL DISCUSSION OF RESULT

Inescapability of the discrepancy on the Birge-Bond diagram

In Fig. 14 for comparison with the observed thresholds we have plotted points W_1 and W_2

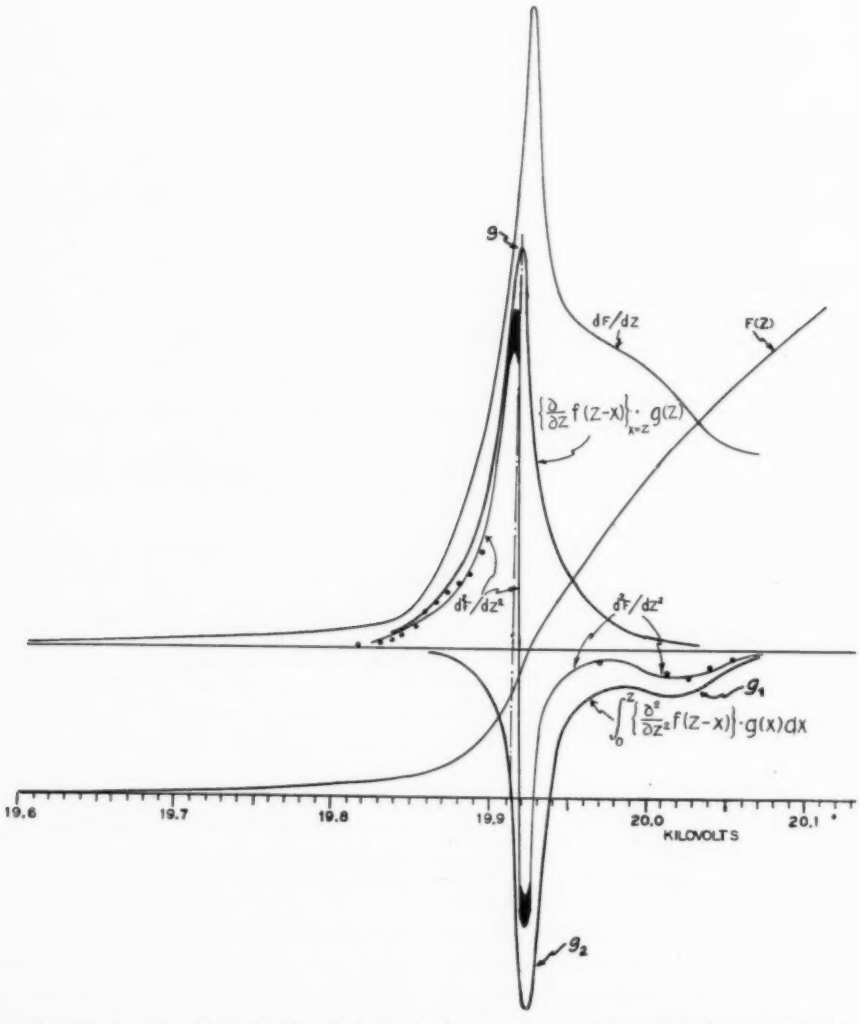

FIG. 21. Location of threshold of higher voltage isochromat with second derivative analysis. The upright g curve contributed by the second term of the right hand member of Eq. (17) and the two displaced and inverted g curves from the first terms of that equation are clear cut. The blackened peaks of the second derivative curve indicate approximately the uncertainty in the value of the second derivative at these points.

where the threshold would have to be in order to make the results of this experiment harmonize with the results of experiments I and II on the Birge-Bond diagram of Fig. 1. Clearly it is very difficult to believe that the thresholds can in reality be at W_1 and W_2 through some vagary of the smearing effect of the g curve. The presence of the knee K_2 would be very difficult to understand if W_1 and W_2 were the true thresholds.

The value of h/e indicated by Fig. 14 is 1.3762×10^{-17}. This is the value computed if we assume the ruled grating wave-lengths of x-rays to be correct in absolute units (Mo $K\beta_2 = 0.6210 \times 10^{-8}$ cm, $WL\beta_1 = 1.2818 \times 10^{-8}$ cm).[15] We may

[15] On the Siegbahn scale of x-ray wave-lengths (in which d_1 for calcite = 3.02904) according to Larsson, Phil. Mag. **3**, 1136 (1927) the wave-length of Mo $K\beta_2$ is 0.619698 while according to Friman, Zeits. f. Physik **39**, 813 (1926) the wave-length of WL β_1 is 1.27917. Both of these values are in

from this also compute $e/h^{3/4}$ independent of any such assumption as to the absolute value of x-ray wave-lengths. This yields the result $e/h^{3/4} = 2.0720 \times 10^{10}$ in rather good agreement with the value obtained by Kirkpatrick and Ross. The slight disagreement is extremely small in comparison to the discrepancy between this experiment and experiments I and II of the Birge-Bond diagram. Our slight disagreement with Ross and Kirkpatrick is in part accounted for by the existence of the knee K_2 of which they were not aware but this is not sufficient to explain all of it and we do not know the cause of the remainder.

It is worth pointing out that if the discrepancy between the results of this experiment (III) and the results of experiments I and II on the Birge-Bond diagram is to be blamed on this experiment (III) our results would indicate that the photons of a given wave-length or frequency appear *too soon* that is at voltages applied to the x-ray tube *lower* than one would expect from conclusions based on I and II. This is much more difficult to understand than would be a discrepancy in the other direction. Two possible causes for such a shift of the threshold voltage to lower values have been suggested but we believe that strong evidence can be presented against these suggestions.

Attempts to account for the discrepancy from causes inherent in the present experiment

First suggestion.—It is suggested that the vigorous ejection by the primary cathode rays of secondary electrons from the target in the region of the focal spot perhaps maintains a positively charged very thin layer at this point which for some reason is not neutralized at a sufficiently rapid rate by electron flow in the metal target to prevent the building up of a considerably more positive potential locally than the potential of the target as a whole measured by the potentiometer. Those infrequent electron collisions which take place very close to the surface of the target and result in the "hardest" x-rays emitted will have the advantage of the extra work done on the cathode rays by the field of this positive layer.

There are at least three objections to this hypothesis. One is that to explain the threshold shift in the case of our 20,000 volt isochromat it would require the positive layer to be about 70 volts more positive than the target. On the other hand it is very difficult to see how such a layer could be many atoms thick. This then would mean that between this layer and the metal target behind it there would exist electrical fields of staggering proportions—billions of volts per centimeter. It becomes terribly difficult to imagine any mechanism of metallic conductivity to explain how such fields are maintained. Furthermore any such explanation must also explain why when the tube is operated around 10,000 volts the threshold shift is only of the order of 30 or 35 volts instead of 70 in the case of 20,000 volt operation. Note that from Fig. 14 one is obliged to find an explanation in terms of a *shift proportional to voltage*. Further investigation is, of course, needed to establish with accuracy just how linear this proportionality is. Finally this explanation must contain some reason to explain why the threshold shift is independent of the cathode-ray current in the tube.

Second suggestion.—It is suggested that photoelectrons are ejected from the cathode and from its focusing cup both of which are subjected to intense x-rays from the target and that these have a preponderant initial energy of some 70 volts for the 20,000 volt x-rays and 35 volts for the 10,000 volt x-rays. These photoelectrons will strike the target then with the requisite excess of energy over the energy to be expected from ordinary thermally emitted electrons to explain the shift in the threshold.

If this were correct one would expect to see the slope of the isochromat increase with increasing voltage all the way up to (or perhaps abruptly at) the points W_1 and W_2, Fig. 14, where one expects to see the spectrum from the ordinary thermally emitted electrons first appear. Instead the curve bends the other way. Work[16] done on the velocity distribution of both primary and secondary electrons ejected by x-rays shows that

good accord with other observers. Bearden (see reference 20) has carefully reviewed the evidence from different sources and finds very convincingly that over a wide range of wave-lengths the ruled grating scale differs from his crystal scale (where $d_{\infty} = 3.0281$, however) by the amount $(\lambda_g - \lambda_c)/\lambda_c = 0.248$ percent. Or reducing this to the Siegbahn scale above it is 0.2035 percent. In this way we get for the ruled grating values of the wave-lengths of Mo $K\beta_2$ and WL β_1 0.6210×10^{-8} cm, and 1.2818×10^{-8} cm, respectively.

[16] L. Simons, Proc. Phys. Soc. London **37**, 58 (1924).

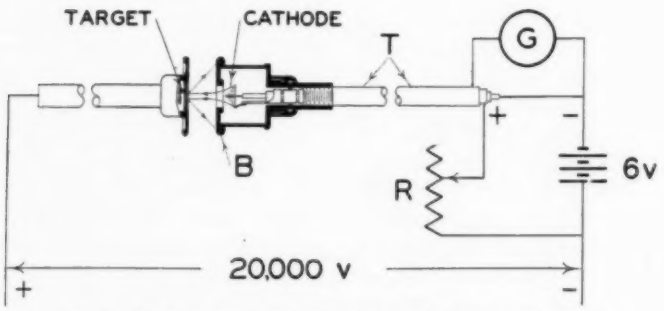

FIG. 22. Showing target and cathode to scale in x-ray tube test for proportionate amount of excess energy electrons by photoelectric ejection. Connection of galvanometer is also shown.

the great bulk of such electrons are secondaries ejected by the fast photoelectrons and that these secondaries have a well marked peak in their velocity distribution curve at a velocity corresponding to about 3.5 volts, a velocity far too low to explain the required shift in the threshold point. Furthermore, strange as it may seem, the most copiously occurring voltage of these secondary electrons, 3.5 volts, is independent of the voltage of the x-rays indirectly responsible for them. Further work[17] shows that for x-rays as far down in the scale as 270 volts ($K\alpha$ line of carbon) the bulk of the ejected electrons have much the same velocity distribution as those ejected by much harder x-rays of the order of those in this experiment. It thus becomes very hard to see how such an effect could give a shift of the threshold *proportional to voltage*. The strongest objection of all, however, is based on the intensity to be expected from such excess energy electrons. In the two references cited[16, 17] the *total* emitted electron currents had to be measured by electrometer and electroscope methods and were probably of the order of 10^{-14} amperes at most. We have made a very rough computation based on energy considerations and the known efficiency of production of x-rays to place an upper limit on the ratio of the total number of such excess energy electrons that could be produced to the number of cathode-ray electrons. This computation repeatedly gives the benefit of the doubt to the side of more rather than less of these electrons and is probably a very gross over estimate. The extreme upper limit fixed in this way for the excess energy electrons of all kinds is 1 percent of the total cathode-ray current. Since this computation may, however, be in error for some reason we have felt it safer to measure in a rough experiment the order of magnitude of the photoelectron current to be expected. The 30 kilowatt (continuous rating) x-ray tube which forms a part of the Watters Memorial Laboratory equipment of this Institute is designed with the cathode filament enclosed in a shield consisting of a cylindrical steel box B from which both terminals of the cathode are insulated as shown in Fig. 22. This box is carried on the end of a steel tube T which completely encloses and shields the cathode leads. The cathode rays stream through the hole in the box and its flat steel end is bathed in the x-rays generated when these cathode rays strike the gold surfaced target distant from the flat front of the cathode box by only $1\frac{1}{4}''$ measured normally. It is evident from the scale drawing that the front of this box subtends a large solid angle at the focal spot. (It is in fact a much larger solid angle than that subtended by the steel focusing cup in the tube used in the main part of the experiment described in this paper.) Any photoelectrons ejected from this steel surface will be instantly transported to the target and the electron current thus leaving the box was measured by means of a galvanometer G connected as shown in Fig. 22. The connection through the galvanometer to the box was such as to make the box slightly more electronegative than the most negative emitting part of the hot filament. With 10 ma thermionic current and 20,000 volts very steady potential (reproducing the conditions of our main experi-

[17] E. Radberg, Proc. Roy. Soc. **120**, 385 (1928).

ment) the total electron current leaving the shield was 0.02 milliampere or only 0.2 percent of the thermionic current. However, a part of this must be regarded as a spurious effect since with only the filament operating but no high voltage and therefore no x-rays we could still get galvanometer deflections indicating electron currents leaving the shield of 0.007 milliampere. Furthermore with the high voltage of 20,000 volts applied but with the cathode cold so as to give no thermionic current the galvanometer still indicated an apparent 0.0035 milliampere of electron current flowing out of the shield probably the result of insulator leaks. Thus there seems no doubt that the photoelectrically ejected electrons *of all velocities* together constituted considerably less than 0.2 percent of the cathode rays striking the target.

One must think then of this excess energy class of electrons, even if it be homogeneous and of initial velocity 70 volts, as itself generating a continuous x-ray spectrum with a threshold at shorter wave-lengths but in its entirety only 0.2 percent (and probably less than this) as intense as the total continuous spectrum from the ordinary thermally emitted electrons whose threshold corresponds to some point like W_1 or W_2 of Fig. 14. It strains one's credulity to the breaking point to believe that a shift of the threshold of the isochromats shown in Fig. 14 could be explained by such a mechanism.

The discrepancy situation on the Birge-Bond diagram

We believe that from the discrepancy exemplified by points I, II and III on the Birge-Bond diagram arises a situation well worth reemphasizing and one which both experimental and theoretical physicists should take very seriously. The better to illustrate the serious nature of this situation we summarize below the formulae applying in each of the three experiments and the various measured quantities entering into the determination. Let us regard each experiment as a method of determining e as a function of measured values and the unknown, h, so that the result of any experiment could be written in the type form

$$e = h^p \cdot [\text{function of measured constants}].$$

For experiment I, $p=0$ for II $p=3/5$, for III the present experiment, $p=3/4$ or unity depending on the assumptions made. Since the two unknowns e and h are involved two experiments are necessary in general for a determination and since there are three ways of pairing these three experiments there result three independent determinations (or if we count both of the alternative ways of interpreting III we really get four independent determinations). Now it appears that each of the three experiments yields results discordant with the remaining two. After the summary of each experiment, therefore, we list just how large a change in any single factor entering into the experiment would be required to harmonize its results with the other two points on the Bond diagram. In every case the cause of the discrepancy is assumed to be concentrated in one factor alone.

I. X-ray crystal determination of e alone

In this experiment[18] e is computed from the Faraday constant and Avogadro's number. This latter is computed from the experimentally determined density of the crystal and absolute size and shape of its lattice cell. To determine this latter in its turn the absolute values of x-ray wave-lengths as determined with ruled gratings are used. The procedure and its result is summed up in the following formulae and definitions:

$$e = 2d^3 Q \rho \Phi(\beta) M^{-1} = 4.805 \times 10^{-10} \text{ e.s.u.},$$

where $d = n\lambda / \{2 \sin\theta (1 - \delta/\sin^2\theta)\}$,

Q = Faraday constant,

M = molecular wt. of $CaCO_3$,

ρ = density of calcite,

$\Phi(\beta)p^3$ = vol. of unit cleavage cell where p is the perpendicular distance between any two parallel faces,

$\delta = 1 - \mu = 2 \times 10^{-6}$; $\sin\theta = 0.117$,

$d_n = d(1 - \delta/\sin^2\theta)$ is independent of λ and depends only on n,

$d/d_n = 0.999865$ in the first order.

[18] The following incomplete list of references is pertinent to work related to this experiment; on absolute values of x-ray wave-lengths, Söderman, Nature **135**, 67 (1935); E. Bäcklin, Nature **135**, 32 (1935) and Zeits. f. Physik **93**, 450 (1935); J. A. Bearden, Phys. Rev. **47**, 883 (1935); **48**, 385 (1935). On crystal reflection angles, grating constants, crystal densities and Avogadro's number, Larsson, Phil. Mag. **3**, 1136 (1927); A. H. Compton, Rev. Sci. Inst. **2**, 365 (1931); J. H. Williams, Phys. Rev. **40**, 636 (1932); Bearden, Phys. Rev. **38**, 1389 (1931); Defoe and Compton, Phys. Rev. **25**, 618 (1925), Bearden, Phys. Rev. **38**, 1389 (1931), also references 23 and 24. H. N. Beets, Phys. Rev. **25**, 624 (1925).

In order that the results of this experiment shall harmonize with II and III_1 (for significance of III_1, see below) e must be lowered to 4.768 which requires a change of 0.75 percent in either e, Q, ρ, $\Phi(\beta)$ or M, or a change of 0.25 percent in either d, θ or λ. In order that the results of this experiment shall harmonize with II and III_2, e must be lowered to 4.785, a change of 0.4 percent in either e, Q, ρ, $\Phi(\beta)$ or M or a change of 0.13 percent in d, θ or λ.

II. The point obtained from e/m and R_∞

The Rydberg constant R_∞ in cm^{-1} units is given by

$$R_\infty = (2\pi^2 e^5)/(h^3 c^2 (e/m)),$$

where e is in absolute e.s.u. and e/m is in abs. e.m.u. Solving this for e we have

$$e = h^{3/5}[c^{2/5}(e/m)^{1/5} 2^{-1/5} \pi^{-2/5} R_\infty^{1/5}].$$

The measured quantities are enclosed in the square brackets

$$R_\infty = 109{,}737.424 \text{ cm}^{-1} \pm 0.06 \text{ cm}^{-1},$$
$$c = 2.99796 \pm 0.00004 \times 10^{10} \text{ cm/sec.},$$
$$e/m = 1.757 \pm 0.0007 \text{ e.m.u./g.}$$

In order for the results of II to agree with I and either III_1 or III_2 we must have one of the following changes: either e/m or R_∞ must be increased 0.73 percent or c must be increased 0.36 percent.

III. Short wave-length limit of the continuous x-ray spectrum

This experiment[19] can be regarded in two ways which we designate III_1 and III_2. According to III_1 no assumption is made as to the absolute value of x-ray wave-lengths. The theory of the inverse photoelectric effect yields the equation

$$h\nu = hc/\lambda = eV,$$

λ is determined from the Bragg equation

$$\lambda = 2d \sin \theta,$$

but d may just as well be regarded as a function of the electronic charge e by the equation given under experiment I as to take the inverse point of view of that experiment. Thus

$$d = e^{1/3} M^{1/3} [2Q\rho\Phi(\beta)]^{-1/3} = Ke^{1/3},$$

where K is a function of measured constants. Eliminating λ and d between these three equations we can solve for e and obtain

$$e = h^{3/4}[2KV \sin \theta]^{-3/4}.$$

According to III_2 we assume that the ruled grating measurements give the correct value of λ, then

$$hc/\lambda = eV,$$
$$e = h[c/(V\lambda)].$$

In order to make this experiment agree with I and II as we have already pointed out V must be increased by 0.25 percent or in Fig. 14 the thresholds must be at W_1 and W_2, a most difficult thing to accept.

It seems worth while pointing out that more difficulties in reconciling points on the Birge-Bond diagram would be eliminated by a change in the absolute determinations of the x-ray wave-lengths by means of ruled gratings or by a change in the Faraday constant than by any other revisions. The striking agreements between various determinations of x-ray wave-lengths by means of ruled gratings by different workers and by dispersion measurements, notably the one by Bearden using diamond as the dispersive medium are very convincing.[20] It is not likely that the Faraday constant can be in error by the requisite amount to explain the discrepancy in question since two completely independent methods of determining it agree very well. We refer to the well-known electrochemical determinations on the one hand and to certain spectroscopic determinations on the other hand whose significance was recently called to our attention by W. V. Houston. This interesting and important check is obtained by comparison of the results of the two spectroscopic methods of determining the specific charge e/m of the electron by the Zeeman effect and by the relative displacement of lines in the spectra of the two hydrogen isotopes. The latter method, which is in reality a determination of M/m, involves the Faraday

[19] Duane and Hunt, Phys. Rev. **6**, 166 (1915); Blake and Duane, Phys. Rev. **10**, 624 (1917); Duane, Palmer and Yeh, Proc. Nat. Acad. Sci. **7**, 237 (1921); J. Opt. Soc. Am. **5**, 376 (1921); H. Feder, Ann. d. Physik **51**, 497 (1929); Kirkpatrick and Ross, Phys. Rev. **45**, 454 (1934); Schaitberger, Ann. d. Physik **24**, 84 (1935).

[20] J. A. Bearden, Phys. Rev. **47**, 883 (1935); **48**, 385 (1935).

constant for the computation of e/m while the former method does not. Now it transpires that when the electrochemical value of the Faraday is used these two methods agree very satisfactorily giving the same value of e/m. This result has been independently obtained in three different laboratories by Gibbs, by Shane and Spedding and very recently by W. V. Houston. We believe this establishes the electrochemical value of the Faraday as free from any error of sufficient magnitude to explain the discrepancy in question.

Of course, the above statements of percentage modifications in measured quantities requisite to harmonize the diagram are based on the assumption that the trouble is entirely localized in one place. It is possible that the discrepancy is to be blamed on the cumulative effect of several superposed small errors in several quantities but after careful consideration of such possibilities as applied to points I, II and III we feel inclined to reject them.

Finally there is the possibility that something is fundamentally wrong with the theories at the foundation of these experiments. In experiment I the theory of the diffraction grating with x-ray at grazing incidence seems to have been pretty thoroughly settled by Eckart.[21] The validity of the x-ray crystal method of determining Avogadro's number seems well established by the experiments of Allison and Armstrong,[22] Y. Tu[23] and DuMond and Bollman[24] unless perchance one could question the applicability of Euclidian geometry to the crystal lattice so as to vitiate the computation of volume from linear dimensions.

In experiment II it is indeed hard to see how the formula for R_∞ can be changed by 1 percent and still leave the Balmer formula with all of its well-known accuracy. Modifications in the formula for R_∞ yielding a relative change of the order of α^2 may indeed be possible but what seems needed is something more nearly of the order of α. The authors are in close contact in this laboratory with highly reliable workers who have repeatedly determined (e/m) both by deflection[25] and spectroscopic[26] methods and we can find no loophole in this quarter either of a theoretical or experimental nature sufficient to explain the required change of about 3/4 percent.

As for the theory of experiment III only the conservation of energy in elementary processes seems to be involved. Elsasser has pointed out that since experiment III is the only one which involves relativistic velocities it is here that one feels a theoretical modification is most likely to be necessary. Such a modification must be of a most fundamental nature to explain, if possible with retention of the conservation of energy, what now appears to be a conversion of electron energy into photon energy at the highly favorable efficiency of 100.25 percent.

We are thus faced with a dilemma which we feel should be very seriously considered both by theoretical and experimental physicists.

The authors consider the present experiment as merely preliminary and they project a much more thorough continuation of this work both at higher and at lower voltages and with better spectral resolution. The latter will be made possible by the recent completion of an extremely powerful source of x-rays. In the quantum law usually written $eV=h\nu$ which should to conform with the quantities actually measured be written $\lambda V=(hc/e)$ it will be interesting to see whether each member of the last equation is really a constant strictly independent of λ and V over a wide range of these variables.

The funds for this investigation were derived from the gift of Dr. Leon L. Watters of New York City for research work in x-rays and atomic structure known as the Watters Memorial Research Fund given by Dr. Watters as a memorial to his wife, Frances Hayes Watters. We are grateful for this opportunity to express our deep appreciation of his gift.

[21] C. Eckart, Phys. Rev. **44**, 12 (1933).
[22] Allison and Armstrong, Phys. Rev. **26**, 701 (1925). See Allison's excellent discussion of these points in Compton and Allison's *X-Rays in Theory and Experiment*, p. 698.
[23] Y. Tu, Phys. Rev. **40**, 662 (1932).
[24] DuMond and Bollman, Phys. Rev. **50**, 524 (1936).
[25] F. Dunnington, Phys. Rev. **43**, 404 (1933).
[26] Campbell and Houston, Phys. Rev. **39**, 601 (1932); Kinsler and Houston, Phys. Rev. **45**, 104 (1934); **46**, 533 (1934).

Infrared Absorption of Dilute Solutions of HCl and HBr

C. E. Leberknight and John A. Ord
Carnegie Institute of Technology, Pittsburgh, Pennsylvania

(Received January 14, 1937)

The infrared absorption of dilute solutions of HCl and HBr in benzene, chlorbenzene, carbon tetrachloride, and tin tetrachloride, was investigated by a prism grating spectrograph of high dispersion with effective slit widths of between one and two wave numbers. There was found a single absorption band for all solutions with the exception of tin tetrachloride which showed a double band for HCl and a single band for HBr located at the position of one of the HCl bands. These results for tin tetrachloride are attributed to the formation of H_2SnCl_6 in the case of the HCl solution, and to the formation of a compound in such a manner that free HCl was liberated in the case of the HBr solution. From the experimental values of the areas under the curves, their half-widths, and the maximum extinction, it is concluded that the dissolved molecules could be treated as a dilute gas composed of damped simple harmonic oscillators. From the half-widths of the bands the damping constants of the dissolved molecules are calculated, and the force constants are determined from the position of the peaks of the absorption bands. In all cases the value of the force constant is diminished from its value for the molecule in the vapor state. The ratio of the change in the force constant of HCl to the change in the constant of HBr in the solvents, benzene, chlorbenzene, and carbon tetrachloride, is close to 1.32 which is the ratio of the dipole moments of the two substances in the vapor state. Likewise, the ratio of the half-widths of the bands for the two molecules is close to 1.32. Values of the Einstein coefficient of absorption and values of ϵ in the equation, $\mu=\mu_0+\epsilon(r-r_0)$ for the electric moment of the molecules are calculated.

IT is evident that the forces existing between molecules in the liquid state affect the dynamical properties of the individual molecules. These properties, in many cases, can be investigated by means of infrared absorption measurements, and the experimentally simplest of such are probably those that can be made on dilute solutions of diatomic polar molecules. Experiments on such solutions will yield information concerning the interaction of the dissolved polar molecules with their environment. The effect of the environment, in general, will be to alter the dynamical behavior of the solute molecules as evidenced, in the case of infrared absorption measurements, by shifts in position of the absorption bands and by changes in their shape and in tensity. West and Arthur[1] have shown by Raman photographs, Plyler[2] and Williams,[3] and West and Edwards,[4] by infrared absorption measurements, with solutions of HCl, that the position of the band due to HCl is shifted by amounts which depend upon the solvent. Now, most solvents which do not dissociate HCl have strong bands in the region of the HCl fundamental absorption band, and this fact necessitates the use of an instrument of large dispersion and resolving power if it is desired to study the position of the infrared absorption bands and particularly their shape and intensity. It is therefore the purpose of this paper to discuss quantitatively some measurements made on dilute solutions of HCl and HBr, with an instrument of such dispersion and resolving power that the position of the bands could be obtained accurately and the form of the absorption curves could be studied.

All measurements were made with an instrument of the prism grating type having a theoretical resolving power of about 15,000 in the first order. The effective slit widths were between one and two wave numbers. The instrument was calibrated by observing the higher orders of the visible mercury lines in the exit slit; this method permitted an accuracy in the calibration of approximately 0.2 wave numbers. Intensity measurements were made by a compensating vacuum thermocouple connected to a voltage sensitive galvanometer. The galvanometer deflections were so amplified by an optical relay that it was possible to work always with deflections of 20 cm or more when the radiation was passed through the cell containing the solvent. The stability of the receiving and amplifying system was such

[1] W. West and P. Arthur, J. Chem. Phys. **2**, 215 (1934).
[2] E. K. Plyler and D. Williams, Phys. Rev. **49**, 215 (1936).
[3] D. Williams, Phys. Rev. **50**, 719 (1936).
[4] W. West and R. T. Edwards, Phys. Rev. **49**, 405 (1936).

that all deflections were subject to an error of not more than one millimeter.

Eastman C. P. benzene, chlorbenzene, and carbon tetrachloride, and Baker and Adamson tin tetrachloride were used as solvents. Where necessary they were refluxed over P_2O_5 to remove any trace of water. HCl was prepared by permitting sulphuric acid to act on sodium chloride, dried, and then bubbled through the various solvents. HBr was obtained by the action of phosphoric acid on potassium bromide crystals, dried, and likewise bubbled into solution. Concentrations were determined by extraction with water and titration with standard acid and alkali solutions with methyl orange as an indicator.

Adjustable brass cells coated with fish glue (which is insoluble in the solvents used) and fitted with microscope cover glasses for windows were used in making all observations. For each solution two cells were prepared as nearly alike as possible. The solution was placed in one cell, the solvent in the other, and successive observations made on the solution and solvent for each setting of the instrument. After the desired portion of the spectrum had been investigated, the cell containing the solution was emptied and filled with solvent. The above process was then repeated with both cells containing solvent. By first comparing solution to solvent, all effects due to the solvent alone were eliminated, while a comparison made with both cells containing the solvent was a necessary precaution taken to prevent errors due to slight differences in the cells. After each complete set of readings on any one solution, the instrument was recalibrated.

In Fig. 1 are shown the extinction curves obtained for HCl and HBr in solutions of benzene, chlorbenzene, carbon tetrachloride, and tin tetra-

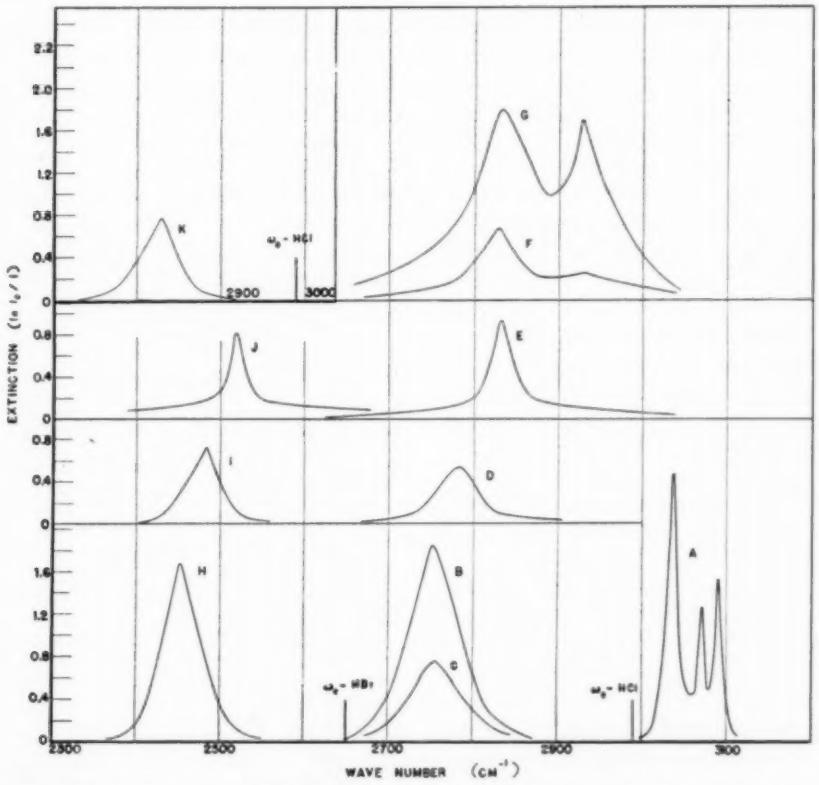

FIG. 1. Extinction curves for HCl and HBr in solutions of benzene, chlorobenzene, carbon tetrachloride and tin tetrachloride.

TABLE I. *Data and computations made from the curves of Fig. 1. E_m is the measured maximum extinction defined as $E=ln\ (I_0/I)=kt$, where t is the thickness of the cell, I is the intensity of the energy transmitted through the solution and I_0 the intensity transmitted through the dummy cell containing only the solvent. N is the normality of the solution. The area in column 6 is twice the area under the curve between two points where the extinction has half its maximum value. γ is the half-width of the bands.*

SOLUTION	CURVE	E_m	"f" cm	N	Area kt_1 cm^{-1}	"γ" cm^{-1}	$A/\gamma E_m$
HCl-C_6H_6	*B*	1.82	0.033	0.153	199	70	1.56
HCl-C_6H_6	*C*	0.75	0.033	0.060	82	71	1.54
HCl-C_6H_5Cl	*D*	0.52	0.033	0.122	48	58	1.59
HCl-CCl_4	*E*	0.92	0.115	0.037	48	34	1.53
HCl-$SnCl_4$	*F*		0.250				
HCl-$SnCl_4$	*G*		0.500				
HBr-C_6H_6	*H*	1.66	0.033	0.443	134	53	1.52
HBr-C_6H_5Cl	*I*	0.71		0.110	48	44	1.54
HBr-CCl_4	*J*	0.73	0.243	0.170	29	25	1.59
HBr-$SnCl_4$	*K*	0.77	0.300		58	49	1.54

chloride; an additional curve for pure benzene (A) is included in order to show that with the dispersion used in the experiments it was possible to work near the region of strong solvent bands even when benzene and chlorbenzene were used as solvents. The first five columns of Table I list the data for the various curves. [Column 1 lists the solution, column 2 refers to the particular curve in Fig. 1, column 3 lists the measured maximum extinction, column 4, the thickness of the cells, and column 5, the normalities of the solutions.] All curves in Fig. 1 are plotted with extinction against wave number, where the extinction is defined as $E=\ln\ (I_0/I)=kt$. In this expression t is the thickness of the cell, I is the intensity of the energy transmitted through the solution, and I_0 is the intensity transmitted through the dummy cell containing only the solvent. This procedure is permissible since the two readings were taken within a few seconds of each other, and since the intensity of the energy emitted by the source remained constant for a considerable period of time. Hence k can be taken as the extinction coefficient of the solute. It should be noted that in all cases the width of the band is considerably larger than the effective slit width which was always between one and two wave numbers.

An inspection of the curves shows that they are symmetrical and similar in shape to the extinction curve of a dilute gas composed of damped simple harmonic oscillators. If they can be treated as such, then it can be shown[5] that a relation exists between the total area under the curve, the maximum extinction, and the half-width, namely, $A/\gamma E_m=\pi/2$; also, the total area under the curve included between the two points where the extinction has half its maximum value. In Table I is listed twice this latter area as determined by a planimeter. The last two columns list the half-widths of the bands in cm^{-1} and the quotient of the total area by the product of the maximum extinction and the half-width. In all cases it is seen that this value is close to $\pi/2$. From the data listed in the table for the two benzene solutions of different HCl concentrations, it is evident that Beer's law holds (i.e., the maximum extinction is proportional to the concentrations). The ratio of the normalities is 2.45 while the ratio of the maximum extinctions is 2.43.

In Table II is listed the various constants of the HCl and HBr molecules in the different solvents considering them as damped simple harmonic oscillators. The error in the values of the Einstein coefficient of absorption B_0' and of ϵ may be as high as 10 percent, due mainly to uncertainties in the thickness of the cells, especially the thinner ones. The experimental error in the positions of the peaks of the absorption bands and in their half-widths is probably not more

TABLE II. *Constants of HCl and HBr molecules in the different solvents considering them as damped simple harmonic oscillators satisfying the equation $md^2q/dt^2+bdq/dt+fq=0$. ω_0 is the position of the peak of the absorption band. ω_e is the position of the band when the molecule is in the vapor state. (ω_e was taken as 2989 cm^{-1} for HCl and 2650 cm^{-1} for HBr. These are the positions of the fundamental for harmonic vibrations of the molecule.) The reduced mass m was taken as 1.615×10^{-24} g for HCl and 1.641×10^{-24} g for HBr. The damping constant "b" was determined from the half-width while "f" is the force constant determined from the equation $m(2\pi\nu)^2=f$. B is the Einstein coefficient of absorption and ϵ is the coefficient in the equation* for the electric moment of the molecule. $\mu=\mu_0+\epsilon(r-r_0)$.*

SOLUTION	ω_0 cm^{-1}	$\omega_0-\omega_e$ cm^{-1}	"b"$\times$ 10^{13}	"f"$\times$ 10^{-5}	$B_0'\times$ 10^{-15}	$\epsilon\times10^{19}$ e.s.u.
HCl-C_6H_6	2753	−236	213	43.61	110	3.0
HCl-C_6H_5Cl	2783	−206	176	44.57	32	1.6
HCl-CCl_4	2833	−156	103	46.19	30	1.6
HCl-$SnCl_4$	2833			46.19		
HBr-C_6H_6	2453	−197	164	35.09	28	1.5
HBr-C_6H_5Cl	2483	−167	136	35.95		
HBr-CCl_4	2519	−131	77	37.00	4	0.6
HBr-$SnCl_4$	2833		152	46.19		

* L. Pauling and E. B. Wilson: *Introduction to Quantum Mechanics* (McGraw-Hill Book Company, Inc., New York, 1935), p. 309.

[5] Füchtbauer, Physik. Zeits. **21**, 322 (1920).

than one wave number, since different runs checked each other to within this amount.

An inspection of the values of the molecular constants of HCl and HBr in the various solvents shows that they vary considerably with the nature of the solvent; there is one similarity, though, in the fact that as the force constant changes in the different solutions, the damping constant varies in a like manner. In all cases the effect of the environment is to decrease the force constant of the molecule. Contrary to the results found by Williams[5] for HCl, this decrease is larger in benzene than in chlorbenzene, since the shift of the bands for both HCl and HBr in solution is greater in benzene. The values of ϵ are all greater for the molecules in solution than in the vapor state.[6] In the benzene, chlorbenzene, and carbon tetrachloride solutions there is only a single absorption band, but in the tin tetrachloride solutions there is a double band for HCl and a single band for HBr. This single band for HBr lies at 2833 cm^{-1} which is the location of one of the HCl bands; the other is at 2930 cm^{-1} for both solutions of different thickness and different concentration. With the concentration used in the experiment, no absorption could be found in the neighborhood of the other HBr bands. It is evident that in the $SnCl_4-HCl$ solution some of the HCl enters into combination to form H_2SnCl_6, and hence there is a mixture of free and combined HCl giving rise to two absorption bands; also, when HBr is dissolved in $SnCl_4$, it must enter into combination in such a manner that free HCl is liberated, and hence only the HCl absorption band is observed.

[6] E. Bartholomé, Zeits. f. physik. Chemie **B23**, 131 (1933).

TABLE III. *Comparison of damping constants "b" and of changes in force function for HCl and HBr in various solvents.*

SOLVENT	$\frac{"b"(HCl)}{"b"(HBr)}$	$\frac{\Delta f(HCl)}{\Delta f(HBr)}$
C_6H_6	1.33	1.33
C_6H_5Cl	1.30	1.36
CCl_4	1.34	1.32

In Table III is shown the ratio of the damping constants and the change in the force constants of HCl and HBr in the three solvents, benzene, chlorbenzene and carbon tetrachloride. The change in the force constant is the difference in the constant for the molecule in solution and its value for the molecule in the vapor state determined from the value of ω_e. All values of the ratios are seen to be close to 1.32, which is the ratio of the dipole moments of the two substances in the vapor state. If it be assumed that the intermolecular potential depends upon the electric moment of the dissolved molecules it is reasonable to suppose that the alteration in their force constants by environment should depend upon the value of their electric moments.

A Resonance Process in the Disintegration of Boron by Protons

J. H. Williams, W. H. Wells,* J. T. Tate and E. L. Hill
University of Minnesota, Minneapolis, Minnesota

(Received January 27, 1937)

An experimental investigation of the efficiency of production of α-particles from boron as a function of the energy of the bombarding protons is reported. Of the two established processes,

$$_5B^{11}+{}_1H^1\rightarrow 3\,{}_2He^4+Q_1$$

and

$$_5B^{11}+{}_1H^1\rightarrow {}_4Be^8+{}_2He^4+Q_2,$$

the second exhibits peculiarities in its efficiency curve whereas the first increases exponentially with proton energy. This irregularity is interpreted as the occurrence of a resonance process in the second disintegration, the resonance peak occurring at 180 kv. A discussion of the possible theoretical interpretations of the process is given. Absolute yields for a thick boron target at various proton energies are given.

Introduction

THE disintegration of boron by proton bombardment has been studied by the Cambridge group[1] and by Kirchner and Neuert.[2] As a result the following processes appear to be established:

$$_5B^{11}+{}_1H^1\rightarrow 3\,{}_2He^4+Q_1, \quad (1)$$

$$_5B^{11}+{}_1H^1\rightarrow {}_4Be^8+{}_2He^4+Q_2. \quad (2)$$

Process (1) predominates even at low voltages, and gives rise to a continuous distribution of α-particles having a maximum at a range of 24 mm. Reaction (2) gives about 1 percent as many α-particles (at 150 kv) and is responsible for the appearance of a small homogeneous group having a range of about 4.5 cm.

In their careful examination of the energy distribution of the α-particles, Cockcroft and Lewis[3] noted that the yields from the two processes did not vary in the same way with the energy of the incident protons; i.e., the two reactions have different efficiency curves. This work has been carried further in this laboratory, and the curves for the yields have been obtained up to about 250 kv. In agreement with Cockcroft and Lewis we find markedly different yield voltage curves from (1) and (2), that for the latter exhibiting a resonance effect. The preliminary results of this work have been published.[4]

Apparatus

A resistance controlled transformer-kenetron-condenser set was adapted to deliver potentials up to 275 kv which could be manually controlled to fluctuations in the output of one percent. The voltage was measured by a high resistance voltmeter constructed from 150 individually calibrated 10-megohm metallized resistors. This voltage accelerated protons from a low voltage arc[5] connected in such a manner that only the measured external voltage was effective. The magnetically resolved proton beam of 2 to 5 microamperes was focused to a spot diameter of less than 5 mm. By means of a high resistance potentiometer in series with the cylindrical accelerating tube elements, a constant focus was obtained over a wide range of voltages.[6] The α-particles emitted from a *thick* fused B_2O_3 target inclined at 45° were observed at an angle of 90° from the proton beam. They were detected by an ionization chamber which was 7 mm deep, connected to an amplifier of the Dunning type.[7] The pulses were recorded by a scale-of-eight thyratron counter[8] adjusted to count all α-particles which entered appreciably into the ionization chamber.

Preliminary experiments to test the apparatus included measurements of the disintegration efficiency of protons on thick LiCl targets. The fact that the values obtained agreed to within 10 percent of the absolute yields given

* Now at Westinghouse Electric & Manufacturing Co. Research Laboratories, East Pittsburgh, Pennsylvania.

[1] Oliphant, Kempton and Rutherford, Proc. Roy. Soc. **A150**, 241 (1935).

[2] Kirchner and Neuert, Physik. Zeits. **34**, 897 (1933); Neuert, Physik. Zeits. **36**, 629 (1935).

[3] Cockcroft and Lewis, Proc. Roy. Soc. **A154**, 246 (1936).

[4] Williams and Wells, Phys. Rev. **50**, 187 (1936).

[5] Tuve, Dahl and Van Atta, Phys. Rev. **46**, 1072 (1934).

[6] Hansen and Webster, Rev. Sci. Inst. **7**, 17 (1936).

[7] Dunning, Rev. Sci. Inst. **5**, 387 (1934).

[8] Shepherd and Haxby, Rev. Sci. Inst. **7**, 425 (1936).

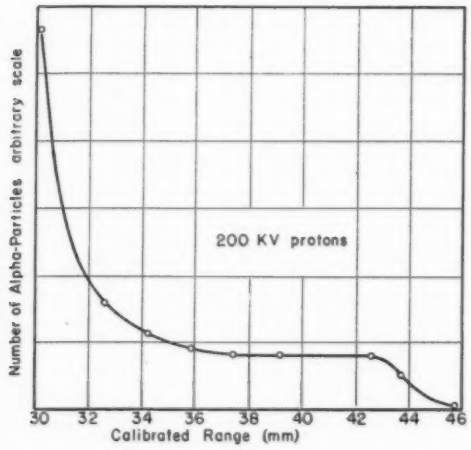

FIG. 1. Number of α-particles from a boron target under proton bombardment reaching a deep ionization chamber as a function of absorber between target and chamber. The absolute values for the abscissae are obtained from comparison with the results of Kirchner and Neuert.

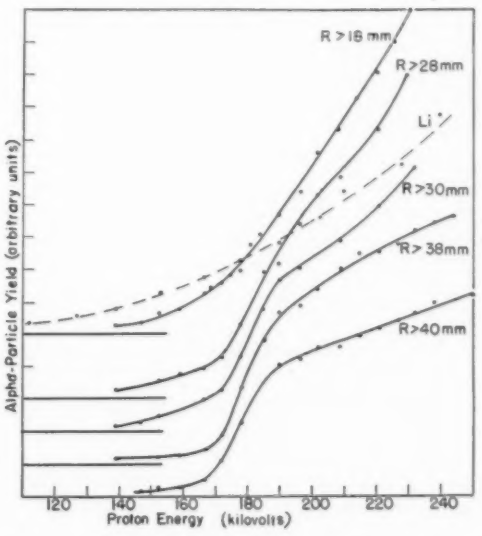

FIG. 2. Yield curves for α-particles from the disintegration of boron by protons. The yields are in arbitrary units and the zeros for the various curves are shifted vertically as indicated. For comparison purposes the yield curve for the α-particles from lithium bombarded with protons is included.

by the Wisconsin group[9] was taken as evidence for the satisfactory behavior of the apparatus.

EXPERIMENTAL PROCEDURE

Protons accelerated by a constant potential of 200 kv were allowed to strike the thick B_2O_3 target, and the number of emitted α-particles entering a *deep* ionization chamber were observed when various thicknesses of mica and air were inserted between the target and the chamber. These observations are shown in Fig. 1. They serve to indicate the presence of the homogeneous group of α-particles attributed to reaction (2) and by comparison with the results of Kirchner and Neuert[2] give a calibration of the range scale of our detecting apparatus. No attempt was made to obtain the shape of this number *vs.* range curve sufficiently accurately to contribute any information as to the nature of reaction (1), since the present method is in this respect experimentally inherently inferior to that of Kirchner and Neuert[2] and that of Dee and Gilbert.[10]

With the range scale thus calibrated we obtained, with range as a parameter, the number of α-particles emitted in a calculated solid angle as a function of proton energy. Since the ionization chamber records all α-particles which enter it, the yield curves will be for all α-particles having a range greater than that necessary to reach the ionization chamber. This experimental condition undoubtedly contributes to the difficulty of interpreting the yield curves, but does not mask their significance. Representative observed efficiency curves are shown in Fig. 2.

It is seen that the main group of α-particles of range greater than 18 mm follows an ordinary excitation curve with no evidence of marked irregularities. However, when sufficient mica is introduced to remove most of the α-particles from (1), so that the majority of those recorded are of range greater than 38 mm, the efficiency curve is found to be markedly different. The yield expected from a *thin* target, obtained by differentiating the thick target curve with respect to the 3/2 power of the accelerating voltage[9] is shown in Fig. 3 (cf. the next section for discussion).

The several curves of increasing range from 28 mm to 40 mm show different slopes at voltages greater than 200 kv. We interpret this as due

[9] Herb, Parkinson and Kerst, Phys. Rev. **48**, 118 (1935); Heydenberg, Zahn and King, Phys. Rev. **49**, 100 (1936).
[10] Dee and Gilbert, Proc. Roy. Soc. **A154**, 279 (1936).

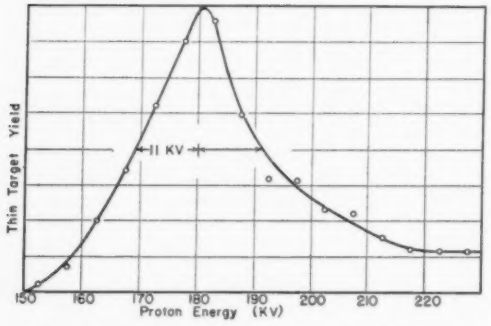

FIG. 3. The yield of long range α-particles expected from a thin target of boron as a function of the bombarding proton's energy. The curve is obtained by differentiating the observed thick target curve with respect to (voltage)$^{\frac{1}{2}}$.

either to the onset of further modes of disintegration or to the inclusion of a small number of α-particles from the continuous distribution of disintegration (1). An examination of Fig. 5 of Cockcroft and Lewis' paper[3] shows that the number-*vs.*-range curve for (1) changes its shape with increasing voltage in a manner such that the continuous distribution extends to greater ranges at the higher voltages. From this point of view the efficiency curve of α-particles of some definite range, say 38 mm, would not decrease exponentially to zero with diminishing incident proton energies, but would have an apparently definite "excitation potential."

An attempt was made to overcome the effect of measuring α-particles from (1) by working at ranges greater than 43 mm. Since the yield of α-particles from (2) is small, it is necessary to arrange the geometry of the ionization chamber to subtend a large solid angle at the target. This imposes the condition that α-particles pass from the focal spot to the ionization chamber over a wide range of angles distributed about 90° from the direction of the proton beam. Consequently only a certain fraction of the 45 mm range α-particles were able to pass through the 43 mm of mica and air absorber between the target and the chamber. In changing the voltage during the measurement of an efficiency curve, very slight changes in the size and position of the focal spot gave gross changes in the number of α-particles which were able to reach the ionization chamber. This effect, although unimportant for absorbers of less than 40 mm stopping power, made accurate relative measurements impossible at greater thicknesses of absorber.

An effort was made to investigate the similar disintegration

$$_5B^{10}+{}_1H^2\rightarrow {}_4Be^8+{}_2He^4+Q_3 \qquad (3)$$

to test whether any correlation could be found in the yield curves, but with the available accelerating voltages it was not possible to obtain satisfactory efficiency curves, since the yields from (3) are small compared to those from (1) and (2) at low energies. However, we did obtain qualitative measurements on the number-*vs.*-range curve, which were in agreement with the results of Cockcroft and Lewis[3] in showing the presence of an homogeneous group of particles arising from (3).

EXPERIMENTAL RESULTS

From our voltage yield curve we can conclude that the yield from reaction (1) follows a Gamow type curve within our experimental error. The yield of 45 mm particles attributed to (2) shows, on the other hand, a distinct resonance effect in the neighborhood of 180 kv. Making reasonable corrections for the contributions of the tail end of the low energy continuous distribution to the high energy group of α-particles, we find that the "thin target" efficiency curve[9] has a half-width of about 11 kv at half-maximum. As the energy of the incident protons was very steady, it is felt that the error in this value should not exceed 3 kv. Fig. 3 shows a typical "differentiated" curve (i.e., differentiated with respect to $V^{\frac{1}{2}}$).

Qualitative results for the yield of α-particles per proton calculated for a pure boron target by multiplying the observations on the thick B_2O_3 target by 34/10 are:

RANGE	>18 mm	>40 mm
150 kv	1.68×10^{-9}	1.79×10^{-11}
175	7.06	17.4
200	18.4	49.7
225	32.3	59.7

The relative yields from the two disintegrations may be compared to Kirchner and Neuert's value of 1:200 at 150 kv, Oliphant, Kempton and

Rutherford's value at 1:70 at an unstated voltage, and Cockcroft and Lewis' values 1:60 at 185 kv and 1:240 at 360 kv.

Discussion

A general formal theory of resonances in nuclear processes has been given by Breit and Wigner,[11] with special consideration of neutron capture or scattering processes with or without γ-ray emission. As regards the latter, γ-rays have been observed[12] from boron bombarded with protons of 900 kv energy, but their intensities appeared to be very strong functions of the voltage, and were inappreciable below 700 kv. The emission of the γ-rays was postulated to be a direct capture of the proton without disintegration; i.e.,

$$_5B^{11}+{}_1H^1\rightarrow{}_6C^{12}+h\nu.$$

If this be the case, there is no obvious reason why γ-ray emission should not appear as an alternative reaction to the two modes of disintegration considered here, even at the lower voltages used by us, unless, as suggested by Crane, Delsasso, Fowler and Lauritsen, the probability of emission of the γ-rays is abnormally high in the region of 900 kv bombarding energy.[13]

The energy balance which is obtained without consideration of possible *simultaneous* γ-ray emission seems to be so good that little room is left for the disposal of much energy in this way, and we provisionally assume that when one or the other disintegration occurs, no γ-ray is emitted. The possible influence of an *alternative* process of γ-ray emission must be left open at the moment.

According to current ideas on the dynamics of disintegration processes, it is convenient to consider that they occur through a transient intermediary stage of an excited "compound" nucleus so that we write them as

$$_5B^{11}+{}_1H^1\rightarrow{}_6C^{12*}\rightarrow 3\,{}_2He^4, \qquad (1')$$

$$\rightarrow{}_6C^{12**}\rightarrow{}_4Be^8+{}_2He^4. \qquad (2')$$

It is of interest to decide, if possible, whether the two levels of the excited C^{12} nucleus implied in (1′) and (2′) are the same. Save for a possible influence of the resonance phenomenon itself in producing a shift in the levels,[14] if two different levels are involved they should differ in energy merely by the binding energy of $_4Be^8$. At the present time this is an uncertain quantity, so that it is not possible to come to any conclusion on this basis. Considered as excited levels of $_6C^{12}$ they lie well within the continuum of energy levels above the first "dissociation potential"

$$_6C^{12}+(\sim 7.5\text{ Mev})\rightarrow 3\,{}_2He^4.$$

The "resonance levels" referred to might better be spoken of as "pre-dissociation levels" lying at about 16.1 Mev above the normal state of $_6C^{12}$.

From our experimental results it seems most probable that the two excited levels involved in (1′) and (2′) are distinct from each other, and that (1′) and (2′) represent independent modes of capture and disintegration rather than alternative disintegrations from one single resonance level. The reason for supposing this is as follows: Suppose that (1′) and (2′) both went through the same excited level of $_6C^{12}$. Let γ_0 be the contribution to the width of the intermediate level due to transitions from the initial proton state, and γ_1 and γ_2 be the half-widths of the transitions out of this state, while $\gamma=\gamma_0+\gamma_1+\gamma_2$. Then the corresponding cross sections in the immediate neighborhood of the resonance energy may be written on the resonance theory in the approximate forms[15]

$$\sigma_1\sim A_1\lambda^2\frac{\gamma_0\gamma_1}{(V-V_r)^2+\gamma^2},$$

$$\sigma_2\sim A_2\lambda^2\frac{\gamma_0\gamma_2}{(V-V_r)^2+\gamma^2},$$

where A_1 and A_2 are nearly equal and vary only slowly with V close to the resonance potential V_r. From these formulas one would expect that *both* processes should show the resonance phenom-

[11] Breit and Wigner, Phys. Rev. **49**, 519 (1936). Cf. also Dirac, *Quantum Mechanics*, Second Edition, p. 203.

[12] Crane, Delsasso, Fowler and Lauritsen, Phys. Rev. **48**, 102 (1935).

[13] It would be interesting to extend the disintegration measurements to this region to look for further resonance effects.

[14] Breit and Wigner, reference 11, p. 526.

[15] Cf. Breit and Wigner, reference 11, Eq. (14) for the analogous case of neutron scattering or capture with γ-ray emission. In the formulas in the text we have not considered the effect of the variation in the Gamow penetration factor over the width of the resonance level. Its inclusion should hardly affect the general conclusion.

enon, and that their corresponding cross sections should be roughly in the ratio of their corresponding half-widths; i.e., the ratio of the corresponding yields. Since (1′) is a much more prolific reaction than (2′), one would then expect to find a large resonance in the main group of α-particles. While this might be somewhat masked by the apparent exponential increase in the yield which is observed, yet the absence of any observable resonance in (1′) leads us to consider that the dynamics of the two disintegration processes probably involve two different modes of "capture" of the proton.

We can estimate roughly the relative probabilities of "capture" into the two excited levels as follows: We find, in agreement with Kirchner and Neuert[2] that about 100 times as many α-particles are observed in the main group as in the small high energy group. From (2′) we would expect to be able to observe only one α-particle per disintegration even if the Be^8 nucleus should be unstable and disintegrate, since the resulting α-particles would have very small energies. It has further been shown by Dee and Gilbert[10] that the most probable disintegration from (1′) is such that one α-particle receives very little energy, the other two dividing the energy roughly evenly. From such a break-up there are then two particles available for measurement. This gives for the relative number of disintegrations from (1′) and (2′) about 50 to 1. If we neglect the probabilities of other modes of passage out of the excited levels (or better, assume that they are equally important for both) then we can use this figure as a rough measure of the probabilities of "capture" into the two levels.[16] The most important correction to this seems likely to come from the possible influence of γ-ray emission, mentioned above.

This ratio suggests that the two processes (1′) and (2′) may result from interactions of s and p protons, respectively, with the B^{11} nucleus, the gross difference being due primarily to the influence of the angular momentum of the p protons in keeping them away from the nucleus. The resonance would then be a resonance of the p protons. Check calculations on the potential well model are being made to test this hypothesis, but without definite results to date.

While no detailed theory can be given at the moment, a suggestion may be made from the observed value of the width of the resonance region on the nature of the mechanism of the disintegration. The observed value of about 11 kv for the half-width indicates a mean lifetime of the excited state involved in (2′) of about 10^{-18} or 10^{-19} sec. If the initial state of the nucleus is represented by one particle wave functions say as in a Hartree model, without any more tendency towards the formation of specific groups than is implied in the use of a self-consistent field and a shell structure modeled after that of the external electrons, it would seem that the probability for the formation of the structures actually observed in the disintegration would be much too low. Particularly as in the present case where there must be the formation of three α-particles which must then distribute the available kinetic energy among themselves in a manner distinctly different from that to be expected *a priori*.[10] The inference is that it would be advantageous to allow in the theory for a predisposition for the preformation of the group structures which make their appearance on disintegration.[17] It is hoped to return to this problem in a more definite way in a later communication.

We wish to express our sincere thanks to Mr. W. G. Shepherd and Mr. R. O. Haxby for invaluable assistance with the recording apparatus. This research was supported by a grant from the Graduate School of the University of Minnesota.

[16] This statement is only of tentative and approximate significance since the mathematical theory of the disintegration through a resonance level does not provide that the probability of disintegration is equal to the product of a probability for capture and a probability for disintegration after capture. Instead the total probability is determined by a formula of the general type

$$(\alpha/\hbar^2)\left|\sum_k \frac{(a|H'|k)(k|H'|b)}{(E-E_k)+i\beta}\right|^2,$$

where a and b refer to the initial and final states; i.e., before and after disintegration, and k refers to the intermediate states within the resonance band. α and β are constants. This allows for the possibility of an interference between the different modes of resonance capture within the resonance band. It is only under special circumstances in which this interference is unimportant that the above expression can be reduced to the form

$$g(E_0)\frac{|(a|H'|k)|^2|(k|H'|b)|^2}{(E-E_0)^2+\beta^2},$$

where E_0 is the energy at the maximum of the resonance band and $g(E_0)$ is a weighting factor.

[17] Wells and Hill, Phys. Rev. **49**, 858 (1936).

The Induced Radioactivity of Calcium*

HAROLD WALKE†
University of California, Berkeley, California
(Received January 27, 1937)

A study has been made of the radioactivities induced in calcium by bombardment with high energy deuterons, alpha-particles and neutrons. Following irradiation by deuterons, the active samples have been separated chemically into fractions containing scandium, calcium and potassium. Most of the activity was found in the scandium precipitate, the decay curve of which has been analyzed into three components with half-lives of 53 ± 3 minutes, 4.0 ± 0.1 hours, and 52 ± 2 hours. The thick target yields of these active isotopes computed for an infinite duration of bombardment are 5.4×10^7, 3.6×10^7 and 3×10^8 deuterons per active atom. It is suggested that these periods are to be associated with Sc^{44}, Sc^{43} and Sc^{41}, respectively. The active calcium has been found to be due to Ca^{45}, the half-life of which is 2.4 ± 0.2 hours. The thick target yield of this isotope is approximately 9.0×10^6 deuterons per active atom. The 4-hour period has been identified with Sc^{43}, as the intense activity observed when calcium was bombarded with 0.2 microampere of 11 Mev alpha-particles decays with a single period of this value. The yield of Sc^{43} in this reaction is one active atom for 2×10^5 alpha-particles. Ca^{45} has also been produced by activating calcium with slow neutrons and by bombarding titanium with fast neutrons. It is shown that the 16-hour period previously reported was probably due to magnesium or sodium impurity and not to the formation of K^{42}, as the period of this isotope has been found to be 12.2 ± 0.2 hours.

INTRODUCTION

THE isotopes of calcium as given by Aston[1] are as follows:

Mass number	40	42	43	44
Percentage abundance	96.76	0.77	0.17	2.30

As recent work has shown that reactions of the type

$$_zA^N + {}_1H^2 \rightarrow {}_zA^{N+1} + {}_1H^1$$

in which the neutron of the deuteron is captured by the bombarded nucleus (the Oppenheimer-Phillips[2] reaction) are very probable among the elements of medium atomic number, it was anticipated that under bombardment by high speed deuterons the radioactive isotopes Ca^{41} and Ca^{45} would be formed, the former decaying to the stable K^{41} by positron emission and the latter emitting negative electrons to form Sc^{45}. The investigation to be discussed was carried out in order to search for Ca^{41}, for it was thought that a proof that this isotope is positron radioactive would preclude K^{41} as the source of the natural radioactivity of potassium.

APPARATUS

The cyclotron in the radiation laboratory was used as a source of deuterons, alpha-particles and neutrons. The deuterons of 5.5 Mev energy can now be passed into a bombarding chamber which is outside of the wall of the cyclotron and by means of a vacuum gate it is possible to bombard the water-cooled targets without causing the beam of ions to pass through a platinum window. In consequence the actual current arriving at the target has been increased by 50 percent and the total current measured can now be used for activation. In the experiments to be described the bombarding currents varied from 5 to 20 microamperes.

The alpha-particles were produced by replacing the deuterium in the chamber by helium and accelerating the doubly ionized helium ions. In this way a current of 0.2 to 0.3 microampere of alpha-particles with 11 million volts energy was obtained. It is of interest to point out that this current corresponds to the total number of alpha-particles emitted by approximately 4.5 grams of pure radium.

The neutrons were produced by allowing the deuteron beam to fall on a target of pure beryllium. With the new target chamber it is possible to place samples within a few inches of the bombarded beryllium. In consequence a very powerful neutron source was used corresponding to about 10^5 curies of radon plus beryllium. Slow neutron effects were observed by enclosing samples in thick blocks of paraffin wax while fast neutron activities were produced by placing

* Presented before the Physical Society, Pasadena Meeting, Dec. 1936.
† Commonwealth Fund Fellow.
[1] Aston, Proc. Roy. Soc. **A149**, 396 (1935).
[2] Oppenheimer and Phillips, Phys. Rev. **48**, 500 (1935).

the samples in a cadmium box which was surrounded with boron and lithium compounds.

All the observations of the decay of the active bodies were carried out with a Lauritsen type quartz fiber electroscope. Absorption measurements were made by placing aluminum sheets between the source and the window of the electroscope. The experimental points shown on the various curves have all been corrected for the natural leak of the electroscope.

Activation by Deuterons

Preliminary experiments with calcium fluoride targets had shown that the radioactivity induced in calcium by deuteron bombardment is complex in character. Accordingly, in recent experiments, calcite crystals and calcium metal, following activation, have been separated chemically into three fractions containing scandium, calcium and potassium.

Chemical separation

The following procedure[3] was used. The activated target was dissolved in dilute hydrochloric acid, the resulting solution being boiled to expel F^{17}, N^{13}, etc. Excess of ammonium chloride was added to prevent as far as possible the precipitation of calcium as hydroxide in the separation of scandium. A small quantity of aluminum nitrate solution was added, followed by excess of ammonia. The scandium and aluminum were thus precipitated as hydroxides. The precipitate was filtered off and washed thoroughly with ammonia and ammonium chloride solution.

The filtrate was boiled and sodium oxalate gradually added. The precipitated calcium oxalate was filtered off and washed with warm ammonium oxalate (in which scandium oxalate is soluble). The second filtrate was then heated with bromine water until the remaining ammonia was expelled as nitrogen. Finally a little potassium chloride was added and potassium precipitated by the addition of sodium cobaltinitrite reagent.

It was found difficult to separate the potassium free of calcium, as the calcium oxalate precipitate was usually very finely divided and passed through the filter paper. This difficulty has recently been overcome by the use of a very hard filter paper.

As a result of such chemical separations it has been established that most of the activity is due to scandium isotopes.

Decay of the calcium precipitate

The relatively weak calcium activity (intensity $1\frac{1}{2}$ hours after activation 0.05 of the scandium activity) decays with a period of about 2.4 hours. The thick target yield computed for equilibrium by correcting for the finite length of the bombardment is 9.0×10^{8} deuterons per active atom. (Due to several uncertainties, such as the calibration of the electroscope, fluctuations in the bombarding current, etc., values of the yields of active atoms given are somewhat approximate.)

There is, in addition, a trace of a longer period, the initial intensity of which is little greater than the natural leak of the electroscope. On account of statistical fluctuations observations of such a weak activity are difficult to make. However, they have been made and it seems not at all unlikely that it is due to a small amount of scandium contamination, as the period would appear to be of the order 50–90 hours. The initial intensity of this period corresponds to about one percent of the total calcium activity.

By deflecting the particles emitted from the calcium fraction in a magnetic field[4] it has been found that they are negatively charged. Visual observation using a Wilson chamber and a magnetic field have confirmed this fact, though the occurrence of an occasional low energy positron is not precluded. These are probably due to the trace of scandium contamination. Gamma-rays are also emitted, rough absorption measurements in aluminum suggesting that these have an energy less than 0.5 Mev. The absorption curve shows, however, that the range of the electrons in aluminum is 0.89 g/cm² so that by Feather's rule their maximum energy is approximately 1.9 Mev.

Thus the radioactive calcium isotope is probably Ca^{45} produced by the reaction:

$$Ca^{44}+H^{2}\rightarrow Ca^{45}+H^{1}$$

[3] I am grateful to Dr. W. Libby for suggesting this procedure.

[4] I wish to thank Dr. A. H. Snell for assistance with this experiment.

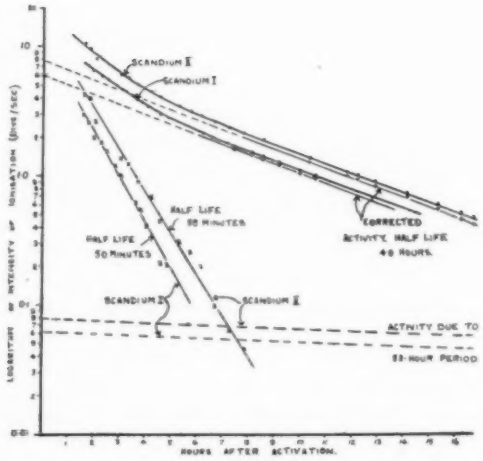

FIG. 1. Decay curves of active scandium separated from calcite crystals after irradiation with deuterons. The points indicated thus: · represent the total activity. Those marked + have been corrected for the activity due to the 52-hour period and the *x*'s are the values obtained after subtraction of both the 52-hour and the 4-hour activities.

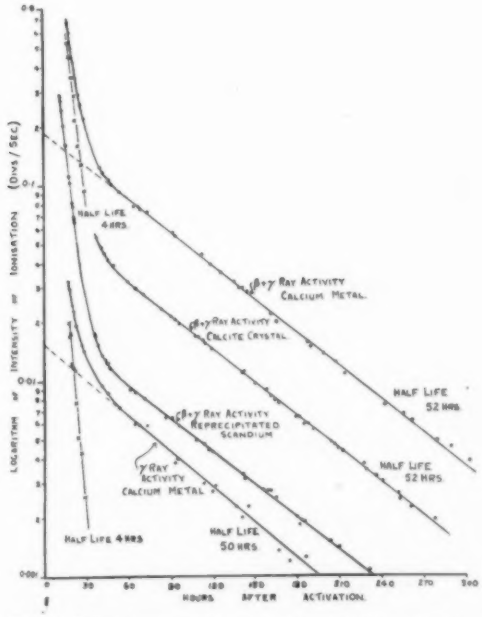
HALF LIFE 4 HRS
β+γ RAY ACTIVITY CALCIUM METAL
β+γ RAY ACTIVITY CALCITE CRYSTAL
HALF LIFE 52 HRS
β+γ RAY ACTIVITY REPRECIPITATED SCANDIUM
HALF LIFE 52 HRS
γ RAY ACTIVITY CALCIUM METAL
HALF LIFE 4 HRS
HALF LIFE 50 HRS
HOURS AFTER ACTIVATION.

FIG. 2. Decay curves of long period activities of various scandium precipitates from calcium activated by deuterons. The *x*'s are the values obtained after subtraction of the corresponding 52-hour activity.

and decaying with a half-life of 2.4 ± 0.2 hours to form the only known stable scandium isotope.

No definite evidence of positrons due to Ca^{41} has been obtained. In view of the very great abundance of Ca^{40} and the high probability of the formation of Ca^{41} by the Oppenheimer-Phillips type of reaction

$$Ca^{40}+H^2\rightarrow Ca^{41}+H^1,$$

this negative result suggests that Ca^{41} is either only just unstable, so that its half-life is very long, or on the other hand, that it is so short lived that its activity has not been detected.

Decay of the scandium precipitate

The decay of the very active scandium precipitate has been observed for more than 300 hours. The curve obtained is readily divisible into three well-defined parts with periods of 53 ± 3 minutes, 4.0 ± 0.1 hours, and 52 ± 2 hours. In Fig. 1 are shown the earlier portions of two such decay curves and it can be seen that there are two periods with half-lives of 4.0 hours and about 53 minutes. The value of the short period is not easily determined accurately on account of having to correct for the two longer periods. In Fig. 2 are shown decay curves of the long period activity. The gamma-ray decay was observed by placing aluminum 0.39 cm in thickness between the active sample and the electroscope window.

The thick target saturation yields corrected for the finite time of bombardment are as follows:

HALF-LIFE	YIELD (Deuterons per active atom)
53 ± 3 minutes	5.4×10^7
4.0 ± 0.1 hours	3.6×10^7
52 ± 2 hours	3.0×10^8

Absorption measurements were made 0.5 hour and 13 hours after the chemical separation was complete. The absorption curves obtained are shown in Fig. 3. It can be seen that the short-lived isotope emits more penetrating beta-rays than the isotope associated with the 4-hour period. The approximate ranges of the beta-rays in aluminum are 0.82 g/cm² and 0.65 g/cm², respectively, corresponding by Feather's rule, to maximum energies of 1.8 Mev and 1.4 Mev. Cloud chamber observations[5] show that the

[5] I am indebted to Mr. L. J. Laslett and Dr. D. Hurst for help with these experiments.

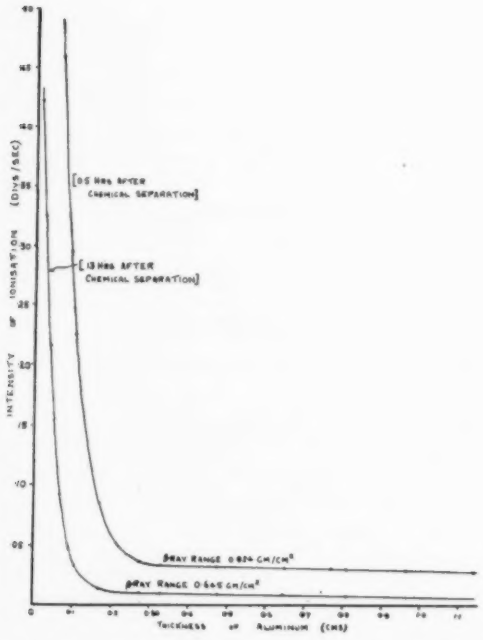
INTENSITY OF IONISATION (DIVS/SEC)
[05 HRS AFTER CHEMICAL SEPARATION]
[13 HRS AFTER CHEMICAL SEPARATION]
β RAY RANGE 0·824 GM/CM²
β RAY RANGE 0·645 GM/CM²
THICKNESS OF ALUMINIUM (CMS)

FIG. 3. Absorption curves of radiations emitted by radioactive scandium precipitates.

emitted particles are mainly positrons, though a few negative electrons were seen. The latter were probably due to Compton recoil electrons from the positron annihilation radiation and to a small amount of contamination from Ca^{45}.

In attempting to identify these radioactive bodies we may make use of the periods of already known unstable scandium isotopes. Zyw[6] has observed an induced radioactivity in potassium when bombarded with alpha-particles which decays to half value in 3 hours. As K^{39} is by far the most abundant isotope it is probable that the activity discovered by Zyw is due to Sc^{42} thus:

$$K^{39}+He^{4}\rightarrow Sc^{42}+n^{1}; \qquad Sc^{42}\rightarrow Ca^{42}+e^{+}.$$

Moreover, von Hevesy[7] has observed a very long lived scandium isotope Sc^{46} when scandium is activated with slow neutrons. The half-life is quoted[8] as being greater than a year.

As the formation of these isotopes under deuteron bombardment would involve the improbable reactions:

$$Ca^{40,\,44}+H^{2}\rightarrow Sc^{42,\,46}+\gamma,$$

in which radiative capture of the deuteron occurred, and as these periods do not agree with the three observed, it seems likely that the deuteron induced radioactivities are due to Sc^{41}, Sc^{43} and Sc^{44} formed by the reactions:

$$Ca^{40,\,42,\,43}+H^{2}\rightarrow Sc^{41,\,43,\,44}+n^{1}, \qquad (I)$$

in which the stable calcium isotopes capture the proton of the deuteron to give rise to the unstable scandium isotopes. As will be shown later the 4-hour period is due to Sc^{43}.

The question of Sc^{41} is of interest, for one would expect that it would decay thus:

$$Sc^{41}\rightarrow Ca^{41}+e^{+}; \qquad Ca^{41}\rightarrow K^{41}+e^{+},$$

resulting in two successive positron emissions and the formation of the unstable Ca^{41} which would then decay to form the only known stable isotope with the mass number 41, K^{41}. Thus one would anticipate that a radioactive calcium isotope would grow in the scandium precipitate. However, no evidence for the decay of Ca^{41} was obtained from the calcium precipitate and no activity could be detected in a calcium oxalate precipitate formed by adding a little inactive calcium chloride to a portion of the original scandium precipitate which had decayed for 14 hours and which was dissolved in dilute hydrochloric acid. Moreover, the reprecipitated scandium decayed in the same manner as the sample which had not been so treated (see Fig. 2.)

Professor Oppenheimer has pointed out that the reaction

$$Ca^{40}+H^{2}\rightarrow Ca^{41}+H^{1}$$

is a very probable one. The fact that no evidence of the decay of this isotope has been observed suggests that it is either nearly stable and of long half-life or so short lived as not to be detectable. The relatively high intensity of the 52-hour period could be explained if this period were associated with Sc^{41} formed thus:

$$Ca^{40}+H^{2}\rightarrow Sc^{41}+n^{1},$$

which then decayed to give the as yet undetected Ca^{41}. The short period of 53 minutes would then be associated with Sc^{44}. Summarizing we may

[6] Zyw, Nature **134**, 64 (1934).
[7] von Hevesy, Nature **135**, 1051 (1935).
[8] Rasetti, *Elements of Nuclear Physics* (Prentice-Hall, 1936), p. 273.

say that there are three periods associated with the scandium precipitate separated chemically from calcium after activation with 5.5 Mev deuterons with half-lives of 53 ± 3 minutes, 4.0 ± 0.1 hours and 52 ± 2 hours. The 4-hour period is due to Sc^{43}, the other periods being probably due to Sc^{44} and Sc^{41} formed by reactions (I).*

Decay of the potassium precipitate

The radioactivity associated with the potassium precipitate is usually masked by contamination of Ca^{45}. Moreover, a sample which showed merely a trace of such short period was only weakly active, the corrected intensity 9 hours after activation being only three times as great as the natural leak of the electroscope. However, the observations fit fairly well a single straight line corresponding to a half-life of 10.5 hours. The intensity of the activity is so small that it may be due to a small amount of some impurity. As, however, the period does not agree with that of any well-known contaminant, it is possible that this radioactive body is an isotope of potassium, in which case it is probably K^{38} produced thus:

$$Ca^{40}+H^2\rightarrow K^{38}+He^4; \qquad K^{38}\rightarrow A^{38}+e^+$$

and decaying by emitting positrons to form A^{38}. The only other radioactive potassium isotope which could be produced is K^{42} by the reaction

$$Ca^{44}+H^2\rightarrow K^{42}+He^4; \qquad K^{42}\rightarrow Ca^{42}+e^-;$$

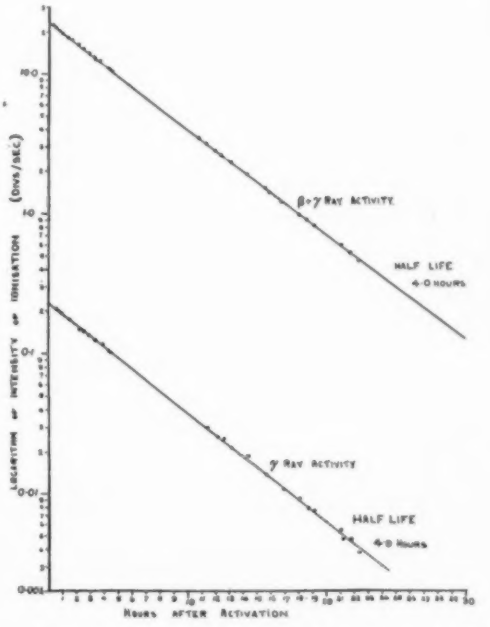

FIG. 4. Decay curve of calcium metal after activation by alpha-particles.

but as will be discussed later the half-life of this isotope is 12.2 hours.

ACTIVATION BY ALPHA-PARTICLES

Frisch[9] has bombarded calcium with alpha-particles and has detected an induced radioactivity, the decay period of which he reported as "4.4 hours with a possible error of 10 percent." He showed that the particles emitted were positrons and from their intensity deduced that the effect was due to Ca^{40}. Chemical tests proved that the active isotope followed the reactions of scandium and he concluded that the activity was due to Sc^{43}. This has been confirmed by Pollard and Brasefield[10] who have detected the protons emitted in the reaction

$$Ca^{40}+He^4\rightarrow Sc^{43}+H^1.$$

The period given by Frisch[9] agrees within the limits of error with the 4-hour period observed with deuterons. It has recently been proved that the two radioactive isotopes are

* *Note added in proof.* Recently radioactive scandium has been separated chemically from potassium fluoride after bombardment with 0.1 microampere of 11 Mev alpha-particles. By deflecting the emitted particles in a magnetic field it has been established that they are positrons. The decay curve shows the presence of two isotopes with half-lives of 4.1 ± 0.2 hours and 52 ± 2 hours. As the long period agrees with that observed in the scandium precipitate from calcium + deuterons it must be associated with Sc^{44} thus:

$$Ca^{43}+H^2\rightarrow Sc^{44}+n^1;\ Sc^{44}\rightarrow Ca^{44}+e^+$$
$$K^{41}+He^4\rightarrow Sc^{44}+n^1.$$

The 4.1 hour period is then due to Sc^{42} produced by the reaction:

$$K^{39}+He^4\rightarrow Sc^{42}+n^1;\ Sc^{42}\rightarrow Ca^{42}+e^+.$$

Thus we have:

Radioactive isotope	Half-life
Sc^{41}	53 ± 3 minutes
Sc^{42}	4.1 ± 0.2 hours
Sc^{43}	4.0 ± 0.1 hours
Sc^{44}	52 ± 2 hours

[9] Frisch, Nature **136**, 220 (1935).
[10] Pollard and Brasefield, Phys. Rev. **51**, 8 (1937).

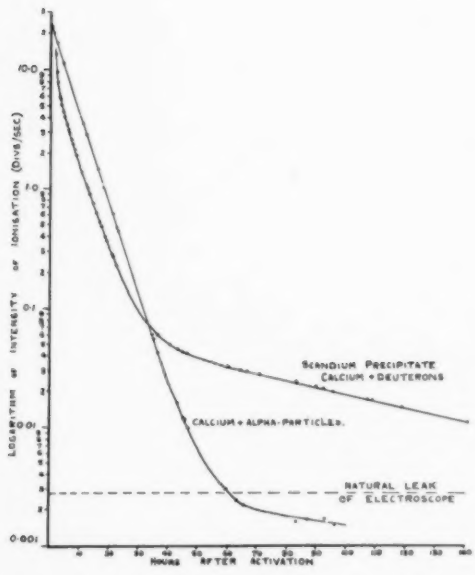

FIG. 5. Comparison between alpha-particle and deuteron induced activities.

identical by repeating Frisch's experiments using the artificially accelerated alpha-particles with 11 million volts energy. A sample of calcium metal was bombarded for about half an hour with 0.2 microampere of the ions and was found to be extremely active (initial intensity $10^5\times$ the natural leak of the electroscope). The activity decayed with a single period the half-life of which is 4.0 hours with an accuracy of about 1–2 percent. The decay curve is shown in Fig. 4.

The thick target saturation yield corrected for the finite period of bombardment is 2×10^5 alpha-particles per active atom.

Absorption measurements show the emitted positrons to have the same range in aluminum as those ejected by the active isotope with the 4-hour period formed by the deuteron activation. It is thus clear that Sc^{43} has been produced by the two reactions:

$$Ca^{42}+H^2\rightarrow Sc^{43}+n^1; \qquad Sc^{43}\rightarrow Ca^{43}+e^+,$$
$$Ca^{40}+He^4\rightarrow Sc^{43}+H^1,$$

its half-life being 4.0 ± 0.1 hours.

There was very little contamination of the alpha-particle beam by deuterons as can be seen from Fig. 5 which shows a comparison between the decay of the deuteron and alpha-particle induced activities. There is evidence of a very weak longer period, the initial intensity of which is 1/100,000 of the initial total intensity. It is probable that this is due to deuterons, though there is no trace of the corresponding short period.

ACTIVATION BY NEUTRONS

Fermi and his co-workers[11] irradiated CaF_2 in water for 14 hours using a strong source of neutrons consisting of 600 millicuries of radon mixed with beryllium but failed to detect any induced radioactivity. On the other hand, Hevesy and Levi[12] irradiated calcium carbonate with neutrons and observed two periods of 4 hours and 16 hours, respectively. In the chemical separation they added sodium chloride to the solution formed by dissolving the irradiated calcium carbonate in dilute hydrochloric acid and after precipitating the calcium as oxalate found the 16-hour activity in the sodium chloride filtrate. The low intensity of the activity they ascribed to the low abundance of Ca^{42}, the reaction postulated being:

$$Ca^{42}+n^1\rightarrow K^{42}+H^1; \qquad K^{42}\rightarrow Ca^{42}+e^-.$$

The author has repeated these experiments on calcium carbonate and has observed such a weak activity. The decay curve obtained is shown in Fig. 6 and is divisible into two portions. The value of the long period, however, was found to be 14.5 hours (corresponding to the 16-hour period reported by Hevesy and Levi[12]) and this is so close to the half-life of Na^{24} (14.8

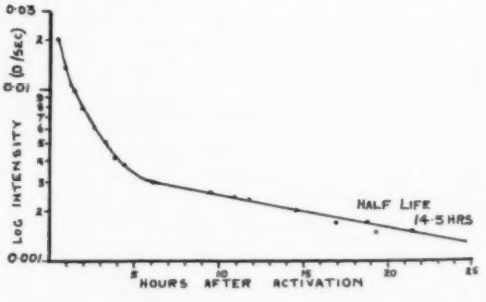

FIG. 6. Decay curve of calcium carbonate following activation by neutrons.

[11] Fermi *et al.*, Proc. Roy. Soc. **A149**, 522 (1935).
[12] Hevesy and Levi, Nature **135**, 580 (1935).

hours[12]) that it is very probably due to the presence of this isotope formed from sodium or magnesium contamination thus:

$$Na^{23}+n^1\rightarrow Na^{24}+\gamma; \qquad Na^{24}\rightarrow Mg^{24}+e^-,$$
$$Mg^{24}+n^1\rightarrow Na^{24}+H^1.$$

The activity is certainly not due to K^{42}, for three samples of potassium salts irradiated with slow neutrons were made strongly radioactive, the decay curves being excellent straight lines corresponding to a half-life of 12.2 ± 0.2 hours.

Calcium metal

On the other hand two samples of calcium metal from different sources when strongly irradiated with slow neutrons were rendered active and, as shown in Fig. 7, the radioactive isotope decays to half-value in 2.4 ± 0.2 hours in agreement with the period of Ca^{45} formed by deuteron bombardment. It was established that this period is not due to silicon present as impurity, for samples of silicic acid were irradiated at the same time and under the same conditions and as can be seen from Fig. 7 the activity induced is only one-fifth as intense as in the calcium. Moreover, the period of Ca^{45}, 2.4 ± 0.2 hours is less than that of Si^{31}, 2.7 ± 0.2 hours.

The weak short-lived activity observed has a half-life close to 30 minutes and may be due to a fast neutron reaction. On the other hand, as the calcium metal was cleaned with hydrochloric acid, this may be due to traces of chlorine contamination. This seems likely, for when calcium metal was bombarded with fast neutrons only a very weak activity was observed, the initial intensity of which was three times as great as the natural leak of the electroscope. There was evidence for a short period, but the shape of the decay curve is such that the activity may well be due to a small number of slow neutrons. There is no evidence for a 12-hour period, which suggests that if the reaction proposed by Hevesy,[12] *viz.*

$$Ca^{42}+n^1\rightarrow K^{42}+H^1$$

occurs at all the resultant activity is so weak that it has not yet been observed.

However, the possibility that the short period is due to a fast neutron disintegration of calcium is not definitely excluded.

[12] Van Voorhis, Phys. Rev. **49**, 889 (1936).

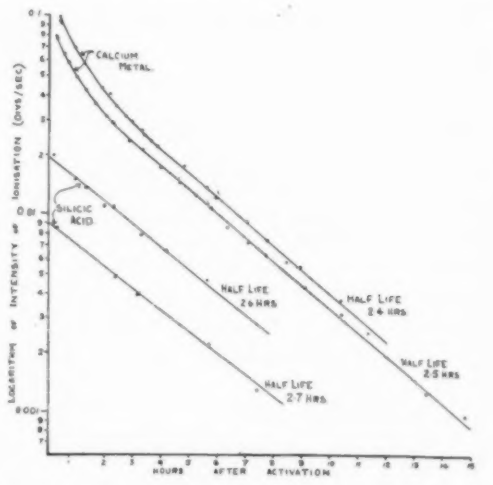

FIG. 7. Decay curves of calcium metal after irradiation with slow neutrons.

Titanium metal

Further evidence confirming the half-life of Ca^{45} has been obtained by bombarding titanium metal with fast neutrons. An analysis of the decay curve of the radioactivity induced shows the presence of a very short period, probably due to Ti^{51} (half-life 3.0 minutes[9]) together with a new period of 2.3 hours which agrees with the half-life of Ca^{45}. As the most abundant isotope of titanium, Ti^{48}, is present to an extent of 78 percent, it appears probable that the reaction:

$$Ti^{48}+n^1\rightarrow Ca^{45}+He^4$$

has been detected.

ACKNOWLEDGMENTS

The author is very greatly indebted to Professor E. O. Lawrence both for the privilege of working in the radiation laboratory and for his continued encouragement. Moreover, it gives the author pleasure to express his appreciation of the friendship and cooperation of the staff of the radiation laboratory and he thanks them for valuable suggestions and discussions. The experimental work has been aided by grants from the Research Corporation, the Chemical Foundation and the Josiah Macy Jr. Foundation.

A New Method of Analysis of the Structure of H_α and D_α

W. V. HOUSTON
California Institute of Technology, Pasadena, California
(Received December 28, 1936)

The interferometer pattern due to a group of spectral lines can be expressed as a Fourier series, and the coefficients of this series can be regarded as the quantities to be measured. These coefficients can also be computed in terms of the positions, intensities, and the parameters describing the shapes of the lines. Although the equations cannot be explicitly solved for the latter quantities in terms of the Fourier coefficients, numerical means can be used to find the parameters which best reproduce the observed values. This method has been applied to two plates of H_α and D_α. The results indicate that to fit the observations with the four strongest lines given by the theory it is necessary to make the separations of the two most intense components some 2 percent less than the theoretical value.

ONE of the principal difficulties in the analysis of fine structure patterns, especially in the light elements, lies in the fact that the widths of the component lines are of the same order of magnitude as their separations. This makes the object under consideration really a continuous spectrum whose intensity distribution must be analyzed, rather than a spectrum of discrete lines. Such a spectrum requires a quite different method of description and must be characterized by a different set of numbers than a true line spectrum. When an interferometer is used to study the spectrum the periodicity of the pattern suggests the use of a Fourier series for describing it, and the method of analysis to be described is one in which the coefficients of this Fourier series are regarded as the characteristics of the spectrum. To compare the observations with spectroscopic theory, however, these characteristic coefficients must be interpreted in terms of intensities and positions of elementary component lines.

METHOD OF ANALYSIS

Consider first the Fabry-Perot interferometer pattern to be expected from a single elementary line. After it has been expressed in terms of intensity as a function of the distance from the center of the pattern, the scale can be made linear by squaring the abscissae. The intensity will then be a periodic function whose period can be determined with considerable accuracy. The range of wave-length represented by the separation of successive orders is called the spectral range and may be designated by s. This quantity is strictly a function of the order of interference, but it varies so slowly that over the three or four orders in which one is usually interested it may be treated as constant. Then let $\theta=2\pi\lambda/s$ be the variable in terms of which the pattern is to be described. θ may be called the angular order of interference.

If the line under consideration were strictly monochromatic, and if the resolving power of the interferometer were infinitely high, the intensity of the pattern would be zero except for a series of points separated by the distance 2π. However, neither of these conditions is satisfied and one needs to consider three principal causes of line breadth.

(*a*) The natural width, due to the finite lifetimes of the states involved, or classically due to the damping of the oscillations, gives a line whose shape is

$$I_n(\theta-\theta_0)=\beta/\{(\theta-\theta_0)^2+\beta\}^2. \qquad (1)$$

θ_0 is the position of the maximum, and β is a constant which depends upon the lifetimes of the initial and final states. The broadening due to collisions gives a line of the same shape so that these two effects can be treated together by giving to β a suitable value.

(*b*) In hydrogen the most important source of broadening is the Doppler effect caused by the motion of the emitting atoms. This gives a line whose form is

$$I_D(\theta-\theta_0)=e^{-\alpha(\theta-\theta_0)}. \qquad (2)$$

The quantity α depends upon the mass of the emitting molecule and the temperature. $\alpha = Ms^2\nu^2/8\pi RT$, where M is the molecular weight, ν is the frequency of the center of the line, R is the gas constant and T is the absolute temperature.

(*c*) The third source of broadening is the finite resolving power of the interferometer. This causes an apparent line form given by

$$I_i(\theta-\theta_0) = 1 + 2\sum_{n=1}^{\infty} r^n \cos n(\theta-\theta_0), \qquad (3)$$

where r is the reflecting power of the interferometer plates.

These three functions can be combined to give the resultant form of the interference fringes due to a single line.

$$J(\theta, \theta_0) = \int_{-\infty}^{\infty} d\theta_2 \int_{-\infty}^{\infty} d\theta_1 I_i(\theta-\theta_2) I_D(\theta_2-\theta_1) \times I_n(\theta_1-\theta_0) \qquad (4)$$

$$= B_0' + \sum_{n=1}^{\infty} (B_n' \cos n\theta + A_n' \sin n\theta),$$

where $B_0' = \pi^{\frac{1}{2}}$, $B_n' = 2\pi^{\frac{1}{2}} r^n e^{-n^2/4\alpha - n\beta} \cos n\theta_0$,

$$A_n' = 2\pi^{\frac{1}{2}} r^n e^{-n^2/4\alpha - n\beta} \sin n\theta_0.$$

These expressions for the coefficients assume a line of unit intensity, and they are of course all proportional to the intensity.

If the pattern is due to a superposition of different elementary lines, the coefficients of the Fourier series (4) are superpositions of contributions from the different lines. Hence

$$B_0 = \pi^{\frac{1}{2}} \sum_{j=1}^{N} I_j,$$

$$B_n = 2\pi^{\frac{1}{2}} r^n e^{-n^2/4\alpha} \sum_{j=1}^{N} e^{-\beta_j n} I_j \cos n\theta_j, \qquad (5)$$

$$A_n = 2\pi^{\frac{1}{2}} r^n e^{-n^2/4\alpha} \sum_{j=1}^{N} e^{-\beta_j n} I_j \sin n\theta_j.$$

In these expressions the subscript j denotes a quantity belonging to the jth elementary line. The quantities I_j are the various intensities.

Eq. (5) is the desired connection between the quantities predicted by the usual spectroscopic theory, and the Fourier coefficients characteristic of the pattern. If all of the theoretical quantities were known it would only be necessary to calculate the Fourier coefficients and compare them with the observed ones. However, the theoretical quantities are not always satisfactorily known. The temperature in a discharge tube is only roughly known; the relative intensities of the lines in a pattern are often dependent upon the conditions of excitation; and the width parameter β is not usually known with any accuracy. Furthermore, although relative positions are usually given by the theory, the origin of θ is not easily determined experimentally. The practical problem is thus to invert the equations (5) and to determine from the observed Fourier coefficients the parameters of the component lines. Of course, this cannot be uniquely done since there is an infinity of coefficients from which to determine a finite number of parameters, and due to experimental errors the coefficients will not be strictly consistent. It is thus necessary to adopt a criterion for what constitutes the best set of parameters and then to find them, essentially by trial.

Let $J(\theta)$ be the interferometer pattern which would be obtained from the assumed parameters, and let $K(\theta)$ be the observed pattern. Let the patterns be expressed as Fourier series in which the coefficients of the observed pattern are designated by asterisks. Then the quantity

$$\Delta = \frac{1}{\pi} \int_0^{2\pi} \{J(\theta) - K(\theta)\}^2 d\theta \qquad (6)$$

may be taken as a measure of the difference between the two curves. By this criterion all parts of the curve of equal extent in θ are given equal weights. The quantity Δ can then be expressed in terms of the Fourier coefficients.

$$\Delta = 2(B_0 - B_0^*)^2 + \sum_{n=1}^{\infty} \{(B_n - B_n^*)^2 + (A_n - A_n^*)^2\}. \qquad (7)$$

The derivative of Δ with respect to any parameter can be determined from this equation, so that after a set of parameters has been tried they can be changed in the proper direction to produce a reduction in Δ. When the derivatives

TABLE I.

PLATE	86				78			
	H_α		D_α		H_α		D_α	
LINE	OBS.	CALC.	OBS.	CALC.	OBS.	CALC.	OBS.	CALC.
B_0	93.28		75.12		103.76		70.10	
B_1	6.07	5.95	1.47	1.28	1.78	2.12	2.28	2.87
B_2	42.81	43.54	56.55	55.42	42.05	41.65	41.04	41.43
B_3	4.86	3.48	7.12	6.47	2.33	1.63	4.55	3.37
B_4	1.49	2.03	6.38	8.77	0.63	1.85	5.00	4.82
B_5	0.14	0.06	−0.08	0.45	−0.65	−0.01	−0.09	0.32
B_6	0.16	0.02	0.77	0.73	−0.30	0.02	−1.12	0.27
A_1	0.63	0.78	1.08	0.57	4.63	4.39	1.84	2.40
A_2	3.19	4.10	2.08	1.53	−0.70	−1.16	4.76	4.91
A_3	−2.24	−3.12	−8.73	−7.15	−1.87	−1.51	1.40	−0.59
A_4	1.22	1.11	4.89	4.28	−0.64	0.52	3.27	2.72
A_5	−0.42	−0.14	0.66	−1.74	−0.18	−0.06	0.67	−0.42
A_6	−0.55	0.01	−0.15	0.43	0.44	0.00	0.13	0.30
Δ	4.78		17.26		4.72		11.38	
r	0.82		0.84		0.70		0.71	
α	1.20		2.30		1.25		2.50	
I_1	100		100		100		100	
I_2	89		96		98		91	
I_3	21		22		21		19	
I_4	12		10		13		11	
θ_1	2°		1°		2°		6°	
θ_2	191°		190°		184.7°		189°	
θ_3	120°		121°		120°		135°	
θ_4	340°		335°		335°		340°	
d	.817872 cm		.817872		.801310		.801310	
$\Delta\nu_0$	.61117 cm^{-1}		.61117		.62380		.62380	
$\Delta\nu_{12}$	.320 cm^{-1}		.320		.317		.317	
$\Delta\nu_{23}$	.120 cm^{-1}		.117		.112		.094	
$\Delta\nu_{14}$	.037 cm^{-1}		.044		.047		.045	
Δp	6.7804				6.6366			
$\Delta\nu$	4.1440 cm^{-1}				4.1399			
e/m	1.7592×10^7				1.7610×10^7			

with respect to all of the parameters are small and change sign with a small change in the parameters, the set of parameters is called the best.

APPLICATION TO H_α AND D_α.

Table I shows the results of the application of this method of analysis to two plates of H_α and D_α. These plates were taken with a grating spectrograph of two meters focal length equipped with a grating of 48,000 lines per inch. This provided enough dispersion to separate the two lines. Intensity marks were photographed on each plate. A microphotometer curve was made of each pattern and this was transformed into a curve of intensity as a function of the distance from the center of the pattern. The abscissae were then squared and two or three orders were averaged together to give the pattern to be analyzed. To permit this averaging it was necessary to apply a correction which took account of the lack of uniformity of illumination of the slit. This correction was determined from the relative intensities of the maxima and minima in successive orders.

To determine the Fourier coefficients, ordinates were taken from the curves at intervals corresponding to 3°. These were multiplied by the corresponding values of the trigonometric functions and the products added. Since the analysis is based on the true Fourier coefficients, and not on a set which will give an exact fit for a certain finite number of ordinates, it is necessary to determine them by a process of integration such as this, rather than by fitting the curve at some selected points. It was concluded from the behavior of the coefficients, that the functions of 6θ could be used, but for higher multiples of θ the coefficients were deemed not to have much significance because of experimental uncertainties.

After the Fourier coefficients had been measured a set of trial parameters was selected. These represented estimates of the breadth parameters and of the positions and intensities of four component lines. The possible fifth line was neglected because of its low intensity. Since the coefficient B_0 is the sum of the intensities, it was used to eliminate the intensity of the first component. From the assumed parameters the corresponding Fourier coefficients were computed, and then either by inspection of the result, or by working out the derivatives of Δ with respect to the various parameters, changes were made and the calculation repeated. By continuing this process the parameters listed in the table were obtained. These are not necessarily the final results which would be obtained if the process were carried out indefinitely, but they make the value of Δ relatively small, and the derivatives of Δ also small. Their accuracy is probably about all that is justified by the accuracy of the photometry.

In this analysis the parameter β was neglected. The natural width of most of the component lines is dominated by the width of the $2p$ level. This is such as to give to β a value of 0.1. However, if all of the component lines have the same value of β the effect on the Fourier coefficients can be produced by a reduction in the reflection coefficient r. Portions of the components designated as 2 and 3 are due, however, to transitions to the $2s$ level. If this level were isolated it would be metastable and very narrow. Since it coincides with the $2p_4$ level it is subject to a

good deal of perturbation, and hence is probably much broadened. For this reason, as well as to avoid the introduction of more parameters than would be justified by the number of usable Fourier coefficients, all of the lines were treated as having the same natural breadth, and this was included in the parameter r.

In the table are listed the observed and computed values of the Fourier coefficients, and the values of the parameters which were used in the computations. For ease in comparison I_1 was set at 100 in each case. d is the separation of the interferometer plates in cm, $\Delta\nu_0$ is the wave number difference corresponding to unit difference in order of interference. This has been corrected for the index of refraction of air. The succeeding $\Delta\nu$'s represent the wave number differences between the components designated by the subscripts. Δp is the difference in order of interference between the two strong components of H_α and D_α and $\Delta\nu$ is the corresponding wave number difference.

The two plates analyzed were taken under slightly different conditions. The interferometer separations were different as indicated. For plate 86 the current density was about 25 ma per sq. cm while for plate 78 it was about 45 ma per sq. cm. The pressure of helium in both cases was about 0.5 mm. The hydrogen pressure was small but unknown since it was due to the dissociation of the water frozen to the walls of the discharge tube. The effect of the difference in current shows up in the different values of r. This indicates a rather considerable broadening due to the increase in current. The values of α correspond to temperatures in the neighborhood of 100°K. The values of $\Delta\nu_{12}$ differ by about 1 percent between the two plates although they are both definitely less than the value 0.328 cm^{-1} given by the theory. To make sure of this difference an attempt was made to use parameters corresponding to this separation in the analysis of D_α on plate 86. The minimum value of Δ which could be obtained in this way was nearly twice the value given in the table.

One might suspect that the difference between the two plates indicates a trend toward the theoretical value as the current is decreased. A study of several more plates will be necessary to establish the presence or absence of such a trend, but the fact that for plate 86 the value of r is as high as can be expected after allowing for the 0.1 taken off by the natural width suggests that in this case the external disturbances have been reduced to a very small value, but that the assumed four-line structure is inadequate to explain the observations if the theoretical separations are to be used. This is in agreement with the previous conclusions of Dr. Hsieh and myself,[1] and of Gibbs and Williams,[2] although Shane and Spedding[3] concluded that they had no evidence of deviations from the theory.

---

[1] Houston and Hsieh, Phys. Rev. **45**, 263 (1934).
[2] Williams and Gibbs, Phys. Rev. **49**, 416 (1936).
[3] Shane and Spedding, Phys. Rev. **47**, 33 (1935).

Resonance Effects in Nuclear Processes

H. A. BETHE
Cornell University, Ithaca, New York
AND
G. PLACZEK
Universitetets Institut for teoretisk Fysik, Copenhagen, Denmark

(Received November 9, 1936)

A general formula is developed for the probability of nuclear processes with particular consideration of resonance (§2). The dependence of the cross section on the energy of the incident particle can be divided into two parts: Firstly, the dependence over energy regions small compared to nuclear energies, and secondly that over large energy regions, of the order of a million volts or more. The first dependence is completely given by the resonance formula; it shows resonance maxima and besides a simple general trend with the particle energy such as the $1/v$ law. The dependence over large energy regions cannot be found without referring to a special nuclear model. (If the problem of nuclei were a one-body rather than a many-body problem, there would be only the dependence over large energy regions. Thus much more theoretical information of a general nature can be obtained for the many-body than for the one-body problem.) The nuclear processes may be divided into several classes according to whether light quanta or material particles are concerned. The selection rules for the various kinds of processes are given (§3). Another useful classification is according to the speed of the particles involved: Slow particles are such whose wave-length is long compared to nuclear dimensions. This means energies below about 300,000 volts for heavy, 1 MV for light nuclei. γ-rays are to be classed as fast particles. When a slow particle *produces* a nuclear reaction, the cross section contains a *factor* $1/v$ (v = velocity of the incident particle) besides the resonance factor; when a slow particle *is produced*, a *factor* v' (v' = velocity of the outgoing particle) appears in the cross section. If the reaction involves only fast particles, the resonance factor is the only significant one; the same is true for the scattering of slow particles. Explicit formulae for the various cases are given. The problem of the wave functions to be chosen for the incident particle is discussed in §4. Arguments are given for using wave functions in a *repulsive* potential, corresponding to the assumption that the particle as a free particle cannot exist inside the nucleus. The "potential scattering" arising as a consequence of this assumption, is discussed and compared to the resonance scattering. In §§5 to 7 the capture of slow neutrons is discussed. The influence of the Doppler effect on the capture cross section is taken into account. Expressions are derived for the activation and for the absorption coefficient with self-indication, both for resonance and for thermal neutrons. These expressions allow for the influence of the line shape in the former case and for the $1/v$ law in the latter. Methods for the determination of the energy, radiation width and neutron width of the compound levels are discussed (§6) and applied (§7) to Ag, Rh, I and Cd. The importance of the interference of several resonance levels is emphasized, particularly for the capture of thermal neutrons. The properties of fast neutrons are briefly discussed (§8). In the case of charged particles (§10), the width of the resonance levels is reduced by the potential barrier. The width of resonance levels observed in the simple capture of protons is found in agreement with reasonable expectations. The widths of the levels in reactions produced by α-particles are probably smaller than has been observed. In the reaction of charged particles with heavy nuclei, no resonance effects can be observed because the energy of the incident particles cannot be defined accurately enough. The photodissociation of nuclei by γ-rays (§11) is not the inverse process of the radiative capture of particles. The cross section for the photodissociation of a heavy nucleus is about 10^{-28} cm² if the energy of the particle produced (neutron) is larger than about 1 MV. This should make the process just observable. The scattering of γ-rays by heavy nuclei has a cross section of the same order which makes it unobservably small compared to the Klein-Nishina scattering.

I. GENERAL THEORY

§1. Introduction

EVEN in the early experiments on the interaction of α-particles and protons with nuclei it was found that scattering and disintegration showed maxima at certain energies which were ascribed to a resonance phenomenon. With improved technique, it was shown that many of these resonances were much sharper than was at first believed. Still more striking resonance effects have been revealed by the more recent experiments with slow neutrons.

The α-particle and proton resonances were formerly interpreted from a one-particle viewpoint, the incident particle being considered as moving in the potential field of the nucleus and as having certain virtual energy levels in that field. However, this picture has proved quite untenable in view of the neutron evidence. In

connection with this evidence, Bohr[1] has emphasized that the problem of nuclear dynamics is essentially a many-body problem and has shown how the experimental results in nuclear physics can be understood from this standpoint.

In particular, the theory of resonance effects is altered in the following way: In the one-particle picture, the distance between adjacent energy levels will be of the order of a few hundred thousand volts, i.e., smaller than, but still comparable to, nuclear binding energies. The width of these resonance levels would be of the same order as their distance apart.[2]

In the many-particle picture the distance between levels decreases extremely rapidly with increasing excitation energy and increasing number of particles in the nucleus.[1] At the same time, the levels are very much sharper than in the one-particle picture. Both spacing and width of the levels are negligibly small compared to nuclear binding energies except for very light nuclei.

This fact causes interesting variations of the probability of nuclear processes over energy regions small compared to nuclear binding energies about which general theoretical information may be obtained. In the one-particle picture, because of the large spacing of the resonance levels the dependence over *small* energy intervals is governed only by trivial factors such as the $1/v$ law for the capture of neutrons.[3] Over *large* energy intervals, the probability depends on the particular model for the process considered.[4]

It is the purpose of this paper to develop the theory of the variations over small energy regions. The formulae obtained are similar to those of Breit and Wigner.[5]

§2. The generalized dispersion formula

The problem of nuclear dynamics is only slightly more general than the ordinary problem of scattering of light. A nuclear process may generally be described as follows: A particle P (e.g., a light quantum, α-particle, proton, neutron, etc.) falls on an initial nucleus A in its ground state. A compound nucleus C is formed. This nucleus then emits a particle Q which may be either of the same or a different kind from the incident particle P. In this process, a residual nucleus B is left which may or may not be in an excited state.

The compound nucleus C possesses a large number of energy levels E_r. It may be considered in a Hohlraum which contains particles of various sorts Q', all of which can interact with the nucleus C. The Hamiltonian $H_{Q'}$ of the interaction depends on the coordinates and possibly on the momenta of particle Q' and on the internal state of the nucleus. Because of this interaction, the nucleus C may emit particles or be formed by the absorption of a particle. The combination of absorption and emission leads to the transformation $A+P\rightarrow C\rightarrow B+Q$ described above. This transformation can occur for any energy of the incident particle P whether E_A+E_P is equal to one of the levels E_r of the compound nucleus or not. This is the case because the levels E_r are broadened by the interaction with the particle-Hohlraum.

According to the foregoing, the problem can be treated by the well-known methods of the Dirac radiation theory. Following the customary procedure, we consider only the second-order perturbation, i.e., the lowest order in which the process $A+P\rightarrow C\rightarrow B+Q$ can occur, and neglect higher orders. This is justified if and only if the widths of all energy levels of nucleus C is small compared to the spacing of the levels.[6, 6a] We

[1] Bohr, Nature **137**, 344 (1936). See also, Bohr and Kalckar, "On the Mechanism of Nuclear Reactions," Kgl. Dansk Vidsk Selsk. Math. Phys. Medd. (1937) where a quantum-mechanical formulation of the general viewpoint developed in the former paper is given, as well as a detailed discussion of a number of typical nuclear reactions from this point of view.

[2] The width would be smaller for charged particles of "medium" energy, i.e., such energy that the penetrability of the Coulomb potential barrier is small compared to unity but still large enough to make the disintegration observable. We shall come back to this case in §10.

[3] Amaldi, d'Agostino, Fermi, Pontecorvo, Rasetti and Segrè, Proc. Roy. Soc. **A149**, 522 (1935); Bethe, Phys. Rev. **47**, 747 (1935); Perrin and Elsasser, Comptes rendus **200**, 450 (1935).

[4] Cf., eg., Ostrofsky, Breit and Johnson, Phys. Rev. **49**, 22 (1936).

[5] Breit and Wigner, Phys. Rev. **49**, 519 (1936).

[6] It might be thought that such a condition would lead to difficulties in the case of the ordinary theory of scattering of light by atoms when the atom has a continuous spectrum. That this is not the case, may be shown by considering, in the usual way, the continuous spectrum as the limiting case of a discrete spectrum, e.g., by considering the atom as enclosed in a Hohlraum of volume Ω. Then the spacing between the atomic energy levels will be inversely propor-

shall show in §4, that this condition is probably fulfilled for our problem but not very well fulfilled for highly excited states of the compound nucleus.

For the present, we assume the perturbation theory to be valid. Then the Dirac radiation theory yields for the probability of the process considered

$$w^{P}{}_{Q}{}^{p}{}_{q}=\frac{2\pi}{h}\left|\sum_{r}\frac{H^{P}{}_{r}{}^{p}H^{r}{}_{Qq}}{E_A+E_P-E_r+i\pi\sum_{Q'q'}|H^{r}{}_{Q'q'}|^2}\right|^2. \quad (1)$$

$H^{P}{}_{r}{}^{p}$ is the matrix element of the interaction between particle P and the nucleus referring to the state r of the nucleus C and to the given state p of the incident particle P. The sum over Q' extends over all kinds of particles which can be emitted by the compound nucleus. The index q' distinguishes various kinetic energies of the outgoing particles Q' which correspond to various excited states of the residual nucleus B. E_A is the energy of the initial nucleus A in the ground state, E_P the kinetic energy of the incident particle and E_r the energy of the state of the compound nucleus considered. In all the matrix elements $H^{Q}{}_{r}{}^{q}$, $H^{Q'}{}_{r}{}^{q'}$ the energy of the particle is determined by the requirement of conservation of energy, e.g., the kinetic energy of particle Q' must be taken as $E_{Q'}(q')=E_A+E_P-E_{B'}(q')$ where $E_{B'}(q')$ is the energy of the nucleus B' in the state in which it is left after the emission of particle Q'. All particle wave functions are normalized per unit energy. The sum over $Q'q'$ in the denominator of (1) represents the total probability of disintegration of the nuclear level r, multiplied by $\hbar$. We shall denote this expression by γ_r, and may consider it as composed of the contributions of the disintegrations with emission of the various sorts of particles Q', *viz.*

$$\gamma_r=\sum_{Q'}\gamma^{r}{}_{Q'}, \quad (2)$$

$$\gamma^{r}{}_{Q'}=\sum_{q'}\gamma^{r}{}_{Q'q'}, \quad (2a)$$

$$\gamma^{r}{}_{Q'q'}=2\pi|H^{r}{}_{Q'q'}|^2. \quad (2b)$$

$\gamma^{r}{}_{Q'q'}/\hbar$ is the probability, per unit time, that nucleus C in state r disintegrates into a particle of kind Q' and a residual nucleus B' in the state defined by q'.

Because of the normalization of the particle wave functions per unit energy, the matrix elements $H^{r}{}_{Qq}$ have the dimension (energy)$^{\frac{1}{2}}$, and therefore the γ's in (2) have the dimension of an energy as it should be. The total expression (1) has the dimension energy^{-1} time^{-1}; it represents the probability that the process $A+P\rightarrow C\rightarrow B+Q$ is caused by a particle P in any of the Hohlraum states of energy around E_P, times the number of Hohlraum states per unit energy. The advantages of the normalization per unit energy are, firstly, that the volume of the Hohlraum does not appear in the formulae, only to drop out in the final result, and secondly, that the disintegration probability of a nuclear state is directly given by the squares of the matrix elements H, without any factors except 2π.

In order to obtain the *cross section* of our process from (1), we have to change from normalization per unit energy to normalization per unit incident current. A plane wave, normalized per unit incident current, has the form

$$\psi_{\text{curr}}=v^{-\frac{1}{2}}e^{ik\cdot r}, \quad (3)$$

where k is the "wave vector" ($k=$ momentum$/\hbar$) and v the velocity. For normalization per unit energy we have

$$\psi_E=\left(\frac{4\pi k^2dk}{(2\pi)^3dE}\right)^{\frac{1}{2}}e^{ik\cdot r}. \quad (4)$$

Using the well-known formula

$$v=dE/\hbar dk \quad (5)$$

we find

$$\psi_{\text{curr}}=\psi_E(2\pi^2\lambda^2\hbar)^{\frac{1}{2}}, \quad (6)$$

where

$$\lambda=1/k \quad (6a)$$

is the wave-length of the incident particle, divided by 2π. Therefore the cross section is

---

tional to Ω. But the same will be true for the radiative width of the levels. This can be seen by using the fact that an electron will only radiate if it comes near the atom, the probability for which is inversely proportional to Ω. The *ratio* of width to spacing is independent of Ω, and very small compared to unity, *viz.* of the order $e^2\omega/mc^2$ for radiation of the frequency ω.

[6a] This condition is also necessary in order to make the width of each level independent of the simultaneous excitation of other levels. For a more detailed discussion, cf. Bethe and Livingston, Rev. Mod. Phys., to appear shortly.

$$\sigma^{PQ^{P}q}=2\pi^2\hbar\lambda^2 w^{PQ^{P}q} \tag{7}$$

$$=4\pi^3\lambda^2\left|\sum_r \frac{H^{Pr^{P}}H^{rQq}}{E_A+E_P-E_r+\frac{1}{2}i\gamma_r}\right|^2. \tag{8}$$

In general, the levels of initial, compound and final nucleus will be degenerate. This fact is considered in detail in the appendix. The result is given in (217). If we transform from the probability to the cross section according to (8), we find

$$\sigma^{PQ^{P}q}=\frac{\pi\lambda^2}{(2s+1)(2i+1)}\sum_{lj l'j' J}(2J+1)\times\left|\sum_r \frac{u^{rA^{J}}{}_{pIlj}u^{rB^{J}}{}_{qI'l'j'}}{E_A+E_P-E_{rJ}+\frac{1}{2}i\gamma_{rJ}}\right|^2, \tag{9}$$

where l, s and j are orbital momentum, spin[7] and total angular momentum of the incident particle; l', s' and j' the same quantities for the outgoing particle; i, J and i' the angular momenta of initial, compound and final nucleus; and prq denote all other quantum numbers of the three nuclei. The letters A, B, P, Q defining the various nuclei and particles precede the indices determining the state of the respective particle. $(u^{rB^{J}}{}_{qI'l'j'})^2$ is the sum of $2\pi|H^{rB^{J}}{}_{q}{}^{M}{}_{I'm'sI'l'j'\mu'}|^2$ over the various magnetic substates $m'\mu'$ of the degenerate final state q, the magnetic substate M of rJ being kept fixed. u is directly connected with the γ by

$$\gamma^{rA^{J}}{}_{pIlj}=(u^{rA^{J}}{}_{pIlj})^2. \tag{10}$$

γ_{rJ} is the total disintegration probability of the level rJ

$$\gamma_{rJ}=\sum_{Q'}\gamma^{rQ'^{J}}=\sum_{Q'q'l'j'}\gamma^{rB'^{J}}{}_{q'l'Q'l'j'}. \tag{11}$$

Formula (9) simplifies considerably if only *one* level rJ of the compound nucleus contributes to the cross section, which will be the case if the energy of the incident particle is sufficiently near the resonance energy $E_{rJ}-E_A$. Then the sum over r reduces to a single term which may be written in the form

$$\sigma^{PQ^{P}q}=\pi\lambda^2\frac{2J+1}{(2s+1)(2i+1)}\times\frac{\gamma^{rP^{J}}{}_{p}\gamma^{rQ^{J}}{}_{q}}{(E_A+E_P-E_{rJ})^2+\frac{1}{4}\gamma^2{}_{rJ}} \tag{12}$$

with $\gamma^{rP^{J}}{}_{p}=\sum_{lj}\gamma^{rA^{J}}{}_{pIlj}=\sum_{lj}(u^{rA^{J}}{}_{pIlj})^2$. (13)

Formula (12) is known as the "one level formula"; it agrees with the formula of Breit and Wigner except for the slightly more complicated statistical weight factor in front, and it is the formula most used in applications.

As already mentioned, the matrix elements $H^{rB^{J}}{}_{qI'Q'l'}$ and therefore $u^{rB^{J}}{}_{qI'Q'l'}$ and $\gamma^{rB^{J}}{}_{qI'Q'j'}$ have to be taken for *that* kinetic energy of the particle Q' for which energy is conserved, *viz.*,[8]

$$E_{Q'}(q')=E_A+E_P-E_{B'}(q'). \tag{14}$$

The γ's will thus be functions of the energy of the incident particle, E_P. If we would insert, instead of the actual particle energy E_P, the energy corresponding to exact resonance with the state r of the compound nucleus, i.e., $E_{rJ}-E_A$, the probability γ_{rJ} would go over into the width Γ_{rJ} of the level rJ. The γ's may therefore be called "effective widths."

The dependence of the γ's and the u's on the energy comes from the normalization of the particle wave function. A wave function of a free particle of orbital momentum l, normalized per unit energy, has the form[9]

$$\psi_P=\left(\frac{2}{\pi}\frac{dk}{dE}\right)^{\frac{1}{2}}\frac{1}{r}\chi_l(kr)\,Y_{lm}(\vartheta,\varphi). \tag{15}$$

Here k is the wave number of the particle,

$$E=(\hbar^2/2m)k^2, \tag{16}$$

its energy, Y_{lm} a normalized spherical harmonic and χ_l *that* solution of the radial wave equation

$$\frac{d^2\chi_l}{dr^2}+\left(k^2-\frac{l(l+1)}{r^2}\right)\chi_l=0, \tag{17}$$

[7] For light quanta, $2s+1=2$ because of the two directions of polarization, but $s=0$ for selection rules (cf. end of appendix). $l=1, 2, \cdots$ for dipole, quadrupole $\cdots$ radiation.

[8] If the nucleus B' is left in an excited state, $E_{Q'}$ is defined only to an accuracy of the order of the width of the level $E_{B'}$. In this case, $u^{rQ'^{J}}{}_{q'}$ and the term $\gamma^{rQ'^{J}}{}_{q'}$ in γ_{rJ} must be averaged over this width. This is, however, of no practical importance.

[9] *Handbuch der Physik* 24/1, p. 292. For our purpose the Coulomb field should be neglected.

which behaves asymptotically as $\sin(kr-\frac{1}{2}l\pi)$. At small r,

$$\chi_l=\frac{1}{1^2\cdot 3^2\cdot\ldots\cdot(2l-1)^2(2l+1)}(kr)^{l+1}. \quad (18)$$

If the wave-length is large compared to nuclear dimensions, the matrix element $\int\psi_A\psi_P H\psi_C d\tau$ contains the wave function ψ_P only for small values of its argument kr. Therefore the matrix element depends on k as

$$(dk/dE)^{\frac{1}{2}}k^{l+1}. \quad (19)$$

This remains true even if one does not use free particle wave functions but rather the wave functions for an attractive or repulsive field of nuclear dimensions. As we shall show in §4, a repulsive field seems to be the most satisfactory assumption. For the present, we assume an arbitrary field, attractive or repulsive, to act on the particle for $r<R$ (R = nuclear radius) while the potential is zero for $r>R$. Then the logarithmic derivative of the wave function χ'/χ will have a certain value κ for $r=R$ which depends on the potential but not sensitively on the kinetic energy of the particle as long as this energy is small compared to the potential. Outside, i.e., for $r>R$, χ will again be a solution of the free particle wave Eq. (17) but in general not the "regular" solution (18) but a linear combination of the regular and the irregular solution. The latter behaves for large r's as $\cos(kr-\frac{1}{2}l\pi)$ and for small values of r as

$$\varphi_l=1^2\cdot 3^2\cdot\ldots\cdot(2l-1)^2(kr)^{-l}. \quad (20)$$

The correct solution which joins smoothly to the interior solution, will have the asymptotic form

$$\sin(kr-\tfrac{1}{2}l\pi+\delta)=\cos\delta\sin(kr-\tfrac{1}{2}l\pi)+\sin\delta\cos(kr-\tfrac{1}{2}l\pi)$$

and therefore the general form

$$\cos\delta\,\chi_l+\sin\delta\,\varphi_l=\cos\delta(\chi_l+\tan\delta\,\varphi_l). \quad (21)$$

Therefore we have for $r=R$

$$\chi'/\chi=(\chi'_l+\tan\delta\,\varphi'_l)/(\chi_l+\tan\delta\,\varphi_l)=\kappa \quad (22)$$

because κ is the value of χ'/χ for the interior wave function. With (18) and (20), we find from (22)

$$\tan\delta=\frac{\chi'_l-\kappa\chi_l}{\kappa\varphi_l-\varphi'_l}=\frac{1}{1^2\cdot 3^2\cdot\ldots\cdot(2l-1)^2(2l+1)}\times(kR)^{2l+1}\frac{l+1-\kappa R}{l+\kappa R}=a(kR)^{2l+1}, \quad (23)$$

where a is a factor of order unity which depends on the special form of the potential acting on the particle but not on k. Since kR is supposed to be small compared to unity, δ will in general be very small. Then $\cos\delta\approx 1$ so that we have from (21), (18) and (20):

$$\chi(R)=\chi_l+a(kR)^{2l+1}\varphi_l=\frac{(kR)^{l+1}}{1^2\cdot 3^2\cdot\ldots\cdot(2l-1)^2(l+\kappa R)}. \quad (24)$$

This depends on the energy as k^{l+1} just as without any potential acting on the particle.

Since dE/dk is proportional to k (cf. 16), the matrix element is, according to (19), proportional to k^{l+1}. Thus we may write

$$u^r{}_{Q^J{}_q}=b^r{}_{Q^J{}_q}k^{l+\frac{1}{2}}=b^r{}_{Q^J{}_q}\lambda^{-(l+\frac{1}{2})} \quad (25)$$

and, because of (13)

$$\gamma^r{}_{Q^J{}_q}=(b^r{}_{Q^J{}_q})^2\lambda^{-(2l+1)}. \quad (25a)$$

However, if the wave-length is long, only the partial wave $l=0$ is of any importance. Therefore, for long particle wave-length, the important u's behave as $k^{\frac{1}{2}}$ which is proportional to $v^{\frac{1}{2}}$ so that

$$u^r{}_{Q^J{}_q}=b^r{}_{Q^J{}_q}\lambda^{-\frac{1}{2}}=a^r{}_{Q^J{}_q}v^{\frac{1}{2}}=c^r{}_{Q^J{}_q}E^{\frac{1}{2}}, \quad (26)$$

where abc are constants independent of the energy of the particle.

For fast particles, the dependence of u on the energy is not quite so simple because formula (18) for χ_l can no longer be used throughout the nucleus. Moreover, orbital momenta larger than zero will become important. Formula (26) can, however, be safely applied for neutrons and protons if the energy does not exceed about 300,000 volts for interaction with heavy nuclei, and about 1 MV for light nuclei. For α-particles, the limits are one-quarter of these figures.

The nonapplicability of (26) for fast particles does not cause any difficulties for our purposes. If the energy of the incident particle is as large as a few hundred thousand volts or more, we restrict ourselves to variations of the energy small compared to the energy of the incident particle itself (cf. the program outlined in §1). Then the variation of k^{l+1} in (25) is negligible, and although u is no longer given by (25), the order of magnitude of its variation with energy will be the same and will therefore also be negligible. We may then replace the u by its value for exact resonance, $U^r{}_{P^J{}_p}$. This is equivalent to the replacement of the effective width γ by the "true width" Γ discussed above, since by definition $u^2=\gamma$, $U^2=\Gamma$.

Alternatively,[10] we may still retain formally the relations (25) (25a) with the only difference that b is now no longer exactly constant but varies slowly with the energy. This variation is again outside the scope of our considerations

[10] This alternative is useful in order to write the same formulae for fast and slow particles.

because it is only appreciable over energy regions of the order of nuclear energies.

The restriction to variations of the energy small compared to a few hundred thousand volts, is quite irrelevant for heavy nuclei, since in this case the compound nucleus possesses very narrowly spaced energy levels in the energy region considered, i.e., about 10 MV above its ground state.[1] For light nuclei, cases may arise where the spacing between the resonance levels is more than a few hundred thousand volts, in this case no simple dependence of the cross section on the energy for fast particles can be deduced from our considerations.

The true widths Γ and the U's may also be introduced for slow particles. In this case, since $l=0$, we have from (26)

$$u^{r}{}_{Q}{}^{J}{}_{q}=U^{r}{}_{Q}{}^{J}{}_{q}(\lambda^{r}{}_{Q}{}^{J}{}_{q}/\lambda)^{\frac{1}{2}}=U^{r}{}_{Q}{}^{J}{}_{q}(E/E^{r}{}_{Q}{}^{J}{}_{q})^{\frac{1}{2}}, \quad (27a)$$

$$\gamma^{r}{}_{Q}{}^{J}{}_{q}=\Gamma^{r}{}_{Q}{}^{J}{}_{q}(\lambda^{r}{}_{Q}{}^{J}{}_{q}/\lambda)=\Gamma^{r}{}_{Q}{}^{J}{}_{q}(E/E^{r}{}_{Q}{}^{J}{}_{q})^{\frac{1}{2}}, \quad (27b)$$

where $\lambda^{r}{}_{Q}{}^{J}{}_{q}$ and $E^{r}{}_{Q}{}^{J}{}_{q}$ are the wave-length and energy corresponding to exact resonance.

These formulae are directly applicable only if the energy of particle Q corresponding to exact resonance, $E^{r}{}_{Q}{}^{J}{}_{q}=E_{rJ}-E_{B}(q)$ is positive and not too large. If the resonance energy is negative, the true width is zero.[11] However, a quantity $\Gamma^{r}{}_{Q}{}^{J}{}_{q}$ may be defined such that (27b) holds, and this Γ has *cet. par.* the same magnitude as if the resonance energy were $|E_Q|$ instead of $-|E_Q|$. For $\lambda^{r}{}_{Q}{}^{J}{}_{q}$ we have also to insert the wave-length for the energy $|E_Q|$. The same argument holds for U.

We shall now consider the case of light quanta. For dipole radiation, the γ's have the familiar form

$$\gamma^{r}{}_{Q}{}^{J}{}_{q}=\lambda^{-3}(b^{r}{}_{Q}{}^{J}{}_{q})^{2}, \quad (28)$$

where the magnitude of the b's is related to the matrix elements of the electric moment vector X by

$$(b^{r}{}_{Q}{}^{J}{}_{q})^{2}=\tfrac{2}{3}|X^{r}{}_{Q}{}^{J}{}_{q}|^{2}, \quad (29)$$

while the sign of b may be found from the explicit evaluation of the matrix elements of the electric moment.[12] The u's may be expressed by the b's

$$u^{r}{}_{Q}{}^{J}{}_{q}=b^{r}{}_{Q}{}^{J}{}_{q}\lambda^{-\frac{1}{2}}. \quad (30)$$

As in (27), we may express u and γ by the quantities U and Γ for exact resonance, *viz.*

$$\begin{aligned} u^{r}{}_{Q}{}^{J}{}_{q}&=U^{r}{}_{Q}{}^{J}{}_{q}(\lambda^{r}{}_{Q}{}^{J}{}_{q}/\lambda)^{\frac{1}{2}},\\ \gamma^{r}{}_{Q}{}^{J}{}_{q}&=\Gamma^{r}{}_{Q}{}^{J}{}_{q}(\lambda^{r}{}_{Q}{}^{J}{}_{q}/\lambda)^{2}. \end{aligned} \quad (31)$$

For quadrupole radiation, similar formulae hold; only the exponent of λ is 5/2 instead of 3/2.

To derive these formulae, we may again use (19) but we must consider that for light dE/dk is independent of k, *viz.*, equal to hc. Moreover, the interaction with particles is not proportional to the density of the light quanta but to the electric field strength $\mathbf{E}$. For unit density of light quanta we have $\mathbf{E}^{2}/8\pi=h\nu$; therefore $\mathbf{E}\propto\nu^{\frac{1}{2}}\propto k^{\frac{1}{2}}$, which introduces another factor $k^{\frac{1}{2}}$ in the matrix element. The matrix element is therefore proportional to $k^{l+\frac{1}{2}}=\lambda^{-(l+\frac{1}{2})}$, which is $\lambda^{-\frac{1}{2}}$ for dipole radiation ($l=0$) and $\lambda^{-5/2}$ for quadrupole radiation. We may *formally* retain the same formula for light as for particles if we arbitrarily determine that, for light quanta, l shall denote the total momentum j rather than the orbital momentum; since the total momentum is one unit larger than the orbital momentum (cf. appendix, end; j is 1, 2, $\cdots$ for dipole, quadrupole . . . radiation), we thus come back to our previous formulae. This is, however, entirely accidental. The dependence of u and γ on the wave-length of the γ-rays is of no practical importance, for the same reasons as discussed for fast particles.

If we insert (25) and (30) into (9) we find for the cross section corresponding to the transition from a definite l to a definite l':

$$\sigma^{P}{}_{Q}{}^{p}{}_{q}{}^{l}{}_{l'}=\frac{\pi}{(2s+1)(2i+1)}\lambda^{1-2l}\lambda^{l'-1-2l'}\sum_{J_{11'}}(2J+1)\times\left|\sum_{\tau}\frac{b^{r}{}_{A}{}^{J}{}_{p_{1}P_{11}}b^{r}{}_{B}{}^{J}{}_{q_{1}'Q_{11'}}}{E_{A}+E_{P}-E_{rJ}+\frac{1}{2}i\gamma_{rJ}}\right|^{2}, \quad (32)$$

$$\begin{aligned} b^{r}{}_{A}{}^{J}{}_{p}\ldots&=U^{r}{}_{A}{}^{J}{}_{p}\ldots(\lambda^{r}{}_{A}{}^{J}{}_{p})^{l+\frac{1}{2}},\\ b^{r}{}_{B}{}^{J}{}_{q}\ldots&=U^{r}{}_{B}{}^{J}{}_{q}\ldots(\lambda^{r}{}_{B}{}^{J}{}_{q})^{l'+\frac{1}{2}}, \end{aligned} \quad (32a)$$

[11] This is not strictly correct. It is true that a negative energy level of nucleus C would have exactly zero width if only particles of kind Q could be emitted. However, in reality there is always a finite probability of emission of particles other than Q, at least the emission of γ-rays is possible in any case. This possibility broadens the negative energy level of the nucleus, and the broadened level may extend into the region of positive energies. For this reason, also the emission of a particle of kind Q by the negative level becomes possible so that the emission of Q may give some contribution to the true width of the negative level. However, this contribution has no relation to the $\Gamma^{r}{}_{Q}{}^{J}{}_{q}$ used in (27b.)

[12] Cf. Placzek, *Handbuch der Radiologie*, second edition, Vol. 6/2, p. 245, formula (27), or appendix of this article.

where λ and λ' are the wave-lengths of incident and outgoing particle, l and l' the corresponding orbital momenta and s, s' the spins. i, J and i' are the angular momenta of initial, compound and final nucleus. b is defined in (25) and (30) and γ in (11). The b's are exact constants if the wave-length of the particle is long compared to nuclear dimensions, while for short wave-length they are slowly varying functions of the energy, the variation being irrelevant for our considerations (see above). In the case of long wave-length, only $l=0$ is important for particles and $l=1$ for light. If only one level of the compound nucleus is important, (32) reduces similarly to (9), to the "one-level formula"

$$\sigma^{P}{}_{Q^{p}{}_{q}{}^{l}{}_{l'}}=\frac{\pi}{(2s+1)(2i+1)}\frac{(\lambda^{r}{}_{P^{J}{}_{p}})^{2l+1}}{\lambda^{2l-1}}$$

$$\times\left(\frac{\lambda^{r}{}_{Q^{J}{}_{q}}}{\lambda'}\right)^{2l'+1}\frac{\Gamma^{r}{}_{P^{J}{}_{pl}}\Gamma^{r}{}_{Q^{J}{}_{ql'}}}{(E_{A}+E_{P}-E_{rJ})^{2}+\frac{1}{4}\gamma^{2}{}_{rJ}}, \quad (33)$$

where

$$\Gamma^{r}{}_{P^{J}{}_{pl}}=\sum_{j}(U^{r}{}_{A^{J}{}_{p}jP\,lj})^{2} \quad (33a)$$

is that part of the true width of the level rJ which corresponds to the emission of particles of sort P with orbital momentum l such that the residual nucleus A is left in state p.

Formulae (32), (33) solve the problem stated at the beginning of this section. They express the cross section of nuclear processes in terms of constants (or, in the case of fast particles, quantities varying only over energy regions of the order of nuclear energies) and of simple functions of the energy of the incident particle.

§3. The processes of nuclear dynamics

For the discussion of (32), (33), we may systematize the nuclear processes according to two schemes. Firstly, we may distinguish according to the particles involved, and secondly, between fast and slow particles.

According to the particles involved, we have four groups of processes:

(1) Incident: light quantum, outgoing: light quantum. Scattering of γ-rays.

(2) Incident: light quantum, outgoing: corpuscle.[13] Photodissociation.

(3) Incident: corpuscle, outgoing: light quantum. Radiative capture.

(4) Incident: corpuscle, outgoing: corpuscle.

(a) Outgoing corpuscle same kind as incident. Elastic and inelastic scattering.

(b) Outgoing corpuscle different from incident. Corpuscle transmutation.

The distinction between the types 1 to 4 of processes is of importance primarily for the selection rules. *The selection rules* for the compound nucleus and either initial or final nucleus are

$$|i-J|\leqslant j\leqslant l+s,\quad i+J\geqslant j\geqslant|l-s|. \quad (34)$$

The parity (even or odd character) of the states of the two nuclei is the same if l is even, and is different if l is odd.

Between initial and final nucleus, we have the selection rule

$$|i'-i|\leqslant l+l'+s+s', \quad (35)$$

$i'+i$ must be larger than or equal to the smallest difference between any of the numbers $|l-s|\cdots l+s$ and any of the numbers $|l'-s'|\cdots l'+s'$. The parity remains unchanged if $l-l'$ is even and changes if $l-l'$ is odd.

(35) represents the selection rules between initial and final nucleus, if states of the compound nucleus with *every* J value possible according to (34) contribute to the cross section. If this is not the case, a more stringent rule than (35) applies which may be found directly from (34) considering the contributing states of the compound nucleus.

For radiation, $s=0$ and $l=1$ for dipole, $l=2$ for quadrupole radiation (cf. appendix). For corpuscles, the selection rules are simplified if the corpuscles are slow (λ large compared to nuclear dimension) because then $l=0$.

The more important selection rule is the one determining the J of the compound nucleus. In the case of incident radiation or slow corpuscles, the explicit selection rules are given in Table I.

According to *velocities*, we distinguish between slow and fast particles. We call a particle "slow" if its wave-length is large compared to nuclear dimensions. For corpuscles this means that the energy must be small compared to a few hundred

[13] We denote by "corpuscle" a material particle, while the term "particle" shall, in this section, include light quanta.

thousand volts. γ-rays are always to be considered as fast.

A. Incident particle fast, outgoing particle fast. —In this case, the variation of the λ-factors in (32) with energy is negligible, and the λ's may be replaced by the corresponding resonance λ's. Introducing the quantity U (cf. (25), (27a)) we have then

$$\sigma^{P}{}_{Q^{P}{}_{q}}=\frac{\pi}{(2s+1)(2i+1)}\lambda^{2}\sum_{ij\Gamma'j'J}(2J+1)\times\left|\sum_{r}\frac{U^{r}{}_{A}{}^{J}{}_{pPl_{s}}U^{r}{}_{B}{}^{J}{}_{qQ^{l's'}}}{E_{A}+E_{P}-E_{r}+\frac{1}{2}i\gamma_{rJ}}\right|^{2}. \quad (36)$$

This formula applies to the scattering of γ-rays,[14] to the capture and the elastic scattering of fast corpuscles. To the photodissociation, the inelastic scattering of fast corpuscles and the particle transmutation produced by fast corpuscles it applies if the outgoing corpuscle is fast.

TABLE I. *Selection rule between initial and compound nucleus.*

PARTICLE	J	SPECIAL RULES	PARITY
Light, dipole radiation	$i, i\pm1$	$0\to0$ forbidden	changes
Light, quadrupole rad.	$i, i\pm1, i\pm2$	$0\to0$, $0\to1$, $\frac{1}{2}\to\frac{1}{2}$ forbidden	unchanged
Slow protons or neutrons	$i\pm\frac{1}{2}$	—	unchanged
Slow α-particles	i	—	unchanged
Slow deuterons	$i, i\pm1$	$0\to0$ forbidden	unchanged

[14] Formula (36) differs from the Kramers-Heisenberg formula in three respects: Firstly, the apparent dependence on λ is different; secondly, it contains for each rJ only a term with the difference of the incident energy $h\nu$ and the resonance energies E_r-E_A while the Kramers-Heisenberg formula contains also another term with denominators of the form $E_r-E_A+h\nu$. Thirdly, in (36) the scattering amplitudes due to states with different J do not interfere. The correct dependence on wave-length is given in the original formula (32). However, as we have mentioned above, this dependence is negligible for our purpose. The terms with $E_r-E_A+h\nu$ have purposely been neglected in (1) because they are of no practical importance in all cases we are interested in. For particles, E_r-E_A and E_P are each of the order Mc^2 where M is the mass of particle P. Therefore the terms with the sum in the denominator are entirely negligible (Besides, even the occurrence of these terms for particles is theoretically doubtful). In the case of γ-rays, the circumstances are not quite so extreme; but we may still neglect the sum terms because in this paper we deal only with processes leading to highly excited states of the compound nucleus. Then $h\nu$ and E_r-E_A are of the order 10 MV. On the other hand, the terms which give the main contributions to (36) contain energy differences of the order of the distance between neighboring energy levels of the compound nucleus which is very small compared to 10 MV. The third difference mentioned above is connected to the second because interference between the scattering amplitudes due to different J's occurs in the Kramers-Heisenberg formula only because of the presence of the "sum terms."

The cross section (36) shows resonance maxima, which, for heavy nuclei, occur at frequent intervals. Apart from these maxima, there is no general trend of the cross section as a function of energy over regions small compared to nuclear energies, since the variation of λ over such regions is negligible.

The total actual width γ_{rJ} is given by (11). In this formula, we may replace the contributions $\gamma^{r}{}_{Q'}{}^{J}{}_{q'}$ by their values at exact resonance for all those emitted particles Q' which have high energy. It is, however, possible that the compound nucleus may also be capable of emitting slow particles. This may, e.g., happen if γ-rays are scattered by a nucleus which at the same time may be dissociated by these γ-rays with the emission of a slow corpuscle. The contributions $\gamma^{r}{}_{Q'}{}^{J}{}_{q'}$ due to these slow particles depend sensitively on the energy. Formula (11) may thus be rewritten

$$\gamma_{rJ}(E_P)=\sum_{\substack{\text{fast}\\\text{particles}}}\Gamma^{r}{}_{Q'}{}^{J}{}_{q'}+\sum_{\substack{\text{slow}\\\text{particles}}}(c^{r}{}_{Q'}{}^{J}{}_{q'})^{2}E_{Q'q'}{}^{\frac{1}{2}}, \quad (37)$$

where $E_{Q'}$ depends on the energy of the incident particle according to (14). If no slow particles are emitted, or if, as is true in most cases, the second sum is negligible compared to the first by virtue of the small factors $E_{Q'}{}^{\frac{1}{2}}$, the total actual width γ_{rJ} may be replaced by the total true width Γ_{rJ} which is independent of E_P. However, it may occur that the coefficients $c^{r}{}_{Q'}{}^{J}{}_{q'}$ are very large, so that the second sum becomes comparable to the first.

B. Incident particle slow, outgoing particle fast. —The variation of λ' in (32) with energy is negligible. For the incident particle, $l=0$ and $j=s$. We have then

$$\sigma^{P}{}_{Q^{P}{}_{q}}=\frac{\pi}{(2s+1)(2i+1)}\lambda\sum_{J\Gamma'j'}(2J+1)\times\left|\sum_{r}\frac{b^{r}{}_{P}{}^{J}{}_{p}\,U^{r}{}_{B}{}^{J}{}_{qQ\Gamma'j'}}{E_{A}+E_{P}-E_{r}+\frac{1}{2}i\gamma_{rJ}}\right|^{2}. \quad (38)$$

This formula applies to the radiative capture of slow particles, and to transmutations produced by slow particles. It is important mainly for slow neutron phenomena, and also for the disintegration of very light nuclei by slow protons.

Apart from the resonance maxima, the cross section is proportional to the wave-length λ of the incident particle. For very small energies, there will always be a region in which the factor λ is predominant ("1/v law"). How small these energies must be, depends on the spacing and width of the resonance levels. These questions and their application on slow neutrons will be discussed in detail in §5. γ_{rJ} is again given by

(37) and may be replaced by $\Gamma_{\tau J}$ if the contribution of the incident particle (and possibly other slow particles which may be emitted by the compound nucleus) to γ is small compared to the total $\gamma_{\tau J}$.

C. Incident particle fast, outgoing particle slow. —The cross section is

$$\sigma^{P}{}_{Q}{}^{p}{}_{q}=\frac{\pi}{(2s+1)(2i+1)}\frac{\lambda^2}{\lambda'}\sum_{Jlj}(2J+1)\times\left|\sum_{\tau}\frac{U^{\tau}{}_{A}{}^{J}{}_{pPlj}\,b^{\tau}{}_{Q}{}^{J}{}_{q}}{E_A+E_P-E_\tau+\frac{1}{2}i\gamma_{\tau J}}\right|^2. \quad (39)$$

(39) applies to photodissociation with the emission of a slow particle, and to particle transmutations and inelastic scattering if the incident particle is fast and the outgoing one slow. Apart from resonance, the cross section decreases as the velocity of the outgoing particle, i.e., as $(E_P+E_A-E_B)^{\frac{1}{2}}$. About the width γ, see case *A*.

D. Incident particle slow, outgoing particle slow. —We have

$$\sigma^{P}{}_{Q}{}^{p}{}_{q}=\frac{\pi}{(2s+1)(2i+1)}\frac{\lambda}{\lambda'}\sum_{J}(2J+1)\times\left|\sum_{\tau}\frac{b^{\tau}{}_{P}{}^{J}{}_{p}\,b^{\tau}{}_{Q}{}^{J}{}_{q}}{E_A+E_P-E_\tau+\frac{1}{2}i\gamma_{\tau J}}\right|^2. \quad (40)$$

This cross section is, apart from resonance, proportional to the ratio of the velocities of outgoing and incident particle. For $\gamma_{\tau J}$ the arguments given in *A* apply again, because there is, besides the possibility of emission of slow particles, always the possibility of emission of γ-radiation, and in some cases of fast corpuscles.

(40) applies to transmutations in which both the incident and the outgoing particle are slow. By far the most important case is the elastic scattering of slow particles. In this case, the cross section does not depend on λ except for the resonance factor.

There is also some simplification of the formula (40) for the case of elastic scattering of slow particles,[15] because in this case $b^{\tau}{}_{P}{}^{J}{}_{p}=b^{\tau}{}_{Q}{}^{J}{}_{q}$. Only the square of b occurs in the cross section while the sign of b does not matter. b^2 may be expressed by Γ according to (25a), (27b), and we have

$$\sigma^{P}{}_{P}{}^{p}{}_{p}=\frac{\pi}{(2s+1)(2i+1)}\sum_{J}(2J+1)\times\left|\sum_{\tau}\frac{\Gamma^{\tau}{}_{P}{}^{J}{}_{p}\,\lambda^{\tau}{}_{P}{}^{J}{}_{p}}{E_A+E_P-E_{\tau J}+\frac{1}{2}i\gamma_{\tau J}}\right|^2. \quad (41)$$

It must be noted that all formulae for the cross section refer to a coordinate system in which the *center of gravity* of incident particle and nucleus is *at rest*. To obtain the cross section in the system of the observer we have to multiply by the ratio of the incident currents in the two systems, i.e., by $v_{\text{center of gravity}}/v_{\text{observer}}$. In the case *B* discussed above, we have therefore to put the factor λ in (38) equal to $\hbar/M_{\text{red}}v_{\text{obs}}$ where M_{red} is the reduced mass and v_{obs} the velocity relative to the observer, while all the other quantities in (38) are to be taken in the center of gravity system. In the particular case of the $1/v$ law, the cross section is therefore independent of the velocity of the initial nucleus. If the $1/v$ law does not hold, the motion of the initial nucleus has an effect on the phenomena with slow incident particles.[16]

In concluding this section, we may say a few words about *inverse processes*. For a given process $A+P\rightarrow B+Q$ and its inverse we have the statistical relation

$$g_{BQq}\sigma^{B}{}_{A}{}^{Q}{}_{P}{}^{q}{}_{p}\lambda_{Qq}{}^{-2}=g_{APp}\sigma^{A}{}_{B}{}^{P}{}_{Q}{}^{p}{}_{q}\lambda_{Pp}{}^{-2}. \quad (42)$$

However, it must be kept in mind that the concept of inverse processes has only limited applications. If we take a given incident particle with given velocity, the outgoing particle Q may, in general, have any of a great number of different energies, corresponding to different states of the resultant nucleus B. The only inverse process which can be produced experimentally, is that starting from nucleus B in the ground state, and the particle Q with the corresponding kinetic energy. This process will, again, lead to many different energies of particle P and different excited states of nucleus A. Therefore only a

[15] A similar simplification of (36) for the elastic scattering of *fast* particles is not possible because (36) contains b's referring to different lj and $l'j'$ so that the numerator of (36) does not reduce simply to a square, even for elastic scattering. The only exception is the scattering of γ-rays for which only the term $l=1$, $j=1$ is important so that a formula similar to (41) holds.

[16] A discussion of these effects will be given in a paper by Placzek and Teller, to appear shortly in the Phys. Rev.

small, very often a negligible, part of the experimentally observed cross section in the process $A+P\rightarrow B+Q$, is related by (42) to a part of the cross section in process $B+Q\rightarrow A+P$. Only for light nuclei, where the number of levels is small, inverse processes can be observed. Even here, it is necessary to make sure in every case that the processes compared lead to the ground states of the respective final nuclei.

§4. Particle wave functions and potential scattering[17]

We have shown in the preceding sections how the probability of nuclear processes may be reduced to the knowledge of certain matrix elements H or U. We shall now discuss how these matrix elements are to be calculated from the wave functions of the nuclei A B C and of the particle (P or Q).

The matrix element $H^{p}{}_{r}{}^{p}$ is

$$H^{p}{}_{r}{}^{p}=\int \psi_{Ap}\psi_{Pp}H\psi_{Cr}{}^{*}d\tau, \qquad (43)$$

where ψ_{Ap} is the eigenfunction of the initial nucleus A in state p, ψ_{Cr} that of the compound nucleus in state r, ψ_{Pp} that of the incident particle and H the Hamiltonian of the interaction between incident particle and initial nucleus. If the nuclear forces are known, H is given; and by solving the Schrödinger equation the nuclear wave functions ψ_{Ap} and ψ_{Cr} may be obtained without ambiguity. Thus the only factor in (43) about which doubt may arise, is the particle wave function ψ_{Pp}.

We know about ψ_{Pp} its asymptotic behavior at infinity: it is a plane or spherical wave, normalized per unit energy. However, in (43) we need the wave function ψ_{Pp} *inside* the nucleus. To obtain ψ_{Pp} inside, we may suppose that it is the solution of a Schrödinger equation with a certain potential $V(r_P)$. This assumption is convenient in order to make the functions ψ_{Pp}, corresponding to different states p of the particle, orthogonal to each other. At large distances r_P from the nucleus, the potential $V(r_P)$ will of course be zero if the particle is a neutron, and it will be the Coulomb potential for charged particles.

About the behavior of the potential V *inside* the nucleus, three different assumptions may be made:

(a) V is negative (attractive potential),
(b) V is zero (free particles),
(c) V is positive (repulsive potential).

Assumption (c) expresses the idea that the nucleus is (practically) impenetrable for incident particles: This is quite plausible, because a particle falling on the surface of a nucleus will give part of its energy to the nuclear particles and will thus become amalgamated with the initial nucleus, forming the compound nucleus. This will prevent the particle from traversing the nucleus unperturbed. This assumption (c) seems most in accord with the general ideas of the compound nucleus.

Previously it has been argued (cf. references 3 and 5) that the most obvious choice of the particle potential $V(r)$ is to take it equal to the average potential energy of the particle in the field of the initial nucleus A, i.e.,

$$V(r_P)=\int H(r_A, r_P)\,|\psi_{Ap}(r_A)|^{2}d\tau_A \qquad (44)$$

where r_A denotes all the coordinates of the particles inside nucleus A. This average potential is certainly attractive. However, we shall show in the following that assumptions (a) and (b) are to be rejected in favor of (c).

The three assumptions (a), (b) and (c) will give widely different results for the matrix elements H, or the widths γ. Obviously, (a) will in general give the largest result because with assumption (a) we may have a resonance phenomenon already for the incident particle.[3] If such a one-body-resonance occurs, ψ_{Pp} will evidently be very large inside the nucleus and therefore the matrix element H will be large. On the other hand, assumption (c) will give the smallest matrix elements: In case (*c*), the wave function ψ_{Pp} will decrease exponentially as we go from the surface of the nucleus inside. The rate of decay of ψ_{Pp} is determined by the magnitude of $V(r_P)$ inside the nucleus. If we assume V of the order of nuclear binding energies, and the energy of the particle E_P small compared to V, ψ_{Pp} will decrease to $1/e$ of its value in a distance of the order of the range of the nuclear forces (say, $2\cdot 10^{-13}$ cm). Therefore the whole contribution

[17] Our thanks are due to Professor E. Teller, to whom we owe most of the ideas presented in this chapter.

to the matrix element (43) will come from a surface layer whose thickness is of the order of the range of the nuclear forces, while in case (*a*) and (*b*) the whole volume of the nucleus contributes. Moreover, the wave function ψ_{Pp} will be smaller than for a free particle even right at the surface (cf. 50). The matrix elements in case (*c*) will, therefore, in general be smaller than in case (*b*).

Evidently, only one of the three values obtained for the matrix element H by the three assumptions (a), (b) and (c) can give the correct width of the level r of the compound nucleus. On the other hand, if we continue the perturbation calculation to sufficiently high approximations, we shall obtain the correct answer from whatever wave functions for the incident particle we have started. Therefore, if we start from the "wrong" wave functions, the first approximation is not sufficient to calculate the width of a nuclear level, and the second approximation will not be sufficient to give the correct dispersion formula.

The condition for a good wave function is the smallness of the higher approximations of the perturbation theory. This condition will be best fulfilled if the matrix elements H are as small as possible. Therefore, *assumption (c) will come nearest to the truth.*

After having decided for assumption (c), the question arises how to choose height and radius of the repulsive potential V. On one hand, a high repulsive potential makes the wave function ψ_{Pp} fall off more steeply and therefore makes the matrix elements in the average smaller. On the other hand, the perturbing potential H must, of course, include the auxiliary potential V with opposite sign: If V is chosen too large, this will again increase the average matrix element. This increase will (again in the average) be small as long as V is small compared to the average nuclear forces, a good measure of which are the nuclear binding energies. Therefore it seems an appropriate choice to make V of the same order as a nuclear binding energy, i.e., about 10 MV.

For the radius of the potential V, the obvious choice is the nuclear radius itself. A smaller radius would again make the matrix elements larger. A larger radius of the potential is even more to be avoided: The perturbation theory as used in this paper, is based on an expansion of a certain function, *viz.*, $F=H\psi_A\psi_P$, in terms of the wave functions of the compound nucleus. This is only possible if in the region in which F is appreciable, the wave functions ψ_C form a complete (or practically complete) system. But this is, obviously, only the case if F is only large inside the nuclear radius. Therefore ψ_P must only fall off inside that radius.

An indication for the importance of higher approximations and therefore of the accuracy of the wave functions chosen may be obtained from the elastic scattering. The scattering of slow particles, e.g., slow neutrons, consists in our scheme of three parts:

(1) The scattering of zero order which is already contained in the "unperturbed" wave functions ψ_P of the incident particle. It is due to the existence of the potential V and amounts, for slow neutrons, to a scattering cross section[18]

$$\sigma_1=4\pi R^2, \tag{45}$$

where R is the radius of the sphere inside which the repulsive potential exists. This part may be called potential scattering in the narrower sense.

(2) The contribution of the low energy levels of the compound nucleus. This contribution shows resonance maxima; in between the maxima it is very small compared to σ_1, because the neutron width of the levels of the compound nucleus is small compared to the spacing of the levels.

(3) The contribution of the high levels of the compound nucleus. For a given neutron wave function, the matrix elements $H^P{}_{r^P}$ will, in the average, be of the same order of magnitude for high levels r of the compound nucleus as for low ones, because there is no essential difference in character between the levels. Only when the energy E_r becomes very high, the matrix elements will fall off with increasing energy. Let us say that this will be the case for $E_r>E_c$. The critical energy E_c will be of the order of 20 or 30 MV, as may be estimated without great difficulty.[19]

The *density* of nuclear levels, i.e., the number of levels per unit energy, increases rapidly with

[18] Cf. Mott and Massey, *Atomic Collisions*, p. 30.

[19] Bethe and Livingston, "Nuclear Physics," Part B, to appear shortly in Rev. Mod. Phys.

increasing energy E_r. For a special model, this increase has been calculated.[20] Now the contributions of the various levels to the elastic scattering (41) all have the same sign. Therefore the most important contributions will come from very high levels where the density of levels is already large and the matrix elements have not yet decreased, i.e., from the levels in the neighborhood of E_c. *These high levels of the compound nucleus are responsible for all the difficulties in the convergence of the perturbation calculation mentioned above.* Therefore the condition for convergence is that the contribution of the high levels should not be too large.

The contribution of the high levels to the scattering can easily be estimated. The resonance denominators in (1) may all be replaced by $-E_c$ where E_c is the critical energy at which the matrix elements begin to fall off.[21] Then we have

$$w^{P_P P_P} = \frac{2\pi}{hE_c^2}\left|\sum_r |H^{P_r P}|^2\right| = \frac{2\pi}{hE_c^2}|(H^2)^{P_P P_P}|^2, \quad (46)$$

using the fact that the wave functions ψ_{C_r} of the compound nucleus form a complete system. The cross section is obtained by multiplying the probability (46) by $2\pi^2\hbar\lambda^2$ (cf. (7)) so that

$$\sigma_3 = \frac{4\pi^3\lambda^2}{E_c^2}\left|\int H^2 |\psi_A|^2 |\psi_{P_P}|^2 d\tau\right|^2. \quad (47)$$

We denote by $d\tau_A$ the volume element in the configuration space of all particles contained in the nucleus A and by $d\tau_P$ that of the incident particle, so that $d\tau_A d\tau_P = d\tau$. Then, because of normalization,

$$\int |\psi_A|^2 d\tau_A = 1 \quad (48)$$

and

$$\int H^2 |\psi_A|^2 d\tau_A = U^2(r_P), \quad (49)$$

where U is an energy of the order of magnitude of a nuclear interaction (about 10 MV), which is an irregularly varying function of the position r_P of the particle. Of the wave function of the particle, only the part $l=0$ is important because we assume the particle to be slow. Considering the normalization per unit energy, we have

$$\psi_{P_P} = (M^2 v/2\pi^2\hbar^3)^{\frac{1}{2}} \sin k(r-r_0)/kr \text{ for } r>R, \quad (50)$$

$$\psi_{P_P} = (M^2 v/2\pi^2\hbar^3)^{\frac{1}{2}}(1/\kappa r)e^{-\kappa(R-r)} \text{ for } r<R, \quad (50a)$$

with

$$\kappa = (2MV)^{\frac{1}{2}}/\hbar, \quad (50b)$$

$$r_0 = R - 1/\kappa. \quad (50c)$$

Quantities of the relative order $1/\kappa R$ have been neglected. Then we have

$$\int H^2 |\psi_A|^2 |\psi_{P_P}|^2 d\tau = \frac{4\pi}{2\pi^2}\frac{M^2 v}{\hbar^3}\int^R \frac{U^2 r^2 dr}{\kappa^2 r^2} e^{-2\kappa(R-r)} = \frac{1}{\pi}\frac{M^2 v}{\hbar^3\kappa^3}\overline{U^2} = \frac{1}{\pi}\frac{1}{2V\kappa\lambda}\overline{U^2} \quad (51)$$

where $\lambda = \hbar/Mv$ is the wave-length of the incident particle. Inserting into (47), we have

$$\sigma_3 = \frac{\pi}{\kappa^2}\left(\frac{\overline{U^2}}{E_c V}\right)^2. \quad (52)$$

U, E_c and V are all of the same order of magnitude; probably E_c is a little larger than the other quantities. To stay on the safe side, we replace the ratio $\overline{U^2}/E_c V$ by unity. $1/\kappa$ is about $2\cdot 10^{-13}$ cm, i.e., one-fifth of the nuclear radius. Thus σ_3 is about a hundred times smaller than σ_1, (cf. 45). This would justify our choice of the wave function. It must, of course, be admitted that some of the estimates leading to (52) are very crude so that we prefer to regard our wave function still as provisional.

On the other hand, we can see immediately from our estimate that plane waves (possibility (b) above) and *a fortiori* an attractive potential (assumption (a)) are out of the question. For plane waves, κ^{-3} in (51) would be replaced by $\frac{3}{2}R^3$ so that (52) would be multiplied by a factor $4/9(\kappa R)^6$, i.e., about $5^6\cdot 4/9 \approx 7000$. The contribution of the high nuclear levels to the scattering would then be enormous, and by analogy we must conclude that the contribution of these levels to the higher approximations of the perturbation theory would also be extremely large

[20] Bethe, Phys. Rev. **50**, 332 (1936).

[21] More accurately, E_c is the energy for which the product of the average square of the matrix element and the density of the levels reaches its maximum.

so that the dispersion formula based on the second-order perturbation would be quite insufficient. The assumption of an impenetrable nucleus is, therefore, at present the most satisfactory for the calculation of particle wave functions.

Our estimates show also that with the use of the correct wave functions, the higher approximations of the perturbation theory may be neglected, which justifies formula (1).

As regards the elastic scattering itself, the contribution of the high levels is, of course, not so small as it might seem from the comparison of σ_3 and σ_1. Actually, the "direct scattering" σ_1 and the contribution σ_3 of the high levels interfere with each other. Now the scattering due to the high levels is certainly in phase with the incident wave just as is the light scattered by an atom if the frequency of the light is below the resonance frequency. On the other hand, the scattered wave due to the impenetrability of the nucleus, has certainly a phase opposite to that of the incident wave. Therefore the amplitudes of the two scattered waves must be subtracted from each other, so that the total potential scattering is

$$\sigma_{\text{pot}}=(\sigma_1^{\frac{1}{2}}-\sigma_3^{\frac{1}{2}})^2. \tag{53}$$

Since σ_3 is about one percent of σ_1, the total potential scattering will be about 20 percent less than the scattering from a hard sphere of radius R.

Near resonance, the resonance scattering σ_2 must be added to the potential scattering. Again there will be interference between the two kinds of scattering which, in the general case, is complicated by the fact that there is only interference between waves of the same total angular momentum J. The potential scattering must therefore be analyzed according to J. The phases are equal if the energy is above, opposite below the resonance level. Neglecting the contribution σ_3, the total elastic scattering cross section becomes for slow particles (cf. 41)

$$\sigma^{P_P P_p}=\frac{\pi}{(2s+1)(2i+1)}\sum_J(2J+1)\times\left|2R+\sum_r\frac{\Gamma^r{}_{P^J{}_p}\lambda^r{}_{P^J{}_p}}{E_A+E_P-E_{rJ}+\frac{1}{2}i\gamma_{rJ}}\right|^2. \tag{54}$$

If only one level is important, this reduces to

$$\sigma^{P_P P_p}=4\pi R^2+\frac{\pi(2J+1)\Gamma^r{}_{P^J{}_p}\lambda^r{}_{P^J{}_p}}{(2s+1)(2i+1)}\times\frac{4R(E_A+E_P-E_{rJ})+\Gamma^r{}_{P^J{}_p}\lambda^r{}_{P^J{}_p}}{(E_A+E_P-E_{rJ})^2+\frac{1}{4}\gamma^2{}_{rJ}}. \tag{55}$$

This cross section has its maximum at an energy E_P slightly higher than the resonance energy $E_{rJ}-E_A$, and a minimum at some energy below the resonance energy. If $\Gamma^r{}_{P^J{}_p}\lambda^r{}_{P^J{}_p}/\gamma_{rJ}R\gg 1$ (large resonance scattering), the maximum cross section is approximately

$$\sigma_{\max}=\frac{4\pi(2J+1)}{(2s+1)(2i+1)}\left(\frac{\Gamma^r{}_{P^J{}_p}}{\Gamma_{rJ}}\right)^2\lambda^2, \tag{56}$$

the minimum

$$\sigma_{\min}=4\pi R^2\left(1-\frac{2J+1}{(2s+1)(2i+1)}\right). \tag{57}$$

The elastic cross section will always be at least of the order of σ_1 unless i or s is zero.

II. Applications

§5. Capture of slow neutrons: theory

A. General formula.—For the capture cross section of a slow neutron with emission of fast particles or light quanta we have (cf. (38), $s=\frac{1}{2}$, (26), (27a))

$$\sigma^{P_Q P_q}=\frac{\pi}{2}\frac{\lambda}{2i+1}\sum_{JI'i'}(2J+1)\times\left|\sum_r\frac{\lambda^r{}_{P^J{}_p}{}^{\frac{1}{2}}U^r{}_{P^J{}_p Q^J{}_q I' i'}}{E_A+E_P-E_{rJ}+\frac{1}{2}i\gamma_{rJ}}\right|^2. \tag{58}$$

This gives the capture cross section for a process which leads to a definite final level q of the remaining nucleus. Especially for radiative capture a great number of final levels will be possible. Hence for obtaining the observed cross section (58) has to be summed over all these final states. This makes the application of the formula rather cumbersome, and the effects of the interference become complicated, even if only a small number of compound states contribute to (58). We shall therefore, in the following, only consider two

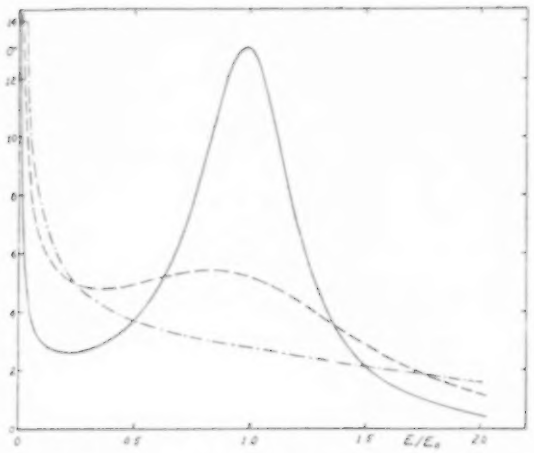

FIG. 1. The cross section as a function of energy for various ratios of width to resonance energy. Abscissa: energy as a fraction of the resonance energy. Ordinate: cross section. The curves are adjusted so that the area is unity in each case. ——— Width $\Gamma=\frac{1}{2}E_0$ (pronounced resonance); – – – – $\Gamma=\sqrt{2}E_0$ (case of Cd); —·—·— $\Gamma=4E_0$ (almost $1/v$ law).

important limiting cases which permit the discussion of some but by far not all applications.

First, we shall discuss the case that only a single compound state is of importance in the sum in (58), and hence (58) can be simplified according to (12). (12) will be generally applicable for light nuclei because of the small density of energy levels; for heavier nuclei it will often be true in the immediate neighborhood of the resonance.

Secondly, we shall consider the case of constant capture probability which leads to the $1/v$ law. As already mentioned in §3B, it is quite generally true that for low energies σ varies as $1/v$. The extension of the energy region in which this is the case is, however, very different according to the circumstances and will be discussed below.

B. Single resonance level.—(58) reduces to (cf. (12))

$$\sigma=\sigma_{0N}\frac{(\Gamma/\gamma)^2}{1+((E-E_g)/(\gamma/2))^2}\left(\frac{|E_g|}{E}\right)^{\frac{1}{2}} \tag{59}$$

with

$$\sigma_{0N}=2\pi\lambda_g^2\frac{\Gamma_n\Gamma_r}{\Gamma^2}\left(1\pm\frac{1}{2i+1}\right)$$

$$=\frac{1.30\cdot10^{-18}}{|E_g|}\frac{\Gamma_r\Gamma_n}{\Gamma^2}\left(1\pm\frac{1}{2i+1}\right). \tag{60}$$

Here, E_g and E are the energy of the level and the neutron, respectively, both measured from zero kinetic energy of the neutron. Hence E_g can be positive as well as negative. Γ_n is the neutron width at the resonance energy E_g, Γ_r the radiation width or width for emission of a fast particle, γ is the total width $(\gamma=\Gamma_r+\Gamma_n(E/|E_g|)^{\frac{1}{2}})$ and $\Gamma=\gamma(E_g)$ the total width at the resonance energy. All energies are measured in volts, σ in cm². The factor $1\pm1/2i+1$ corresponds to the two possibilities $J=i\pm\frac{1}{2}$; for $i=0$, it has to be replaced by 2. If, as is true in most of the cases to be considered afterwards, the contribution of the neutron width to the total width is negligible, γ can be considered as independent of the energy E and replaced by $\Gamma=\Gamma_r$. We shall in the following, if not otherwise stated, always make this assumption. Then we have

$$\sigma=\sigma_{0N}\frac{1}{1+((E-E_g)/(\Gamma/2))^2}\left(\frac{|E_g|}{E}\right)^{\frac{1}{2}}; \tag{61}$$

$$\sigma_{0N}=\frac{1.30\cdot10^{-18}}{|E_g|}\cdot\frac{\Gamma_n}{\Gamma_r}\left(1\pm\frac{1}{2i+1}\right). \tag{61a}$$

If $E_g>0$, and $\Gamma/E_g\ll1$, the cross section has, according to (61), a maximum for $E=E_g$ and a minimum for $E=E_g/5$. For larger values of the ratio $\Gamma/|E_g|$ the extrema get less pronounced, their positions come nearer together and finally coalesce at $\frac{3}{5}E_g$ for $\Gamma/E_g=4/\sqrt{5}=1.79$. Generally we have

$$E_{\substack{\max\\\min}}=\frac{E_g}{5}\left\{3\pm2\left(1-\frac{5}{16}\left(\frac{\Gamma}{E_g}\right)^2\right)^{\frac{1}{2}}\right\}. \tag{62}$$

For $\Gamma/E_g\geq1.79$ there is no longer a maximum and minimum, and the cross section increases continuously with decreasing E up to the $1/v$-region.

If $E_g<0$, the cross section increases monotonously with decreasing energy for all values of Γ/E_g. Fig. 1 illustrates the energy dependence of the cross section for a number of values of the ratio $\Gamma/E_g=c$.

The form (61) of the cross section is modified by the motion of the capturing nuclei. For free nuclei,[22] this leads to a Doppler broadening of the amount:

$$\Delta=4(mE_gkT/M)^{\frac{1}{2}} \tag{63}$$

[22] For the discussion of the validity of the assumption of free nuclei in the cases treated in the present paper cf. G. Placzek and E. Teller, reference 16.

(m, M mass of the neutron and capturing nucleus).[23]

C. Immediate neighborhood of the resonance.— For

$$\frac{|E_g-E|}{E_g}\ll 1, \quad \frac{\Delta}{E_g}\ll 1,^{24}$$

the combination of Doppler and natural width leads to the result familiar from optics:

$$\sigma=\sigma_{0N}\psi(\xi, x), \tag{64a}$$

$$\psi(\xi, x)=\frac{\xi}{\sqrt{\pi}}\int_{-\infty}^{\infty}\frac{e^{-\xi^2(x-y)^2}}{1+y^2}dy, \tag{64}$$

$$x=\frac{E_g-E}{\Gamma/2}, \quad \xi=\Gamma/\Delta. \tag{64b}$$

The maximum cross section σ_0 is

$$\sigma_0=\sigma_{0N}\psi(\xi, 0)=\sigma_{0N}\frac{\xi}{\sqrt{\pi}}\int_{-\infty}^{\infty}\frac{e^{-\xi^2y^2}}{1+y^2}dy$$
$$=\sigma_{0N}\sqrt{\pi}\xi e^{\xi^2}\{1-\Phi(\xi)\}, \tag{65}$$

where $\Phi(\xi)$ is the Gaussian error function

$$\Phi(\xi)=2\pi^{-\frac{1}{2}}\int_0^{\xi}e^{-t^2}dt.$$

For $\xi\gg 1$ (natural width) (64), (65) go over into[25]

$$\sigma=\sigma_{0N}(1/(1+x^2)), \tag{66}$$

$$\sigma_0=\sigma_{0N}. \tag{66a}$$

For $\xi\ll 1$, $\xi x<1$ (Doppler width)

$$\sigma=\sigma_{0D}e^{-((E-E_0)/(\Delta/2))^2} \tag{67}$$

with

$$\sigma_{0D}=\sqrt{\pi}\xi\sigma_{0N}$$
$$=2.31\cdot 10^{-18}\cdot\frac{\Gamma_n}{\Delta E_g}\left(1\pm\frac{1}{2i+1}\right). \tag{67a}$$

With the help of (64) and (65) we can calculate the cross section for the important case, that the same substance is used as absorber and indicator (self-indication)[26, 27]

$$\sigma_g=\int\sigma^2dE/\int\sigma dE. \tag{68}$$

If $\Gamma/E_g\ll 1$, the integration can be extended from $x=-\infty$ to $x=\infty$ without appreciable error, as in this case only those regions contribute to the integral, in which the condition $|E_g-E|\ll E_g$ is fulfilled and hence (64) is valid. The result of the integration[28] is:

---

[23] If the resonance energy is $E_g=\frac{1}{2}mv_g^2$ in the system where the capturing particle is at rest, we have for the energy in the system of the observer

$$E=\tfrac{1}{2}m(v_g-u_x)^2, \tag{63a}$$

where u_x is the velocity component of the capturing particle in the direction of the incident particle. Supposing $|u_x|\ll|v_g|$ i.e., $E_g\gg kTm/M$ we may neglect the term with u_x^2 and obtain from (63a)

$$E_g-E=u_x(2mE_g)^{\frac{1}{2}}. \tag{63b}$$

Now the probability that u_x lies between u_x and u_x+du_x is

$$w(u_x)du_x=(M/2\pi kT)^{\frac{1}{2}}e^{-Mu_x^2/2kT}du_x. \tag{63c}$$

Hence from (63b) and (63c)

$$w(E)dE=2\pi^{-\frac{1}{2}}e^{-4(E-E_g)^2/\Delta^2}dE/\Delta, \tag{63d}$$

where

$$\Delta=4(mE_gkT/M)^{\frac{1}{2}}. \tag{63}$$

In the relativistic case we have instead of (63b)

$$E_g-E=u_xp,$$

(p momentum of the incident particle) and hence

$$\Delta=2p_g(2kT/M)^{\frac{1}{2}}. \tag{63e}$$

(63e) is valid both for light quanta and for particles; it reduces for light to the familiar expression

$$\Delta=2(\hbar\omega/c)(2kT/M)^{\frac{1}{2}}. \tag{63f}$$

The Doppler width for particles is equal to the Doppler width for light quanta with the same momentum.

[24] This latter assumption was already used in the derivation of (63), because it is equivalent with $u_x\ll v$. It is fulfilled for all practical cases.

[25] The factor $(|E_g|/E)^{\frac{1}{2}}$ in (59) does not appear in (64a) as E_g-E was supposed small compared with E_g.

[26] We denote throughout with the indices 0 and g the maximum cross section for monochromatic incident particles and the effective cross section for self-indication while the letters N and D refer to natural and Doppler width, respectively.

[27] (68) holds, of course, only for thin absorbers.

[28] Instead of the integral $\int\psi^2(\xi, x)dx$ which occurs in (68) (cf. (64)), we calculate immediately the somewhat more general integral $\int\psi(\xi, x)\psi(\eta, x)dx$. Using the definition (64), we have

$$I=\int\psi(\xi, x)\psi(\eta, x)dx$$
$$=\frac{\xi\eta}{\pi}\int_{-\infty}^{\infty}\int\int dxdydz\frac{e^{-\xi^2(x-y)^2}}{1+y^2}\frac{e^{-\eta^2(x-z)^2}}{1+z^2}. \tag{69a}$$

We integrate first over x and obtain

$$I=\frac{\xi\eta}{\pi^{\frac{1}{2}}(\xi^2+\eta^2)^{\frac{1}{2}}}\int_{-\infty}^{\infty}\int dydz\frac{e^{-\xi^2\eta^2(y-z)^2/(\xi^2+\eta^2)}}{(1+y^2)(1+z^2)}. \tag{69b}$$

Here we introduce the new coordinates $u=\frac{1}{2}(y+z)$ and $v=\frac{1}{2}(y-z)$. The integration over u is straightforward and yields

$$I=\tfrac{1}{2}\pi^{\frac{1}{2}}\zeta\int_{-\infty}^{+\infty}dve^{-\zeta^2v^2}/(1+v^2) \tag{69c}$$

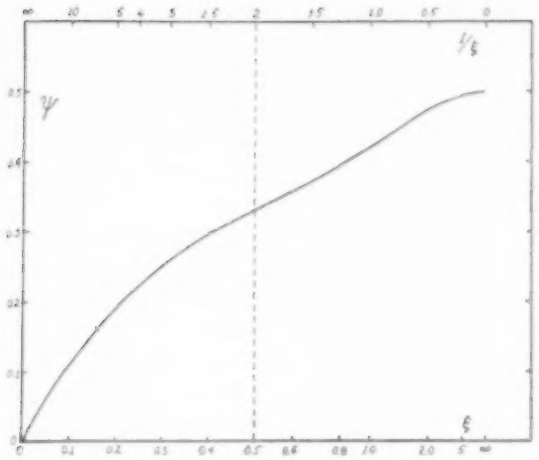

FIG. 2. The ratio χ of the average absorption of the resonance group to the absorption coefficient at exact resonance, as a function of the ratio ξ of natural to Doppler width. Note the change of scale at $\xi=0.5$. (By mistake the ordinate in the figure is marked "ψ" instead of "χ").

$$\sigma_g=\sigma_{0N}\frac{\int_{-\infty}^{\infty}\psi^2dx}{\int_{-\infty}^{\infty}\psi dx}=\tfrac{1}{2}\sigma_{0N}\psi(\xi\sqrt{2},0). \qquad (69)$$

The cross section with self-indication is thus equal to half the maximal cross section, measured at $\frac{1}{2}$ of the original temperature. Hence, for $\xi\gg1$ (natural width), as there is no effect of the temperature, $\sigma_{gN}=\frac{1}{2}\sigma_{0N}$ while for $\xi\ll1$ (Doppler width) $\sigma_{gD}=\sigma_{0D}/\sqrt{2}$ since the Doppler width (*viz.* (63)) is proportional to the square root of the temperature and the maximal cross section in this case (*viz.* (67a)) proportional to ξ.

From (65) and (69) we obtain:

$$\sigma_g=\sigma_{0N}\chi(\xi), \qquad (70)$$

$$\chi(\xi)=\tfrac{1}{2}\psi(\xi\sqrt{2},0)=(\pi/2)^{\frac{1}{2}}\xi e^{2\xi^2}\{1-\Phi(\xi\sqrt{2})\}. \qquad (70a)$$

For $\xi\gg1$

$$\sigma_g=\sigma_{gN}\left\{1-\frac{1}{4\xi^2}+\frac{1\cdot3}{(4\xi^2)^2}-\frac{1\cdot3\cdot5}{(4\xi^2)^3}+\cdots\right\}, \qquad (71)$$

$$\sigma_{gN}=\tfrac{1}{2}\sigma_{0N}. \qquad (71a)$$

For $\xi\ll1$

$$\sigma_g=\sigma_{gD}\{1-2(2/\pi)^{\frac{1}{2}}\xi+2\xi^2-(8/3)(2/\pi)^{\frac{1}{2}}\xi^3+2\xi^4-\cdots\}, \qquad (72)$$

$$\sigma_{gD}=\sigma_{0N}(\pi/2)^{\frac{1}{2}}\xi=1.63\cdot10^{-18}(\Gamma_n/\Delta E_g). \qquad (72a)$$

A plot of the function $\chi(\xi)$ is given in Fig. 2. If the Doppler width is not negligible with respect to the natural width, the cross section for self-indication σ_g will depend on ξ and hence on the temperature of the absorber and indicator. Measurements of the temperature-dependence of σ_g in a region where both widths are comparable, may therefore serve to determine ξ and, if the energy E_g is known, also Γ_r.[29] If indicator and absorber are held at different temperatures, the temperature to be introduced in the ξ in (70), (71), (72) is (cf. (69d) and (63)), the arithmetic mean $\frac{1}{2}(T_1+T_2)$.

The capture cross section is not only important for absorption experiments but also for the measurement of the activation. Amaldi and Fermi[30] have given a relation between absorption coefficient, activation and width. The absorption coefficient was supposed to be constant within the line. Instead of this assumption we shall use (64). For the activation (number of disintegrations per second after infinite time of neutron irradiation = number of neutrons captured per second) of a thin layer we have

$$A=\delta F\int\rho(E)v\kappa(E)dE, \qquad (73)$$

δ and F thickness (in g/cm²) and surface of indicator, $\rho(E)dE$ density of neutrons of energy E per cm³; v velocity; κ absorption coefficient in cm²/g ($\kappa=L\sigma/A$; L, Avogadros number; A, atomic weight).

According to Amaldi and Fermi, the density of neutrons above 1 volt is

$$\rho(E)dE=(1/v)ql_gdE/E, \qquad (74)$$

q number of neutrons emitted by the source per second and cm³, l_g mean free path of neutrons

with $\zeta=2\xi\eta(\xi^2+\eta^2)^{-\frac{1}{2}}$. (69d)

But the integral in (69c) is exactly the same as in (65), so that we find

$$I=\tfrac{1}{2}\pi\psi(\zeta,0). \qquad (69e)$$

In the special case $\xi=\eta$ (69d) reduces to

$$\zeta=\xi\sqrt{2}. \qquad (69f)$$

The integral in the denominator of (68) gives simply $\pi\sigma_{0N}$ which, together with (69e) (69f), leads immediately to (69).

[29] This was first pointed out by O. R. Frisch, who also reported about preliminary experiments of this kind at the Copenhagen conference (June, 1936).

[30] Amaldi and Fermi, Ricerca Sci. **7/1**, no. 11–12 (1936) and Phys. Rev. **50**, 899 (1936).

of energy E_g in paraffin. Introducing (74), (64) and (70) into (73) we have

$$A_g=\delta Fq\frac{l_g}{E_g}\int\kappa(E)dE=\frac{\delta Fql_g}{E_g}\kappa_{0N}\int_{-\infty}^{\infty}\psi dE$$
$$=\frac{\delta Fql_g}{E_g}\kappa_{0N}\frac{\Gamma}{2}\pi=\frac{\delta Fql_g}{E_g}\kappa_g\frac{\Gamma}{\chi}\cdot\frac{\pi}{2}. \quad (75)$$

Γ/χ can be considered as a measure of the effective width, we have

$$\text{for}\qquad \xi\gg 1,\quad \Gamma/\chi=2\Gamma$$
$$\xi\ll 1,\quad \Gamma/\chi=(2/\pi)^{\frac{1}{2}}\Delta. \quad (76)$$

We may also write (75) (cf. (61a))

$$A_g=\frac{\pi}{2}\frac{\delta Fql_g}{M}\cdot 1.30\cdot 10^{-18}\frac{\Gamma_n}{E_g^{\,2}}\left(1\pm\frac{1}{2i+1}\right)$$
$$=\frac{\pi}{2}\frac{\delta Fql_g}{M}\cdot 1.30\cdot 10^{-18}\frac{\Gamma_n'}{E_g^{\frac{1}{2}}}\left(1\pm\frac{1}{2i+1}\right), \quad (77)$$

where
$$\Gamma_n'=\Gamma_nE_g^{-\frac{1}{2}} \quad (77a)$$

is the neutron width at 1 volt and M the atomic mass in grams. Thus, the activation is proportional to the neutron width and varies with the position of a level with given properties (symbolized by Γ_n') as $E_g^{-\frac{1}{2}}$.

D. The 1/v region.—The condition for the validity of the $1/v$ law is that the variation of the $1/v$ factor with the energy is large compared to the variation of the capture probability. Thus, according to (61)

$$\left|\left(\frac{|E_g|}{E}\right)^{\frac{1}{2}}\frac{d}{dE}\frac{1}{1+((E_g-E)/(\Gamma/2)^2)}\right|$$
$$\ll\left|\frac{1}{1+((E_g-E)/(\Gamma/2))^2}\frac{d}{dE}\left(\frac{|E_g|}{E}\right)^{\frac{1}{2}}\right|, \quad (78a)$$

which gives
$$\frac{4E|E_g-E|}{(\Gamma/2)^2+(E_g-E)^2}\ll 1. \quad (78)$$

We see that (78) is always satisfied if *either*[31]

$$E\ll\tfrac{1}{4}|E_g| \quad (79)$$

or
$$E\ll\tfrac{1}{4}\Gamma. \quad (80)$$

[31] We may write (78) in the form
$$E\ll\tfrac{1}{4}\Gamma|\tfrac{1}{2}\Gamma/|E_g-E|+|E_g-E|/\tfrac{1}{2}\Gamma|$$
from which (79) and (80) are obvious.

A more complete expression for the extension of the $1/v$ range as a function of E_g and Γ is obtained by putting the left side of (78) equal to a small quantity ϵ and solving this as an equation for E. In this way it is seen that the $1/v$ range may even extend to much higher energies than indicated by (79) and (80).

Thus the $1/v$ law certainly holds if the incident energy is small compared to the *larger* of the two quantities E_g and Γ.[32] No serious error will be committed by applying this condition also in the cases, where the one-level formula is to be replaced by the general formula (58), provided it holds for all the compound levels contributing to the sum.

Actually, the extension of the $1/v$ range is very different according to the position and width of the resonance levels. It is a fraction of a volt for nuclei like Ag and Rh (see below), and considerably higher for light elements, because of the smaller density of nuclear levels. It is true that accidentally the first resonance level may lie at a low energy even for light nuclei. Even then, the $1/v$ law will hold up to fairly high energies if the capture of the neutron is followed by the emission of a charged particle. For in this case the width of the level will be of the order of several 10,000 volts (cf. §6) so that the validity of the $1/v$ law is ensured at least up to several thousand volts, irrespective of the position of the resonance level. Considerations of this kind have led to the use of the absorption in boron, caused by the reaction

$${}_5B^{10}+{}_0n^1={}_5B^{11}={}_3Li^7+{}_2He^4$$

as an energy gauge for slow neutrons.[33] This method will be discussed in §6A1.

For the radiative capture of neutrons by light nuclei two cases may occur. In the usual case of a high resonance level we shall have a wide $1/v$ range but the cross section will *cet. par.* be smaller than for the emission of particles in the ratio of the γ-ray to the particle width. The γ-ray width may be of the order of 1 volt (cf. §10) which

[32] If, however, the contribution of the neutron width to the total width is not negligible, this condition is not strictly sufficient because of the energy dependence of γ. In this case (80) is invalidated, but (79) remains sufficient with the supplementary condition $\gamma_n\ll E_g$ as can be derived from (59).

[33] Frisch and Placzek, Nature **137**, 357 (1936); Weekes, Livingston and Bethe, Phys. Rev. **49**, 471 (1936).

makes the radiative capture by a factor of the order of 10,000 less probable than the emission of particles. A large cross section for radiative capture by light nuclei can only occur if the first resonance level lies exceptionally low; in this case, however, the $1/v$ law will break down at quite a low energy.

For a great number of nuclei the $1/v$ law holds in the region of thermal energies. We shall therefore in the following give expressions for the cross section of and the activation by thermal neutrons, assuming this law for absorber and indicator. The question, how far the so-called C neutrons (i.e., neutrons stopped by cadmium) are identical with thermal neutrons, shall not be discussed at this stage.

For the total density of thermal neutrons, we have (cf. Amaldi and Fermi,[30] or (83d) for large x)

$$\int_{\text{th}} \rho(E)dE = q'\tau, \tag{81}$$

where q', the total number of neutrons produced per cm³ and second, is different from the q used in (74) because of the different density distribution in paraffin of resonance and thermal neutrons. Integrating over the whole volume, we get the total number Q of neutrons produced per second:

$$Q = \int q\,dV = \int q'\,dV. \tag{82}$$

τ is the lifetime of a thermal neutron in paraffin. We may put

$$\tau = Nl/\bar{v} = Nl(8kT/\pi m)^{-\frac{1}{2}}. \tag{83}$$

N: number of collisions of a thermal neutron in paraffin before its capture, l: mean free path of a thermal neutron.[34]

Assuming complete thermal equilibrium, we get for the energy distribution of the thermal neutrons

$$\rho(E)dE = \frac{q'\tau E^{\frac{1}{2}}e^{-E/kT}}{(\pi/4)^{\frac{1}{2}}(kT)^{\frac{1}{2}}}dE. \tag{84}$$

If the indicator is covered on one side by Cd which absorbs the thermal neutrons, the density

---

[34] That this particular average of v has to be taken (rather than, say, $\tau = Nlv^{-1}$) can be seen by going back to the theory of diffusion of neutrons (cf. Amaldi and Fermi, reference 30).

The stationarity equation for the neutron diffusion is

$$D\Delta F - F/\tau + q' = 0, \tag{83a}$$

where $F(x, y, z)$ is the total neutron density per cm³, τ the mean life of a neutron in paraffin, q' the number of neutrons produced by the source per cm³ and sec., and

$$D = \tfrac{1}{3}l\bar{v}, \tag{83b}$$

the diffusion coefficient of thermal neutrons. τ is independent of the neutron velocity. We solve (83a) for the case that a Cd absorber, sufficient to absorb all thermal neutrons, is placed at $x=0$. This corresponds in first approximation to the boundary condition

$$F = 0 \qquad \text{at} \qquad x = 0. \tag{83c}$$

(We shall find below that F is not exactly zero; in fact, it is just the value of F for $x=0$ we wish to calculate. But it is sufficient for our arguments that F at $x=0$ is small compared to its value in the paraffin.) The solution of (83a) with the boundary condition (83c) is for $x>0$

$$F = q'\tau(1 - e^{-x(D\tau)^{-\frac{1}{2}}}). \tag{83d}$$

The current of neutrons near $x=0$ is then

$$S = D(dF/dx)_0 = q'L, \tag{83e}$$

where

$$L = (D\tau)^{\frac{1}{2}} \tag{83f}$$

is the "diffusion length" measured by Amaldi and Fermi. The neutron current determines the activity produced in a detector. If the angular distribution of the neutrons is

$$f(\vartheta) = a\cos\vartheta + b\cos^2\vartheta, \tag{83g}$$

the activity produced in a thin detector of thickness δ and absorption coefficient κ will be

$$A = S\kappa\delta\frac{\int_0^{\pi/2}(a + b\cos\vartheta)\sin\vartheta d\vartheta}{\int_0^{\pi/2}(a\cos\vartheta + b\cos^2\vartheta)\sin\vartheta d\vartheta} = S\kappa\delta\frac{a + \frac{1}{2}b}{\frac{1}{2}a + \frac{1}{3}b}. \tag{83h}$$

For the neutrons emerging from paraffin, we have (Amaldi and Fermi, (5))

$$b = a\sqrt{3}, \qquad A = S\kappa\delta\sqrt{3}. \tag{83i}$$

On the other hand, *inside* a uniform paraffin block the activity would be

$$A = F_0\bar{v}\kappa\delta, \tag{83j}$$

where $\bar{v}$ is the average velocity and F_0 the density of the neutrons. From (83i) and (83j) we obtain the "effective density" at the surface

$$F' = 3^{\frac{1}{2}}S/\bar{v} = 3^{\frac{1}{2}}q'L/\bar{v}. \tag{83k}$$

Now the number of collisions before capture N is *defined* by Amaldi and Fermi in terms of the observed diffusion length L and the observed mean free path l by the relation

$$L = l(N/3)^{\frac{1}{2}}. \tag{83l}$$

Inserting this in (83k), we find

$$F' = q'lN^{\frac{1}{2}}/\bar{v}, \tag{83m}$$

which is identical with (81) (83) (85). It might be objected against (83h) and (83j) that the absorption coefficient κ depends on the velocity. This objection is not valid because the energy distribution of the thermal neutrons emerging from the paraffin near the Cd absorber is the same as that in the interior of the paraffin: In both cases, the number of neutrons of energy E striking the detector per sec., is proportional to the number of such neutrons in the Maxwell distribution, times the neutron velocity.

is hereby reduced by the factor (cf. Amaldi and Fermi,[30] and reference 34)

$$\rho'/\rho = 1/N^{\frac{1}{2}}. \tag{85}$$

Thus we have

$$\rho'(E)dE = \frac{q'l(\frac{1}{2}Nm)^{\frac{1}{2}}}{(kT)^2} E^{\frac{1}{2}} e^{-E/kT} dE. \tag{86}$$

With the help of (86) we can calculate the cross section and activation.

Putting $\sigma = XE^{-\frac{1}{2}}$, where X is a constant, and considering that also the sensitivity of the indicator varies with $1/v$ which compensates the v factor coming in by the change from density to current, we have

$$\sigma_{\text{th}} = \frac{\int \sigma \rho' dE}{\int \rho' dE} = \frac{X}{((\pi/4)kT)^{\frac{1}{2}}} \tag{87}$$

and hence $$\sigma(E) = \sigma_{\text{th}}(\tfrac{1}{4}\pi kT/E)^{\frac{1}{2}}. \tag{88}$$

Thus, the effective energy for the absorption of thermal neutrons in a thin layer is $(\pi/4)kT$.

For the activation by thermal neutrons B_{th} we get from (86) and (88):

$$B_{\text{th}} = \delta F \int \kappa(E) v \rho'(E) dE = \tfrac{1}{4}\pi \delta F q' N^{\frac{1}{2}} l \kappa_{\text{th}} \tag{89}$$

(κ_{th} absorption coefficient in cm^2/g, $\kappa_{\text{th}} = \sigma_{\text{th}}/M$).

§6. Slow neutrons: Methods for the determination of energy, neutron and radiation width of the compound levels

In the following we discuss the application of the formulae derived in §5 to the determination of the constants E_g, Γ_n and Γ_γ from absorption and activation experiments. We shall limit ourselves throughout to a consideration of the case of thin absorbers and indicators. Corrections for finite thickness, which become important in nearly all practical cases, will be discussed in a subsequent paper by one of the authors (H.A.B.). When refering to experimental data, we shall not recorrect the values for cross section and activation for finite thickness, but use the values as given and corrected by the respective authors. The constants thus obtained must therefore be considered as provisional.

The application of the preceding formulae is based on the possibility of isolating, among the neutrons emerging from paraffin, (*a*) thermal neutrons, (*b*) neutrons, the capture of which leads to a *definite* level of the compound nucleus formed in the capture process (resonance neutrons), The only means of isolating the thermal neutrons is at present the absorption in cadmium. As is shown by various experiments, practically all thermal neutrons are stopped by 0.45 g/cm^2 Cd. Under the assumption, that the numerosity of the thermal neutrons is very large compared to the numerosity of the neutrons of higher energies absorbed by Cd, the thermal neutrons have therefore been identified with the so-called *C* neutrons, i.e., neutrons stopped by 0.45 g/cm^2 Cd. It is, however, probable—see below—that the Cd level responsible for this absorption lies at about 0.1 volt and has a width of 0.2 volt, so that the strong absorption in 0.45 g/cm^2 Cd extends to about 0.3 volt.

Hence, a certain number of neutrons of energies considerably higher than thermal energies will be among the *C* neutrons. The fact, that the slowing down process in paraffin in the region between the energy of the chemical hydrogen bond ($\frac{1}{3}-\frac{1}{8}$ volt) and the thermal region is rather inefficient, increases the number of neutrons in this region. Furthermore, in the thermal region itself, the energy distribution of the neutrons will not be accurately represented by the Maxwell curve, as the neutrons slowed down in paraffin are captured by the hydrogen nuclei before complete thermal equilibrium is reached.

No accurate estimates of the magnitude of these effects are at present available, but it seems from a theoretical discussion that they are not very large,[19] so that at least the order of magnitude of the results will not be changed. This is also shown by the fact that the energy distribution curve of the neutrons, as found with the mechanical velocity selector of Cd sheets, has a maximum in the thermal region.[35] Therefore we shall in this paper retain throughout the identification of *C* neutrons and thermal neutrons, substituting thus σ_{th}, κ_{th}, and B_{th} by σ_c, κ_c, and B_c and using for the effective energy of the *C* neutrons with $1/v$ indication the value $E_c = (\pi/4)kT$ (cf. (88)).

[35] Dunning, Pegram, Fink, Mitchell and Segrè, Phys. Rev. **48**, 704 (1935).

For the isolation of the resonance neutrons the absorption or indication in the element to be investigated is used. A source of uncertainty lies in the fact, that the resonance neutrons thus defined may belong not to a single resonance level but to several of them. The total resonance activation A_{res} observed will then be the sum of the activations of the single compound levels, so that we have (cf. (77)):

$$A_{res}=\sum_g A_g=c\sum_g(\Gamma'_{ng}/E_g^{\frac{1}{2}}), \qquad (90)$$

where c is a constant, and Γ'_{ng} the reduced neutron width of the level E_g (i.e., neutron width at 1 volt; cf. (77), (77a)). Except for the irregular variation of Γ'_{ng}, the contributions of the higher levels to the activation will decrease as $E_g^{-\frac{1}{2}}$. For a quite schematic picture of the situation, we may assume the levels to be equally spaced with a distance D corresponding to the actual *mean* distance and Γ'_{ng} to be the same for all levels. Then we see that the importance of the contributions of the higher levels to the activation will be determined by the ratio of the energy of the first positive level E_1 to the mean distance D. Indeed we have

$$A_{res}=A_1\cdot\sum_{g=1}\{1+(g-1)(D/E_1)\}^{-\frac{1}{2}} \qquad (91)$$

and may now distinguish three cases:

(a) $E_1\ll D$. The activation is practically determined by the first level. This case will be realized, if resonance capture is observed in a light element, because here the resonance activation will in general only be observable if E_1 by accident lies exceptionally low.[36] Occasionally, this may also occur for a heavy element.

(b) $E_1\sim D$. The total contribution of the higher levels to the activation is of the same order of magnitude as the contribution of the first level and is caused by a great number of levels; e.g., for $E_1=\frac{1}{2}D$ we have $A_{res}=2.6A_1$, and the activation due to the levels with $g>50$ is still 30 percent of the activation of the first level.

We shall later give arguments to the effect that this case is more or less realized for elements like Ag, Rh, In; D being of the order of some volts.

(c) $E_1\gg D$. Each of a great number of higher levels produces an activation of the order of the effect of the first one. This may occasionally happen for a heavier nucleus. It seems (cf. below) that iodine may come near to this case.

In a similar way, the influence of the higher levels on the absorption coefficient with self-indication can be discussed.

A certain—though not very sharp—control of the effect of higher levels is supplied by the analysis of the absorption curves with self-indication, supplemented with boron absorption curves. Such an analysis would permit one to detect a pronounced heterogeneity of the neutrons.[37] (Cf. Fermi's groups *A* and *B* in Ag.) In the following, we shall give formulae under the assumption, that only a single level is effective, and discuss for every method how the results are modified by the presence of several levels.

A. Determination of energy

1. Absorption in boron[38]

Case a. Resonance energy larger than the cadmium absorption limit.—The absorption coefficient in boron for the neutrons penetrating cadmium and indicated by the element under investigation is compared to the absorption coefficient of the *C* neutrons in boron, measured with a boron chamber or another indicator obeying the $1/v$ law in the thermal region. Because of the $1/v$ law for the capture in boron, the reasons for which have been given in §5D, and because of (88), we have for the resonance energy:[39]

[36] It is true that with decreasing atomic number, not only the mean distance D of the levels, but also the neutron width $\bar{\Gamma}_n$ increases rapidly, so that for a light nucleus a noticeable activation might still be produced by resonance neutrons of much higher energy than for a heavy nucleus. It is, however, probable, that the neutron width increases less rapidly than $D^{\frac{1}{2}}$, so that here the possibility for the detection of resonance-capture is in general limited to the case $E_1\ll D$.

[37] Also if only a single resonance level is of importance, the heterogeneity caused by the variation of the absorption coefficient within the line will manifest itself in the absorption curves. It will often be possible, however, to decide with the help of the constants determined according to Section C whether this reason is sufficient to explain the shape of the absorption curves or whether the presence of several levels must be assumed.

[38] Frisch and Placzek, reference 33. Weekes, Livingston and Bethe, reference 33. Collie, Nature **137**, 619 (1936). Amaldi and Fermi, reference 30. Halban and Preiswerk, Helv. Phys. Acta **9**, 318 (1936). Goldsmith and Rasetti, Phys. Rev. **50**, 328 (1936). Goldsmith and Manley, Phys. Rev., in press.

[39] Goldsmith-Rasetti take kT instead of $\pi/4\ kT$ as a correction for the hardening of the thermal neutrons in the thick layers used. The actual value of E_c is probably still a little higher because of the reasons exposed at the beginning of this section.

$$E_g = E_c \left(\frac{\kappa^{\text{boron}}{}_c}{\kappa^{\text{boron}}{}_g} \right)^2 = \frac{\pi}{4} kT \left(\frac{\kappa^{\text{boron}}{}_c}{\kappa^{\text{boron}}{}_g} \right)^2. \quad (92)$$

If several resonance levels are effective, the energy determined according to (92) will be a rather ill defined mean value, namely (cf. 90)

$$E_{res} = \left(\frac{\sum_g \Gamma'_{ng} E_g^{-1}}{\sum_g \Gamma'_{ng} E_g^{-2}} \right)^2. \quad (93)$$

If all Γ'_{ng} are equal, and $E_1 = D$ (cf. above), this gives $E_{res} = 2.5 E_1$.

(93) holds for a thin boron layer; for thick layers, the influence of the higher levels will be still more pronounced. It is therefore essential to base the energy determination on complete absorption curves and not on single points. Furthermore the influence of the higher levels may be reduced by defining the resonance neutrons not by the indication alone, but also by the absorption, which can be done by adding to the cadmium filter a filter consisting of the same element as the indicator.

At present, the energy values found by different observers with the boron method seem to differ to a certain extent in some cases. The reason for this appears to be not so much lack of precision of the measurements, but different—and perhaps insufficient—correction for geometrical factors.

Case b. E_g smaller than the Cd absorption limit. If the resonance energy is smaller than the energy at which Cd becomes transparent (about 0.3 volt, *viz.* below), the boron method in the form described will not be applicable. Here, instead, some information about the position of the level may be obtained by the study of the boron absorption with boron indication of the neutrons stopped by and penetrating through layers of various thickness of the element to be investigated, as was done originally in the case of cadmium.[40]

Important supplementary information about the position of low energy levels may be obtained from the rotating wheel experiment,[41] as will be discussed for the case of cadmium (§7B).

[40] Frisch and Placzek, reference 33.

[41] Rasetti, Segrè, Fink, Dunning and Pegram, Phys. Rev. **49**, 104 (1936); Rasetti, Mitchell, Fink and Pegram, Phys. Rev. **49**, 777 (1936).

The extension of both methods to other elements, where the presence of a low level is suspected (Dy, Sm, Gd) is made difficult by the rarity of most of these elements, which forbids the use of absorbers of sufficient dimensions.

2. Other methods

The energy of resonance neutrons may also be estimated by the study of the diffusion of the resonance neutrons in paraffin.[42] It seems, however, that these methods are hardly accurate enough to give quantitative results; they may chiefly serve to check the relative order of the energies as given by the boron method.

B. Neutron width

The neutron width may be found directly from the resonance activation with the help of (77), if the absolute number of the neutrons q is known. To determine q, we will use the procedure of Amaldi and Fermi, who express q by the thermal activation and cross section. Integrating resonance and thermal activations over the whole paraffin volume, we get from (77), (89) and (82):

$$\Gamma_n = \frac{C E_g^2 \sigma_c}{1.30 \cdot 10^{-18}}, \quad (94)[43]$$

where

$$C = \tfrac{1}{2} \frac{\int A_g dV}{\int B_g dV} \frac{N \bar{l}}{l_g}. \quad (94a)$$

For purposes of comparison it is better to use the reduced neutron width Γ'_n (neutron width at 1 volt, $\Gamma'_n = \Gamma_n E_g^{-1}$)

$$\Gamma'_n = \frac{C E_g^{\frac{1}{2}} \sigma_c}{1.30 \cdot 10^{-18}}. \quad (95)$$

(95) is very useful as it gives an expression for the neutron width which, being independent of ξ, holds irrespective of the form of the line.

In the case of the presence of several resonance levels, the Γ'_n determined from (95) will be considerably too large. Indeed, we have from (95), (90) and (93)

$$(\Gamma'_n)_a = \frac{(\sum \Gamma'_{ng} E_g^{-1})^4}{(\sum \Gamma'_{ng} E_g^{-2})^3}. \quad (96)$$

[42] Halban-Preiswerk, Comptes rendus **202**, 849 (1936); Amaldi-Fermi, reference 30.

[43] Here and in the following, we shall always incorporate the unknown factor $(1 \pm 1/(2i+1))$ in the neutron width, i.e., write Γ_n instead of $\Gamma_n(1 \pm 1/(2i+1))$.

which is a weighted sum rather than a mean value. This is also clear from the fact that Γ'_n is proportional to the activation. In the special case (cf. above, after (91) and after (93)) that all Γ'_{ng} are equal, and $E_1 = D$, we have $(\Gamma'_n)_a = 10.4\ \Gamma'_{ng}$.

A way of estimating Γ'_n, if E_g lies near the thermal region, will be discussed for the example of cadmium.

C. Effective width Γ_r/χ and radiation width Γ_r

The effective width can be found—as shown by Amaldi and Fermi—from the resonance activation and absorption coefficient for self-indication. For the relative effective width $(\Gamma_r/\chi)/E_g$ we find from (75), (89), (82) and (94a)

$$(\Gamma_r/\chi(\xi))/E_g = C\kappa_c/\kappa_g \tag{97}$$

For $\xi \gg 1$ and $\xi \ll 1$ we may express the effective width by the natural and Doppler width, respectively. Thus (cf. 70 to 72a)

for $\xi \gg 1$:

$$\Gamma_r/E_g = \tfrac{1}{2} C\kappa_c/\kappa_g \cdot (1 - 1/4\xi^2 + \cdots) \tag{97a}$$

for $\xi \ll 1$:

$$\Delta/E_g = (\pi/2)^{\frac{1}{2}} \cdot C\kappa_c/\kappa_g (1 - (8/\pi)^{\frac{1}{2}}\xi + \cdots). \tag{97b}$$

The relative width found by Amaldi and Fermi under the assumption of constant cross section both for resonance and thermal neutrons is $2C(\kappa_c/\kappa_g)$, their values have hence to be divided by 4 in the case of natural and by $(8/\pi)^{\frac{1}{2}}$ in the case of Doppler width.[44] (97) also provides a mean for checking the assumptions $\Gamma_r \ll E_g$, $\Delta \ll E_g$, made for the derivation of the formulae in §5C. (Δ/E_g can, of course, also be directly calculated, *viz.* (63), if E_g is known from the boron method.)

Instead of finding from (97) the effective width, we may use the relation also as an equation for ξ and hence for Γ_r. Dividing both sides of (97) by Δ, we get

$$\frac{\chi(\xi)}{\xi} = 4\left(\frac{kTm/M}{E_g}\right)^{\frac{1}{2}} \cdot \frac{\kappa_g}{\kappa_c} \cdot \frac{1}{C}, \tag{98}$$

from which ξ may be determined. If, however, ξ is small, (98) is very insensitive, since for $\xi \ll 1$, $\chi(\xi)$ is proportional to ξ. Thus small natural widths cannot be determined in the presence of large Doppler widths.

The presence of several levels has a similar effect upon the radiation width Γ_r determined from (98) as upon the neutron width Γ_n. If all levels have natural width, the Γ_r found from (98) is

$$(\Gamma_r)_a = \frac{(\sum \Gamma'_{ng} E_g^{-1})^4}{(\sum (\Gamma'^2_{ng}/\Gamma_{rg}) E_g^{-2})(\sum \Gamma'_{ng} E_g^{-2})^2}, \tag{99}$$

which, as in the case of $(\Gamma_n)_a$, is a sum rather than a mean value. In the special case that all Γ'_{ng} and all Γ_{rg} are equal, that the levels are equally spaced and $E_1 = D$, we have $\Gamma_r = 10.4\ \Gamma_{rg}$.

In the formulae derived up to now, the one level formula (61) was only made use of in the immediate neighborhood of the resonance but no relation was assumed between the cross section for thermal neutrons σ_c and the resonance cross section σ_g. If we suppose that the thermal cross section σ_c is determined by the influence of a single resonance level, the comparison between thermal and resonance cross section gives us another method for finding the radiation width.[45] It is obvious, that this assumption, which involves the extrapolation of the one level formula up to the thermal region, is a much more special one than the assumption discussed before, *viz.* that the measured resonance absorption is mainly due to one compound level only.

Firstly, for the thermal cross section the levels of negative energy E_g, which do not contribute to the absorption, are of as much importance as the levels of positive energy. Secondly, the interference of the capturing amplitudes in (58) may considerably increase the effect of the higher levels. The importance of formulae based on this assumption will therefore consist not so much in that they supply an independent method to determine Γ_r, but rather in that they give a possibility of finding out in actual cases, to what extent the thermal cross section is connected to the measured resonance absorption.

If $E_g \gg kT$, we have from (61), (63) and (70)[46]

[44] Cf. however, reference 49.

[45] Bethe, Phys. Rev. **49**, 888 (1936).

[46] The formulae which are based on the extrapolation of the one level formula in the thermal region are marked by an asterisk.

$$\sigma_c = \frac{\sigma_{0N}}{2} \frac{\Gamma_r^2}{E_g^{\frac{1}{2}}(\pi kT)^{\frac{1}{2}}} = \sigma_g \cdot \frac{8}{\pi^{\frac{1}{2}}} \frac{m}{M} \frac{\xi^2}{\chi(\xi)} \left(\frac{kT}{E_g}\right)^{\frac{1}{2}}. \quad (100)^*$$

This gives for the relative radiation width Γ_r/E_g for $\xi \gg 1$ (cf. 71):

$$\Gamma_r/E_g = (\sigma_c/\sigma_g)^{\frac{1}{2}}(\pi kT/E_g)^{\frac{1}{2}}(1 - 1/8\xi^2 + \cdots) \quad (101a)^*$$

for $\xi \ll 1$ (cf. 72, 72a);

$$\frac{\Gamma_r}{E_g} = \frac{\sigma_c}{\sigma_g} \frac{\pi}{8^{\frac{1}{2}}} \left(\frac{M}{m}\right)^{\frac{1}{2}} (1 - (8/\pi)^{\frac{1}{2}}\xi - \cdots). \quad (101b)^*$$

More generally, we may consider (100) as an equation for ξ

$$\frac{\chi(\xi)}{\xi^2} = \frac{8}{\pi^{\frac{1}{2}}} \frac{m}{M} \frac{\sigma_g}{\sigma_c} \left(\frac{kT}{E_g}\right)^{\frac{1}{2}}. \quad (102)^*$$

Instead of the ratio of the absorption coefficients, we may also use the ratio of the activations C. Introducing (100) into the expression for the thermal activation (89), or also expressing the ratio of the absorption coefficients in (97) by (100), we get a very simple relation between the ratio of the activations and ξ, *viz.*:

$$\xi = \left(\frac{\pi}{4} \frac{M}{m}\right)^{\frac{1}{2}} \Big/ C. \quad (103)^*$$

We have now 3 relations for ξ, the general relation (98) and the two relations (102) and (103) which make use of the assumption (100). Of these 3 relations, however, only two are independent, as for instance by dividing (98) by (103) we get (102). We may find out in each case how far the thermal cross section is connected with the level causing the resonance absorption, by comparing the ξ found from (103) with the ξ supplied by the general formula (98). In this connection attention must be paid to the fact, that the ratio of the two ξ's depends rather sensitively on the value of C; e.g., for $\xi \gg 1$, ξ is proportional to C (cf. 98), while ξ_{act} [so we shall denote from now on the ξ determined from (103)] is, proportional to $1/C$, so that, ξ/ξ_{act} is proportional to C^2.

§7. Discussion of experimental data on slow neutrons

A. $E_g \gg kT$. Complete data on energies, absorption coefficients and activations are available for the elements Rh, Ag (22nd period, group *A*) and I. The values for the resonance absorption coefficients κ_g and the resonance activations A_g are not very certain, owing to the difficulties of correction for finite thickness of the indicators and absorbers used. The following discussion should therefore be considered as demonstrating how the preceding formulae should be used in the analysis of the experiments, rather than as a derivation of final results.

1. *Rhodium (group D).*—For the energy, determined by the boron method, we take $E_g = 1.1$ volts.[47] This corresponds to a Doppler width of 0.066 volt. The absorption coefficient for C neutrons is 0.7 cm^2/g,[48] corresponding to a cross section of $120 \cdot 10^{-24}$ cm^2. For the ratio of the activations, one finds from Amaldi-Fermi's data $C = 0.77$.[49] From these data, we get for the neutron width $\Gamma_n = 8.6 \cdot 10^{-5}$ volt and the reduced neutron width $\Gamma'_n = 8.2 \cdot 10^{-5}$ volt.

The resonance absorption coefficient κ_g is given as 4.0 cm^2/g by v. Halban,[50] while Amaldi and Fermi find $\kappa_g = 1.8$. From (97) and (98) we have (the constants following from the latter value of κ_g are put in brackets) $\Gamma_r/\chi = 0.15$ (0.33), $\xi = 0.90$ (2.4), $\Gamma_r = 0.060$ (0.16).

Supposing that the cross section for neutrons of thermal energy is entirely caused by the resonance level, to which the constants now determined refer, we would get from the activations according to (103)* $\xi_{act} = 11.5$, and from the

[47] Goldsmith-Rasetti, Phys. Rev. **50**, 328 (1936).

[48] Amaldi and Fermi, reference 30.

[49] This value is obtained by using Amaldi and Fermi's correction for finite thickness, based on the assumption of a constant resonance absorption coefficient. The correction is numerically rather important, it increases the measured value of C by a factor 1.55 in the present case. The consideration of the fact that due to the variation of the capture cross section in the resonance region—the apparent absorption coefficient of resonance neutrons is lowered by their passage through thick layers, would tend to diminish the corrective factor and thus diminish the value of C. The correct procedure would be to use Amaldi-Fermi's value as a zero approximation in (97) and (98), recorrect it by introducing the line-shape thus determined, and recalculate the constants with the recorrected value of C. The lowering of the above value of C, caused by this effect, may well be upset, if Amaldi-Fermi's value for κ_g, used also for the correction of C, should prove to be too low, as would be the case according to v. Halban (see below).

[50] Private communication.

cross sections, cf. (102)*, $\xi_\sigma = 3.2$ (5.2). If, therefore, the observed resonance level were the only one contributing to the thermal cross section, the thermal activation and cross section would be by the ratio ξ_{act}/ξ, i.e., 12.8 times (4.8 times), smaller than the observed values.

If we assume, therefore, that the main resonance absorption is caused by a single level at 1.1 volts, we may conclude that—as far as we can trust the measurements and especially if v. Halban's value for the resonance cross section proves to be right—the chief contribution to the thermal cross section does not come from this resonance level, but from other (higher or negative) levels.[50a]

2. *Silver.*—The resonance neutrons of Ag (22″-period) have been divided into two groups. About two-thirds of the resonance activation are absorbed in a thin sheet of Ag and called group *A*. The other third (group *B*) seems to consist of much harder components.

For the energy of group *A*, we take $E_\varrho = 2.5$ volts,[47] which gives the Doppler width $\Delta = 0.096$ volt.

The absorption coefficients for thermal and resonance neutrons are[30] $\kappa_\varrho = 20 \text{cm}^2/\text{g}$, $\kappa_c = 0.25$ cm^2/g, the ratio of the activations $C = 1.52$.

Now we must take account of the fact that Ag consists of two isotopes of nearly equal abundance, of which only one absorbs group *A*, giving rise to the 22″ period. Thus we have for the cross section σ_ϱ obtained from κ_ϱ : $\sigma_\varrho = 2\kappa_\varrho M = 7000 \cdot 10^{-24}$ cm². To the cross section in the thermal region both isotopes contribute. The ratio of the thermal activations for the short and the long period was found to be 3 : 1.[10] The thermal cross section of the isotope absorbing group *A* is therefore $\sigma_c = \frac{1}{2}\kappa_c M = 70 \cdot 10^{-24}$ cm². The thermal activation measured by Amaldi and Fermi refers to both periods. Therefore, the absorption coefficients to be introduced in (98) are the directly measured absorption coefficients, while in (102) enter the actual cross sections of the capturing isotope. If we use in all the formulae the measured absorption coefficients (or correspondent apparent cross sections $\sigma = M\kappa$) and the thermal activation referring to both periods, then the value of Γ_n and Γ'_n obtained from (94) and (95) have to be multiplied by 2, χ/ξ^2 from (102) by 4/3 and ξ from (103) by $\frac{1}{4}$.

Taking these factors into account, one finds $\Gamma_n = 7 \cdot 10^{-4}$ volts, $\Gamma'_n = 4 \cdot 10^{-4}$ volts.

From (98) we get $\chi/\xi = 2.02$. From this, we cannot calculate ξ, because the maximum value of χ/ξ for $\xi = 0$ is $(\pi/2)^{\frac{1}{2}} = 1.25$. We may only conclude that ξ is probably smaller than 1. In other words: the effective width Γ_r/χ determined from (97) turns out to be smaller than the Doppler width calculated from the boron determined energy. Indeed (97) gives $\Gamma_r/\chi = 0.047$ volt, which, if the line has pure Doppler form, would correspond to a Doppler width of 0.060 volt, while the Doppler width from the boron energy is 0.096 volt. This difference may well be due to experimental error.

From the ratio of the activations (103) one finds $\xi_{act} = 6.0$, from the ratio of the cross sections $\xi = 1$. As in Rh, the one level formula gives too high values for ξ. This means, as already mentioned, that if the resonance level with the width determined from (98) would alone be effective, the activation and cross section in the thermal region would be smaller than observed. The discrepancies are much more striking than in the case of Rh and cannot be removed by considerations as those described in reference 50*a*.

The existence of higher levels in the Ag isotope which absorbs group *A* is proved by the existence of group *B*, the mean energy of which is estimated by the boron method to be 4.5 volts.[47] The fact that this group is much less absorbable in Ag seems to show that either the neutron widths of the respective levels are smaller or the radiation width larger than those of group *A*. If the latter is the case, the effect of these levels upon the thermal cross section would be more important than the contribution of the level corresponding to group *A*.

3. *Iodine.*—The data for iodine are the least accurate ones. The resonance energy lies high: $E_\varrho \sim 80$ volts.[47] The thermal activation has not been given by Fermi and Amaldi, because they eliminated q in this case with the help of the thermal cross section and activation for Rh. Herefrom and from the thermal absorption coefficient $\kappa_c = 0.024$ cm^2/g[51] the thermal activation can be recalculated, which gives $C = 2.16$. For the resonance absorption coefficient Amaldi and Fermi give $\kappa_\varrho = 0.38$ cm^2/g.

[50a] *Note added in proof:* The calculations described are very sensitive to the assumptions about the mean free path of thermal and faster neutrons in paraffin. Reasons can be given (reference 19) for the assumption that l_ϱ is only 0.8 to 0.9 cm rather than 1.1 cm as Amaldi and Fermi assume. This improves the agreement considerably so that it can, at the moment, not be excluded that the chief contribution to the thermal cross section of Rh comes from the "*D*" level.

[51] Frisch, private communication.

The constants derived from these values, together with the constants for Rh and Ag, are shown in Table II. The very high values for the neutron as well as for the radiation width[52] of iodine suggest, that the resonance activation of iodine is due to a number of levels of about equal effect (case *c*, beginning of §6), in which case the observed width would be something like the sum of the widths of the single levels.

In toto, the whole situation may be compatible with the following picture:

If we consider the series of elements Rh, Ag, In, I, which, being not very different as to their mass and all containing an even number of neutrons and an odd number of protons, should exhibit a certain similarity as to their mean density of energy levels[20] although individual variations are by no means excluded. We note that for Rh, Ag and In the boron method gives resonance energies of a few volts, while for iodine the resonance energy lies much higher. It may therefore be that the mean distance of levels in all these elements is of the order of a few volts. For Rh, Ag and In, then, the energy of the first level is of the same order as the mean distance, and the resonance activation of these elements consists therefore of a large effect of one level, the position of which coincides roughly with the measured resonance energy, and smaller contributions of a number of higher levels.

In iodine, on the other hand, the energy of the first levels would be by chance several times larger than the mean distance. Therefore, no single level has a prominent influence upon the resonance activation. The energy measured is then a mean value over many levels, which may extend from about 20 or 30 volts upwards, and the measured widths are the weighted sum of the widths of these levels. It may even be that the actual width of most of these levels is already practically Doppler width.

How far this picture coincides with the facts may be ascertained to a certain extent by the accurate study of the absorption curves with self-indication and the refinement of the boron method by its combination with varied filterings.

[52] According to recent measurements of Frisch, κ_g seems to be much higher than given by Amaldi and Fermi, i.e., about 2–3 cm²/g. This would reduce considerably the value of the radiation width and also create with respect to the ratio ξ_{act}/ξ a situation more similar to Ag and Rh.

B. $E_g \approx kT$.

4. *Cadmium.*—The absorption coefficient in boron, measured with boron indication, of the neutrons penetrating cadmium is about 7 times smaller than the boron absorption coefficient for *C* neutrons.[53] From this it follows, that Cd has a resonance level at an energy considerably lower than one volt. This energy may, according to these data, be positive as well as negative. Rasetti, Segrè, Fink, Dunning, Pegram[41] have shown that the absorption of a Cd wheel is lowered when it rotates with a velocity component in the direction of the velocity of the incident neutrons. From this it follows that the capture probability in the thermal region increases with increasing energy. This proves, that the level has a positive energy and lies above the thermal energy. Still a little more follows from a quantitative discussion.

The relative change in the absorption measured in this experiment is directly equal to the relative change in the capture probability $\Delta p/p$. We have:

$$\frac{\Delta p}{p} = \frac{1}{p}\frac{dp}{dE}\cdot\Delta E = \frac{2(E_g - E)}{(E_g - E)^2 + (\tfrac{1}{2}\Gamma)^2}\cdot\Delta E \qquad (104)$$

(ΔE is the change in the effective energy of the neutrons caused by the rotation of the wheel). We may now define an energy u by

$$u = p/\Delta p\cdot\Delta E. \qquad (105)$$

Then we have from (104)

$$u = \frac{(\tfrac{1}{2}\Gamma)^2 + (E_g - E)^2}{2(E_g - E)} \qquad (106)$$

From (106) we see, that, if $u > 0$

$$E_g - E < 2u, \qquad (107a)$$

$$\Gamma < 2u, \qquad (107b)$$

$$(E_g - E)^2 + (\tfrac{1}{2}\Gamma)^2 < 4u^2. \qquad (107c)$$

From the measurements, u comes out to be 0.10 volt, hence

$$E_g - E < 0.20 \text{ volt}, \qquad (108a)$$

$$\Gamma < 0.20 \text{ volt}, \qquad (108b)$$

$$((E_g - E)^2 + (\tfrac{1}{2}\Gamma)^2)^{\frac{1}{2}} < 0.20 \text{ volt}. \qquad (108c)$$

[53] Frisch and Placzek, reference 33, Collie, reference 38.

We may now try to get further information by using Amaldi-Fermi's cadmium absorption curve measured with Rh indication. From this curve, the Cd absorption coefficient for the Rh resonance (D) neutrons may be estimated to be about 270 times smaller than for the C neutrons. Assuming that the Cd cross section for D neutrons is entirely determined by the resonance level near thermal energy, which is of course very doubtful, especially in the light of the evidence of section A, we have from (61):

$$\frac{\sigma_D}{\sigma_{\text{th}}}=\frac{E_{\text{th}}^{\frac{1}{2}}}{E_D^{\frac{1}{2}}}\cdot\frac{(E_\varrho-E_{\text{th}})^2+(\tfrac{1}{2}\Gamma)^2}{(E_D-E_\varrho)^2}. \tag{109}$$

Combining (109) with (106), we find $E_\varrho=0.14$ volt, $\Gamma=0.20$ volt. With these values, the cross section (cf. Fig. 1) would have a very flat minimum at about 0.05 volt and a very flat maximum at 0.12 volt, the maximum being only about 12 percent higher than the minimum.

To find the neutron width, we must decide to which of the many Cd isotopes the resonance level is to be ascribed. The most probable assumption is, that it belongs to an isotope with odd mass, as these isotopes have the largest level density.[20] As both odd isotopes (111 and 113) have about equal abundance (12 percent and 10 percent, respectively), it does not matter very much for the cross section, to which of the two isotopes the level belongs.

Inserting the thermal cross section, which—corrected for the abundance with this assumption—is $25{,}000\cdot10^{-24}$ cm^2, and the above values for E_ϱ and Γ_τ into (61), we find for the cross section at resonance $\sigma_{0N}=25{,}000\cdot10^{-24}$ cm^2, i.e., the same value as at thermal energy. This gives for the neutron width $\Gamma_n=5\cdot10^{-4}$ volt and the reduced neutron width $\Gamma'_n=1.5\cdot10^{-3}$ volt.

§8. Fast neutrons[54]

The present theory is quantitatively applicable to fast neutrons only as long as the mean distance of the compound levels remains large compared to the neutron and the radiation width,[55a] i.e., $\Gamma_n\ll D$, $\Gamma_\tau\ll D$.

Even in the energy region where this condition still holds, the cross section will in general exhibit no maxima because of the Doppler effect. At an energy of 2 million volts, the Doppler width for an element of mass 100 will be about 100 volts, which is probably more than the mean level distance of most of the elements in this region. Apart from this fact, the actual inhomogeneity of fast neutron beams will, even with artificial production, not be lower than a few thousand volts, so that resonance phenomena, even if present, may only be detected if D is larger than this energy inhomogeneity. In all other cases, a mean absorption will be observed, given by[55]

$$\sigma=\frac{\pi^2R^2}{2i+1}\frac{\Gamma_n}{D}. \tag{110}$$

Γ_n is the mean neutron width of the levels in the energy region concerned, and R the nuclear radius. The formula is obtained by considering the influence of the various orbital momenta of the incident particle. (110) comprises capture and scattering except potential scattering. As already emphasized by Bohr,[1] most of the scattering (except the potential scattering) will be inelastic.[56]

[54] For a detailed discussion of the properties of fast neutrons we refer to Bohr and Kalckar, reference 1.

[55a] For the case of large width, cf. reference 19.

[55] Cf., Bethe, Phys. Rev. **50**, 332 (1936); Bethe and Livingston, reference 19.

[56] For the experimental evidence, cf. Werthenstein, Nature **135**, 747 (1935); Ehrenberg, Nature **136**, 870 (1935).

TABLE II.

Element	E_ϱ	K_ϱ	K_τ	C	$\sigma_\varrho\cdot10^{24}$	$\sigma_c\cdot10^{24}$	Δ	Γ_τ	$\Gamma_n\cdot10^4$	$\Gamma'_n\cdot10^4$	ξ	ξ_{act}
Rh	1.1[a]	1.8[b]	0.7[b]	0.77	310	120	0.066	0.16	0.86	0.82	2.4	11.5
		4.0[c]			680	67	0.096	0.060	6.6	4.2	0.90	6
Ag(22″)	2.5[a]	20[b]	0.25[b]	1.52	7100	5	0.50	<0.05	500	56	≪1	4.6
I	80[a]	0.38[b]	0.024[d]	2.2	80	25,000		5.5	5	15	11	
Cd	0.14		13.5					0.2				

[a] Goldsmith-Rasetti, reference 46.
[b] Amaldi-Fermi, reference 30.
[c] v. Halban, reference 38.
[d] Frisch, reference 51.

Two kinds of inelastic processes may occur. Either the compound level created by the capture of a fast neutron may emit a neutron of lower energy, leaving the final nucleus in an excited state, which then emits a γ quantum (ordinary inelastic scattering). Or the compound level originally formed may first go over by γ-ray emission to a lower state of the compound nucleus, which then decays further under emission of a neutron (inelastic scattering of the second kind). The latter type of processes must be taken into account for the calculation of the capture cross section: It has a lowering effect on the probability of capture because not all radiative processes lead to capture. However, it is likely that the probability of the inelastic scattering of the second kind is smaller than the capture cross section, because the γ-rays emitted have lower frequency in the case of the scattering of the second kind, and the emission probability is *cet. par.* proportional to the third power of the frequency of the γ-ray. Only if the neutrons have very high energies, will the inelastic scattering of the second kind be important.

Experimentally, not very much is known about the capture of fast neutrons. The earlier conception, according to which the observed capture effects should be attributed to the effect of small admixtures of slow neutrons,[57] seems not to agree very well with numerosity considerations, and it is more likely, that at least a part of the observed effects is to be ascribed to the fast neutrons. Conclusions about the ratio of neutron and radiation width in the range of high neutron energies, based on the comparison of capture and scattering cross section, are therefore hardly possible.

In this state of affairs, it seems more promising to estimate the neutron width at high energies by simply extrapolating the data from slow neutron experiments. Assuming the $E^{\frac{1}{2}}$ law for the neutron width which will hold as long as the wave-length is large compared to nuclear dimensions, and supposing, as in §4, that there are no systematic differences between the matrix elements for high and for low energies, we would get from the slow neutron data for Rh and Ag a neutron width of 0.1–1 volt for energies of some million volts. This would mean, that in that region neutron and radiation width have about the same order of magnitude. However, it must be kept in mind that this extrapolation gives only the *partial* neutron width corresponding to a process in which the final nucleus is left in the *ground* state. If the neutron energy is sufficient for inelastic scattering, i.e., if the final nucleus may be left in excited states after the reemission of the neutron, the total neutron width will be much larger, approximately in proportion to the number of possible final levels. Then the inelastic scattering will be much more probable than the capture.

[57] Bethe, Phys. Rev. **47**, 797 (1935).

§9. Elastic scattering of neutrons

The theoretical discussion of the scattering has been given in §4. Experimentally, the scattering of slow neutrons, of thermal as well as higher energies, has been investigated.[58] The cross sections observed with various elements are of the order of magnitude of nuclear dimensions. No case of resonance scattering has been found thus far.

For fast neutrons, it is again difficult to separate inelastic[56] from elastic scattering. Assuming that the "total absorption" of fast neutrons observed[59] is due to elastic scattering, Rabi[60] found good agreement with the theoretical potential scattering for hard spheres. This corresponds to the assumption about the potential which we showed in §4 to be most likely correct.

§10. Transmutations involving charged particles

If the particle Q is charged, the matrix element $U^r{}_Q{}^J{}_q$ involves two factors, firstly a factor due to the electrostatic potential barrier between the particle and the nucleus, and secondly, a factor giving the probability of the concentration of the nuclear energy on the particle Q. The latter factor is quite analogous to the case of neutrons, and is the more interesting part. In order to obtain it from the experimental data, the first (penetration) factor must be split off, using the well-known formulae for the penetration through a potential barrier. A convenient form for the penetration factor is[19]

[58] Dunning, Pegram, Fink and D. P. Mitchell, Phys. Rev. **48**, 265 (1935). Wick and Pontecorvo, Ric. Sci. **2**, 3/4 and 4/5 (1936). A. C. G. Mitchell and Murphy, Phys. Rev. **48**, 653 (1935). A. C. G. Mitchell, Murphy and Longer, Phys. Rev. **49**, 401 (1936). A. C. G. Mitchell, Murphy and Whittaker, Phys. Rev. **50**, 132 (1936).

[59] Dunning *et. al.* reference 58.

[60] Rabi, Phys. Rev. **43**, 838 (1933). It may seem satisfactory that Rabi deduced from the scattering effective radii somewhat larger than the then accepted nuclear radius whereas we have shown (§4) that the cross section of the potential scattering should be slightly smaller than the geometrical cross section of the nucleus. This difference would compensate for the increase in the nuclear radius necessitated by the Bohr theory (cf. reference 55).

$$P_Q = \exp[-2g\gamma(E_Q/U_0)] \quad (111)$$

where
$$g = 0.38(M_Q Z_Q)^{\frac{1}{2}} Z_B^{\frac{1}{2}} M_B^{1/6}, \quad (111a)$$

$$\gamma(x) = x^{-\frac{1}{2}} \arccos x^{\frac{1}{2}} - (1-x)^{\frac{1}{2}} \quad (111b)$$

with M_Q and M_B the atomic weights of the particle Q and the nucleus $B(O^{16}=16)$, Z_Q and Z_B the respective nuclear charges and 0.38 a constant derived from the observed radii of heavy nuclei. A curve for $\gamma(x)$ is given in the report by Bethe and Livingston.[19] E_Q is the absolute kinetic energy of the incident particle, and U_0 the height of the potential barrier,

$$U_0 = 0.70 Z_Q Z_B (M_B + M_Q)/M_B^{4/3} \text{ MV}. \quad (111c)$$

Since the penetrability (111) falls very rapidly with decreasing particle energy, charged particles can only appear in nuclear reactions if their energy is not too small compared to the height of the potential barrier. (For quantitative data, cf. reference 19.) Because of the considerable energy required, it is not possible to define the energy of the incident particle accurately enough to observe reasonances if the resonance levels are closely spaced. Therefore *no resonance effects will be observable with charged particles and heavy nuclei* (cf., however, the case of Pt below).

On the other hand, if the energy is high enough to make the process observable, there is still a rapid increase of the probability with increasing particle energy. This increase is apt to mask resonance effects if the resonance is broad and not very pronounced. Consequently, the best chance for observing resonance with charged particles is if the resonance is narrow. The process most suitable for resonance is therefore the simple capture of particles with the emission of γ-rays, provided that no other process is possible for the given energy and angular momentum of the incident particle.

In fact, the most striking resonance effects have been observed for the simple capture of protons by nuclei. The processes studied in detail are[61]

$$Li^7 + H^1 = Be^8 + \gamma \quad \text{I},$$
$$C^{12} + H^1 = N^{13} + \gamma \quad \text{II},$$
$$F^{19} + H^1 = Ne^{20} + \gamma \quad \text{III}.$$

[61] Hafstad and Tuve, Phys. Rev. **47**, 506 (1935). Hafstad, Heydenburg and Tuve, Phys. Rev. **50**, 504 (1936). For detailed theoretical discussions, see Hafstad, Heydenburg and Tuve; Bohr and Kalckar, reference 1.

For process I and III, the width of the resonance has been measured and found to be small, for II the resonance is also known to be narrow. The reactions have been studied by measuring the γ-rays.

In case II, the capture reaction is the only one which can occur on energetic grounds. All other reactions, e.g., $C^{12}+H^1=B^9+He^4$, $C^{12}+H^1=C^{11}+H^2$, $C^{12}+H^1=N^{12}+n^1$ would be very highly endoergic and can therefore not take place with protons of relatively low energy (below 1 MV). In case I and III, other reactions are energetically allowed, *viz.* in the first case,

$$Li^7 + H^1 = 2He^4 \quad \text{(Ia)}$$

and in case III

$$F^{19} + H^1 = O^{16} + He^4 \quad \text{(IIIa)}$$

However, there are very strict selection rules for parity and angular momentum, particularly in case I.

The wave function of the α-particle in its ground state will certainly be even. The same will be true of the wave function describing the relative motion of the two α-particles formed in reaction Ia, because they obey Bose statistics. Therefore only *even* states of the compound nucleus Be^8 can disintegrate into two α-particles. Similarly, the spin of the α-particle is zero. The wave function of the relative motion of two α-particles contains only even spherical harmonics, again because it is symmetrical in the two particles (Bose statistics). Therefore a state of Be^8 must have even angular momentum J in order to disintegrate into two α-particles. For compound states with odd parity or odd J, reaction Ia is impossible, such states can only disintegrate into the original particles Li^7+H^1, or into a light quantum plus a Be^8 nucleus in a lower state.

In case IIIa, the situation is not quite so clear. It is true that the ground state of O^{16}, just as that of He^4, is even and has spin zero. But the wave function describing the relative motion of O^{16} and He^4 has no particular parity and contains in principle terms of all angular momenta because there are no symmetry requirements. Possibly, the compound state responsible for the resonance observed in case III has very high angular

momentum so that its disintegration probability into $O^{16}+He^4$ is small though not negligible.

The observed width of the resonance level in reaction I, is 11 kv. The contribution of the emission of γ-rays to the width is negligible, from estimates of the absolute yield of the capture process it turns out to be a few volts[61] (see below) which is compatible with the neutron evidence (§7). The observed width is therefore to be attributed to the process $Be^8 \rightarrow Li^7+H^1$. To obtain the width free from the influence of the Coulomb field, we divide the observed width by the penetrability of the potential barrier. Inserting $Z_Q=1$, $Z_B=3$, $M_Q=1$, we find $g=0.83$ and for the height of the potential barrier $U_0=1.25$ MV. With $E=0.44$ MV for the energy of the incident proton, we have $x=0.35$ and $\gamma(x)=0.78$ and, according to (111), the penetrability becomes $P=e^{-1.66\cdot 0.78}=1/3.6$. Therefore the width of the level would be $3.6\cdot 11{,}000=40{,}000$ volts if the potential barrier were absent.

The "width for one volt energy without potential barrier"

$$\gamma' = \gamma E^{-\frac{1}{2}} \tag{112}$$

is, in our case, $\gamma' = 40{,}000/340{,}000^{\frac{1}{2}} = 70$ volts.[62] This value is, of course, very much (about 100,000 times) larger than the width of neutron resonance levels in heavy nuclei (§7) corresponding to the much larger average distance between levels, which, for Be^8, may be of the order of one MV or more, as compared to a few volts in heavy nuclei.

In the neighborhood of the resonance, the influence of other levels of the compound nucleus can certainly be neglected so that the one-level formula (12) may be used. The angular momenta are in our case $s=\frac{1}{2}$ (proton), $i=3/2$ (Li^7) and very probably $J=1$ (excited Be^8). The width $\gamma^r{}_p{}^J{}_p$ corresponds to the emission of protons such that the residual Li^7 is left in the ground state. But with the energy available, it is impossible that protons can be emitted by the compound nucleus and at the same time the Li^7 nucleus be left in an excited state. Therefore $\gamma^r{}_p{}^J{}_p$ is identical with the total proton width of the level and thus practically identical with the total over-all width γ, because the γ-ray width is negligible and other particles cannot be emitted.

We sum (12) over all possible excited states Q in which the nucleus may be left after emission of the γ-ray,[63] insert the values for s, i and J and obtain

$$\sigma_c = \frac{3}{2}\pi\lambda^2 \frac{\gamma\gamma_r}{4(E-E_0)^2+\gamma^2}, \tag{113}$$

where γ_r is the radiation width, γ the proton width and E_0 the energy of the resonance level. At exact resonance,

$$\sigma_{res} = \frac{3}{2}\pi\lambda^2\gamma_r/\gamma. \tag{114}$$

The experimental cross section is not well known; a crude determination[61] gave 10^{-27} cm^2. Since the resonance energy is 440 kv, we have $\lambda = 7.8\cdot 10^{-13}$ (reduced proton mass!) and

$$\gamma_r = \frac{10^{-27}}{280\cdot 10^{-26}}\gamma = 3.5\cdot 10^{-4}\gamma = 4 \text{ volts}. \tag{115}$$

The scattering of protons will also be influenced by the resonance level; we have

$$\sigma_{sc} = \frac{3}{2}\pi\lambda^2 \frac{\gamma^2}{4(E-E_0)^2+\gamma^2}. \tag{116}$$

At exact resonance, $\sigma_{sc}=(3/2)\pi\lambda^2$. With the given resonance energy of 440 kv, we have therefore $\sigma = 2.8\cdot 10^{-24}$ cm^2. This is to be compared to the Rutherford scattering in the Coulomb field which is about $1\cdot 10^{-24}$ cm^2 for backward scattering and $4\cdot 10^{-24}$ cm^2 for scattering at right angles. Thus the increase in the scattering cross section at resonance should be observable.

The apparent width of the resonance in the capture of protons by fluorine (case III above) in the experiments of Halfstad and Tuve is equal to the inhomogeneity of the proton beam, i.e., about 4 kv for the resonance at 330 kv, and about 15 kv for the levels at 890 and 940 kv.

[62] $340{,}000 = 440{,}000\cdot(7/8)^2$ volts is the relative kinetic energy of the proton with respect to the center of gravity.

[63] In the particular case of the capture of protons by Li^7, there seems to be only one state in which the final nucleus may be left, *viz.* the ground state. At least the most recent experiments (Fowler, Delsasso and Lauritsen, Phys. Rev. **50**, 389 (1936)) make it probable that only a single γ-ray line of 17 MV energy is emitted in the reaction. *Note added in proof:* This conclusion is again made doubtful by the results of Crane, Phys. Rev. **51**, 49 (1937).

Therefore, it can only be said that the actual width of the resonance levels must be smaller than, say, 3 and 10 kv, respectively. The widths should, at least for the lower resonance level, in fact be expected to be much smaller than for the Li^7+H-reaction; firstly because of the higher potential barrier of F, and secondly because the energy levels of the heavier compound nucleus Ne^{20} are denser and therefore would be narrower even without the higher potential barrier. For fluorine, we have (cf. (111)) $g=1.77$ and $U_0=2.50$. Therefore the penetrability becomes $P=1/5000$ for 330 kv and $P=1/13$ for 920 kv (average of 890 and 940). Thus we conclude from the experimental results that the widths without potential barrier would be smaller than $3\cdot 5000=15{,}000$ kv and $10\cdot 13=130$ kv, respectively. The very large result obtained for the level at 330 kv means that this level must actually be very much narrower than 3 kv, it is probably only a few volts wide. The second figure obtained would correspond to a γ' (cf. 112) of $130{,}000/830{,}000^{\frac{1}{2}}=140$ volts which also seems to be too large compared to the width $\gamma'=80$ volts of the Be^8 level (cf. above); it should be expected that γ' is smaller for the compound nucleus Ne^{20} than for Be^8; therefore the actual width should be less than one-half the upper limit given by the experiments of Hafstad, Heydenburg and Tuve. Thus the experiments are compatible with simple theoretical considerations. It must, however, be kept in mind that the theoretical results were obtained under the assumption that the width is entirely due to the proton, which need not be true (cf. above, selection rules).

Apart from the three cases mentioned, simple capture of protons has also been observed for B^{10} (detected by the radioactivity of C^{11})[64] and for Be^9 and B^{11} (detected by the γ-rays).[65] The process does no doubt occur with practically every initial nucleus, and will presumably show resonance features in most cases. However, in some cases no resonance level in the experimentally investigated region may be available; in other cases there may be other processes allowed besides the simple capture, and these other processes may lead to the emission of fast particles and may make the resonance very broad and accordingly the maximum cross section very small. The alternative reaction most likely to occur is the type giving α-particles, according to the scheme

$$Z^A+H^1\rightarrow(Z-1)^{A-3}+He^4.$$

No reaction of this type is energetically possible for N^{14} and O^{16} because the resulting nuclei C^{11} and N^{13} would have too high internal energies. Therefore the simple capture of protons by N^{14} and O^{16} should show sharp resonances provided there are suitably situated resonance levels in the respective compound nuclei O^{15} and F^{17}.

Simple capture of other projectiles, notably deuterons and α-particles, has never been observed and should be hard to observe. In particular deuterons can, because of their large internal energy, cause a great variety of more probable reactions with almost every nucleus, *viz.* the reactions leading to the emission of neutrons, protons and α-particles, respectively. This prevents the existence of sharp resonance levels. Moreover, the three reactions mentioned will, in many cases, leave the residual nucleus in an excited state, so that γ-rays are given off after the reactions. This makes it difficult to identify the simple capture process by observing the γ-rays except if very accurate measurements of their energy are available. Finally, the nucleus produced by the simple capture will usually not be radioactive so that the radioactivity is also not available for the detection of the simple capture process.

The same arguments apply to the simple capture of α-particles. However, in this case there are two nuclei for which the simple capture might be observable, *viz.* C^{12} and O^{16}. These two nuclei cannot be disintegrated by α-particles in any other way. The greatest difficulty with α-particles is the small intensity available.

Resonance phenomena have also been observed for processes other than the simple capture, *viz.* for reactions produced by α-particles and giving protons and neutrons, according to the schemes

$$Z^A+He^4=(Z+1)^{A+3}+H^1 \quad (\alpha p),$$
$$Z^A+He^4=(Z+2)^{A+3}+n^1 \quad (\alpha n).$$

[64] Crane and Lauritsen, Phys. Rev. **45**, 497 (1934).
[65] Crane, Delsasso, Fowler and Lauritsen, Phys. Rev. **47**, 782 and **48**, 102 (1935).

For the αp reaction, resonance has been observed[66] with B^{10}, N^{14}, F^{19}, Na^{23}, Mg, Al^{27}. In the case of the αn reaction, the only case where resonance has been observed with certainty, is $Be^9+He^4 \rightarrow C^{12}+n^1$. The case best investigated is the αp-reaction $Al^{27}+He^4=Si^{30}+H^1$. Seven resonance levels are known.[67] The average spacing is about 300,000 volts which seems very reasonable. The width of the levels apparent in the experiments is about half this amount, but no doubt the greater part of this figure is due to the inhomogeneity of the incident beam and the actual width of the levels is probably quite small.

A fluctuation of the yield with energy has also been reported for the radioactivity induced in Pt by deuteron bombardment.[68] This is certainly not a resonance phenomenon. For, with deuterons of about 4 MV energy, the energy of the compound nucleus is at least about 15 MV above the ground state. Considering the high atomic weight of Pt, the energy levels of the compound nucleus must be exceedingly dense, their spacing should be only a small fraction of a volt.[20] On the other hand, the reported maxima and minima in the yield are spaced several hundred thousand volts apart. However, it is quite possible that there are slow fluctuations of the cross section, due to fluctuations in the density of levels or in the magnitude of the matrix elements.

§11. Phenomena produced by γ-rays

As mentioned already in §3, there are two phenomena which may be caused by γ-rays: The photodissociation, and the scattering of γ-rays by the nucleus.

If the photodissociation were the inverse of the capture of particles, it would be exceedingly probable. E.g., for the capture of resonance neutrons we have found (§7) cross sections up to the order of 10^{-20} cm^2 the neutron energy being around 2 volts. According to (42), the probabilities of two mutually inverse processes are apart from simple statistical factors of the order unity, proportional to the squares of the wave-lengths of the respective incident particles. Now for neutrons of 2 volt energy, λ is of the order $3\cdot10^{-10}$ cm, whereas for γ-rays of 10 MV energy (corresponding to the binding energy of neutrons in heavy nuclei) we have $\lambda_\gamma \approx 2\cdot10^{-12}$ cm. Therefore $(\lambda_\gamma/\lambda_n)^2=1/20{,}000$, and the cross section for photodissociation would turn out to be of the order 10^{-25} to 10^{-24} cm^2, i.e., an exceedingly large cross section compared to other phenomena produced by γ-rays.

In reality, however, the photodissociation is not the inverse of the neutron capture, as already mentioned briefly at the end of §3. When a slow neutron is captured, any of a great number of different γ-rays may be emitted, corresponding to different excitation states q of the final nucleus B. Only for a very small fraction of all capture processes, the final nucleus will be left in the ground state. In the photodissociation, we start from a nucleus B in the ground state and irradiate it with γ-rays of the appropriate energy. The photodissociation is thus the inverse of that part of the capture process in which the final nucleus is left in the ground state. A simple estimate shows that the cross section for photodissociation is thereby reduced by a factor of about 10^5 which would make it practically unobservable for the neutron energy of 2 volts used above.

If only one level of the compound nucleus contributes, the cross section for the photoelectric dissociation is (cf. 12)

$$\sigma=\frac{\pi\lambda_\gamma^2(2J+1)}{2(2i+1)}\,\frac{\gamma_{r0}\gamma_n}{(h\nu-E_0)^2+\frac{1}{4}(\gamma_r+\gamma_n)^2}, \qquad (117)$$

where λ_γ is the wave-length of the γ-ray, i and J are the angular momenta of the initial nucleus in the ground state and in the excited ("compound") state to which it is raised by absorbing the γ-ray and $h\nu$ and E_0 are the energies of the γ-ray and the compound state. γ_n is the width of the compound level corresponding to the emission of neutrons, or generally of the particles which are formed in the photodissociation, γ_r the total γ-ray width and γ_{r0} that part of the γ-ray width which corresponds to a transition to the ground state. For not very light nuclei, the spacing between the resonance levels is so narrow that it is impossible to define the energy

[66] For references to the very extensive literature, cf. the report by Bethe and Livingston, reference 19.
[67] Chadwick and Feather, *Internat. Conf. on Physics* (London, 1934), p. 95.
[68] Cork and Lawrence, Phys. Rev. **49**, 788 (1936).

of the γ-ray accurately enough to obtain resonance. Therefore we must average (117) over an energy region large compared to the spacing D between levels, and obtain

$$\sigma_{a\nu}=\pi^2\lambda_\gamma{}^2\frac{(2J+1)_{av}}{2i+1}\frac{\gamma_{r0}\gamma_n}{(\gamma_r+\gamma_n)D}. \tag{118}$$

Since J may have the values $i-1$, i or $i+1$, we may put the average value of $(2J+1)/(2i+1)$ equal to unity.

(118) is obviously very small if $\gamma_n \ll \gamma_r$, i.e., if the dissociation leads to the emission of slow particles. If the particles emitted are fast,[69] and particularly if the residual nucleus may be left in several excited states, γ_n will be larger than γ_r. Then (118) reduces to

$$\sigma_a=\pi^2\lambda_\gamma{}^2\gamma_{r0}/D. \tag{119}$$

In order to estimate γ_{r0}, we assume that, in the average, the partial radiation width of the compound state corresponding to the transition to *any* lower state is, in the average, simply proportional to the third power of the frequency of the γ-ray. Then the ratio of the total radiation width γ_r to the contribution of the ground state γ_{r0} is of the same order as but smaller than the number of energy levels below the compound state in question, which again is of the order of but smaller than $h\nu/D$. Thus we may write

$$\gamma_{r0}/\gamma=\kappa D/h\nu, \tag{120}$$

where κ is a numerical factor which may be of the order 100 to 1000. Thus

$$\sigma_a=\pi^2\kappa\lambda_\gamma{}^2\gamma_r/h\nu. \tag{121}$$

With $h\nu=10$ MV, $\lambda_\gamma=2\cdot10^{-12}$, $\kappa=500$, we have

$$\sigma_a=2\cdot10^{-27}\gamma_r \text{ cm}^2. \tag{121a}$$

Assuming γ_r to be about 0.1 volt, the cross section for photodissociation would be of the order $2\cdot10^{-28}$ cm^2 which would be just observable if γ-rays of sufficient energy (10 MV) are available with an intensity of the same order as that of the Th C′ γ-rays. It should be mentioned that the product nucleus may be left in an excited state if the energy of the γ-ray is sufficient. This does not increase the probability of the photodissociation.

The *scattering* cross section for γ-rays is to the cross section for photodissociation as γ_r to γ_n. Not making the assumption $\gamma_r \ll \gamma_n$, we have therefore, analogous to (121), for the average cross section

$$(\sigma_{Sc\gamma})_a=2\cdot10^{-27}\gamma_r{}^2/(\gamma_r+\gamma_n). \tag{122}$$

This is of the order 10^{-28} cm^2 if $\gamma_n<\gamma_r$, i.e., if photodissociation is either energetically quite impossible or leads to the emission of slow neutrons. (122) is still smaller if the γ-rays are energetic enough to produce fast neutrons by photodissociation so that $\gamma_n>\gamma_r$. In any case, the nuclear scattering of γ-rays is entirely negligible compared to the Klein-Nishina scattering which is of the order 10^{-26} cm^2.

Appendix

In this appendix we shall consider the influence of the angular momenta of the various nuclei involved, on the probability of the nuclear processes. We denote by J the angular momentum of the compound nucleus C, by M its component in a given (z-) direction, and by r all quantum numbers of the state of the compound nucleus except the angular momentum. Similarly, i, m, p are the total angular momentum, its z component, and a symbol abbreviating the other quantum numbers for the initial nucleus A, $i'm'q$ have the same significance for the final nucleus B. The incident particle P may be characterized by an orbital momentum l, a spin s, their components μ_l and μ_s, their resultant (total angular momentum) j and its z component μ. The quantities $l's'\mu_l'\mu_s'j'\mu'$ refer to the outgoing particle Q. We shall also use, for incident and outgoing particle, plane waves. In this case, the state of the incident particle is defined by a unit vector $\mathfrak{k}=\mathbf{k}/k$ in its direction of motion, and by s and μ_s. If a plane wave is used to describe the incident particle, the z axis (axis of quantization) will be chosen parallel to the direction of motion; if a spherical wave of given l is used, the direction of z is arbitrary.

We assume first that the incident particle has a wave function corresponding to a definite j and μ. The probability of the elementary process is (cf. (1))

$$w^A{}_B{}^p{}_q{}^i{}_{i'}{}^m{}_{m'}{}^P{}_Q{}^j{}_{j'}{}^\mu{}_{\mu'}=\frac{2\pi}{\hbar}\times\left|\sum_{rJM}\frac{H^A{}_r{}^P{}_J{}^i{}_M{}^{mP j\mu}H^r{}_B{}^J{}_q{}^M{}_{i'm'Qj'\mu'}}{E_A+E_P-E_{rJ}+\pi i\sum_{Q'q'i''m''j''\mu''}|H^r{}_B{}^J{}_{q'}{}^M{}_{i''m''Q'j''\mu''}|^2}\right|^2. \tag{201}$$

[69] According to the end of §8, the neutron width will be of the same order as the γ-ray width for neutron energies of about 1 MV or more. This is true if the residual nucleus after the emission of the neutron can only be left in the ground state. If it can also be left in an excited state, a smaller neutron energy is sufficient to make $\gamma_n=\gamma_r$.

We are interested in the *total* transition probability to *all* substates $m'\mu'$ of the final system, averaged over all possible directions of the angular momentum of the initial nucleus and the incident particle, i.e. over all m and μ. This probability is

$$w^{A}{}_{B}{}^{p}{}_{q}{}^{i}{}_{i'}{}^{P}{}_{Q}{}^{j}{}_{j'}=\frac{1}{(2i+1)(2j+1)}\sum_{m\mu m'\mu'} w^{A}{}_{B}{}^{p}{}_{q}{}^{i}{}_{i'}{}^{m}{}_{m'}{}^{P}{}_{Q}{}^{j}{}_{j'}{}^{\mu}{}_{\mu'}. \quad (202)$$

The matrix elements may be written

$$H^{r}{}_{A}{}^{J}{}_{p}{}^{M}{}_{imPj\mu}=u^{r}{}_{A}{}^{J}{}_{piPj}C^{J}{}_{i}{}^{M}{}_{mj\mu}, \quad (203)$$

where the coefficients C depend only on spacial symmetry while u depends on the special properties of the system considered. The C's fulfill the well-known orthogonality relation

$$\sum_{m\mu} C^{J}{}_{i}{}^{M}{}_{mj\mu}C^{J'}{}_{i}{}^{M'}{}_{m}{}^{*}{}_{j\mu}=\delta_{JJ'}\delta_{MM'}c^{J}{}_{ij}. \quad (204)$$

The normalization coefficient $c^{J}{}_{ij}$ is arbitrary; it is convenient to choose

$$c^{J}{}_{ij}=1/2\pi. \quad (205)$$

This also normalizes the quantities u introduced in (203).

With (203) to (205) we get immediately

$$\gamma^{r}{}_{A}{}^{J}{}_{piPj}=2\pi\sum_{m\mu}|H^{r}{}_{A}{}^{J}{}_{p}{}^{M}{}_{imPj\mu}|^{2}$$
$$=(u^{r}{}_{A}{}^{J}{}_{piPj})^{2}2\pi\sum_{m\mu}|C^{J}{}_{i}{}^{M}{}_{mj\mu}|^{2}=(u^{r}{}_{A}{}^{J}{}_{piPj})^{2}, \quad (206)$$

so that the last term in the denominator of (201) becomes

$$\tfrac{1}{2}i\gamma_{rJ}=\tfrac{1}{2}i\sum_{Q'q'i'j'}\gamma^{r}{}_{B}{}^{J}{}_{q'i'Q'j'}=\tfrac{1}{2}i\sum(u^{r}{}_{B}{}^{J}{}_{q'i'Q'j'})^{2}. \quad (207)$$

Considering that H is Hermitian, i.e.,

$$H^{A}{}_{r}{}^{P}{}_{J}{}^{i}{}_{M}{}^{mPj\mu}=H^{r}{}_{A}{}^{J}{}_{p}{}^{M}{}_{i}{}^{*}{}_{mPj\mu}, \quad (208)$$

we have further

$$w^{A}{}_{B}{}^{p}{}_{q}{}^{i}{}_{i'}{}^{P}{}_{Q}{}^{j}{}_{j'}=\frac{2\pi}{(2i+1)(2j+1)\hbar}\sum_{m\mu m'\mu'}$$
$$\times\left|\sum_{rJM}\frac{u^{r}{}_{A}{}^{J}{}_{piPj}\,u^{r}{}_{B}{}^{J}{}_{qi'Qj'}C^{J}{}_{i}{}^{M}{}_{m}{}^{*}{}_{j\mu}C^{J}{}_{i'}{}^{M}{}_{m'j'\mu'}}{E_A+E_P-E_{rJ}+\frac{1}{2}i\gamma_{rJ}}\right|^{2}$$
$$=\frac{2\pi}{(2i+1)(2j+1)\hbar}\sum_{JJ'}S_J S^{*}{}_{J'}\sum_{mm'\mu\mu'MM'}$$
$$\times C^{J}{}_{i}{}^{M}{}_{m}{}^{*}{}_{j\mu}C^{J}{}_{i'}{}^{M}{}_{m'j'\mu'}C^{J'}{}_{i}{}^{M'}{}_{m}{}_{j\mu}C^{J'}{}_{i'}{}^{M'}{}_{m'}{}^{*}{}_{j'\mu'} \quad (209)$$

with

$$S_J=\sum_{r}\frac{u^{r}{}_{A}{}^{J}{}_{piPj}\,u^{r}{}_{B}{}^{J}{}_{qi'Qj'}}{E_A+E_P-E_{rJ}+\frac{1}{2}i\gamma_{rJ}}. \quad (210)$$

The last sum in (209) may be summed first over m and μ, then over m' and μ', using the relations (204), (205). The result is

$$(2\pi)^{-2}\sum_{MM'}\delta_{MM'}\delta_{JJ'}=(2\pi)^{-2}(2J+1)\delta_{JJ'}. \quad (211)$$

This relation shows that the contributions of *compound states of different angular momentum JJ' do not interfere.* The probability w becomes

$$w^{A}{}_{B}{}^{p}{}_{q}{}^{i}{}_{i'}{}^{P}{}_{Q}{}^{j}{}_{j'}=\frac{1}{2\pi\hbar(2i+1)(2j+1)}\sum_{J}(2J+1)$$
$$\times\left|\sum_{r}\frac{u^{r}{}_{A}{}^{J}{}_{piPj}\,u^{r}{}_{B}{}^{J}{}_{qi'Qj'}}{E_A+E_P-E_{rJ}+\frac{1}{2}i\gamma_{rJ}}\right|^{2}. \quad (212)$$

It may be mentioned that it is not necessary to average over the magnetic quantum number μ of the incident particle but that the result (212) applies also to each magnetic state μ separately. This may be shown by a somewhat more detailed investigation of the properties of the C's.

We now consider the case that the initial and final state of the particle is characterised by definite values of $ls\mu_l$ and μ_s rather than of j and μ. This case may be reduced to the one previously treated with the help of the C's. These coefficients appear in all problems in which two angular momenta are compounded to form a resultant, such as i and j to form J in our previous problem, and l and s to form j in our present one. Accordingly, we may write

$$H^{r}{}_{A}{}^{J}{}_{p}{}^{M}{}_{iPls\mu_l\mu_s}=\sum_{j\mu}C^{j}{}_{l}{}^{\mu}{}_{\mu_l s\mu_s}H^{r}{}_{A}{}^{J}{}_{p}{}^{M}{}_{iPlsj\mu}$$
$$=\sum_{j\mu}C^{j}{}_{l}{}^{\mu}{}_{\mu_l s\mu_s}C^{J}{}_{i}{}^{M}{}_{mj\mu}u^{r}{}_{A}{}^{J}{}_{piPlsj}. \quad (213)$$

With the help of a calculation on the same lines as our previous one, which we shall give below, it may be shown that states of different j of the incident particle do not interfere, just as states of the compound nucleus of different J do not. The same holds, of course, for states of different j' of the outgoing particle. Consequently,

(1) the total probability of the transitions *to* all states of the outgoing particle with given l' and s' is obtained by *summing* the probabilities for all values of j' which are possible for the given l' and s', i.e. $j'=|l'-s'|$ to $l'+s'$,

(2) the average probability of a transition starting *from* any state of given l and s is obtained by *averaging* the probabilities for all possible values of j, taking account of the statistical weights. Since $2j+1$ is the statistical weight of a state j, and $(2l+1)(2s+1)$ that of all the states ls, we have

$$w^{A}{}_{B}{}^{p}{}_{q}{}^{i}{}_{i'}{}^{P}{}_{Q}{}^{l}{}_{l'}{}^{s}{}_{s'}$$
$$=\frac{1}{(2l+1)(2s+1)}\sum_{jj'}(2j+1)w^{A}{}_{B}{}^{p}{}_{q}{}^{i}{}_{i'}{}^{P}{}_{Q}{}^{l}{}_{l'}{}^{s}{}_{s'}{}^{i}{}_{j'}, \quad (214)$$

or, inserting (212)

$$w^{A}{}_{B}{}^{p}{}_{q}{}^{i}{}_{i'}{}^{P}{}_{Q}{}^{l}{}_{l'}{}^{s}{}_{s'}=\frac{1}{2\pi\hbar(2l+1)(2s+1)(2i+1)}\sum_{Jjj'}(2J+1)$$
$$\times\left|\sum_{r}\frac{u^{r}{}_{A}{}^{J}{}_{piPlsj}u^{r}{}_{B}{}^{J}{}_{qi'Ql's'j'}}{E_A+E_P-E_{rJ}+\frac{1}{2}i\gamma_{rJ}}\right|^{2} \quad (215)$$

with

$$\gamma_{rJ}=\sum_{Q'q'i'l's'j'}(u^{r}{}_{B}{}^{J}{}_{q'i'Q'l's'j'})^{2}. \quad (215a)$$

Formulae (215), (215a) give the probability of the process if the incident particle has given orbital momentum l. In reality, the particle has a given direction of motion $\varkappa$ and must therefore be represented by a plane wave. If the plane wave is normalized per unit energy and per solid angle 4π, its expansion in terms of wave functions with given angular moments, is[70]

$$\delta(\mathbf{r}-\mathbf{r}')=\int dE(d\Omega/4\pi)\psi_{E\boldsymbol{\varkappa}}(\mathbf{r})\psi^{*}_{E\boldsymbol{\varkappa}}(\mathbf{r}')$$
$$=\int dE\sum_{lm}\psi_{Elm}(\mathbf{r})\psi^{*}_{Elm}(\mathbf{r}'). \quad (216a)$$

We insert (216) in the first expression and average over the direction of $\varkappa$, i.e., of the axis of the polar coordinate system to which the spherical harmonic in $\psi_{El0}=\psi_{El}(r)Y_{l0}(\vartheta\varphi)$ refers. The average gives, according to well-known relations between spherical harmonics:

$$\int(d\Omega/4\pi)Y_{l0}(\mathbf{r})Y_{l'0}(\mathbf{r}')=\delta_{ll'}\sum_{m}Y_{lm}(\mathbf{r})Y_{l'm}(\mathbf{r}')/(2l+1) \quad (216b)$$

which reduces the middle expression in (a) to the right-hand expression.

[70] A simple proof of the factor $(2l+1)^{\frac{1}{2}}$ is the following: The δ function may be represented in either of the two ways

$$\psi_{E\mathbf{\kappa}}=\sum_l (2l+1)^{\frac{1}{2}} i^l \psi_{El0}, \tag{216}$$

where ψ_{El0} is real, is normalized per unit energy, and has a magnetic quantum number $\mu_l=0$, i.e., no orbital momentum around the direction $\mathbf{\kappa}$. The factor $(2l+1)^{\frac{1}{2}}$ differs from the familiar $2l+1$ in the expansion of a plane wave in spherical harmonics because we use here normalized spherical harmonics, and the normalized harmonic Y_{l0} is equal to $(2l+1/4\pi)^{\frac{1}{2}}P_l$. It may then be shown along the same lines as before that different l's do not interfere. Since the factor $2l+1$ in (216) cancels the $2l+1$ in the denominator of (215), we have for the total probability

$$w^{rP}{}_{q^p}=\frac{1}{2\pi\hbar(2s+1)(2i+1)}\sum_{Jlj i' j'}(2J+1)\times\left|\sum_r \frac{u^r A^J{}_{piPlsj}\,u^r B^J{}_{qi'Qi's'j'}}{E_A+E_P-E_{rJ}+\frac{1}{2}i\gamma_{rJ}}\right|^2. \tag{217}$$

It remains to show that different j's and l's really do not interfere. The probability may be written

$$w^{rP}{}_{q^p}=\frac{2\pi}{\hbar}\sum_{\mu_s m l' \mu_l' \mu_s' m'}\left|\sum_{ljJMj'\mu'} i^l C^j{}_{l^p 0 \mu_s} C^J{}_{j}{}^{M}{}_{\mu i m}\times\frac{u^r A^J{}_{piPlsj}\,u^r B^J{}_{qi'Qi's'j'} C^J{}_{j'}{}^{M}{}_{\mu'}{}^{*}{}_{i'm'} C^{j'}{}_{l'}{}^{\mu'}{}_{\mu_l'}{}^{*}{}_{s'\mu_s'}}{E_A+E_P-E_{rJ}+\frac{1}{2}i\gamma_{rJ}}\right|^2$$

$$=\frac{2\pi}{\hbar(2s+1)(2i+1)}\sum_{i'll_a j l_a J J_a i'_a l'} S_{ljJj'l'} S^{*}{}_{l_a j_a J_a i'_a l'}\times\sum_{\mu_s m \mu_l' m' \mu_{l_a} M M_a \mu' \mu'_a} C^j{}_{l^p 0 \mu_s} C^{j_a}{}_{l_a}{}^{\mu_{l_a}} {}_{0 \mu_s}{}^{*} C^J{}_{j}{}^{M}{}_{\mu i m} C^{J_a}{}_{j_a}{}^{M_a}{}_{\mu_a}{}^{*}{}_{im}\times C^J{}_{j'}{}^{M}{}_{\mu'}{}^{*}{}_{i'm'} C^{J_a}{}_{j'_a}{}^{M_a}{}_{\mu'_a i' m'} C^{j'}{}_{l'}{}^{\mu'}{}_{\mu_l'}{}^{*}{}_{s'\mu_s'} C^{j'_a}{}_{l'}{}^{\mu'_a}{}_{\mu_l' s' \mu_s'} \tag{218}$$

with $$S_{lJj'l'}=i^l\sum_r \frac{u^r A^J{}_{piPlsj}\,u^r B^J{}_{qi'Qi's'j'}}{E_A+E_P-E_{rJ}+\frac{1}{2}i\gamma_{rJ}}. \tag{218a}$$

The second sum in (218) will be summed,

(1) over μ'_l and μ'_a: The result will vanish unless $j'_a=j'$ and $\mu'_a=\mu'$. This proves that different values of j' do not interfere, and the sum over μ'_a reduces to a single term.

(2) over μ' and m': The result will vanish unless $J_a=J$ and $M_a=M$. Therefore different J's do not interfere, and the sum over M_a reduces to one term.

(3) over M and m. Since we have already proved that $J_a=J$ and $M_a=M$, this sum has the form

$$\sum_{Mm} C^J{}_{j}{}^{M}{}_{\mu i m} C^J{}_{j_a}{}^{M}{}_{\mu_a}{}^{*}{}_{im}=c\delta_{jj_a}\delta_{\mu\mu_a}. \tag{219}$$

This expression differs from the orthogonality relation (204) in that the sum extends over the upper and one lower index, rather than the two lower ones. But the C's are, except for normalization, symmetrical in the three angular momenta J, j and i so that there holds the orthogonality relation (219) similar to (204). C is a constant (in our normalization $2\pi(2J+1)/(2j+1)$). (219) shows that different j's do not interfere and that the sum over μ_a in (218) reduces to one term.

(4) There remains the sum over μ and μ_s. In analogy to (219), we find that it vanishes unless $l=l_a$. This proves (217).

We have, in this derivation, started from particle wave functions with given l, and then constructed plane waves out of these. It is equally possible to start from plane waves. We may write

$$\sigma^{rP}{}_{Q^p q^s}{}_{i i'}{}^{\mathbf{\kappa}}=\int\frac{d\Omega'}{4\pi}\frac{\pi\lambda^2}{(2s+1)(2i+1)}\sum_J(2J+1)\times\left|\sum_r\frac{u^r A^J{}_{piPs}{}^{\mathbf{\kappa}}\,u^r B^J{}_{qi'Qs'}{}^{\mathbf{\kappa}'}}{E_A+E_P-E_{rJ}+\frac{1}{2}i\gamma_{rJ}}\right|^2 \tag{220}$$

and $$\gamma_{rJ}=\sum_{Q'q's'}\int(d\Omega'/4\pi)\,|u^r B^J{}_{q's'Q's'}{}^{\mathbf{\kappa}'}|^2. \tag{221}$$

These relations mean just that the particle wave functions with different $\mathbf{\kappa}$, as well as the functions with different lm, form a complete set. The proof is analogous to that in reference 70. The matrix element $u^r A^J{}_{piPs}{}^{\mathbf{\kappa}}$ may be directly calculated using a plane wave for the particle, the normalization follows most quickly from the fact that the average of $(u^r A^J{}_{piPs}{}^{\mathbf{\kappa}})^2$ over $\mathbf{\kappa}$ represents the total disintegration probability of state rJ with the emission of particle P with energy $E_p(P)$.

Some special considerations are required for light quanta. Corresponding to the two directions of polarization, we have to put the quantity $2s+1$ in the denominators of all formulae equal to 2. (We have to average over the *two* directions of polarization of the incident quantum, just as over the $2s+1$ directions of the spin of a particle.) The selections rules (§3, beginning) on the other hand, cannot be obtained satisfactorily with any value of s (see below), but the value $s=1$ comes nearest to the truth. The reason for this difference is that in the case of light there is a relation between the polarization and the direction of propagation whereas the direction of the spin of a particle is quite independent of its direction of motion. Thus the polarization of the light introduces a spherical harmonic of order one in the matrix element but only a weight factor 2 which would correspond to $s=\frac{1}{2}$. The same fact also prevents the existence of any wave function for a light quantum with total momentum $j=0$.

To investigate the selection rules, we expand a plane light wave $e^{i\mathbf{k}\cdot\mathbf{r}}$ in spherical harmonics with the direction of $\mathbf{k}$ as polar axis (z axis). The two possible directions of polarization x and y are perpendicular to $\mathbf{k}$. The operator of the radiation theory may therefore be written

$$e^{i\mathbf{k}\cdot\mathbf{r}}\frac{\partial}{\partial x}=\sum_L\chi_L(kr)\,Y_{L0}(\vartheta)\left(\sin\vartheta\cos\varphi\frac{\partial}{\partial r}+\cdots\frac{\partial}{\partial\vartheta}+\cdots\frac{\partial}{\partial\varphi}\right)$$

$$=\sum\chi_L(kr)[\alpha_{L+1}(Y_{L+1,1}+Y_{L+1,-1})+\alpha_L(Y_{L-1,1}+Y_{L-1,-1})]\frac{\partial}{\partial r}+\cdots, \tag{222}$$

where the α's are certain coefficients. For each value of L, the total momentum j may thus have the values $j=L+1$ or $L-1$. This would correspond to $s=1$ except for the fact that $j=L$ does not occur for light. Furthermore, $j=0$ which should correspond to $L=1$ does actually not occur at all in (222) because the spherical harmonics Y_{01} and Y_{0-1} do not exist.

We may rewrite (222) using the total momentum j rather than the "orbital" momentum L for labeling the terms:

$$e^{i\mathbf{k}\cdot\mathbf{r}}\frac{\partial}{\partial x}=\sum_{j=1}^{\infty}(Y_{j1}+Y_{j-1})\times\left\{[\alpha_j\chi_{j-1}(kr)+\alpha_{j+1}\chi_{j+1}(kr)]\frac{\partial}{\partial r}+\cdots\right\}. \quad (223)$$

For light, only small values of kr are important because the wave-length of the light is generally large compared to the dimensions of the radiating system. Now, according to (18), we have $\chi_{j-1}\approx(kr)^j$ and $\chi_{j+1}\approx(kr)^{j+2}$ so that the first term in the square bracket in (223) is always much more important than the second. The terms $j=1, 2, 3, \cdots$ (or $L=0, 1, 2, \cdots$) correspond to dipole, quadrupole, octopole . . . radiation.

MARCH 15, 1937 PHYSICAL REVIEW VOLUME 51

Relativistic Wave Functions in the Continuous Spectrum for the Coulomb Field

MORRIS E. ROSE
Cornell University, Ithaca, New York

(Received January 22, 1937)

For purposes of reference the continuous spectrum solutions of the Dirac wave equation for the Coulomb field are given. The solutions in the form of series and integral representations and the asymptotic behavior at large distances are included among the formulae.

THE solutions in the continuous spectrum of the Dirac wave equation for the Coulomb field have been known and used extensively for some time. However, the form in which they appear in the literature is not convenient for some purposes. It is with the intention of furnishing a reference from which one may obtain the wave functions with a minimum expenditure of time and labor that the following formulae are given.

For the sake of simplicity we adopt a system of units in which energy is measured in mc^2, length in $\hbar/mc$ and momentum in mc. The symbols which occur below have the following meanings:

$\psi_1\psi_2\psi_3\psi_4$, the four components of the wave function.
f_l and g_l, radial wave functions.
$Y_{l\mu}$, normalized spherical harmonics (see Eq. (2)).
j, total angular momentum quantum number.
m, magnetic quantum number.
l, auxiliary index characterizing the wave functions. (l is the orbital momentum for the electron *only*, in the nonrelativistic limit.)
W, *absolute* value of the energy.
p, *absolute* value of the momentum $=(W^2-1)^{\frac{1}{2}}$.
α, fine structure constant $=e^2/\hbar c$.
Z, nuclear charge.

The wave functions are of two types:

Type a, $j=l+\frac{1}{2}$,

$$\psi_1=i\left(\frac{l-m+\frac{3}{2}}{2l+3}\right)^{\frac{1}{2}}Y_{l+1,\,m-\frac{1}{2}}f_l,$$
$$\psi_2=i\left(\frac{l+m+\frac{3}{2}}{2l+3}\right)^{\frac{1}{2}}Y_{l+1,\,m+\frac{1}{2}}f_l,$$
$$\psi_3=\left(\frac{l+m+\frac{1}{2}}{2l+1}\right)^{\frac{1}{2}}Y_{l,\,m-\frac{1}{2}}g_l, \quad (1a)$$
$$\psi_4=-\left(\frac{l-m+\frac{1}{2}}{2l+1}\right)^{\frac{1}{2}}Y_{l,\,m+\frac{1}{2}}g_l,$$
$$l\geqq 0, \quad -(l+1)\leqq m-\tfrac{1}{2}\leqq l-1.$$

Type b, $j=l-\frac{1}{2}$,

$$\psi_1=i\left(\frac{l+m-\frac{1}{2}}{2l-1}\right)^{\frac{1}{2}}Y_{l-1,\,m-\frac{1}{2}}f_{-l-1},$$
$$\psi_2=-i\left(\frac{l-m-\frac{1}{2}}{2l-1}\right)^{\frac{1}{2}}Y_{l-1,\,m+\frac{1}{2}}f_{-l-1},$$
$$\psi_3=\left(\frac{l-m+\frac{1}{2}}{2l+1}\right)^{\frac{1}{2}}Y_{l,\,m-\frac{1}{2}}g_{-l-1}, \quad (1b)$$
$$\psi_4=\left(\frac{l+m+\frac{1}{2}}{2l+1}\right)^{\frac{1}{2}}Y_{l,\,m+\frac{1}{2}}g_{-l-1},$$
$$l\geqq 1, \quad -l\leqq m-\tfrac{1}{2}\leqq l-1,$$

$$Y_{l\mu}(\vartheta, \varphi)=\left(\frac{2l+1}{4\pi}\right)^{\frac{1}{2}}\left[\frac{(l-\mu)!}{(l+\mu)!}\right]^{\frac{1}{2}}\frac{\sin^{\mu}\vartheta e^{i\mu\varphi}}{2^l l!}$$
$$\times\left(\frac{d}{d\cos\vartheta}\right)^{l+\mu}(\cos^2\vartheta-1)^l. \quad (2)$$

It is convenient to treat the two types of solutions simultaneously by the introduction of the parameter κ.

$$\kappa=-(j+\tfrac{1}{2})=-(l+1) \quad \text{when} \quad j=l+\tfrac{1}{2},$$
$$=j+\tfrac{1}{2}=l \quad \text{when} \quad j=l-\tfrac{1}{2}.$$

We give the solutions for the radial functions in the positive energy spectrum (electron). Suppressing the index κ,

$$f=(1-W)^{\frac{1}{2}}(G-G^*), \quad g=(1+W)^{\frac{1}{2}}(G+G^*), \quad (3)$$

so that f and g are real.[1] The solutions given below are normalized per unit energy interval.

Series representation:

$$r\begin{Bmatrix}f\\g\end{Bmatrix}=\frac{(1\mp W)^{\frac{1}{2}}(2pr)^{\gamma}e^{\pi\alpha ZW/2p}|\,\Gamma(\gamma+i\alpha ZW/p)\,|}{2(\pi p)^{\frac{1}{2}}\Gamma(2\gamma+1)}$$
$$\times\{e^{-ipr+i\eta}(\gamma+i\alpha ZW/p)F(\gamma+1+i\alpha ZW/p,$$
$$2\gamma+1\,;\,2ipr)\mp\text{c.c.}\}, \quad (4)$$

where c.c. denotes the complex conjugate.

$$\gamma=(\kappa^2-\alpha^2Z^2)^{\frac{1}{2}},$$
$$e^{2i\eta}=-(\kappa-i\alpha Z/p)/(\gamma+i\alpha ZW/p),$$

and F is the confluent hypergeometric function defined by

$$F(a, b\,; x)=\frac{\Gamma(b)}{\Gamma(a)}\sum_{n=0}^{\infty}\frac{\Gamma(a+n)}{\Gamma(b+n)}\frac{x^n}{n!}.$$

Integral representation:

$$r\begin{Bmatrix}f\\g\end{Bmatrix}=\frac{(1\mp W)^{\frac{1}{2}}e^{\pi\alpha ZW/2p}(pr/2)^{\gamma}}{2(\pi p)^{\frac{1}{2}}|\,\Gamma(\gamma+i\alpha ZW/p)\,|}$$
$$\times\left\{e^{i\eta}\int_{-1}^{1}e^{ipru}(1-u)^{\gamma-1-i\alpha ZW/p}\right.$$
$$\left.\times(1+u)^{\gamma+i\alpha ZW/p}du\mp\text{c.c.}\right\}. \quad (5)$$

Asymptotic behavior:

$$rf=-[(W-1)/\pi p]^{\frac{1}{2}}\sin(pr+\delta),$$
$$rg=[(W+1)/\pi p]^{\frac{1}{2}}\cos(pr+\delta), \quad (6)$$
$$\delta=(\alpha ZW/p)\log 2pr-\arg\Gamma(\gamma+i\alpha ZW/p)$$
$$+\eta-\pi\gamma/2.$$

It is, of course, simple to obtain the solutions with any other normalization. For example, to obtain the solutions normalized to one particle in a large sphere of radius R the above solutions need only be multiplied by a factor $(\pi p/WR)^{\frac{1}{2}}$.

The dimensionality of rf (and rg) is (energy length)$^{-\frac{1}{2}}$ for normalization per unit energy interval and (length)$^{-\frac{1}{2}}$ for normalization to one particle in a large sphere. Hence to write the solution in ordinary units, besides replacing W by W/mc^2, p by p/mc and pr by $pr/\hbar$, rf (and rg) should be multiplied by $(\hbar c)^{-\frac{1}{2}}$ and $(mc/\hbar)^{\frac{1}{2}}$ for the two methods of normalization, respectively. The transition to any other system of units is easy. For example, to write the above formulae in atomic (Hartree) units W should be replaced by α^2W, p by αp, pr remains unchanged and rf is to be multiplied by $\alpha^{\frac{1}{2}}$ and $\alpha^{-\frac{1}{2}}$ for the two cases of normalization, respectively.

To obtain the solutions in the negative energy spectrum (positron) we have[1]

$$f=(1+W)^{\frac{1}{2}}(G+G^*), \quad g=(1-W)^{\frac{1}{2}}(G-G^*), \quad (7)$$

in which G and G^* are obtained from the formulae given above by changing the sign of W and $e^{2i\eta}$. Thus, for example, in the asymptotic expressions (6) the forms of f and g are interchanged.

[1] The relative sign of f and g as determined from the differential equations which they must satisfy is obtained correctly if we take $(1-W)^{1/2}=+i(W-1)^{1/2}$.

The Band Spectra of SbF and BiF

GEORGE D. ROCHESTER*
Department of Physics, University of California, Berkeley, California
(Received December 7, 1936)

New band spectra attributed to the molecules SbF and BiF have been excited by active nitrogen. The spectrum of SbF from 2000–5500A is found to have three groups of bands lying in the regions 3600–5200A, 2600–2700A and 2200–2430A. Analysis of the first group shows that sixty-one bands out of sixty-nine can be placed into two systems with the following vibrational constants, in cm^{-1}:—

System	ν_0	ω_e'	$x_e'\omega_e'$	ω_e''	$x_e''\omega_e''$
A_1	21887.5	411.3	1.71	616.9	2.89
A_2	23992.5	420.0	1.75	612.6	2.58

The second group consists of a few isolated bands degraded to shorter wave-lengths and the third of bands in closely spaced sequences and also degraded to shorter wave-lengths. A preliminary analysis indicates that the bands in the latter group can be placed into two systems for which $\omega_e'\sim700$ cm^{-1}, $\omega_e''\sim620$ cm^{-1} and $\Delta\nu_{21}\sim1850$ cm^{-1}. Three new systems of bands, degraded to shorter wave-lengths and forming a triplet system with wide multiplet separations, (7330 cm^{-1} and 4800 cm^{-1}), are found in the spectrum of BiF at 3050–3250A, 2650–2850A and 2250–2350A. Photographs taken with small dispersion indicate that $\omega_e'\sim620$ cm^{-1} and $\omega_e''\sim520$ cm^{-1}.

INTRODUCTION

THE band spectra of the diatomic halides of related elements, e.g., Ca, Sr and Ba, are, in general, very similar. It is observed that each spectrum contains the same number of band systems, arising from electronic states of the same multiplicity, and that corresponding systems move towards longer wave-lengths with increasing molecular weight.

The recent analysis of the band spectra of the diatomic lead halides has enabled a comparison of the spectra of the related molecules PbCl[1] and SnCl to be made, and has shown that whereas the spectrum of SnCl contains several systems arising from doublet electronic states, only one system occurs in PbCl, due, apparently, to a transition between singlet states. Evidently the ultraviolet systems of PbCl are too weak to appear and the other system which should occur if the ground state of the molecule is a doublet, (by analogy with SnCl), is in the infrared or is also too weak to be observed.

It was therefore thought of interest to search for the band spectra of the halides of other related elements and the two chosen for this purpose were the fluorides of antimony and bismuth (SbF and BiF). A band system of BiF lying in the visible region of the spectrum was already known from the work of Howell,[2,3] Rochester[2] and Morgan.[4] No previous observations on the spectrum of SbF appear to have been made.

EXPERIMENTAL

Two methods have been used previously to excite the band spectra of BiF and BiCl, namely, the high frequency discharge[2] and active nitrogen.[5] Both methods were therefore tried in the present case to see which was preferable and the second was finally chosen because of the "purity" of the spectrum it produced. Details of the apparatus used and the method of operation were as described by Mulliken[6] in his early work on the band spectra of the copper halides. To excite the spectrum of SbF, the vapor of SbF_3 was introduced into the stream of active nitrogen by gently warming some commercial antimony trifluoride—the "glow" so produced being pale violet in color—but to vaporize

* Commonwealth Fund Fellow.
[1] G. D. Rochester, Proc. Roy. Soc. **A153**, 407 (1936); F. Morgan, Phys. Rev. **49**, 47 (1936).
[2] H. G. Howell and G. D. Rochester, Univ. Durham Phil. Soc. Proc. **9**, 126 (1934).
[3] H. G. Howell, Proc. Roy. Soc. **A155**, 141 (1936).
[4] F. Morgan, Phys. Rev. **49**, 41 (1936).
[5] P. G. Saper, Phys. Rev. **37**, 1710A (1931).
[6] R. S. Mulliken, Phys. Rev. **26**, 1 (1925).

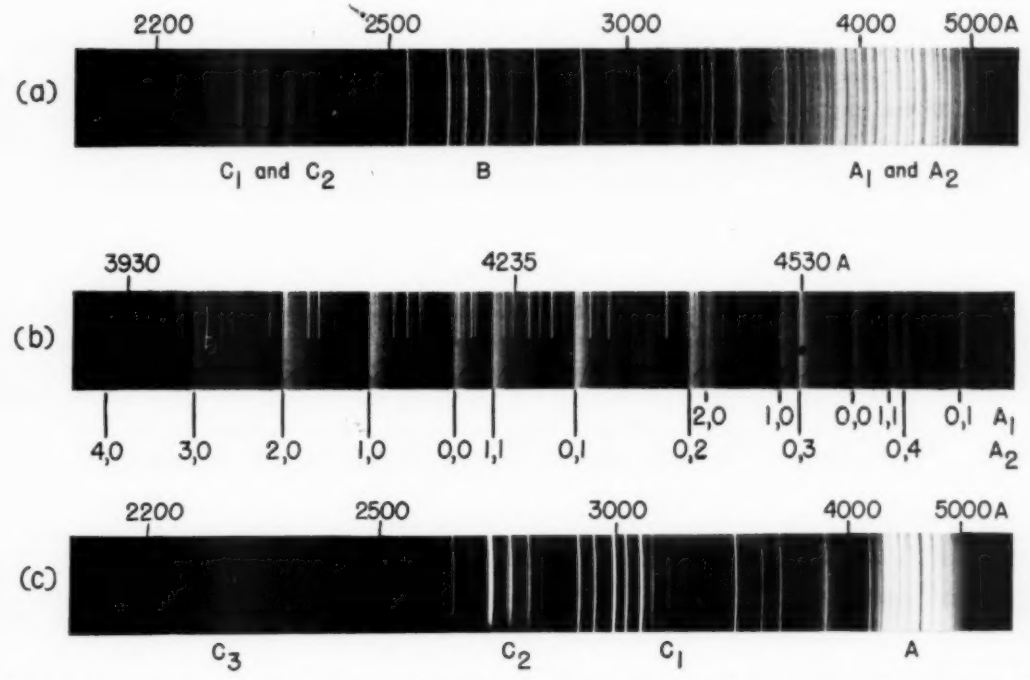

FIG. 1. (a) The band spectrum of SbF between 2200 and 5200A. (b) Systems A_1 and A_2 of SbF. (c) The band spectrum of BiF between 2200 and 5200A.

bismuth trifluoride it was necessary to heat the salt strongly in a quartz tube.

Both spectra when photographed with a Hilger small quartz spectrograph with exposure times varying from three to thirty minutes on fresh Eastman 40 plates revealed groups of bands in the visible and ultraviolet regions of the spectrum. The most intense system in SbF[7] was later photographed on Eastman 33 plates in six hours using a quartz spectrograph with a focal length of three meters and having an average dispersion of 7.5A/mm in the region covered by the bands.

Measurements of these band heads were made on two plates by means of a Société Génevoise Comparator and were reduced to wave-lengths, using iron-arc wave-length standards. Intensities were assigned visually on a 0–10 scale.

[7] While this work was in progress Dr. H. G. Howell of University College, Southampton, England, informed the author that he had independently discovered the band spectrum of SbF and was engaged in the analysis of the ultraviolet part of the spectrum; for this reason only preliminary results for this part of the spectrum are reported.

DESCRIPTION OF THE SPECTRA

Antimony fluoride (SbF)

Photographs of the spectrum of SbF illustrating its main features are reproduced in Figs. 1a and 1b. Fig. 1a, taken with the small quartz spectrograph, shows clearly that the spectrum of SbF has three groups of bands in the region 2000–5200A, namely, at 3600–5200A, 2200–2430A and 2600–2700A. The first group consists of progression type bands degraded to the red end of the spectrum, as may be seen more easily from Fig. 1b, the second of sequence-type bands degraded to shorter wave-lengths, and the third of a few isolated bands also degraded to shorter wave-lengths. Some of the bands in the "visible" systems resemble those of BiF and PbF in having line-like heads, and well-resolved rotational structure at some distance from the heads.

Bismuth fluoride (BiF)

A photograph of the spectrum of BiF taken with the small quartz spectrograph and repro-

duced in Fig. 1c shows that the spectrum extends from 2200–5200A. In addition to the known system of bands at 4200–5500A, degraded to the red end of the spectrum, three new systems of progression type bands, degraded to shorter wave-lengths, at 2250–2350A, 2650–2850A and 3050–3250A can be recognized.[8]

[8] System C_3 is clearly visible on the original plate.

TABLE I. *SbF. System A. (Wave numbers of band heads and differences in cm⁻¹.)*

v' \ v''	0	1	2	3	4	5	6	Mean $\Delta G'$ $\begin{matrix}A_2\\A_1\end{matrix}$
0	23896.0 (10) *2111.5* 21784.5 (6)	23289.0 (10) *2114.5* 21174.5 (7)	22686.5 (10) *2118.0* 20568.5 (3)	22089.0 (9) *2120.5* 19968.5 (1)	21497.5 (6) — —	20910.0 (1) — —		*416.5* *408.3*
1	24313.0 (10) *2119.5* 22193.5 (7)	23705.0 (10) *2123.5* 21581.5 (5)	23103.0 (2) *2125.5* 20977.5 (1)		21913.0 (2) — —	21327.5 (2) — —	20745.5 (0) — —	*412.6* *403.2*
2	24726.0 (10) *2128.0* 22598.0 (7)	24118.5 (2) *2133.5* 21985.0 (1)	23515.0 (2) *2136.0* 21379.0 (0)	22919.0 (3) *2139.0* 20780.0 (0)	22325.0 (1) — —			*410.3* *400.5*
3	25135.0 (8) *2136.5* 22998.5 (3)		23925.5 (3) — —		22736.5 (1) — —	22150.5 (1) — —		*406.5* *397.0*
4	25541.5 (7) *2146.0* 23395.5 (3)	24934.5 (3) *2151.0* 22783.5 (1)	24331.0 (1) — —	23736.0 (1) — —	23144.0 (1) — —			*402.5* *395.0*
5	25944.5 (4) *2154.5* 23790.0 (1)	25337.0 (5) *2158.0* 23179.0 (0)		24138.0 (1) *2166.5* 21971.5 (0)				*398.3* *392.0*
6	26343.0 (2) — —	25736.0 (4) *2166.0* 23579.0 (1)		24535.5 (1) *2171.0* 22364.5 (0)				*395.7* —
7	26739.5 (1) —	26131.0 (2) —	25529.0 (1) —					*394.0* —
8		26525.5 (2) —	25922.5 (2) —					*388.5* —
9			26311.0 (1) —					*383.5* —
10			26694.5 (1) —	26097.5 (1) —				*381.0* —
11				26478.5 (1)	25884.5 (1)			
Mean $\Delta G''$ $\begin{matrix}A_2\\A_1\end{matrix}$	*607.5* *611.6*	*602.8* *605.3*	*596.4* *599.5*	*592.9* —	*586.3* —	*582.0* —		

SbF. Progressions (a) and (b). (Intensities in brackets.)

(a) 27202.5 (3) *601.5* 26601.0 (4) *597.0* 26004.0 (4) *591.5* 25412.5 (3) *587.5* 24825.0 (2)

(b) 25233.5 (2) *580.0* 24653.5 (1) *578.5* 24075.0 (1)

TABLE II. *SbF. Classified bands.*

SYSTEM A_1				SYSTEM A_2						
ν (obs. cm^{-1})	I	$0-C$ (cm^{-1})	v', v''	ν (obs. cm^{-1})	I	$0-C$ (cm^{-1})	v', v''	ν (obs. cm^{-1})	I	$0-C$ (cm^{-1})	v', v''
23790.0	1	0	5, 0	26739.5	1	1.0	7, 0	24138.0	1	1.0	5, 3
23570.0	1	0	6, 1	26694.5	1	0.5	10, 2	24118.5	2	0	2, 1
23395.5	3	−0.5	4, 0	26525.5	2	2.5	8, 1	23925.5	3	0	3, 2
23179.0	0	0	5, 1	26478.5	1	0	11, 3	23896.0	10	−0.5	0, 0
22998.5	3	0	3, 0	26343.0	2	0	6, 0	23736.0	1	1.5	4, 3
22783.5	1	−1.5	4, 1	26311.0	1	2.0	9, 2	23705.0	10	−0.5	1, 1
22598.0	7	1.0	2, 0	26131.0	2	0	7, 1	23515.0	2	−1.0	2, 2
22364.5	0	−1.0	6, 3	26097.5	1	0.5	10, 3	23289.0	10	0	0, 1
22193.5	7	0.5	1, 0	25944.5	4	0.5	5, 0	23144.0	1	1.5	4, 4
21985.0	1	−1.0	2, 1	25922.5	2	0	8, 2	23103.0	2	0	1, 2
21971.5	0	−2.5	5, 3	25884.5	1	−2.1	11, 4	22919.0	3	0	2, 3
21784.5	6	−0.5	0, 0	25736.0	4	0.5	6, 1	22736.5	1	0	3, 4
21581.5	5	−0.5	1, 1	25541.5	7	0	4, 0	22686.5	10	0	0, 2
21379.0	0	−2.0	2, 2	25529.0	1	0.5	7, 2	22325.0	1	−2.0	2, 4
21174.5	7	0.5	0, 1	25337.0	5	0.5	5, 1	22150.5	1	0.5	3, 5
20977.5	1	1.0	1, 2	25135.0	8	−0.5	3, 0	22089.0	9	−0.5	0, 3
20780.0	0	−1.5	2, 3	24934.5	3	0.5	4, 1	21913.0	2	−1.0	1, 4
20568.5	3	0	0, 2	24726.0	10	0	2, 0	21497.5	6	0	0, 4
19968.5	1	−0.5	0, 3	24535.5	1	−0.5	6, 3	21327.5	2	0	1, 5
				24331.0	1	−0.5	4, 2	20910.0	1	−1.0	0, 5
				24313.0	10	0	1, 0	20745.5	0	0	1, 6

VIBRATIONAL ANALYSIS

Antimony fluoride (SbF)

The three groups of bands in this system will be designated systems A, B and C, system A referring to the system with the smallest value of "ν_e."

System A.—In the region 3600–5000A there have been observed sixty-nine bands of which sixty-one can be placed into two systems (designated A_1 and A_2, A_1 referring to the system with the smallest value of ν_e), five in one v'' progression, (designated progression (a)), and three in another, (progression (b)). The wave numbers of the band-heads and the Deslandres schemes are given in Table I. The intensity distributions, also given in Table I, are such as would be expected from the Franck-Condon principle for the observed difference in the ω's of the two electronic states and show that the v numerations can be assigned without ambiguity. Since antimony has two isotopes of masses 121 and 123 and abundances 56 and 44, respectively, it might be expected that the antimony isotope effect could be used to confirm the v numerations; however, a careful examination of the band heads shows that the isotopic heads $Sb^{121}F$ and $Sb^{123}F$ are not resolved with the dispersion used. A slight diffuseness of the band heads at some distance from the system origin may be taken as qualitative evidence of an isotope effect and of the correctness of the quantum number allocations. To within the accuracy of measurement the wave numbers of the band heads are given by the formulae:

$$\nu_1 = 21{,}887.5 + 411.3(v'+\tfrac{1}{2}) - 1.71(v'+\tfrac{1}{2})^2 - 616.9(v''+\tfrac{1}{2}) + 2.89(v''+\tfrac{1}{2})^2,$$

$$\nu_2 = 23{,}992.5 + 420.0(v'+\tfrac{1}{2}) - 1.75(v'+\tfrac{1}{2})^2 - 612.6(v''+\tfrac{1}{2}) + 2.58(v''+\tfrac{1}{2})^2.$$

$0-C$ values for all classified bands are listed in Table II.

Systems B and C.—Pending more detailed analyses[7] only preliminary results, from measurements made on plates taken with small dispersion, will be given. Three bands have been found in System B with heads at 2630A, 2672A and 2714A, forming what is probably a v'' progression since the differences are of the same order as the ω''s of Systems A_1 and A_2:

System B

38,010 (5) *600* 37,410 (4) *580* 36,830 (2).

Sixteen bands have been found in the region 2200–2430A, analysis indicating that they can be placed into two systems with the same upper and lower state differences; $\omega_e' \sim 700$ cm^{-1}, $\omega_e'' \sim 620$ cm^{-1} and $\Delta\nu_{21} \sim 1850$ cm^{-1}.

TABLE III. *BiF. System C. (Wave numbers of band heads and differences in cm⁻¹.)*

v′ \ v″	0	1	2	3	Mean ΔG′
0	44290 (4) *7330* 36960 (10) *4780* 32180 (7)	43770 (7) *7320* 36450 (7) *4790* 31660 (4)	43260 (4) *7340* 35920 (2) *4780* 31140 (2)	42760 (0) *7340* 35420 (0) — —	— *620* *620*
1	37580 (2) *4780* 32800 (2)		36540 (1) *4780* 31760 (1)		
Mean ΔG″	*520*	*520*	*500*		

Discussion

Systems *A* and *C* both appear to result from transitions between doublet electronic levels, but, from the present analysis, it is not possible to state in which levels the multiplicity occurs. It is possible, because of the definite, though small, difference between corresponding ω's of systems A_1 and A_2 that the upper and perhaps the lower electronic states of these systems are multiple. The same may be true of systems C_1 and C_2 but the accuracy of measurement of the band heads, (not $>1A$), is not sufficient to allow a definite statement to be made. The occurrence of apparently doublet multiplicity appears to suggest that the emitting molecule is not SbF, for this molecule, having an even number of electrons, should give rise to electronic states of odd multiplicity. The only other possibility is the molecule SbF^+ but it is very unlikely that the spectrum of this molecule could be excited by active nitrogen. Thus it must be concluded that the observed doublets are two levels of a triplet, the other predicted system being too weak to appear or being outside the region investigated. In the case of system *A* it is possible that one of the progressions (*a*) or (*b*) is part of the third system.

Bismuth fluoride (BiF)

Systems A and B.—These two systems, lying in the visible and near ultraviolet regions of the spectrum have been reported previously.[2–4] Howell[3] observed forty-one bands of system *A* in emission and made an analysis leading to the following vibrational constants, (in cm^{-1}), for the two electronic states involved:

Level	ν_e	ω_e	$x_e\omega_e$	$y_e\omega_e$
A	22959.7	381.0	3.00	0.10
X	0	510.7	2.05	—

Morgan[4] observed twenty-eight bands of the same system in absorption showing that the level *X* is the ground state of the molecule; his analysis is in good agreement with Howell's.

System *B* is a weak system observed by Morgan in absorption; no details concerning its position in the spectrum have yet been given. The corresponding systems in the spectra of BiCl, BiBr and BiI have been observed, however, so it is possible to estimate that it should be at about 3700A. By analogy with the other diatomic bismuth halide spectra it is probable that this system results from a transition between the ground state *X* and a singlet level.

System C.—The analysis of this system has been carried out with measurements made on a plate taken with small dispersion. As Table III clearly shows the system is triplet with wide multiplet separations. It is seen that the values of ω for the upper and lower states are approximately 620 cm^{-1} and 520 cm^{-1}, respectively, showing that the lower state of the system is to be identified with the ground state. The upper state is then a wide triplet with the large separations, 7330 cm^{-1} and 4780 cm^{-1}. The triplet character of the state *C* is in accordance with the even number of electrons in the neutral molecule BiF.

It is a pleasure to express my appreciation of the generous help given me by Professor F. A. Jenkins.

The Spectra of Neutral and Ionized Boron Hydride

G. M. Almy and R. B. Horsfall, Jr.*
Department of Physics, University of Illinois, Urbana, Illinois
(Received December 26, 1936)

The spectrum of boron hydride, as excited in the cathode of a Schüler lamp, consists of at least three systems, $^1\Pi\rightarrow{}^1\Sigma$ of BH, $^3\Sigma\rightarrow{}^3\Pi$ of BH, and a new system, $^2\Pi\rightarrow{}^2\Sigma$, due to BH^+.

BH, $^1\Pi\rightarrow{}^1\Sigma$.—This system has been extended to include the (2,2) band. One is thereby enabled to refine the rotational and vibrational constants of the system and, from a study of dissociation by rotation, to fix the heat of dissociation (D_e) of the normal state at 3.60 ± 0.05 ev.

BH, $^3\Sigma\rightarrow{}^3\Pi$, (0,0) head at λ3694.—The fine multiplet structure of this system has been resolved and the transition, previously reported to be $^3\Pi\rightarrow{}^3\Sigma$, established as $^3\Sigma\rightarrow{}^3\Pi$. The $^3\Pi$ state is regular and near case b ($A/B=+0.47$).

BH^+, $^2\Pi\rightarrow{}^2\Sigma$, (0,0) head at λ3766.—This system is the analog of the green bands of the isoelectronic molecule BeH. Application of the Hill and Van Vleck theory to the $^2\Pi$ state does not yield an A/B which is constant with increasing J. Refinement of the theory to include the rotational D term, along the lines suggested by Gilbert for $^3\Pi$ states, does not greatly improve the situation. The remaining discrepancy is probably due to unobservable $^2\Sigma$ doubling. The Λ type doubling has been evaluated and compared with theory with results very like those in BeH.

THE spectrum of boron hydride was first studied by Lochte-Holtgreven and van der Vleugel[1] and by Paton and Almy.[2] Recently Thunberg[3] has investigated the spectrum, particularly the isotope effect in the singlet bands due to the two boron and two hydrogen isotopes. Photographs of the spectrum as excited in the hollow cathode discharge reveal several new features of the spectrum which are the subject of this paper. First, the $^1\Pi\rightarrow{}^1\Sigma$ system, of which the (0,0) and (1,1) bands have been reported, has been extended to include the (2,2) band. Each of the three bands, moreover, exhibits dissociation by rotation which enables the heat of dissociation to be fixed fairly accurately. Second, the fine structure of the triplet band, discovered by Lochte-Holtgreven and van der Vleugel, has been more clearly resolved than by them and the transition fixed as $^3\Sigma\rightarrow{}^3\Pi$, instead of $^3\Pi\rightarrow{}^3\Sigma$, as reported. The molecular constants, including the electronic coupling coefficient in the $^3\Pi$ state, have been determined. Third, a new system, $^2\Pi(\text{reg})\rightarrow{}^2\Sigma$, due to BH^+, has been photographed and analyzed.

Experimental Details

The hollow cathode lamp used to excite the spectrum is essentially of the Schüler type, modified to permit rapid changes of the cathode and to provide forced water circulation around the cathode. A section of the lamp is shown in Fig. 1. To change the cathode one merely removes the glass cap at the left, fastened by picien, unscrews a cylindrical plug, and removes the cathode with a threaded tool. The lamp is much more convenient in surveying the spectra of a series of elements than the older type in which the cathode was pushed in from the window at the right. In this arrangement the cathode frequently stuck after the lamp had been run for some time and had to be drilled out.

The discharge was excited by a Phanotron bridge set at about 1200 volts a.c., 1 to 1.25 amperes. A copper cathode containing powdered boron was used. Helium and hydrogen were circulated through the lamp, and the proportions of the mixture were varied by controlling the cooling of the charcoal and chabuzite traps in the circulation system. When properly adjusted for photographing on the 21-foot grating the H_α line and the nearby He λ6678 were visually about equally intense and the hydrogen many-lines spectrum was faint when viewed in a hand spectroscope.

The discharge was operated at the lowest pressure which would give a steady intense cathode glow. At higher pressures the band spectra became weaker relative to the line spectra appearing.

Curiously, the bands of CuH were not excited

* Now at Bausch and Lomb Optical Company, Rochester, New York.
[1] W. Lochte-Holtgreven and E. S. van der Vleugel, Zeits. f. Physik **70**, 188 (1931).
[2] R. F. Paton and G. M. Almy, Phys. Rev. **37**, 1710 (1931).
[3] S. F. Thunberg, Zeits. f. Physik **100**, 471 (1936).

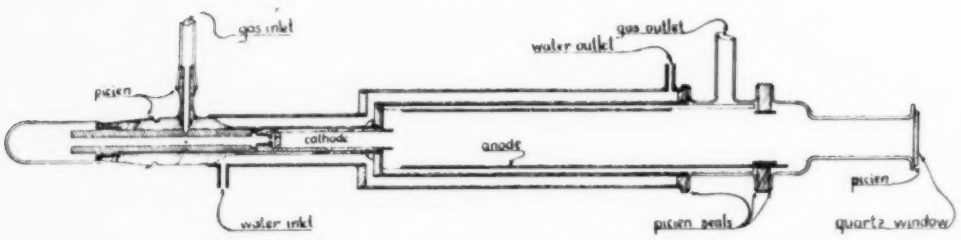

FIG. 1. Section of hollow cathode lamp.

nor do the hydrides of the somewhat similar metals Au and Na appear when these are placed in the cathode. The spectra of the hydrides of the alkaline earths, and of Zn, Cd and Hg, can be obtained with great intensity, as can those of Al and B.

The plates used in the analysis were obtained in the first order of a 21-foot, 30,000-lines-per-inch grating, with an iron arc providing the standard wave-lengths. For interpolating wave numbers directly use was made of the practical formula,

$$\nu = A/(B+x), \tag{1}$$

where A and B are constants and x is the distance along the plate from an arbitrary reference point. This approximate formula follows from the general grating equation,

$$\nu = \frac{n/d}{\sin i + \sin\theta}. \tag{2}$$

$\theta = (D+x)/R$, where D is the distance along the arc from the center of curvature of the grating to the reference point from which x is measured and R is the radius of curvature of the grating. Substitute for θ in Eq. (2), expand $\sin(D+x)/R$, make the approximation, $\sin(x/R) = x/R$ and lump constants to obtain Eq. (1). A correction curve is necessary. This formula is especially useful when a computing machine with automatic division is available.

$^1\Pi \rightarrow {}^1\Sigma$ BAND SYSTEM OF $B^{11}H$

Our determinations of the wave numbers of the (0,0) and (1,1) $^1\Pi \rightarrow {}^1\Sigma$ bands of $B^{11}H$ agree well with those of Thunberg and will not be recorded here. The wave numbers and quantum assignments of the new (2,2) band are given in Table I. We agree that Thunberg's revised numbering of the (0,0) Q branch follows from a consideration of the Λ type doubling, especially from a comparison of this effect in the three bands. The rotational constants of the three bands, obtained by a graphical method, are given in Table II. Thunberg's B_e and α_e of the $^1\Pi$ state need revision because B_v is not a linear function of $(v+\frac{1}{2})$; γ in the table is the constant appearing in $B_v = B_e - \alpha(v+\frac{1}{2}) + \gamma(v+\frac{1}{2})^2$. Otherwise our values of the rotational constants agree with his, generally within the probable errors of calculation (about ± 0.002 for any B_v).

Each of the three bands shows an abnormally sharp drop in intensity of rotational lines, the decrease occurring near $K' = 26$ in the (0,0) band, $K' = 21$ in the (1,1) band, $K' = 14$ in the (2,2) band. The visual estimates of intensity for (2,2) are given in Table I. These observations, combined with the fact that the (3,3) band is not observed on plates on which the (2,2) band is strong, show fairly conclusively that either

TABLE I. *Wave numbers, quantum assignments and intensities (eye-estimates) of the (2,2) band of the $^1\Pi \rightarrow {}^1\Sigma$ system of $B^{11}H$.*

K''	P	INT.	Q	INT.	R	INT.
0					22569.70	2
1			22547.79	5	588.64	2
2	22503.77	0	544.51	5	605.92	2
3	478.87	1	539.74	6	621.51*	6
4	452.57	3	533.30	6	635.35	4
5	424.68	3	525.07	6	647.21	3
6	395.13	4	514.96	6	656.83*	4
7	363.99	2	502.91	6	664.27	2
8	331.09	3	488.63	5	669.12	3
9	296.27	2	472.04	5	671.20	3
10	259.38	2	452.77	5	670.07	3
11	220.21	3	430.65	4	665.52	4
12	178.48	2	405.30	4	656.83*	4
13	133.88	2	376.32	2	643.79	4
14	085.83	od	343.90	1	missing	
15	missing		atomic line	10		
16			missing			

* Indicates superposition.

predissociation or dissociation by rotation takes place in the $^1\Pi$ state. As in the case of the analogous AlH bands, it is undoubtedly the latter. Lochte-Holtgreven and van der Vleugel remarked that at high pressures the lines of higher rotational quantum number in the (0,0) and (1,1) bands became diffuse, which is to be expected when dissociation by rotation is possible.

Since only the diagonal bands ($v'=v''$) are obtained on even the most intense photographs, the individual vibrational constants of the two states cannot be obtained. With three diagonal bands one can obtain the coefficients of the equation,

$$\nu_0(v,v)=\nu_e+(\omega_e'-\omega_e'')(v+\tfrac{1}{2})-(x_e'\omega_e'-x_e''\omega_e'')(v+\tfrac{1}{2})^2. \quad (3)$$

The origins, $\nu_0(v,v)$, were calculated from the frequencies of the first few lines in the P and R branches and the rotational constants of Table II with the results,

$$\nu_0(0,0)=23{,}074.0\ \text{cm}^{-1},$$
$$\nu_0(1,1)=22{,}891.8\ \text{cm}^{-1},$$
$$\nu_0(2,2)=22{,}549.2\ \text{cm}^{-1}.$$

Substituting these in Eq. (3) one obtains on solving,

$$\nu_e=23{,}104.0\ \text{cm}^{-1},$$
$$\omega_e'-\omega_e''=-21.8\ \text{cm}^{-1},$$
$$x_e'\omega_e'-x_e''\omega_e''=80.2\ \text{cm}^{-1}.$$

We may assume that both molecular states arise from a combination of normal $2p^2P$ boron and normal ^2S hydrogen atoms.[4] The lower, $^1\Sigma$ state is tightly bound and, by analogy with AlH, may be expected to show a normal relationship among constants. In particular, from $\omega_e''^2=4B_e''^3/D_e''$, we find $\omega_e''=2366\ \text{cm}^{-1}$; in AlH ω_e'', similarly calculated, agrees excellently with ω_e'' obtained from vibrational analysis, well within the uncertainty due to error in D_e''.[5] Since $\omega_e'-\omega_e''=21.8\ \text{cm}^{-1}$, $\omega_e'=2344\ \text{cm}^{-1}$. This is a more reliable value than $[4B_e'^3/D_e']^{\frac{1}{2}}$, which gives 2300 cm^{-1}, since the upper state is shallow and D_e' less certainly known than D_e''.

To estimate $x_e'\omega_e'$ and $x_e''\omega_e''$ Thunberg uses the semiempirical relation $x_e=0.6\alpha_e/B_e$ and obtains $x_e''\omega_e''=49\ \text{cm}^{-1}$, $x_e'\omega_e'=85$. Our value of $x_e''\omega_e''$ is on this basis about the same. We will accept it as the best available value. Then our relatively exact determination of $x_e'\omega_e'-x_e''\omega_e''$ requires that $x_e'\omega_e'=129\ \text{cm}^{-1}$. Hence the best available constants are:

$$\omega_e''=2366\ \text{cm}^{-1},\qquad \omega_e'=2344\ \text{cm}^{-1},$$
$$x_e'\omega_e'=49\ \text{cm}^{-1},\qquad x_e''\omega_e''=129\ \text{cm}^{-1}.$$

We may now fix limits for the heat of dissociation (also denoted by D_e) of both singlet states of BH. For $^1\Pi$ D_e' certainly lies between the energies of the states $v'=2$, $K'=0$ and $v'=2$, $K'=14$. That is to say, $0.63\ \text{e.v.}<D_e'<0.88\ \text{e.v.}$ The upper limit is further reduced if one admits that the absence of the (3,3) band is due to the instability of the state $v'=3$, $K'=0$; then, $D_e'<0.82$ volt. We conclude that $D_e'=0.73$ volt with a probable error of about 0.05 volt. It follows that for the $^1\Sigma$ ground state,

$$D_e''=\nu_e+D_e'=3.60\pm0.05\ \text{volts}.$$

An alternative method of calculating the heat of dissociation is to use the relation $D_e''=\omega_e''^2/4x_e''\omega_e''$. This gives $D_e''=3.5$ volts. Since the reliability of this method is much inferior to that making use of dissociation by rotation the agreement is to be taken as an indication of the accuracy of $x_e''\omega_e''$, obtained with the use of $x_e''=0.6\alpha_e''/B_e''$.

TABLE II. *Rotational constants of singlet states of B^{11}H (in cm^{-1}).*

CONSTANT	$^1\Sigma$	$^1\Pi$
B_0	11.812	11.918
B_1	11.399	11.187
B_2	10.989	10.246
α_e	0.412	0.521
γ_e		−0.105
B_e	12.018	12.152
D_0	−0.00122	−0.00141
D_1	−0.00118	−0.00165
D_2	−0.00114	−0.00211
D_e	−0.00124	−0.0013
r_e	1.225A	1.219A

[4] R. S. Mulliken, Rev. Mod. Phys. **4**, 1 (1932). The present argument with regard to the triplet states is not given explicitly by Mulliken but is implied in his Fig. 35 which shows the observed and predicted states of BH, and in his discussion of similar examples.

[5] W. Holst and E. Hulthén, Zeits. f. Physik **90**, 712 (1934).

$^3\Sigma\rightarrow{}^3\Pi$ BAND SYSTEM OF B^{11}H

Lochte-Holtgreven and van der Vleugel[1] discovered a band system with (0,0) head at 3694A whose general appearance and rotational

constants are similar to those of the singlet bands. A few lines in the R branch of the (0,0) band were resolved into triplets. Because the two systems were so similar they attributed the triplets to a $^3\Pi \rightarrow {}^3\Sigma$ transition "corresponding" to the $^1\Pi \rightarrow {}^1\Sigma$ transition and, indeed, these are the four states that can arise from normal B and normal H. Since on our plates several lines of the P and R branches are resolved into triplets (Q branch appears as doublets) it is possible to determine the nature of the transition more accurately than has been done. The conclusion, that it is $^3\Sigma \rightarrow {}^3\Pi$, rather than $^3\Pi \rightarrow {}^3\Sigma$, is supported by theoretical considerations which will be discussed.

The wave numbers and quantum assignments appear in Table III. The combination differences,

$$\Delta_2 F_i'(K) = R_i(K) - P_i(K),$$
$$\Delta_2 F_i''(K) = R_i(K-1) - P_i(K+1),$$

where $i=1$, 2, 3 were computed. The spin splitting in both states is evidently small and the states near case b. Since for singlet or pure case b states,

$$\Delta_2 F(K) = 4B(K+\tfrac{1}{2}) + 8D(K+\tfrac{1}{2})^3 + \cdots, \quad (4)$$

we have plotted in Fig. 2, $\Delta_2 F(K)/4(K+\frac{1}{2})$ against $(K+\frac{1}{2})^2$ for the six substates. For a $^3\Sigma$ state the effect of the splitting should be very small for low K and the plots for the three substates should coincide. For a $^3\Pi$ state not pure case b the lines should diverge as K decreases, on account of rotational distortion. It is clear that there is coincidence in the upper state but a definite divergence in the lower, indicating that the transition is $^3\Sigma \rightarrow {}^3\Pi$.

Next we may consider the relation of the molecular states of BH to the atomic states of the separated atoms and of the "united atom," carbon.[4] The normal atomic states, $2s^2 2p\ ^2P$ of B and $1s\ ^2S$ of H give four molecular states $^1\Sigma^+$, $^1\Pi$, $^3\Sigma^+$, $^3\Pi$. The united atom, carbon, has three low atomic states from the configuration $2s^2 2p^2$, namely, ^3P (normal), ^1D, ^1S, which give, on separating the atom, the following molecular states:

$^3\Pi$ and $^3\Sigma^-$ from ^3P,
$^1\Delta$, $^1\Pi$, $^1\Sigma^+$ from ^1D,
$^1\Sigma^+$ from ^1S.

In this group there is no $^3\Sigma^+$; the lowest $^3\Sigma^+$ comes from $2s^2 2p 3s\ ^3P$, 7.4 volts above the ground ^3P. $^3\Sigma^+$ from normal B and normal H is therefore repulsive or, at the least, less attractive than the $^3\Pi$ which goes into normal ^3P on pushing B and H together. On the other hand, $^3\Sigma^-$ from normal ^3P of C cannot dissociate into any observed state of B and normal H. However, the first excited state of B, $2s^2 3s\ ^2S$ (at 4.95 volts) would give $^3\Sigma^+$ with normal H. This is most probably the upper state of the triplet system. In this case it is about 1.6 volts more tightly bound than the lower $^3\Pi$ state since the corresponding atomic transition (4.95 volts) is

TABLE III. *Wave numbers and quantum assignments of* $^3\Sigma \rightarrow {}^3\Pi$ *system of* $B^{11}H$. *Subscript 3 corresponds to* $^3\Pi_2$, $J''=K''-1$; *2 to* $^3\Pi_1$, $J''=K''$; *1 to* $^3\Pi_0$, $J''=K''+1$.

K''	P_3	P_2	P_1	R_3	R_2	R_1	Q_3	Q_2	Q_1
2	27010.08	27007.96	27006.39	27131.19	27129.39	27127.51	27057.98	27056.22?	27054.66
3	26981.96	26980.64	26979.21	151.51	149.62	148.50	054.66	053.34	051.48
4	952.98	951.95	950.94	170.35	169.29	168.33	unresolved	048.72	047.17
5	923.31	922.36	921.69	188.38	187.63	186.78	"	042.94	041.71
6	892.81	892.09	891.43	205.29	204.58	203.80	"	036.07	034.90
7		860.48		220.74	220.17	219.48	"	028.03	026.95
8	829.04	828.51	828.02	235.12	234.48	233.92	"	018.85	017.90
9	795.85	795.49	795.03	unresolved	247.44	"	"	008.56	007.62
10	761.98	761.45	760.87	"	258.86	"	"	26997.11	26996.17
11	unresolved	726.57	unresolved	"	268.65	"	"	984.44	983.59
12	691.26	690.94	690.57	"	277.37	"	"	970.63	969.75
13	654.83	654.47	654.07	"	284.15	"	"	955.73	954.77
14	617.56	617.21	616.82	"	290.14	"	"	939.55	938.62
15	579.41	579.11	578.88	"	294.65	"	"	922.08	unresolved
16	540.69	540.42	540.07	"	297.02 (head)	"	"	903.36	"
17	unresolved	500.39	unresolved				"	883.47	"
18	"	460.63	"				"	862.65	"
19	"	419.66	"				"	840.81	"
20	"	377.91	"						

about 1.6 volts greater than the molecular electronic energy change.

Holst has observed the apparently analogous triplet system in AlH.[6]

The rotational constants of the $^3\Sigma$ state have been obtained graphically from Fig. 2. Eq. (4) applies and shows that the slope of the coincident lines for the three Σ states is $2D_0'$ and that the intercept at $(K+\frac{1}{2})^2=0$ is B_0'. The constants B_0 and D_0 for the $^3\Pi$ state have been determined by Challacombe and Almy[7] using Gilbert's method.[8] The electronic coupling constant λ, or A/B, has also been determined by Gilbert's method and verified by a graphical method suggested by Budo's treatment[9] of the Hill and Van Vleck theory for $^3\Pi$ states. The results are,

$$B_0''= 12.667, \quad B_0'= 12.126,$$
$$D_0''= -0.00122, \quad D_0'= -0.00128,$$
$$r_0''= 1.198\text{A}, \quad r_0'= 1.220\text{A},$$
$$\lambda = +0.47,$$

The $^3\Pi$ state is regular and near case *b*.

The Λ type doubling for each of the three sublevels of the Π state is shown in Table IV and Fig. 3. For pure case *b* the splitting should be the same in each sublevel and proportional to $K(K+1)$.[10] From the graph it appears that there is some departure from pure case *b* Λ type doubling. Following Hebb's treatment of this effect in $^3\Pi$ state, one might make a detailed comparison with theory, but this has not been done. The *cd* designation is based upon the assumption that the upper state is $^3\Sigma^+$.

$^2\Pi \rightarrow {}^2\Sigma^+$ Band System of $B^{11}H^+$

With the hollow cathode source a band appears with *R* head at 3766A, approximately as intense as the triplet band discussed above. A weaker head appears at 3803A. These two heads are assumed to be the (0,0) and (1,1) bands of a system. Only the (0,0) band has been measured and analyzed.

The (0,0) band exhibits *P*, *Q* and *R* branches, each branch consisting of narrow doublets whose interval converges as *K* increases. The wave numbers and quantum assignments appear in Table V. The general features of the system

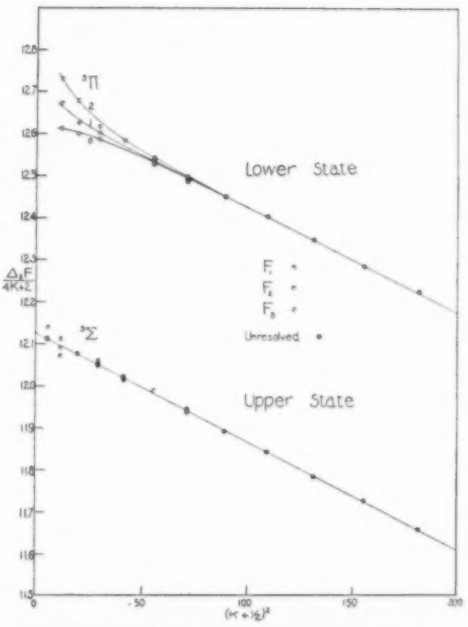

FIG. 2. $\Delta_2F(K)/4K+2$ for each triplet substate.

indicate a transition between a Π and a Σ state and a detailed consideration of missing lines shows that it fits the assignment $^2\Pi(\text{reg}) \rightarrow {}^2\Sigma$ with a $^2\Pi$ state whose coupling is intermediate between the two pure case *b* conditions ($\lambda=0$ and $\lambda=4$). That is to say, the P_1, Q_1, R_1 branches lie to the violet from the P_2, Q_2, R_2 branches, respectively, or, $F_1(K)$ of $^2\Pi$ lie above $F_2(K)$. If λ is less than 0 or greater than +4, $F_2(K)$ lies above $F_1(K)$. To see that the missing lines near the origin are just those one would expect to be missing one may compare Table V with Jevons' *Report on Band Spectra of Diatomic Molecules*, Fig. 40(i).

That the transition is $^2\Pi \rightarrow {}^2\Sigma$ is supported by the behavior of the values of Δ_2F for the two states. For the lower state these differences are identical within errors of observation for the F_1 and F_2 levels. This is characteristic of a $^2\Sigma$ state with negligible doubling. In the upper state Δ_2F_2 and Δ_2F_1 diverge as *K* decreases as when rotational distortion is occurring. Rather fragmentary observations on the isotopic spectrum accompanying the system support the assumption that the molecule is boron hydride. This BH^+ system corresponds to the well-known

[6] W. Holst, Zeits. f. Physik **86**, 338 (1934).
[7] To be published soon.
[8] Cecil Gilbert, Phys. Rev. **49**, 619 (1936).
[9] A. Budo, Zeits. f. Physik **96**, 219 (1935).
[10] M. H. Hebb, Phys. Rev. **49**, 610 (1936).

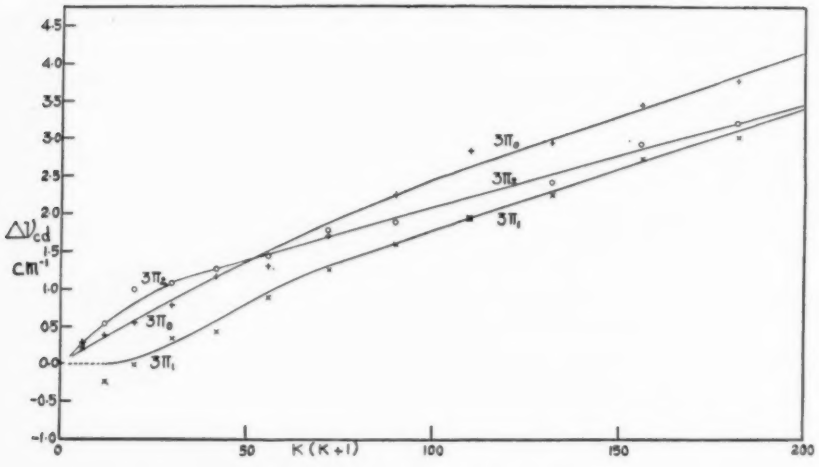

FIG. 3. Λ type doubling of $^3\Pi$ substates.

$^2\Pi \rightarrow {}^2\Sigma$ green BeH bands and to the AlH^+ bands.

Before calculating the rotational and electronic coupling constants of BH^+ we will refine the theory of $^2\Pi$ states somewhat beyond the stage discussed by Hill and Van Vleck.[11] In a recent paper Gilbert[8] has shown how the theory of Van Vleck for $^3\Pi$ states intermediate between case *a* and case *b* may be modified to take better account of the rotational D term. In the improved theory the D term is not considered merely as a fixed term to be added to each component of a molecular multiplet ($DK^2(K+1)^2$ near case *b* or $DJ^2(J+1)^2$ near case *a*) but is included in the Hamiltonian function of the unperturbed (case *a*) system. It is then shown that the D term is not the same for all components of a multiplet. Gilbert gives a neat method for finding the rotational and electronic coupling constants of triplet states under the refined theory. The corresponding theory for doublet states can be written down at once.

THEORY OF $^2\Pi$ STATES

The Hamiltonian for case *a* used by Gilbert is,

$$H_a = H + \mu H^2 + \lambda\Lambda\Sigma,$$

where $\mu = D/B$, $\lambda = A/B$. $H + \lambda\Lambda\Sigma$ is the matrix for case *a* given by Van Vleck, μH^2 is the new term including the effect of the D term. As in Gilbert's paper, Van Vleck's matrices will be divided by B. The elements of $H_a(\Sigma, \Sigma')$ are

$$\begin{Vmatrix} (J^*-7/4)+\mu[(J^*-7/4)^2+(J^*-\tfrac{3}{4})]+\lambda/2 & (J^*-\tfrac{3}{4})^{\frac{1}{2}}[1+2\mu(J^*-\tfrac{3}{4})] \\ (J^*-\tfrac{3}{4})^{\frac{1}{2}}[1+2\mu(J^*-\tfrac{3}{4})] & (J^*+\tfrac{1}{4})+\mu[(J^*+\tfrac{1}{4})^2+(J^*-\tfrac{3}{4})]-\lambda/2 \end{Vmatrix},$$

where $J^* = J(J+1)$.

The energies are the roots of the equation,

$$\begin{vmatrix} \frac{F}{B}-H_a(\tfrac{1}{2},\tfrac{1}{2}) & -H_a(+\tfrac{1}{2},-\tfrac{1}{2}) \\ -H_a(-\tfrac{1}{2},\tfrac{1}{2}) & \frac{F}{B}-H_a(-\tfrac{1}{2},-\tfrac{1}{2}) \end{vmatrix} = 0. \quad (5)$$

TABLE IV. Λ *type doubling of* $^3\Pi$. *Values of* $\Delta\nu_{cd}$ *are listed where* $2\Delta\nu_{cd}(K+\frac{1}{2}) = [R(K)-Q(K+1)] - [Q(K)-P(K+1)]$.

$K+\frac{1}{2}$	$^3\Pi_2$	$^3\Pi_1$	$^3\Pi_0$
$2\frac{1}{2}$	0.25	0.23	0.29
$3\frac{1}{2}$	0.55	−0.23	0.40
$4\frac{1}{2}$	1.00	0.00	0.57
$5\frac{1}{2}$	1.09	0.36	0.80
$6\frac{1}{2}$	1.28	0.45	1.18
$7\frac{1}{2}$	1.45	0.90	1.32
$8\frac{1}{2}$	1.78	1.28	1.71
$9\frac{1}{2}$	1.88	1.61	2.26
$10\frac{1}{2}$	1.94	1.94	2.84
$11\frac{1}{2}$	2.42	2.26	2.95
$12\frac{1}{2}$	2.92	2.74	3.46
$13\frac{1}{2}$	3.22	3.04	3.79
$14\frac{1}{2}$	3.96	3.81	4.16
$15\frac{1}{2}$	4.95	4.81	4.64
$16\frac{1}{2}$	5.29	5.29	5.29

[11] E. L. Hill and J. H. Van Vleck, Phys. Rev. **32**, 250 (1928).

If we let

$$E=\frac{F}{B}-\tfrac{1}{2}[H_a(\tfrac{1}{2},\tfrac{1}{2})+H_a(-\tfrac{1}{2},-\tfrac{1}{2})], \quad (6)$$

the determinant Eq. (5) becomes, on expanding.

$$E^2=\tfrac{1}{4}[H_a(\tfrac{1}{2},\tfrac{1}{2})-H_a(-\tfrac{1}{2},-\tfrac{1}{2})]^2 + H_a^2(\tfrac{1}{2},-\tfrac{1}{2})=\alpha. \quad (7)$$

Then $E=\pm\sqrt{\alpha}$ are the solutions, where

$$\alpha=\frac{(\lambda-2)^2}{4}+\frac{4J^*-3}{4}\left[1+\mu(4J^*+1-2\lambda) +\mu^2\left(\frac{4J^*-1}{2}\right)^2-\mu^2\right]. \quad (8)$$

Finally, from Eq. (6),

$$F(J)=B(J^*-\tfrac{3}{4})+D\left(J^{*2}-\frac{J^*}{2}+\frac{13}{16}\right)\pm B\sqrt{\alpha}. \quad (9)$$

These are the energies of the states for a particular value of J. The upper $(+)$ sign goes with $J=K-\frac{1}{2}$, or F_2 levels. The lower $(-)$ sign, goes with $J=K+\frac{1}{2}$, or F_1 levels. If terms in D are dropped the expression for $F(J)$ reduces to the Hill and Van Vleck formula. If another rotational term is needed FJ^{*3} (not the above F) may be added to each component just as D and F terms have been added in using the Hill and Van Vleck theory.

Calculation of B and D

We may write,

$$\text{Spur } F(J)=B \text{ Spur } H_a =B[H_a(\tfrac{1}{2},\tfrac{1}{2})+H_a(-\tfrac{1}{2},-\tfrac{1}{2})] =-(3/2)B+(13/8)D +(2B-D)J^*+2DJ^{*2}.$$

Hence

$$\Sigma\Delta_2F(J)=\Delta_2F_1(J)+\Delta_2F_2(J) =\text{Spur } F(J+1)-\text{Spur } F(J-1) =8(B+D)(J+\tfrac{1}{2})+16D(J+\tfrac{1}{2})^3. \quad (10)$$

Thus if one plots the mean $\Delta_2F(J)$ divided by $4J+2$ against $(J+\frac{1}{2})^2$ one should obtain a straight line of slope $2D$, intercept, $B+D$. If the line is not straight a correction term $24F(J+\frac{1}{2})^5$ may be added to Eq. (10).

Fortunately this result is, except for the negligible term $8D(J+\frac{1}{2})$ in Eq. (10), exactly the same as in the procedure which has usually been followed in applying the Hill and Van Vleck theory.

TABLE V. *Wave numbers and quantum assignments of (0,0) band of* $^2\Pi\rightarrow{}^2\Sigma^+$ *system of* $B^{11}H^+$. *Subscript 1 corresponds to* $^2\Pi_{\frac{1}{2}}$, $J'=K'+\frac{1}{2}$; *subscript 2 to* $^2\Pi_{\frac{3}{2}}$, $J'=K'-\frac{1}{2}$.

K''	P_1	P_2	Q_1	Q_2	R_1	R_2
0			26368.18		26389.87	
1	26335.39		365.59		410.91	26406.78
2	316.52		361.40	26357.17	430.32	427.55
3	287.48	26283.73	356.14	353.28	448.34	446.32
4	257.71	254.77	349.42	347.17	464.71	463.08
5	226.56	224.50	341.20	339.48	479.45	478.15
6	194.29	192.62	331.34	330.03	492.42	491.34
7	160.46	159.18	319.94	318.80	503.48	502.62
8	125.38	124.33	306.98	305.95	512.85	512.12
9	088.85	088.09	292.38	291.50	520.30	519.61
10	051.18	050.50	276.11	275.48	525.91	525.42
11	012.11	011.54	258.33	257.71	529.59	529.17
12	25971.81	25971.35	238.82	238.33	531.50	530.76
13	930.29	929.86	217.84	217.42	531.00	unresolved
14	887.64	887.19	195.06	194.71	528.65	"
15	843.42	unresolved	170.58	unresolved	524.37	"
16	798.11	"	144.64	"	518.05	"
17	751.69	"	117.12	"	509.58	"
18	704.21	"	088.09	"	499.06	"
19	655.54	"	057.07	"	486.38	"
20	605.81	"	024.63	"	471.42	"
21	554.92	"	25990.61	"	454.49	"
22	503.04	"	955.03	"	435.46	"
23	450.08	"	917.84	"	414.26	"
24	396.27	"	879.44	"	390.35	"

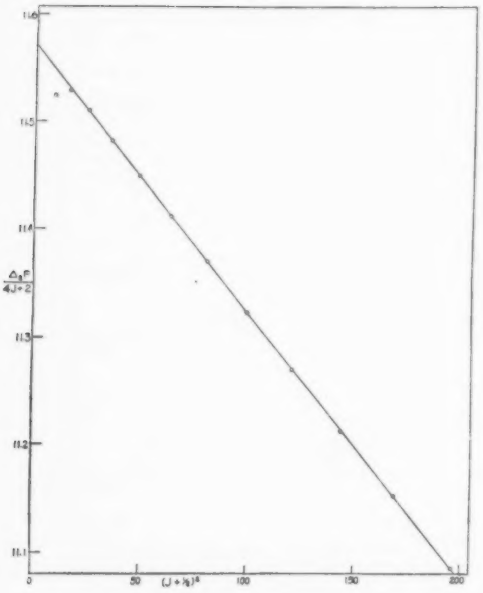

FIG. 4. Mean $\Delta_2 F/4J+2$ for $^2\Pi$ state. The slope is $2D_0$, the intercept $B_0+D_0+\frac{1}{2}q^*$.

We have not, however, considered the effect of Λ type doubling on this calculation. Mulliken and Christy[12] have given a complete expression for the energy of a $^2\Pi$ state with terms for Λ type doubling included (but without D terms). Their equation stands, with the present modification of theory, if the D term of Eq. (9) is added and if $\sqrt{\alpha}$ is substituted for their $X/2$. An examination of their equation shows that if one takes the mean of all four values of $\Delta_2 F(J)$, that is, for $1c$, $1d$, $2c$, $2d$ sublevels, the Λ doubling correction terms subtract off except for a term $\frac{1}{2}q^*(J+\frac{1}{2})$. This term may be considered as a correction on the term in $(J+\frac{1}{2})$ in Eq. (10) so that in the method for evaluating B and D, the intercept is not $B+D$ but $B+D+\frac{1}{2}q^*$. q^* can be determined from a study of the Λ type doubling. Near case b, as in BH^+, it may be taken as the experimentally determined coefficient q_0 in Eq. (13).

Calculation of λ

One may obtain λ from the relation,

$$F_2(J)-F_1(J)=2B\sqrt{\alpha}.$$

[12] R. S. Mulliken and A. Christy, Phys. Rev. **38**, 87 (1931).

α depends upon J (Eq. (8)). One substitutes the observed J doublet intervals on the left and solves for $(\lambda-2)^2$, and hence λ, for various values of J. The ambiguity in λ must be removed by a consideration of missing lines, or of Λ type doubling.

The objection to this method is that it deals with a J doublet for which the interval, especially near case b, is due largely to difference of rotational energy. Hence B and D must be precisely known. Near case a the method should work well but near case b it is better to use K doublets. The width of a K doublet is:

$$\begin{aligned}\Delta\nu_{12}(K)&=F_1(K)-F_2(K)\\&=B[2K+1+4\mu(K+\tfrac{1}{2})^3\\&\qquad-(\sqrt{\alpha_1}+\sqrt{\alpha_2})],\end{aligned}\quad(11)$$

in which α_1 is α with $J=K-\frac{1}{2}$, α_2 is α with $J=K+\frac{1}{2}$. A term $(\mu/2)(K+\frac{1}{2})$ has been dropped. Solving for $(\lambda-2)^2$,

$$(\lambda-2)^2=\frac{[(g(K)-\Delta\nu_{12}/B)^2-f(K)-f(K+1)]^2-4f(K)f(K+1)}{(g(K)-\Delta\nu_{12}/B)^2},\quad(12)$$

in which $g(K)=2K+1+4\mu(K+\frac{1}{2})^2$

$$f(K)=(K^2-1)[1-2\mu\lambda-\mu^2+4(\mu-\mu^2)K^2+4\mu^2K^4].$$

Calculation of band origin

Writing the equations for the frequencies of the Q_1 and Q_2 lines and adding, one may readily show that,

$$\nu_{00}=\frac{Q_2(J)+Q_1(J)}{2}-(B'-B'')J(J+1)+\tfrac{3}{4}B'+\tfrac{1}{4}B''.$$

MOLECULAR CONSTANTS OF BH^+

The rotational constants of the $^2\Pi$ state of BH^+ have been determined graphically in Fig. 4 by the method described, using Eq. (10), and taking into account Λ doubling. The constants for the $^2\Sigma$ state have been obtained by least squares solution for the coefficients in

$$\Delta_2 F(K)/(4K+2)=B+2D(K+\tfrac{1}{2})^2+3F(K+\tfrac{1}{2})^4.$$

Within errors of observation, $\Delta_2 F_1''$ and $\Delta_2 F_2''$

are equal. The results,

$$B_0''= 12.374, \qquad B_0'= 11.565,$$
$$D_0''= -0.00125, \qquad D_0'= -0.00124,$$
$$F_0''= 6.9\times10^{-8},$$
$$r_0''= 1.208\text{A}, \qquad r_0'= 1.248\text{A}.$$
$$\nu_{00}= 26376.2 \text{ cm}^{-1},$$

The coupling constant λ for the $^2\Pi$ state of BH^+ has been determined by applying Eq. (12) to each observed K doublet between $K=2$ and $K=11$. The data were obtained from a careful measurement of the Q branch on a rather faint second order plate. Thus intervals between c levels are used. Since, as is shown below, the Λ doubling is practically the same for the F_1 and F_2 levels, the results would not be appreciably changed if the d levels were used. The results are shown in Fig. 5. A constant value of λ is not obtained. The main reason for refining the theory was to see if one might thereby get a more consistent value of λ than is obtained with the Hill and Van Vleck theory (dotted line in Fig. 5). The situation is not much improved. The remaining discrepancy is presumably due to doubling in the $^2\Sigma$ state. Theoretically if there is a "pure precession" relation between a $^2\Pi$ and a $^2\Sigma$ state, the doubling in the $^2\Sigma$ state is $\Delta\nu_{12}(K) = \gamma(K+\frac{1}{2})$ where $\gamma=\lambda q_0$ and q_0 is a coefficient in the expression for Λ doubling in the $^2\Pi$ state (Eq. (13)). In the case of BH^+ the electron configurations are $2s\sigma^2\,2p\pi$ and $2s\sigma^2\,2p\sigma$ and one may expect approximately pure precession.[12] We find experimentally (below) that $q_0=0.016$ and hence $\gamma=0.02$. Since the observed spin doubling is $\Delta\nu_{12}(^2\Pi)-\Delta\nu_{12}(^2\Sigma)$ the observed intervals should be increased by $0.02(K+\frac{1}{2})$ before λ is evaluated. This change would, as a matter of fact, give a fairly constant λ, though the correction overshoots somewhat (at $K=10$, the corrected λ is 1.30). In the absence of satellite branches, γ can only be determined experimentally from a study of $\Delta_2F(K)$, since $\Delta_2F_1(K) - \Delta_2F_2(K)=2\gamma$. For BH^+ 2γ is 0.04 cm^{-1}. The data on BH^+ are not sufficiently precise to enable an estimate to be made in this way. Since the uncertainty in the $^2\Pi$ doublet interval is least for low K, the best value of λ is obtained in this range. We conclude from Fig. 5 that

$$\lambda = 1.21\pm0.01, \qquad A=\lambda B = 14.0 \text{ cm}^{-1}.$$

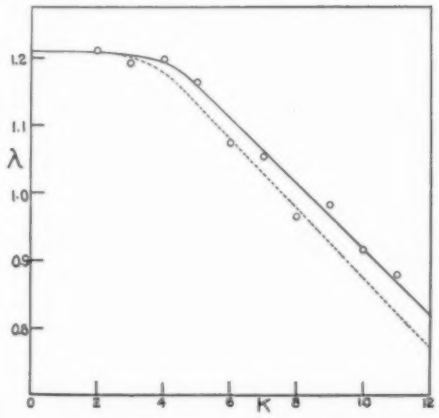

FIG. 5. Values of electronic coupling constant (λ) obtained with Eq. (12) (solid line) and from Hill and Van Vleck theory (dashed line). The plotted points go with the solid line.

In the case of the analogous $^2\Pi$ state of the isoelectronic molecule BeH, Olsson[13] found that the observed doublet intervals fit the Hill and Van Vleck theory without correction for $^2\Sigma$ splitting. This is to be expected because the $^2\Sigma$ splitting is theoretically much smaller than in BH^+, since λ is smaller. That is to say, $\gamma=\lambda q_0 = 0.0029$, using the experimental $q_0=0.0142$. In the range in which the theory was applied $(K<11)\Delta\nu_{12}(^2\Sigma)$ is less than 0.03 cm^{-1} and the correction to the computed λ would be inappreciable.

The Λ type doubling, calculated for each component of the $^2\Pi$ state according to the equation

$$2\Delta\nu_{dc}(K+\tfrac{1}{2}) = [R(K)-Q(K)] - [Q(K+1)-P(K+1)]$$

is plotted in Fig. 6. Van Vleck's theory of Λ type doubling, as formulated and extended by Mulliken and Christy[12] predicts that for either sublevel in case b,

$$\Delta\nu_{dc}(K) = q_0[(K+\tfrac{1}{2})^2+(4D/B)(K+\tfrac{1}{2})^4].$$

$$q_0=\left[\frac{2B_v^2J(J+1)}{\nu(\Pi,\Sigma)}\right] \qquad (13)$$

Negligible terms are dropped. $q_0=[2B_v^2J(J+1)/$

[13] E. Olsson, Zeits. f. Physik **73**, 732 (1932).

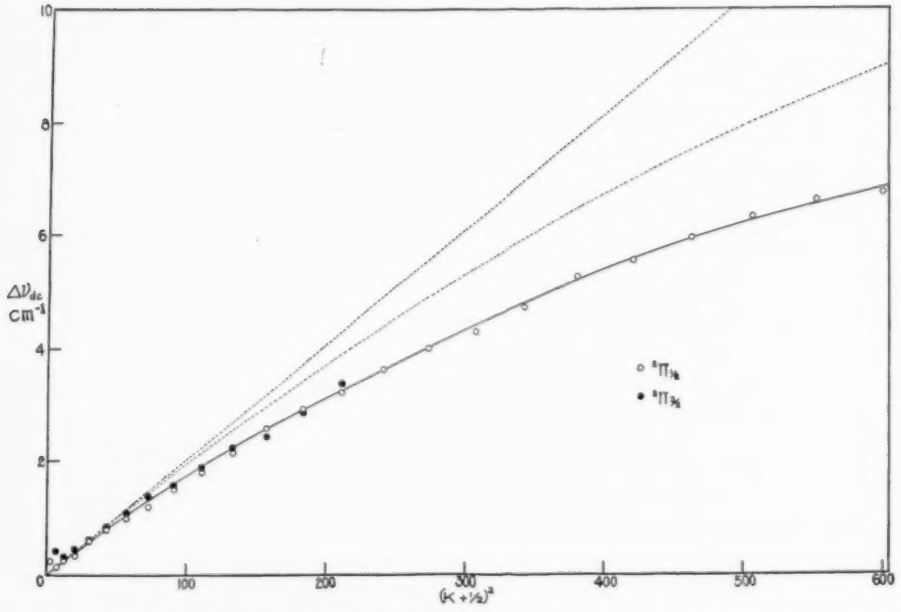

FIG. 6. A type doubling in $^2\Pi$ state of BH^+. Solid curve: $0.0164(K+\frac{1}{2})^2-0.086\times10^{-4}(K+\frac{1}{2})^4$. Upper dashed curve: $q_0(K+\frac{1}{2})^2$. Lower dashed curve: Eq. (13).

$\nu(\Pi, \Sigma)]$, in the case of pure precession. The curve through the plotted points shows that the observed doubling can be fitted accurately by the equation,

$$\Delta\nu_{dc}=0.0164(K+\tfrac{1}{2})^2-0.086\times10^{-4}(K+\tfrac{1}{2})^4,$$

in which the coefficients were obtained by least squares. The corresponding theoretical coefficients are $q_0=0.0204$ and $4q_0D_0/B_0=-0.090\times10^{-4}$. The curves obtained with the latter coefficients, with and without the fourth power term, are shown. The departure from pure precession and the improvement in the shape of the curve when the fourth-power term (due to stretching with rotation) is added is very like that found in BeH.[12]

The Sign of the Magnetic Moment of the K^{39} Nucleus

HENRY CUTLER TORREY*
Columbia University, New York City
(Received January 25, 1937)

The assignment of quantum numbers to the magnetic levels of alkali atoms depends on the sign of the nuclear magnetic moment. If a beam of normal alkali atoms is split in a weak inhomogeneous magnetic field and transitions are then induced among the component magnetic levels, a subsequent strong field analysis of a selected state suffices to identify its quantum numbers and hence to determine the sign of the moment. This method applied to K^{39} determines its nuclear magnetic moment to be positive in contradiction to the findings of Jackson and Kuhn from h.f.s. data. A similar experiment on Na^{23} shows its nuclear moment to be positive in agreement with the h.f.s. result of Granath and Van Atta.

A METHOD for the determination of the signs of nuclear magnetic moments based on the use of nonadiabatic transitions[1] in an atomic beam was suggested by Rabi,[2] and has been used by Kellogg, Rabi and Zacharias[3] to determine this property of the proton and the deuteron. This method has now been extended to include the alkalis and, specifically, to determine the sign of the nuclear magnetic moment of K^{39}.

General Considerations

If a beam of neutral alkali atoms passes through a weak inhomogeneous magnetic field, it is separated into $2(2I+1)$ component magnetic states where I is the nuclear spin. The atoms in $2(I+\frac{1}{2})+1$ of these states have a total angular momentum $F=I+\frac{1}{2}$, while those in the remaining $2(I-\frac{1}{2})+1$ states have $F=I-\frac{1}{2}$. In the case of K^{39}, $I=3/2$[4] and there are eight states in all, for five of which, $F=2$ and for the remaining three, $F=1$. The effective magnetic moments of the atoms in these eight levels as a function of the magnetic field intensity are given by[5]

$$\mu_m=(\mp\delta)\frac{x+2\delta m/(2I+1)}{\{1+[4\delta m/(2I+1)]x+x^2\}^{\frac{1}{2}}}\mu_0, \qquad x=2\mu_0 H/\Delta W, \tag{1}$$

where $\delta=+1$ if the nuclear moment is positive and -1 if negative; μ_0 is the Bohr magneton, H is the external magnetic field intensity, m is the magnetic quantum number and ΔW is the energy separation of the two groups of levels in the absence of magnetic field. These magnetic moments are plotted against x in Figs. 1a and 1b

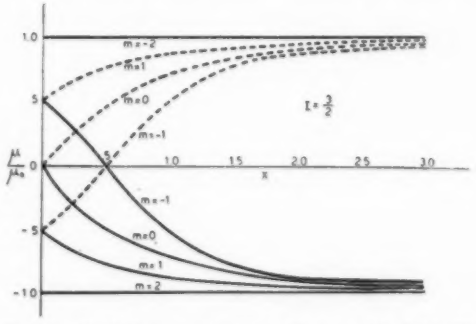

FIG. 1a. Variation of moment with magnetic field. The dotted lines are the moments of the magnetic levels arising from the $F=I-1/2$ state. Nuclear moment assumed positive.

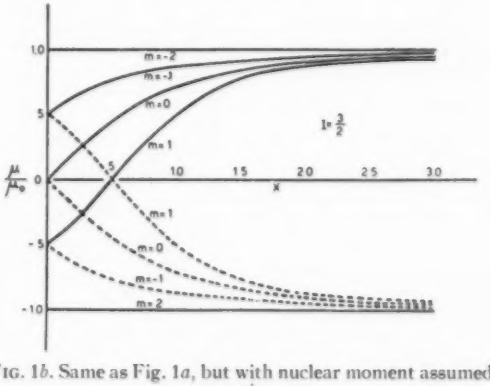

FIG. 1b. Same as Fig. 1a, but with nuclear moment assumed negative.

* University Fellow, Columbia University, 1935–36.
[1] T. E. Phipps and O. Stern, Zeits. f. Physik **73**, 183 (1931); R. Frisch and E. Segrè, Zeits. f. Physik **80**, 610 (1933).
[2] I. I. Rabi, Phys. Rev. **49**, 324 (1936).
[3] J. M. B. Kellogg, I. I. Rabi and J. R. Zacharias, Phys. Rev. **50**, 472 (1936).
[4] S. Millman, Phys. Rev. **47**, 739 (1935).
[5] G. Breit and I. I. Rabi, Phys. Rev. **38**, 2082 (1931).

for nuclear moment positive and negative, respectively. In the case of K^{39} one x unit is equivalent to 159 gauss. As is evident from these curves, the only asymmetries due to the sign of the nuclear magnetic moment consist in the assignment of the quantum numbers m and F to the individual states. Since the magnetic moments are the important quantities in an atomic beam experiment, the sign can be determined only by having recourse to these distinctions.

As was shown by Rabi,[2] it is possible to utilize these differences by causing the atoms of the beam to make transitions among the component magnetic levels. These transitions are produced by passing the beam of atoms through the immediate neighborhood of a point of zero field intensity. Such a region is characterized by a rapid change in direction of the magnetic field intensity along the path of the beam. The spacial quantization of an atom passing through this region is thus subject to perturbation which, in certain cases, is sufficient to induce a nonadiabatic transition to another magnetic state. The probabilities of such transitions for this type of perturbation have been calculated by Majorana[6] in terms of a parameter α, which is, physically, the angle between the two directions, before and after transition, with respect to which the atom is space-quantized with the same quantum number m. It can be shown that α is the same for all m and is given by a certain function of the distance of the beam from the point of zero field and the field intensity at the position of closest approach of the beam to the zero point. Majorana's equations are reproduced in Rabi's paper. In Table I, the transition probabilities for $F=2$ are given in terms of $\cos\alpha/2$ and $\sin\alpha/2$. The transition which is significant in this experiment is the one in which m changes from $-\delta$ to -2δ. Its probability is $4\cos^6\alpha/2\sin^2\alpha/2$ which has the maximum value 0.422 at $\alpha=60°$. The success of the method of nonadiabatic transitions depends largely on the following circumstance: Since the perturbation takes place in very weak fields (less than one gauss), it is not sufficiently powerful to induce transition unless the energy separation of the two states concerned is quite small. This condition obtains among the Zeeman components of either of the two h.f.s. levels, but is not satisfied by the comparatively large interval ΔW. The transitions are therefore subject to the selection rule $\Delta F=0$.[7]

It will be shown later that if the beam is first split in a weak inhomogeneous magnetic field and transitions are then caused to take place, a subsequent analysis of the beam in a second inhomogeneous magnetic field will suffice to identify a given state and hence to determine the sign of the nuclear magnetic moment.

Apparatus

The apparatus is represented diagrammatically in Fig. 2. The essential parts are housed in a brass tube 5 in. inside diameter and $4\frac{1}{2}$ ft. long. This tube is divided by a partition into two chambers. The source chamber contains the oven and is made short so that a pressure of 10^{-5} mm can be tolerated without detriment to the beam intensity. To permit the passage of the beam, the partition separating the two chambers is fitted with a pair of slit jaws which have a separation of about 0.5 mm and form a channel 2 mm long which offers a high resistance to gas flow. Each chamber is evacuated with its own high speed oil diffusion pump of the Zabel[8] type. These two pumps feed into an interstage vacuum provided by a small oil diffusion pump which is backed by a Cenco Megavac.

[6] E. Majorana, Nuovo Cimento **9**, 43 (1932).

[7] L. Motz and M. E. Rose, Phys. Rev. **50**, 348 (1936).

[8] R. M. Zabel, Rev. Sci. Inst. **6**, 54 (1935).

Table I. *Transition probabilities for $F=2$ in terms of $\cos\alpha/2$ and $\sin\alpha/2$.*

m	-2	-1	0	$+1$	$+2$
-2	c^8	$4c^6s^2$	$6c^4s^4$	$4c^2s^6$	s^8
-1	$4c^6s^2$	$c^4(c^2-3s^2)^2$	$6s^2c^2(c^2-s^2)^2$	$s^4(3c^2-s^2)^2$	$4c^2s^6$
0	$6c^4s^4$	$6s^2c^2(c^2-s^2)^2$	$(c^4-4s^2c^2+s^4)^2$	$6s^2c^2(c^2-s^2)^2$	$6c^4s^4$
$+1$	$4c^2s^6$	$s^4(3c^2-s^2)^2$	$6s^2c^2(c^2-s^2)^2$	$c^4(c^2-3s^2)^2$	$4c^6s^2$
$+2$	s^8	$4c^2s^6$	$6c^4s^4$	$4c^6s^2$	c^8

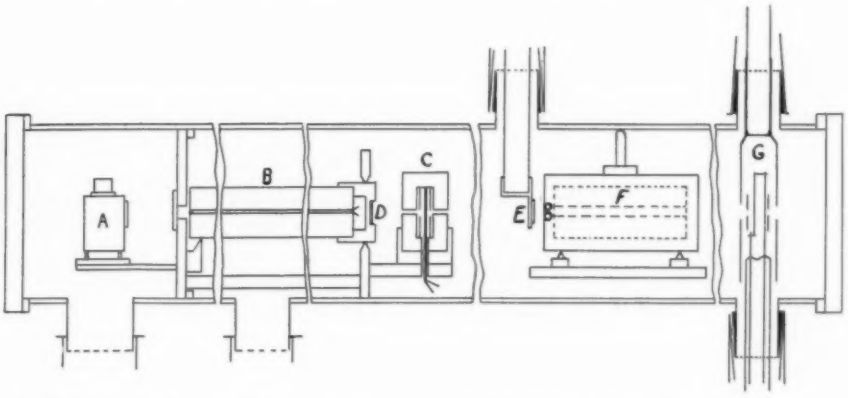

FIG. 2. Schematic diagram of the apparatus. *A*, oven; *B*, *A* field block; *C*, transition field assembly; *D*, collimator slit; *E*, selector slit; *F*, *B* field magnet; *G*, detector.

The beam is produced in a nickel oven (*A*) of conventional design. Its slit has a width of about 0.02 mm.

The first deflecting field or "*A*" field is produced in the manner described by Rabi, Kellogg and Zacharias,[9] by two horizontal straight copper tubes carrying currents in opposite directions. These are held in a duralumin block, 2 ft. long, (shown at *B*) which is supported at the source end by a knife edge and at the other end by two screw points. It is movable for purposes of lineup about a vertical axis through these points by a screw at the source end. The collimator slit, *D*, is rigidly fixed to the end of the field block and is collinear with the axis of the screw points so that a motion of the block about this axis does not shift the beam. The width of this slit is 0.02 mm.

The transitions are produced by sending the beam between two vertical straight copper wires 3.5 mm apart which carry currents of the order of 0.1 amp. in the same direction. These currents produce a magnetic field which changes in direction through 180° along the path of the beam and has a zero point on a line perpendicular to the two wires and joining their centers. The distance of this zero point from the path of the beam as well as the magnetic field intensity at the distance of closest approach to the zero point can be controlled by the currents in the wires. Fig. 3 shows a plot of the lines of force in the neighborhood of the two wires in the special case of equal currents. The region in the neighborhood of these wires is shielded magnetically by a permalloy cylinder. To avoid magnetizing the permalloy the current having passed through the two wires is returned by a cylindrical brass sheath inside the permalloy. This assembly (shown at *C*) immediately follows the collimator slit. The oven, partition, *A* field block, collimator slit, transition field assembly and their supports form a complete unit which can be lined up outside before installation.

The function of the slit shown at *E*, is the selection of part of the beam for future analysis. It is suspended from a double eccentric ground joint. Immediately following the selector slit is the electromagnet (*F*) which produces the analyzing, or "*B*," field. It is placed on the opposite side of the beam to the *A* field block in order to give deflections in the opposite direction. The magnet, a cross section of which is shown in Fig. 4, is a cylindrical shell 4 in. long of Armco iron which is slotted to a width of 3/16 in. along its length. It is activated by a current in eight turns of hollow water-cooled copper tubing. The author is indebted to Professor I. I. Rabi for suggesting this type of magnet which has considerable utility in molecular beam experiments. Its construction is easy and its small size permits inclusion in the vacuum system. Activation by high currents with a low voltage power source is most convenient, as the few turns necessary

[9] I. I. Rabi, J. M. B. Kellogg, J. R. Zacharias, Phys. Rev. **46**, 157 (1934).

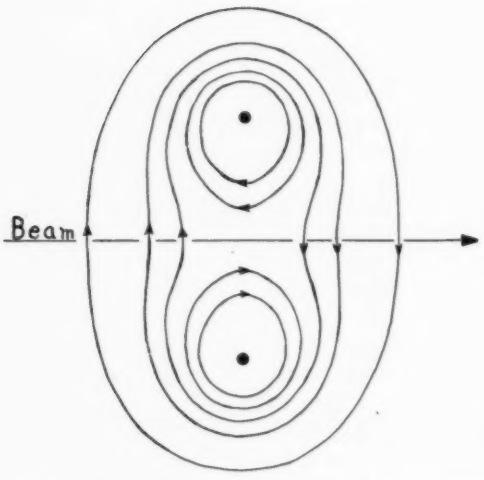

FIG. 3. Lines of force in the neighborhood of the transition field wires in the special case of equal currents.

under these conditions are easily cooled and insulated. The magnet in its present form was developed by Dr. J. R. Zacharias and the author. The magnetic field intensity in the region of the slot opening was measured by a point to point plot of the magneto-resistance of a straight fine bismuth wire. The gradient was then computed from these measurements by numerical differentiation. The direct measurements were preferred to calculation by a Schwarz transformation since the latter is very tedious. The beam is sent along parallel to the axis of the magnet just outside the pole faces, as in this region the gradient is approximately constant over the height of the beam. The power source is a large two volt lead cell with a capacity of 3000 amp. hr. Two volts across the field coil yields a current of 250 amp. and a field of 5000 gauss inside the gap and 4000 gauss at the region traversed by the beam. The ratio of gradient to field at the latter position is about 2 cm^{-1}.

Detection is effected by a surface ionization gauge with a one mil tungsten filament (shown at G). The filament motion is furnished by a double eccentric ground joint.

The distances from the oven slit to the collimator slit, transition field wires, selector slit and detector are respectively 65, 70, 95 and 125 cm.

THE EXPERIMENTAL METHOD

The oven is loaded with a piece of potassium metal and the apparatus is immediately sealed and evacuated. Upon attainment of a sufficiently low pressure, the oven is heated slowly until a beam of desired intensity is obtained. The current in the A field wires is turned on to produce a field of 120 gauss at the region traversed by the beam. The corresponding value of x (cf. Figs. 1a and 1b) is about 3/4. At this field the eight magnetic levels have magnetic moments separated by approximately equal intervals. Since the force on an atom in the y direction in a magnetic field is $\mu_m(\partial H/\partial y)$ when μ_m is the effective magnetic moment of the atom, the deflections produced by the A field are about equally spaced. Four of the eight states are deflected to the right and four to the left. The selector slit, which is so wide that only one jaw is used at a time, is introduced to stop one of the two groups of four states. The remaining atoms all of which have magnetic moments of the same sign are allowed to enter the analyzing field. The magnetic field intensity in this region is so large (over 1000 gauss) that the coupling between the nuclear and electronic spins is destroyed and the atoms of all these four states have the same magnetic moment equal in absolute magnitude to one Bohr magneton. Consequently this field exerts the same force on each atom. By a suitable choice of the current activating this field, it is thus possible to

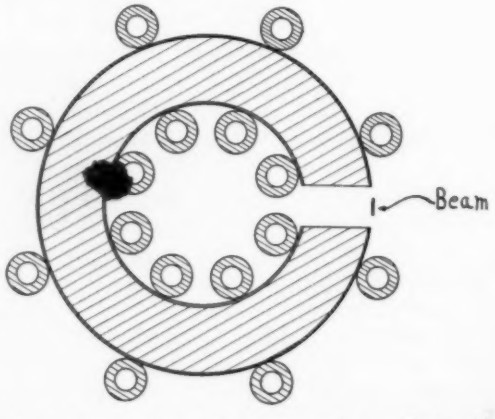

FIG. 4. Cross section of the electromagnet producing the B field.

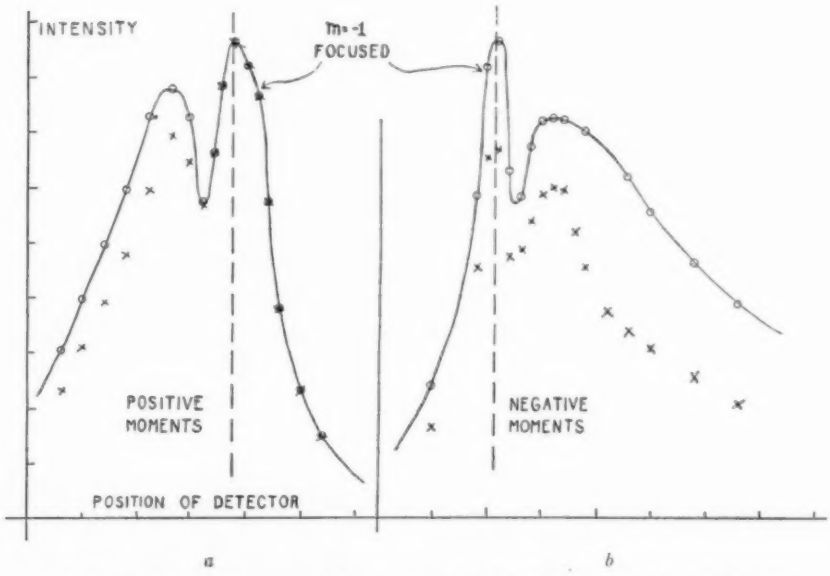

FIG. 5. Effect of nonadiabatic transitions on intensity distribution at detector. Broken line shows position of net zero deflection.

neutralize the deflections received by the atoms of one of the four states in the A field. The atoms of this state are now focused at the detector which has not been moved from its original position at the maximum of the undeflected beam. The atoms of the remaining three states, passed by the selector slit, still have net deflections and miss the detector. Thus the atoms now being focused belong entirely to one of the eight original magnetic levels.

Of the four selected states, the one having $m=-\delta$ is best resolved and, for this reason, the current in the B field is adjusted until the atoms belonging to this state are focused. With no current in the transition field wires, the filament is moved across the beam and the intensity is taken at each position. This yields an intensity distribution curve which shows two peaks: a narrow one at the position of net zero deflection due to the focused atoms and a broad one to one side due to the atoms of the three unfocused states. At each position of the filament, the transition field currents are varied in an effort to alter the intensity. Whenever this is possible, the intensity of maximum change is recorded. Let us inquire as to what effect, if any, transitions may be expected to have on the intensity. If the atoms received by the filament make transitions to states with atomic moments of the same sign[10] in the B field, no change will be noticed in the intensity since the magnetic moment and hence the deflection in the strong B field is unaltered. If, however, the transitions result in change of sign of the net atomic moment, the deflection in the B field will be opposite in direction and these atoms will no longer strike the detector. In general it can be said that transitions are unobservable unless the sign of the atomic moment in the B field is changed, and that observable transitions are manifested by reductions in the intensity at the detector.

Since the value of x in the A field is greater than $\frac{1}{2}$, the three states for which $F=1$ have in this field atomic moments of the same sign. This may be seen by reference to Fig. 1 in which the magnetic moments of these states are represented by the broken line curves. This circumstance, together with the rule that F does not change in a transition, means that an atom,

[10] Atomic moments are not to be confused with nuclear moments.

originally in one of these states, is confined to atomic moments of one sign in the B field and is therefore incapable of making an observable transition. Such is not the case, however, for an atom in one of the five states for which $F=2$. Such an atom always has open to it the possibility of an observable transition consistent with the selection rule.

In view of these considerations, we are led to the following conclusions:

(a) If it is found possible to alter the intensity at a given position of the filament by manipulation of the transition field currents, then at least some of the atoms received at this position have $F=2$.

(b) If no combination of currents in the transition field wires succeeds in altering the intensity at a given position of the filament, then all of the atoms striking the detector at this position have $F=1$.

The latter statement is, of course, only true within the limits of experimental error which may be estimated to be less than 2 percent. It is further qualified by the fact that the maximum probability of an observable transition is usually less than 1. However, these probabilities, given by the matrix elements in Table I, all have maxima in excess of 0.37.

Results

Typical results are shown in Figs. 5a and b which are plots of the intensity at the filament against filament position taken in the manner described above. Fig. 5a shows the results obtained when atoms with positive atomic moments were selected; Fig. 5b shows the corresponding curve for negative atomic moments. The broken line indicates in each case the position of the filament when it is receiving atoms with net zero deflections. The peaks at this position in the two curves, a and b, are due to the focused atoms of the two states for which $m=-\delta$. The crosses give the intensity at each point after the original intensity has been altered as much as possible by manipulation of the transition field currents.

Since the atoms of the state m with positive strong field moments do not show observable transitions, they must belong to the $F=1$ level by the result (b) of the last section. The intensity of the $m=-\delta$ state with negative strong field atomic moments shows a maximum change of 25 percent. This state must, then, be one of the group for which $F=2$ by the result (a) of the last section. It is seen that the atoms of the three unfocused states show observable transitions in both Figs. 5a and 5b. This result should be expected in any case, since at least one of the states composing each selected group has $F=2$.

By an inspection of Fig. 1, it is clear that these results are consistent only with the hypothesis that the hyperfine structure of the $^2S_{\frac{1}{2}}$ state of K^{39} is regular and the nuclear magnetic moment is positive.

Discussion

During the progress of this experiment Jackson and Kuhn[11] published results from the intensities of the h.f.s. of K^{39} to show that the nuclear moment is negative. This result, if valid, would place K^{39} in a unique position since the h.f.s. of the other alkalis so far examined (Li^7, Na^{23}, Rb^{85}, Rb^{87} and Cs^{133}) has been found to be regular. In view of the disagreement of Jackson and Kuhn's result with the findings of the method of nonadiabatic transitions, it should be emphasized that the determination of the sign of the nuclear moment by the latter method depends only on the detection of qualitative differences in the behavior of two states with the same m and different F. The final result is independent of the manner in which the transitions are brought about, provided the selection rule, $\Delta F=0$, is obeyed.

Since the first instance in which it has been possible to compare results of the two methods has led to contradiction, it was thought advisable to make a further comparison on another alkali nucleus. Na^{23} was chosen for this purpose. It should be noted that all above considerations will still apply to sodium since its nuclear spin is also 3/2.

Further Experiments

The apparatus used for K^{39} did not have sufficient resolving power for Na^{23} so that another very similar apparatus was modified for these measurements. The author wishes to thank

[11] D. A. Jackson and H. Kuhn, Nature **137**, 107 (1936).

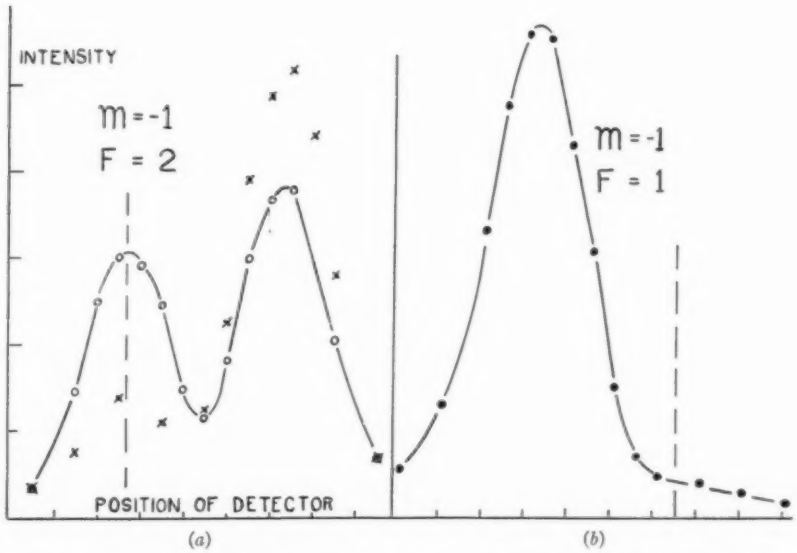

FIG. 6. Asymmetries in deflection patterns of (*a*) $m=-1$ atoms with positive strong field moments, (*b*) $m=-1$ atoms with negative strong field moments.

Dr. Millman and Dr. Zacharias for the loan of this apparatus and for their cooperation in securing the results. After modification to meet the demands of the above method, the only major difference between the two apparatus, aside from resolving power, was in the location of the analyzing field which is now on the same side of the beam as the *A* field block. As a result of this change an atom with a magnetic moment of the same sign in both fields will not be focused. However, selection is now effected not by focusing but by narrowing the selector slit to 0.035 mm so that only atoms of the state in question are passed. The states examined are again the two for which $m=-\delta$. The procedure is now as follows. With all fields off, the filament is placed at the center of the beam. The *A* field is then set at a value of x slightly less than 1/2. The filament is moved slightly to one side so that the atoms which strike it belong only to one of the $m=-\delta$ states. The atoms of the other states have relatively large deflections and miss the detector. The selector slit is introduced to pass the atoms directed towards the filament. The *B* field is now turned on, deflecting these atoms to one side, and the filament is moved the necessary amount to pick up the deflected peak. These preliminary adjustments made, the transition field is turned on and varied in an effort to change the intensity at the final position of the filament. As in the former experiment, transitions, to be observable, must take place to $m=-2\delta$ and this is not possible if the original state has $F=1$. When the state $m=-\delta$ with positive strong field atomic moments was selected in this manner, it was found that no change in intensity to within 1 percent could be produced by the transition field, whereas the peak intensity of the corresponding state with negative moments in the *B* field was reduced from a maximum of 14.2 cm of galvanometer deflection to a minimum of 9.5 cm, a net change of 30 percent. Hence by reference to Figs. 1*a* and 1*b* it is seen that the sign of the nuclear magnetic moment of Na^{23} is positive in agreement with the results of Granath and Van Atta.[12]

In order to effect a direct comparison of the two alkalis, the apparatus was also used with K^{39}. The *A* field was set at a value of x slightly larger than $\frac{1}{2}$; otherwise the preliminary experimental procedure is the same as for Na^{23}. In this case, however, the intensity distribution of the

[12] L. P. Granath and C. M. Van Atta, Phys. Rev. **48**, 725 (1935).

selected atoms was found by moving the filament across the beam (*a*) when the transition field current was set at the value for which the peak intensity was a maximum and (*b*) when this current was set to minimize the peak intensity. The results when the state $m=-\delta$ with negative strong field moments was selected is shown in Fig. 6*a*. The circles are the experimental points for procedure (*a*); the crosses are those for procedure (*b*). The peak in the solid line curve at the position of the dotted line is due to atoms which have made observable transitions, in consequence of which they have received smaller deflections in the *B* field. The other peak in this curve is due to atoms which have not made observable transitions. Since this state shows observable transitions, it must have $F=2$. Fig. 6*b* shows the corresponding situation when atoms of the state $m=-\delta$ with positive strong field atomic moments were selected. Atoms making observable transitions would give rise to a peak at the position of the dotted line. In this case procedures (*a*) and (*b*) are equivalent, since it was found impossible to alter the intensity of the observed peak by varying the transition field currents. It was also impossible to produce a displaced peak in this manner. The absence of observable transitions identifies this state as $F=1$. These results determine the sign of the magnetic moment of the K^{39} nucleus to be positive in agreement with the results of the first experiment.

In conclusion the author wishes to express his gratitude to the members of the molecular beam laboratory for generously contributed assistance and especially to Professor I. I. Rabi who suggested the problem and whose advice and resourcefulness insured its successful solution.

MARCH 15, 1937 PHYSICAL REVIEW VOLUME 51

Effect of CCl_4 Vapor on the Dielectric Strength of Air

M. T. RODINE AND R. G. HERB
Department of Physics, University of Wisconsin, Madison, Wisconsin
(Received January 14, 1937)

The effect of CCl_4 vapor on the dielectric strength of air has been studied at a number of different air pressures up to a maximum of 75 lb./in.^{2}. With air at 25°C and 15 lb. pressure the dielectric strengths of the mixtures relative to pure air ranged from a value of 1.25 for a CCl_4 vapor pressure of 5 percent of saturation to a value of 1.80 for a saturated vapor pressure. At higher air pressures the addition of CCl_4 vapor gives a greater increase in the absolute value of the dielectric strength, but the percentage increase, relative to the pure air, is less than at 15 lb. pressure.

INTRODUCTION

THE effect of CCl_4 vapor on the dielectric strength of air was first noticed three years ago by one of the authors (R.G.H.) while working with an electrostatic generator of the Van de Graaff type which operates in a steel tank under an air pressure up to 45 lb. With air at atmospheric pressure containing a high concentration of CCl_4 vapor the maximum generator potential was found to be about 1.7 times the maximum potential obtainable with pure air.

Qualitative measurements were then made on the breakdown potential of the generator as a function of CCl_4 vapor pressure, with air at atmospheric pressure and also at higher pressures. The electrostatic generator proved to be unsatisfactory, however, for a thorough study of the CCl_4 effect because of sparking along a textolite support which determined an upper voltage limit that could not be improved by higher air pressure or higher concentrations of CCl_4 vapor. A small pressure chamber, equipped with an adjustable sphere gap was therefore constructed and with this apparatus sparking potentials were determined as a function of CCl_4 vapor pressure at a number of different air pressures. Publication of these results was de-

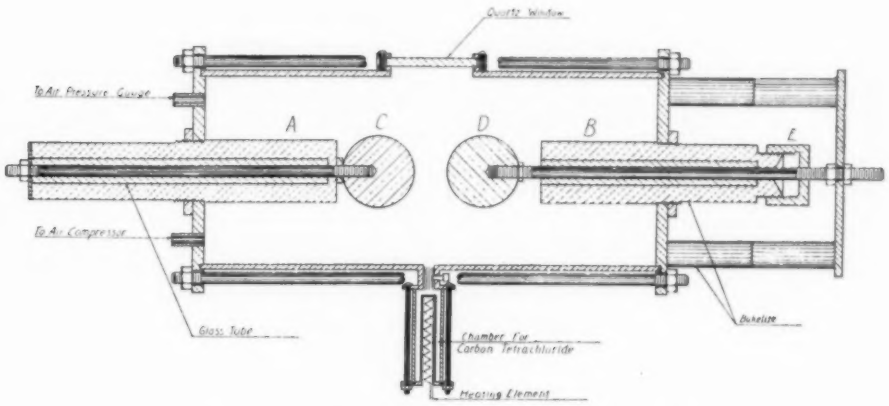

FIG. 1. Pressure chamber for study of sparking potentials.

layed because it was intended to look for similar effects caused by other vapors, but because of a shortage of personnel and equipment the research has been discontinued and the investigation, as reported in this paper, therefore covers only the effect of CCl_4 vapor on the breakdown strength of air.

Recently Joliot, Feldenkrais and Lazard reported[1] the discovery of the CCl_4 effect. They find that an electrostatic generator operated in air containing a high concentration of CCl_4 vapor gives a maximum potential twice as high as when operated in ordinary air. As our results differ considerably from these and since our investigation covers a wide range of air pressures and CCl_4 vapor pressures we believe that this belated report of our work may be of interest.

APPARATUS

Fig. 1 shows the pressure chamber with its adjustable sphere gap. The walls of the chamber are formed of a brass cylinder $4\frac{1}{2}$ inches in diameter, 11 inches long, and $\frac{1}{8}$ inch thick, equipped with brass end plates $\frac{5}{16}$ inches thick. One end plate is soldered to the cylinder and the other, which is removable, is held in place by 6 steel stay rods and is sealed by a rubber gasket. *C* and *D* are brass spheres 5 cm in diameter which are threaded onto brass rods that pass through insulating bushings. Sphere *C* is fixed in position while sphere *D* can be adjusted for different separations by sliding its supporting rod through bushing *B* and stuffing box *E*. The displacement of the supporting rod and consequent displacement of the sphere is measured by means of a traveling microscope mounted on the pressure chamber. A small chamber for vaporization of CCl_4 is located on the bottom part of the main cylinder. The walls of this vaporizer are made up of an outer glass cylinder and a reentrant brass cylinder containing a heating coil. Liquid CCl_4 is injected into the vaporizing chamber through a small hole near the top which is then closed by a threaded plug. The pressure chamber is provided with two windows, one made of glass, to permit observation of the spark discharge, and the other made of quartz so that the spark gap can be illuminated with ultraviolet light.

The apparatus is provided with a calibrated gauge of the dial type for measurement of pressure.

METHOD AND RESULTS

For the necessary high voltage the sphere gap was connected across the terminals of a 125 kv transformer with a 175,000 ohm water resistance in series with each terminal to prevent large surges of current and oscillations. The secondary voltage of the transformer was determined in the following way. The primary voltage was measured by means of a voltmeter and for different sphere separations the value of the

[1] Joliot, Feldenkrais and Lazard, Comptes rendus **202**, 291 (1936).

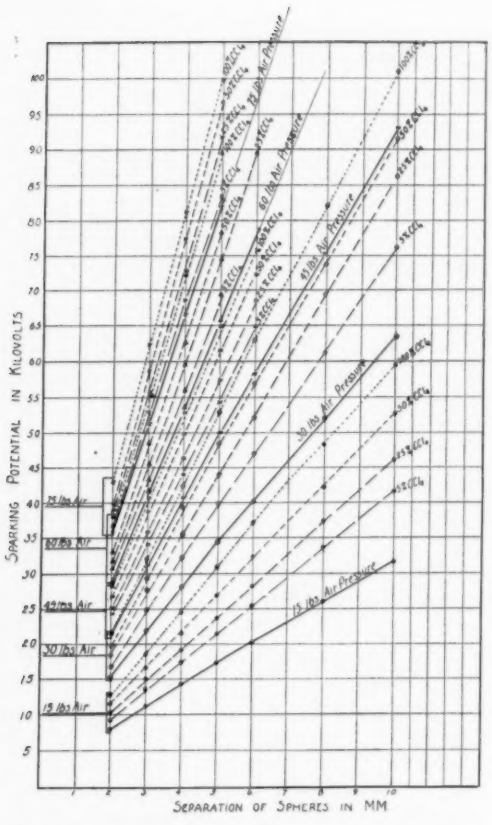

FIG. 2. Curves showing sparking potential as a function of sphere separation. Full lines are for pure air and broken lines for air to which CCl_4 vapor has been added.

primary voltage was recorded as the breakdown occurred at the sphere gap. Using these data and Peek's data on sparking potentials for sphere gaps, with corrections for temperature and barometric pressure, the peak secondary voltage of the transformer was plotted as a function of primary voltage and the resulting calibration curve was used in all subsequent measurements. During these measurements and for all subsequent work the spheres were illuminated with ultraviolet light from a quartz mercury arc lamp to avoid possible trouble from spark lag.

The procedure followed in studying the carbon tetrachloride effect was as follows: With pure dry air in the chamber several runs were taken on sparking potential as a function of sphere separation in order to check the consistency of the results. Sufficient CCl_4 was then introduced, by means of a calibrated glass pipette, to give a vapor pressure of 5 percent of the value for saturation for a temperature of 25°C, and again the sparking potential was determined at a number of sphere separations. The chamber was then flushed out with clean dry air and a check run was taken on pure air before the introduction of a higher concentration of CCl_4. Following this procedure sparking potentials were determined as a function of CCl_4 vapor pressure using air at a number of different pressures up to a maximum of 75 lb./in.^{2}.

Fig. 2 shows the results obtained. The sparking potentials determined by the curves of Fig. 2 for a sphere separation of 5 mm are replotted in Fig. 3 to give the curves showing sparking potential as a function of vapor pressure of CCl_4.

Because of the limited time available for this research sufficient check runs could not be made

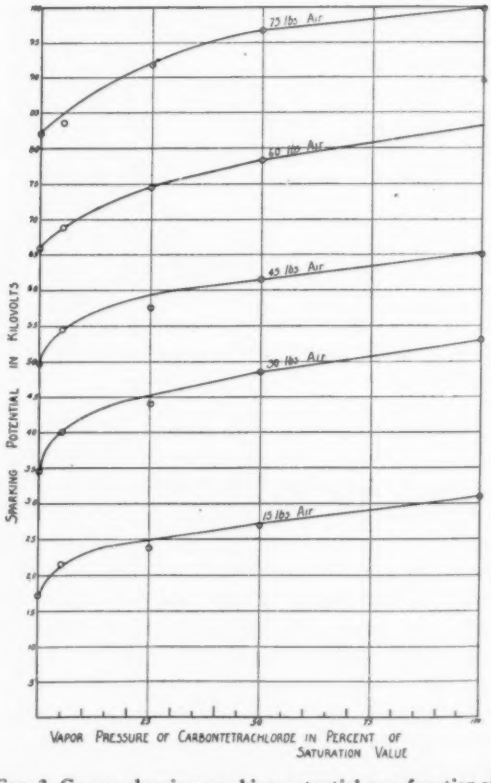
SPARKING POTENTIAL IN KILOVOLTS
VAPOR PRESSURE OF CARBONTETRACHLORDE IN PERCENT OF SATURATION VALUE
75 lbs Air
60 lbs Air
45 lbs Air
30 lbs Air
15 lbs Air

FIG. 3. Curves showing sparking potential as a function of vapor pressure of CCl_4 for several different air pressures.

and therefore no great precision can be claimed for the data. When saturated vapor pressures of CCl_4 were used the values obtained for sparking potentials were found to be very inconsistent and the values plotted are the highest obtained out of several trials. After each spark a light fog due to condensed vapor could be seen in the region of the sphere gap and a second spark would then pass at a very low voltage. At lower concentrations of CCl_4 vapor the sparking potential was found to be independent of the number of sparks which had previously passed, thus showing that any decomposition of the vapor due to spark discharges was not noticeably influencing the results.

Natterer[2] and Wright[3] have measured the dielectric strength of pure CCl_4 vapor. Wright found that its dielectric strength is 20 times as great as that of pure air with the same temperature and pressure. If the dielectric strength of CCl_4 vapor measured by Wright simply added to that of the air with which it is mixed the dielectric strength of the mixture would show a linear increase with vapor pressure of CCl_4, and for a mixture consisting of 15 lb. of air and a 100 percent concentration of CCl_4 vapor at 25°C the dielectric strength would be 3.9 times the value for pure air. The curves of Fig. 3 show, however, that the dielectric strengths of the two components of the mixture do not add together in this simple way and that the actual behavior is more complex. All of the curves rise more rapidly in the region of low concentration of CCl_4 than at high concentrations, although this characteristic behavior is less pronounced at high air pressure.

The lowest curve of Fig. 3 shows that the breakdown potential of air at 15 lb. pressure is increased by the addition of a 50 percent concentration of CCl_4 vapor to a value of about 1.56 times the value for pure air. This increase corresponds to that obtained by the addition of 8.5 lb. of pure air. At high air pressures the increase in sparking potential due to the addition of CCl_4 vapor is somewhat greater than at 15 lb. but the percentage increase becomes much less. These results indicate that carbon tetrachloride vapor would not be of great value for increasing the breakdown strength of air at high pressures. It may be of interest to note that while working with the small electrostatic generator previously referred to, certain results indicated that CCl_4 vapor may be more efficient for suppression of corona discharge than for suppression of sparking.

We wish to express our indebtedness to the late Professor C. E. Mendenhall for advice and support and to D. B. Parkinson and D. W. Kerst for valuable help in part of this work.

[2] K. Natterer, Ann. Phys. Chem. **38**, 663 (1889).
[3] R. Wright, J. Chem. Soc. **111**, 643 (1917).

Quantum Equations in Cosmological Spaces

A. H. TAUB
*Princeton University, Princeton, New Jersey**
(Received November 16, 1936)

The Dirac equations for a free electron in a cosmological space are solved by means of separation of variables. It is shown that the wave functions depend on the angles θ and φ in the same manner as those of a free electron in flat space time. The radial functions are obtained and it is shown that they go over into the usual ones in the limit. The explicit form of the time dependence of the wave functions cannot be obtained until an arbitrary function $R(t)$ is specified. Three different cases are discussed. The energy of the free electron is then determined for each of these. Finally the connection between the equation used here and that proposed by Dirac for the DeSitter space is discussed. It is shown that they are similar and that the imaginary part of the complex mass that he was forced to introduce has a geometrical origin.

1. INTRODUCTION

VARIOUS extensions of the Dirac equation for an electron in arbitrary gravitational and electromagnetic fields have been proposed by Weyl, Fock, Schrödinger, Pauli, Schouten and Van Dantzig, and others. The relations between these equations and the class of equations of the Dirac type (linear, equations which are first order in the derivatives with respect to the coordinates, and which are invariant under arbitrary spin, gauge and coordinate transformations) were discussed in "The Dirac Equation in Projective Relativity."[1] There it is shown that one equation of the class reduces exactly to the Dirac equation for a charged particle in the special relativity case.

In this paper we obtain exact solutions of that equation for the free electron in any cosmological space, i.e., a space time whose metric is of the form[2]

$$ds^2=c^2dt^2-R^2(t)du^2, \tag{1.1}$$

where $R(t)$ is an arbitrary function of t and

$$du^2=h_{ij}dx^idx^j \tag{1.2}$$

defines a three dimensional space of constant Riemannian curvature, ρ^2, which may be positive, negative or zero. The angular functions are the same for the three cases. The radial functions are obtained explicitly for ρ^2 positive and those for the flat spaces are obtained by taking the limit as $\rho\to\infty$. The radial functions for spaces of negative curvature are obtained by making an imaginary transformation ($\rho=i\rho$, and $\alpha=i\alpha$).

The time dependence of the wave functions cannot be obtained until some assumptions are made regarding the arbitrary functions $R(t)$. In the Einstein universe R is a constant and $\rho^2>0$, it is shown that the wave functions contain a factor $e^{i\lambda t}$ where λ depends on the energy of the electron. The case where $\rho^2\geqslant 0$ and $R(t)=e^{ct/a}$ includes the DeSitter universe and the wave functions are obtained explicitly for this case. When $R(t)=ct$ and ρ^2 is negative,[3] the time dependence of the wave functions are obtained explicitly and the radial functions are obtained by an imaginary transformation.

Recently Dirac[4] proposed an equation for an electron in DeSitter space. He used the fact that the DeSitter space may be imbedded in a flat five space and used the coordinates of the latter space in his equation. The equation used here, when written in terms of the coordinates of the flat five space, gives an equation different from Dirac's but very similar to it.

The equation given in D.P.R. is invariant under abitrary spin, gauge and coordinate transformations, where the coordinate transformation

* Now of the University of Washington.

[1] A. H. Taub, O. Veblen and J. v. Neumann, Proc. Nat. Acad. Sci. **20**, 383–385 (1934). Hereafter this paper will be referred to as D.P.R.

[2] H. P. Robertson, "Relativistic Cosmology," Rev. Mod. Phys. **5**, 62 (1933). Hereafter referred to as R.C.

[3] Robertson has shown that this case is equivalent to Milne's world structure: Zeits. f. Astrophys. **7**, 153–166 (1933). Professor Schrödinger discussed the Dirac equation in such a space in lectures at Princeton University during the spring of 1934.

[4] P.A.M. Dirac, Annals of Mathematics **36**, 657 (1935).

does not induce a spin transformation. This equation is[5]

$$\gamma^\alpha\left(\frac{\partial}{\partial x^\alpha}+S_\alpha-\frac{i}{h}\frac{e}{c}\varphi_\alpha\right)\psi=\mu\psi, \tag{1.3}$$

where φ_α is the electromagnetic four vector, $\mu=imc/2h$, m is the mass of the electron, e, its charge, h is Planck's constant divided by 2π, and in a proper choice of spin coordinate system[6]

$$S_\alpha=\gamma_\mu\left(\left\{\begin{matrix}\mu\\ \beta\alpha\end{matrix}\right\}\gamma^\beta+\frac{\partial\gamma^\mu}{\partial x^\alpha}\right). \tag{1.4}$$

The matrices γ_α are defined by means of the gravitational metric tensor $g_{\alpha\beta}$ as solutions of

$$\tfrac{1}{2}(\gamma_\alpha\gamma_\beta+\gamma_\beta\gamma_\alpha)=\tfrac{1}{4}g_{\alpha\beta}\cdot 1 \tag{1.5}$$

and the quantities $\left\{\begin{matrix}\mu\\ \beta\alpha\end{matrix}\right\}$ are the Christoffel symbols of the second kind formed from the $g_{\alpha\beta}$.

2. Computation of S_0 and $\gamma^i S_i$

The quantities S_0 and $\gamma^i S_i$ will now be computed. The nonvanishing Christoffel symbols formed from the $g_{\alpha\beta}$ are[7]

$$\left\{\begin{matrix}i\\ jk\end{matrix}\right\}=\left\{\begin{matrix}i\\ jk\end{matrix}\right\}^*,\quad \left\{\begin{matrix}0\\ ij\end{matrix}\right\}=\frac{RR'}{c^2}h_{ij};\quad \left\{\begin{matrix}i\\ 0j\end{matrix}\right\}=\frac{R'}{R}\delta_j{}^i, \tag{2.1}$$

where the asterisk on the Christoffel symbol indicates that it is to be computed from the coefficients h_{ij} of the line element (1.5) and $R'=dR/dt$. Hence we have from (1.2)

$$S_0=\gamma_0\partial\gamma^0/\partial t+\gamma_i(R'\gamma^i/R+\partial\gamma^i/\partial t).$$

Since g_{00} is a constant, γ_0 and γ^0 may be taken independent of x^α. Therefore

$$S_0=\gamma_i\gamma^iR'/R+\gamma_i\partial\gamma^i/\partial t.$$

Let
$$\gamma_i=iR\sigma_i, \tag{2.2}$$

where
$$\tfrac{1}{2}(\sigma_i\sigma_j+\sigma_j\sigma_i)=\tfrac{1}{4}h_{ij}. \tag{2.3}$$

Then σ_i is independent of t. Also we have

$$\gamma^i=g^{ij}\gamma_j=-h^{ij}\gamma_j/R^2=-i\sigma^i/R. \tag{2.4}$$

Hence
$$S_0=\gamma_i\gamma^iR'/R+\gamma_i(\partial/\partial t)(-i\sigma^i/R)=0. \tag{2.5}$$

From Eq. (1.2) we have

$$S_i=\gamma_\mu\left(\left\{\begin{matrix}\mu\\ \beta i\end{matrix}\right\}\gamma^\beta+\frac{\partial\gamma^\mu}{\partial x^i}\right).$$

In virtue of Eqs. (2.1) and the fact that γ^0 is a constant matrix this reduces to

$$S_i=2\gamma_i\gamma_0\frac{R'}{c^2R}+\left\{\begin{matrix}l\\ ji\end{matrix}\right\}\gamma_l\gamma^j+\gamma_l\frac{\partial\gamma^l}{\partial x^i}. \tag{2.6}$$

From this we obtain

$$\gamma^iS_i=2\gamma^i\gamma_i\gamma_0\frac{R'}{c^2R}+\left\{\begin{matrix}l\\ ji\end{matrix}\right\}\gamma^i\gamma_l\gamma^j+\gamma^i\gamma_l\frac{\partial\gamma^l}{\partial x^i}.$$

[5] The summation convention is used throughout this paper. Also, we shall use the convention that Greek indices take on the four values: 0,1,2,3, whereas Latin indices take the values 1,2,3.

[6] This spin coordinate system is characterized by the fact that the spinors γ_{AB} and $\gamma_{\dot A\dot B}$ are constants in it. See O. Veblen, "Spinors in Projective Relativity," Proc. Nat. Acad. Sci. **19**, 979–989 (1933) for a discussion of these spinors.

[7] R. C. p. 83 (Eq. A. 6).

But $\gamma^i\gamma_i=\frac{3}{4}\cdot 1$ and $\gamma^i\gamma_l=(\frac{1}{2}\delta_l{}^i\cdot 1-\gamma_l\gamma^i)$.

Hence
$$\gamma^iS_i=\frac{3}{2}\gamma_0\frac{R'}{c^2R}+\frac{1}{2}\gamma^j\left\{\begin{matrix}l\\jl\end{matrix}\right\}-\frac{1}{4}\gamma_lg^{ij}\left\{\begin{matrix}l\\ij\end{matrix}\right\}+\gamma^i\gamma_l\frac{\partial\gamma^l}{\partial x^i}$$

or
$$\gamma^iS_i=\frac{3}{2}\gamma_0\frac{R'}{c^2R}+\gamma^j\left(\frac{3}{4}\frac{\partial\log h^{\frac{1}{2}}}{\partial x^i}+\frac{1}{4}h_{lj}\frac{\partial h^{lk}}{\partial x^k}+\gamma_l\frac{\partial\gamma^l}{\partial x^j}\right). \tag{2.7}$$

Since
$$h^{ij}\left\{\begin{matrix}l\\ij\end{matrix}\right\}=-\left(\frac{\partial h^{lk}}{\partial x^k}+h^{lj}\left\{\begin{matrix}k\\jk\end{matrix}\right\}\right).$$

3. No Field

In case $\varphi_a=0$ Eq. (1.1) becomes

$$\left[\gamma^0\left(\frac{\partial}{\partial t}+\frac{3}{2}\frac{R'}{R}\right)-\frac{i\sigma^j}{R}\left(\frac{\partial}{\partial x^j}+\frac{3}{4}\frac{\partial\log h^{\frac{1}{2}}}{\partial x^j}+\frac{1}{4}h_{jl}\frac{\partial h^{lk}}{\partial x^k}+\sigma_l\frac{\partial\sigma^l}{\partial x^j}\right)\right]\psi=\mu\psi. \tag{3.1}$$

We can introduce a coordinate system such that[8]

$$du^2=\rho^2d\alpha^2+\rho^2\sin^2\alpha d\theta^2+\rho^2\sin^2\alpha\sin^2\theta d\varphi^2, \tag{3.2}$$

where ρ is a real constant, if the space defined by du^2 is a space of positive curvature.

In this coordinate system

$$\partial h^{lk}/\partial x^k=0$$

since $h^{lk}=0$ for $l\neq k$ and h^{kk} is independent of x^k. In this coordinate system a solution of the equations (2.3) in a spin coordinate system in which S_a is given by Eq. (1.4), is

$$\begin{aligned}\sigma^1&=(1/\rho)(\sin\theta\cos\varphi\delta_1+\sin\theta\sin\varphi\delta_2+\cos\theta\delta_3),\\ \sigma^2&=(1/\rho\sin\alpha)(\cos\theta\cos\varphi\delta_1+\cos\theta\sin\varphi\delta_2-\sin\theta\delta_3),\\ \sigma^3&=(1/\rho\sin\alpha\sin\theta)(-\sin\varphi\delta_1+\cos\varphi\delta_2),\end{aligned} \tag{3.3}$$

where
$$\tfrac{1}{2}(\delta_a\delta_b+\delta_b\delta_a)=\tfrac{1}{4}\delta_{ab}. \tag{3.4}$$

It is readily found that

$$\sigma_i\frac{\partial\sigma^i}{\partial x^j}=-\frac{1}{2}\frac{\cos\alpha}{\sin\alpha}\delta_j{}^1+\left[2\delta_3(\cos\varphi\delta_1+\sin\varphi\delta_2)-\frac{1}{4}\frac{\cos\theta}{\sin\theta}\right]\delta_j{}^2+2\delta_1\delta_2\delta_j{}^3; \tag{3.5}$$

hence
$$\sigma^i\left(\frac{3}{4}\frac{\partial\log h^{\frac{1}{2}}}{\partial x^i}+\sigma_l\frac{\partial\sigma^l}{\partial x^i}\right)=\sigma^1\frac{\cos\alpha}{\sin\alpha}-\frac{\sigma^1}{\rho\sin\alpha}. \tag{3.6}$$

Thus Eq. (3.1) may be written

$$\left[\gamma^0\left(\frac{\partial}{\partial t}+\frac{3}{2}\frac{R'}{R}\right)-\frac{i}{R}\left(\sigma^1\left(\frac{\partial}{\partial\alpha}+\frac{\cos\alpha}{\sin\alpha}-\frac{1}{\rho\sin\alpha}\right)+\sigma^2\frac{\partial}{\partial\theta}+\sigma^3\frac{\partial}{\partial\varphi}\right)\right]\psi=\mu\psi. \tag{3.7}$$

If $\psi'=R^{\frac{1}{2}}\rho\sin\alpha\psi$, Eq. (3.1) becomes

$$\left(\gamma^0\frac{\partial}{\partial t}-\frac{i}{R}\left[\sigma^1\left(\frac{\partial}{\partial\alpha}-\frac{1}{\rho\sin\alpha}\right)+\sigma^2\frac{\partial}{\partial\theta}+\sigma^3\frac{\partial}{\partial\varphi}\right]\right)\psi=\mu\psi. \tag{3.8}$$

[8] R. C. p. 84 (Eq. B. 8).

The replacement of the wave function ψ by ψ' means that any normalization condition of the type

$$\int \sum_{A=1}^{4} |\psi^A|^2 g^{\frac{1}{2}} dx^1 dx^2 dx^3 = 1$$

is replaced by

$$\int \sum_{A=1}^{4} |\psi^A|^2 d\alpha \sin\theta d\theta d\varphi = 1.$$

Multiplying (3.8) by γ^0 and dropping primes we have

$$\left\{\frac{1}{4c^2}\frac{\partial}{\partial t} - \frac{1}{R}\left(i\gamma^0\sigma^1\left(\frac{\partial}{\partial\alpha} - \frac{1}{\rho\sin\alpha}\right) + i\gamma^0\sigma^2\frac{\partial}{\partial\theta} + i\gamma^0\sigma^3\frac{\partial}{\partial\varphi} - \mu\gamma^0\right)\right\}\psi = 0.$$

Now let $\gamma^0 = (1/2c)\alpha_4$,

$$\begin{aligned} i\gamma^0\sigma^1 &= \beta_\alpha/\rho = (1/\rho)(\sin\theta\cos\varphi\alpha_1 + \sin\theta\sin\varphi\alpha_2 + \cos\theta\alpha_3), \\ i\gamma^0\sigma^2 &= \beta_\theta/\rho\sin\alpha = (1/\rho\sin\alpha)(\cos\theta\cos\varphi\alpha_1 + \cos\theta\sin\varphi\alpha_2 - \sin\theta\alpha_3), \\ i\gamma^0\sigma^3 &= \beta_\varphi/\rho\sin\alpha\sin\theta = (1/\rho\sin\alpha\sin\theta)(-\sin\varphi\alpha_1 + \cos\varphi\alpha_2), \end{aligned} \tag{3.9}$$

where $\alpha_a = 4ci\gamma^0\delta_a$.

Since γ^0 anticommutes with δ_a and since the δ_a anticommute among themselves, we have

$$\tfrac{1}{2}(\alpha_a\alpha_b + \alpha_b\alpha_a) = \delta_{ab} \quad (a, b = 1, 2, 3) \tag{3.10}$$

and

$$\alpha_4\alpha_a + \alpha_a\alpha_4 = 0, \quad (\alpha_4)^2 = 1. \tag{3.11}$$

The matrices α_a and α_4 are the usual Dirac matrices.[9]

Eq. (3.8) may now be written as

$$(h/i)(1/c)(\partial/\partial t)\psi = H\psi, \tag{3.12}$$

where

$$H\psi = \frac{1}{R}\left[\frac{\beta_\alpha}{\rho}\frac{h}{i}\left(\frac{\partial}{\partial\alpha} - \frac{1}{\rho\sin\alpha}\right) + \frac{1}{\rho\sin\alpha}\frac{h}{i}\left(\beta_\theta\frac{\partial}{\partial\theta} + \frac{\beta_\varphi}{\sin\theta}\frac{\partial}{\partial\varphi}\right) + mc\alpha_4\right]\psi. \tag{3.13}$$

4. Angular Momentum Integral

A first integral of Eqs. (3.12) may be obtained by noting that the operator

$$K = -\alpha_4\left[\beta_\alpha\left(\beta_\theta + \frac{\beta_\varphi}{\sin\theta}\frac{\partial}{\partial\varphi}\right) - 1\right] \tag{4.1}$$

commutes with H. To prove this we first write Eq. (3.13) as

$$H = \frac{1}{R\rho}\left[\beta_\alpha\frac{h}{i}\frac{\partial}{\partial\alpha} - \frac{h}{i}\frac{\beta_\alpha\alpha_4}{\sin\alpha}K + mc\alpha_4\right]. \tag{4.2}$$

Since α_4 is a constant and anticommutes with the β's, it commutes with K. We must now prove that β_a commutes with K.

From Eqs. (3.9) we see that

$$\partial\beta_\alpha/\partial\theta = \beta_\theta \quad \text{and} \quad \partial\beta_\alpha/\partial\varphi = \sin\theta\beta_\varphi. \tag{4.3}$$

[9] E. U. Condon: G. H. Shortley, *Theory of Atomic Spectra* (Cambridge Press, 1935), p. 126, Eq. (3).

Hence
$$\alpha_4\left[\beta_\alpha\left(\beta_\theta\frac{\partial}{\partial\theta}+\frac{\beta_\varphi}{\sin\varphi}\frac{\partial}{\partial\varphi}\right)-1\right]\beta_\alpha=2\alpha_4\beta_\alpha+\beta_\alpha\alpha_4\beta_\alpha\left(\beta_\theta\frac{\partial}{\partial\theta}-\frac{\beta_\varphi}{\sin\theta}\frac{\partial}{\partial\varphi}\right)-\alpha_4\beta_\alpha$$
$$=\beta_\alpha\alpha_4\left[\beta_\alpha\left(\beta_\theta\frac{\partial}{\partial\theta}+\frac{\beta_\varphi}{\sin\theta}\frac{\partial}{\partial\varphi}\right)-1\right].$$

The operator defined by Eqs. (4.1) is the operator

$$\alpha_4((2/h^2)L\cdot S+1), \tag{4.4}$$

which occurs in the usual treatment of the Dirac equation as may be seen from Eqs. (3.9). Thus we see that the angular momentum integral of the Dirac equation in flat space holds in the cosmological spaces. That is, the dependence of the wave functions in these spaces on the variables θ and φ is given as in the flat case by solutions of the equations

$$K\psi=k\psi, \tag{4.5}$$

where k is a constant. It follows that k is an integer and equal to $l+1$ where l is the orbital angular momentum quantum number whose z component is labeled by the integer m.

The solutions of Eqs. (4.5) are[10]

$$\psi_1=A_1(\alpha,t)\left(\frac{k+m}{2k-1}\right)^{\frac{1}{2}}\varphi(k-1,m), \qquad \psi_3=A_3(\alpha,t)\left(\frac{k-m}{2k+1}\right)^{\frac{1}{2}}\varphi(k,m),$$
$$\psi_2=A_1(\alpha,t)\left(\frac{k-m-1}{2k-1}\right)^{\frac{1}{2}}\varphi(k-1,m+1), \quad \psi_4=A_3(\alpha,t)\left(\frac{k+m+1}{2k+1}\right)^{\frac{1}{2}}\varphi(k,m+1), \tag{4.6}$$

where $\varphi(l,m)$ is the normalized spherical harmonic and A_1 and A_3 are arbitrary functions.

It is readily verified that

$$\beta_\alpha\varphi=\varphi, \tag{4.7}$$

where φ is the spinor whose components are φ_1, φ_2, φ_3 and φ_4.

The angular part of the wave functions in an arbitrary spherically symmetric electromagnetic field (i.e., one that depends on α and t) are the same as for the free electron, since the operator K will still commute with H if such a field is present.

5. Radial Functions

We now proceed with the determination of the functions A_1 and A_3. Eqs. (3.12) may now be written as

$$\frac{h}{i}\frac{1}{c}\frac{\partial}{\partial t}\psi=\frac{1}{R\rho}\left(\beta_\alpha\frac{h}{i}\frac{\partial}{\partial\alpha}-\frac{h}{i}\frac{\beta_\alpha\alpha_4 k}{\sin\alpha}+mc\alpha_4\right)\psi. \tag{5.1}$$

In virtue of Eqs. (4.6) and (4.7) these equations reduce to

$$R(t)\left(\frac{h}{i}\frac{1}{c}\frac{\partial}{\partial t}-mc\right)A_1=\frac{1}{\rho}\frac{h}{i}\left(\frac{\partial}{\partial\alpha}+\frac{k}{\sin\alpha}\right)A_3, \quad R(t)\left(\frac{h}{i}\frac{1}{c}\frac{\partial}{\partial t}+mc\right)A_3=\frac{1}{\rho}\frac{h}{i}\left(\frac{\partial}{\partial\alpha}-\frac{k}{\sin\alpha}\right)A_1. \tag{5.2}$$

Let[11]
$$\frac{u}{c}=\int_{t_0}^{t}\frac{dt}{R(t)}, \quad \text{that is} \quad \frac{R}{c}\frac{\partial}{\partial t}=\frac{\partial}{\partial u}.$$

[10] Reference 9, pp. 127–128.

[11] Then u as the spatial distance light has traveled during the time $t-t_0$. See R.C. p. 68.

Eqs. (5.2) become

$$\left(\frac{h}{i}\frac{\partial}{\partial u}-mcR(u)\right)A_1=\frac{h}{i\rho}\left(\frac{\partial}{\partial\alpha}+\frac{k}{\sin\alpha}\right)A_3,\quad \left(\frac{h}{i}\frac{\partial}{\partial u}+mcR(u)\right)A_3=\frac{h}{i\rho}\left(\frac{\partial}{\partial\alpha}-\frac{k}{\sin\alpha}\right)A_1. \tag{5.3}$$

We may now obtain a second-order differential equation by eliminating A_3 from the first of these. Thus

$$\left(\frac{h}{i}\frac{\partial}{\partial u}+mcR(u)\right)\left(\frac{h}{i}\frac{\partial}{\partial u}-mcR(u)\right)A_1=\frac{-h^2}{\rho^2}\left(\frac{\partial}{\partial\alpha}+\frac{k}{\sin\alpha}\right)\left(\frac{\partial}{\partial\alpha}-\frac{k}{\sin\alpha}\right)A_1.$$

Let $A_1(\alpha, u)=A_1(\alpha)T_1(u)$, then by separating variables we have

$$\frac{-h^2}{\rho^2}\left[\frac{d^2}{d\alpha_2}+\frac{k^2-k\cos\alpha}{\sin^2\alpha}\right]A_1=W_1^2A_1, \tag{5.4}$$

$$\left[\left(\frac{h}{i}\right)^2\frac{d^2}{du^2}-mc\frac{h}{i}\frac{dR}{du}-R^2m^2c^2\right]T_1=W_1^2T_1, \tag{5.5}$$

where W_1 is a constant.

If we are given the function $R(t)$, $R(u)$ is determined and we can solve Eq. (5.5) for T_1 and thus determine the time dependence of the wave functions. Later we shall assume $R(t)$ has a definite form and solve Eqs. (5.5). The function $A_1(\alpha)$ may be determined from Eq. (5.4). Thus if we set $r=\cos\alpha$, Eq. (5.4) becomes

$$(r^2-1)\frac{d^2A_1}{dr^2}+r\frac{dA_1}{dr}-\left(\frac{\rho^2W_1^2}{h^2}+\frac{k^2-kr}{r^2-1}\right)A_1=0. \tag{5.6}$$

A nonsingular solution of this Riemann P equation is

$$A_1=C_1(1-r)^{k/2}(1+r)^{k+1/2}F\left(\frac{\rho W_1}{h}+\frac{2k+1}{2},\frac{-\rho W_1}{h}+\frac{2k+1}{2};\frac{2k+1}{2};\frac{1-r}{2}\right), \tag{5.7}$$

where C_1 is a constant and F denotes the hypergeometric series and k is assumed to be positive.

Since A_1 must be finite for $\frac{1}{2}(1-r)=\pm1$, the series must contain only a finite number of terms and we must have either

$$-\rho W_1/h+(2k+1)/2=-n \quad \text{or} \quad \rho W_1/h+(2k+1)/2=-n, \tag{5.8}$$

where n is a positive integer. That is,

$$(\rho W_1/h)^2=(n+(2k+1)/2)^2. \tag{5.9}$$

Thus the allowed values of W are determined in terms of k. Since k must be an integer, we see that $(\rho W_1/h)^2$ is the square of a half-integer. We shall show later that the kinetic energy of a free electron is expressible in terms of W_1.

Similarly we may eliminate A_1 from Eqs. (5.3) and we obtain

$$\left(\frac{h}{i}\frac{\partial}{\partial u}-mcR(u)\right)\left(\frac{h}{i}\frac{\partial}{\partial u}+mcR(u)\right)A_3=\frac{-h^2}{\rho^2}\left(\frac{\partial}{\partial\alpha}-\frac{k}{\sin\alpha}\right)\left(\frac{\partial}{\partial\alpha}+\frac{k}{\sin\alpha}\right)A_3.$$

Now let $A_3(\alpha, u)=A_3(\alpha)T_3(u)$; then by separating variables we have

$$-\frac{h^2}{\rho^2}\left[\frac{d^2}{d\alpha^2}-\frac{k^2+k\cos\alpha}{\sin^2\alpha}\right]A_3=W_3^2A_3, \tag{5.10}$$

$$\left[\left(\frac{h}{i}\right)^2\frac{d^2}{du^2}+mc\frac{h}{i}\frac{dR}{du}-R^2n^2c^2\right]T_3=W_3^2T_3. \tag{5.11}$$

Setting $r=\cos\alpha$, Eq. (5.10) becomes

$$(r^2-1)\frac{d^2A_3}{dr^2}+r\frac{dA_3}{dr}-\left(\frac{k^2+kr}{r^2-1}+\frac{W_3^2\rho^2}{h^2}\right)A_3=0. \tag{5.12}$$

A nonsingular solution of this equation is

$$A_3=C_3(1-r)^{k+1/2}(1+r)^{k/2}F\left(\frac{\rho W_3}{h}+\frac{2k+1}{2},\frac{-\rho W_3}{h}+\frac{2k+1}{2},\frac{2k+3}{2},\frac{1-r}{2}\right). \tag{5.13}$$

The condition that A_3 be finite at $\frac{1}{2}(1-r)=\pm1$ implies

$$(\rho W_3/h)^2=(n+(2k+1)/2)^2. \tag{5.14}$$

The functions $A_1(\alpha)$ and $A_3(\alpha)$ given by Eqs. (5.7) and (5.13) will be solutions of Eqs. (5.3) if $W_1=W_3$. We shall henceforth set $W=W_1=W_3$.

In the above we have assumed that k is positive. However, from Eqs. (5.3) we see that if (A_1, A_3) is a solution for positive k then (A_3, A_1) is the solution for negative k.

The constants C_1 and C_3 may be chosen so that

$$\int_0^\pi |A_1|^2d\alpha=\int_0^\pi |A_2|^2d\alpha=1. \tag{5.15}$$

This is readily done by expressing A_1 and A_3 as Jacobi polynomials, and using their orthogonality relations.[12] We readily see that Eqs. (5.15) are satisfied if

$$C_1=\frac{1}{2^k\Gamma((2k+1)/2)}\left(\frac{\Gamma(\rho W/h+(2k+1)/2)}{\Gamma(\rho W/h-(2k-1)/2)}\right)^{\frac{1}{2}},\quad C_3=\frac{\rho W/h}{2^k\Gamma((2k+3)/2)}\left(\frac{\Gamma(\rho W/h+(2k+1)/2)}{\Gamma(\rho W/h-(2k-1)/2)}\right)^{\frac{1}{2}}. \tag{5.16}$$

The neighborhood of the point $\alpha=0$ on the three dimensional sphere of radius ρ goes into a flat three dimensional space as becomes infinite. We shall now show that the functions A_1 and A_3 go over into the usual radial functions as ρ becomes infinite (i.e., Bessel functions).

Let $$\sigma=\lim_{\substack{\alpha\to0\\ \rho\to\infty}}\rho\sin\alpha=R\alpha.$$

Then $$\frac{1-\cos\alpha}{2}=\sin^2\frac{\alpha}{2}\to\frac{\alpha^2}{4}=\frac{\sigma^2}{4\rho^2}$$

and $A_3=C_3(\sigma^2/4\rho^2)^{k+1/2}F(n+2k+1, -n, (2k+3)/2; \sigma^2/4\rho^2)$, where $n=\rho W/h+(2k+1)/2$.

In virtue of Eq. (5.16) we have

$$\lim_{\rho\to\infty}A_3=\frac{1}{2^k}\left(\frac{W}{h}\frac{\sigma}{2}\right)^{\frac{1}{2}}J_{k+\frac{1}{2}}\left(\frac{W}{h}\sigma\right),$$

where J_n is the Bessel function of order n.

[12] H. Bateman: *Partial Differential Equations of Mathematical Physics* (Cambridge Press, 1932), p. 392.

Similarly we can show that

$$\lim_{\rho\to\infty} A_1=\frac{1}{2^k}\left(\frac{W}{h}\frac{\sigma}{2}\right)^{\frac{1}{2}} J_{k-1}\left(\frac{W}{h}\sigma\right).$$

But σ is the distance from the origin to the point whose coordinates are x, y, z. Hence the radial functions we have obtained go over into the usual radial functions as $\rho\to\infty$.

6. Einstein Universe

To obtain the time dependence of the wave functions we must make some assumptions regarding the arbitrary function $R(t)$. The simplest assumption, namely $R(t)$ is constant, corresponds to the Einstein universe.[13] When the radial functions given by Eqs. (5.7) and (5.13) are substituted into Eqs. (5.2) they become

$$\begin{aligned}\left(\frac{h}{i}\frac{1}{c}\frac{d}{dt}-mc\right)T_1&=-i\frac{W}{R}T_3,\\ \left(\frac{h}{i}\frac{1}{c}\frac{d}{dt}+mc\right)T_3&=i\frac{W}{R}T_1.\end{aligned}\tag{6.1}$$

Two linearly independent solutions of these equations are

$$T_1=c_1e^{i/\hbar\lambda t},\quad T_3=ic_3e^{i/\hbar\lambda t},\tag{6.2}$$

and

$$T_1=d_1e^{i/\hbar\lambda t},\quad T_3=id_3e^{-i/\hbar\lambda t},\tag{6.3}$$

where

$$\lambda=\left(m^2c^4+c^2\frac{W^2}{R^2}\right)^{\frac{1}{2}}=\left(m^2c^4+\frac{c^2h^2}{R^2\rho^2}\left(n+\frac{2k+1}{2}\right)^2\right)^{\frac{1}{2}}$$

and c_1, c_3, d_1 and d_3 are constants.

The constant λ is the energy of a free electron in an Einstein space. The existence of the two solutions (6.2) and (6.3) means that both positive and negative energy states are allowable as in flat space. Since n and k are integers we see that the square of the kinetic energy is proportional to the square of half an odd integer.

The existence of two linearly independent solutions for each value of λ corresponding to the two orientations of spin for given energy is obtained as in the usual theory.

Thus there exist four linearly independent solutions of the Dirac equations in an Einstein space. They are of the form

$$\begin{aligned}\psi_1&=a_1e^{\mp i/\hbar\lambda t}A_1(\alpha)\varphi_1(\theta,\varphi)=a_1e^{\mp i/\hbar\lambda t}\Phi_1(\alpha,\theta,\varphi),\\ \psi_2&=a_1e^{\mp i/\hbar\lambda t}A_1(\alpha)\varphi_2(\theta,\varphi)=a_1e^{\mp i/\hbar\lambda t}\Phi_2(\alpha,\theta,\varphi),\\ \psi_3&=a_3e^{\mp i/\hbar\lambda t}A_3(\alpha)\varphi_3(\theta,\varphi)=a_3e^{\mp i/\hbar\lambda t}\Phi_3(\alpha,\theta,\varphi),\\ \psi_4&=a_3e^{\mp i/\hbar\lambda t}A_3(\alpha)\varphi_3(\theta,\varphi)=a_3e^{\mp i/\hbar\lambda t}\Phi_4(\alpha,\theta,\varphi),\end{aligned}\tag{6.4}$$

where φ's are given by Eqs. (4.6), the A's are given by Eqs. (5.7) and (5.13) and a_1 and a_3 are constants.

The current vector whose divergence vanishes as a consequence of the Dirac equations is[14]

$$J^a=\psi^+\gamma^a\psi,\tag{6.5}$$

where $\psi^+=\psi^*\gamma^0$ (ψ^* is the complex conjugate of ψ) and ψ is a solution of Eqs. (1.3). Hence

$$\int J^0dV=\int\sum_{A=1}^{4}|\psi_A|^2dV,\tag{6.6}$$

where dV is an arbitrary three dimensional volume.

In virtue of the normalization conditions we imposed we have

$$\int J^0dV=2(|a_1|^2+|a_3|^2).\tag{6.7}$$

It is evident that we may normalize our constants so that the left member of Eqs. (6.7) is unity.

The form of the wave functions given by Eqs. (6.4) was to be expected since the space with the metric

$$du^2=h_{ij}dx^idx^j$$

is a three dimensional sphere. The wave functions must therefore be a representation of the group

[13] R.C. p. 69.

[14] D.P.R. p. 384. The matrix γ_{AB} may be taken equal to the matrix γ^0.

which leaves this space invariant, namely, the rotations in a flat four space. However, the rotation group in four dimensions is a direct product of two three dimensional rotation groups. Hence the representations of this group are obtained by taking the direct product of representations of the three dimensional groups. The Jacobi polynomials and the spherical harmonics are such representations. Hence we expect that the wave functions for the Einstein space should have as factors Jacobi polynomials in cos α and spherical harmonics in θ and φ.

7. DeSitter Universe

The DeSitter universe is a cosmological space in which $R(t)=e^{ct/a}$ and the three dimensional space whose metric is $du^2=h_{ij}dx^i dx^j$ is a flat space.[15] Hence we may obtain the solutions of the Dirac equations in a DeSitter universe by solving Eqs. (5.2) where $R(t)=e^{ct/a}$ and passing to the limit as $\rho\to\infty$. We have already seen that the radial functions go over into those of the flat space as we pass to the limit. Hence the only difference between the wave functions in this space and in the flat space-time is in the time dependence of the wave functions given by the functions $T_1(t)$ and $T_3(t)$.

Eqs. (5.5) and (5.11) which determine $T_1(t)$ and $T_3(t)$ become

$$\left[\frac{d^2}{du^2}-\frac{\mu^2a^2+\mu a}{u^2}+\frac{W^2}{h^2}\right]T_1=0 \tag{7.1}$$

and

$$\left[\frac{d^2}{du^2}-\frac{\mu^2a^2-\mu a}{u^2}+\frac{W^2}{h^2}\right]T_3=0, \tag{7.2}$$

where $\mu=\frac{mc}{h}i$, $W=\pm\frac{h}{\rho}\left(n+\frac{2k+1}{2}\right)$,

and

$$\frac{u}{c}=\int_{t_0}^{t}e^{-ct/a}dt=-\int_{t}^{\infty}e^{-ct/a}dt=-\frac{a}{c}e^{-ct/a}. \tag{7.3}$$

We must choose such solutions of Eqs. (7.1) and (7.2) which are solutions of Eqs. (6.1).

Eqs. (7.1) and (7.2) are the differential equations for the Bessel functions. Hence for each value of W we have as the two linearly independent solutions of Eqs. (6.1) the functions

$$\begin{aligned} T_1&=c\sqrt{u}J_{\mu a+\frac{1}{2}}(Wu/h);\\ T_3&=c\sqrt{u}J_{\mu a-\frac{1}{2}}(Wu/h) \end{aligned} \tag{7.4}$$

and

$$\begin{aligned} T_1&=d\sqrt{u}J_{-\mu a-\frac{1}{2}}(Wu/h);\\ T_3&=d\sqrt{u}J_{-\mu a+\frac{1}{2}}(Wu/h), \end{aligned} \tag{7.5}$$

where c and d are constants and J_p is a Bessel function of complex order. Thus we again find four linearly independent solutions to the Dirac equations. This corresponds to the fact that there are two orientations of the spin for each of two possible values of the energy.

The constants c and d may be chosen so that the time component of the current vector is one. From Eqs. (6.1) it is evident that

$$\int J^0 dV=2(|T_1|^2+|T_3|^2) \tag{7.6}$$

is a constant. This constant is one for the solutions (7.4) and (7.5) if

$$c=d=\tfrac{1}{2}(|W|/h)^{\frac{1}{2}}\Gamma(\mu a+\tfrac{1}{2}). \tag{7.7}$$

The magnitude of the number μa is the ratio of the radius of the universe to the Compton wave-length. This number is of the order of magnitude of 10^{57}. From the asymptotic expansions of T_1 and T_3 we see that as $a\to\infty$ T_1 and T_3 tend to the exponential functions. Since the functions T_1 and T_3 can be normalized for any value of μa there is no reason for assigning any particular value to this number. However, such might not be the case when there is a field present.

The energy of the electron in this type of a universe is a function of the time. The exact expression for it may be obtained by computing the time-time component of the stress energy tensor given by Fock.[16] However, since a is of the order of 10^{27} cm, we may consider $R=e^{ct/a}$ as a constant and obtain as a first approximation that

$$T_3=cT_1=e^{i\lambda t/h}, \tag{7.8}$$

where c is a constant and λ is the energy and is given as a function of time by the relation

[15] R.C. p. 70.

[16] V. Fock, Zeits. f. Physik **57**, 274 (1929).

$$\frac{\lambda^2}{c^2}-m^2c^2=e^{-2ct/a}\left(\frac{Wh}{\rho}\right)^2\left(n+\frac{2k+1}{2}\right)^2. \quad (7.9)$$

Also we see that λ may take on positive and negative values.

The wave functions for a universe in which $R(t)=e^{ct/a}$ and $\rho^2>0$ are therefore

$$\begin{aligned}\varphi_1&=T_1\Phi_1(\alpha,\theta,\varphi), \quad \varphi_3=T_3\Phi_3(\alpha,\theta,\varphi),\\ \varphi_2&=T_1\Phi_2(\alpha,\theta,\varphi), \quad \varphi_4=T_3\Phi_4(\alpha,\theta,\varphi),\end{aligned} \quad (7.10)$$

where T_1 and T_3 are given by Eqs. (7.6) and (7.7), respectively, and the functions $\Phi(\alpha,\theta,\varphi)$ are given by Eqs. (6.5).

The wave functions for the DeSitter universe are obtained by going to the limit $\rho\to\infty$. They are of the same type as Eqs. (7.10) but we must replace the Jacobi polynomials of $\cos\alpha$ that occur in the functions $\Phi(\alpha,\theta,\varphi)$ by the Bessel functions of $\sigma=\rho\sin\alpha$. The energy in excess of the rest energy need not be an odd integer since $n\to\infty$ as $\rho\to\infty$. Hence we have that the energy of a free electron in DeSitter space is approximately

$$\lambda^2/c^2-m^2c^2=e^{-2ct/a}W, \quad (7.11)$$

where W is a constant.

8. Milne Case

If the three spaces $t=$constant are spaces of negative Riemannian curvature, then we can introduce a coordinate system such that the metric takes on the form

$$du^2=\rho^2(d\alpha^2+\sinh^2\alpha(d\beta^2+\sin^2\beta d\varphi^2)) \quad (8.1)$$

instead of that given in Eqs. (3.2). If we make the imaginary transformation $\rho=i\rho$ and $\alpha=i\alpha$, Eq. (8.1) goes over into Eq. (3.2). Thus the solutions of the Dirac equation for the case of 3 space of negative curvature can be obtained from that of positive curvature by replacing ρ by $i\rho$ and α by $i\alpha$ in the solutions we have obtained. Since this transformation leaves β and φ unaltered, we see that the angular part of the wave functions is the same for both cases. The radial functions differ from those given in Section 5 in that we have Jacobi polynomials in $\cosh\alpha$ instead of $\cos\alpha$.

The time dependence of the wave functions depends again on the nature of $R(t)$. Robertson has shown[2] that Milne's theory of world structure is equivalent to the theory of a cosmological space in which the three spaces t constant are spaces of negative Riemannian curvature and $R(t)=ct$. We shall now obtain the time dependence of the wave functions for this case. The equations determining T_1 and T_3 are

$$\begin{aligned}ct\left(\frac{h}{i}\frac{1}{c}\frac{d}{dt}-mc\right)T_1&=-iWT_3,\\ ct\left(\frac{h}{i}\frac{1}{c}\frac{d}{dt}+mc\right)T_3&=iWT_1,\end{aligned} \quad (8.2)$$

where $$W=\pm\frac{h}{\rho}\left(n+\frac{2k+1}{2}\right).$$

The two second-order equations obtained from Eq. (8.2) by elimination are

$$\left(\frac{d^2}{dt^2}+\frac{1}{t}\frac{d}{dt}-\mu^2c^2-\frac{\mu c}{t}+\frac{W^2}{h^2t^2}\right)T_1=0 \quad (8.3)$$

and

$$\left[\frac{d^2}{dt^2}+\frac{1}{t}\frac{d}{dt}-\mu^2c^2+\frac{\mu c}{t}+\frac{W^2}{h^2t^2}\right]T_3=0, \quad (8.4)$$

where $\mu=imc/h$. The two linearly independent solutions of Eq. (8.3) for each value of W are

$$T_1^{(1)}=c_1e^{\mu ct}e^{iW\log t/h}\times{}_1F_1\left(i\frac{W}{h},\frac{2iW}{h}+1;-2\mu ct\right), \quad (8.5)$$

$$T_1^{(2)}=d_1e^{\mu ct}e^{-iW\log t/h}\times{}_1F_1\left(-i\frac{W}{h},-2\frac{iW}{h}+1,-1\mu ct\right), \quad (8.6)$$

where ${}_1F_1(a,b,x)$ is the confluent hypergeometric function. The two linearly independent solutions of Eq. (8.4) are

$$T_3^{(1)}=c_3e^{-\mu ct}e^{iW\log t/h}\times{}_1F_1\left(i\frac{W}{h},2i\frac{W}{h}+1,2\mu ct\right), \quad (8.7)$$

$$T_3^{(2)}=d_3e^{-\mu ct}e^{-iW\log t/h}\times{}_1F_1\left(-i\frac{W}{h},\frac{-2iW}{h}+1,2\mu ct\right). \quad (8.8)$$

If we take $c_1 \neq 0$ and $d_1 = 0$, then in order to satisfy Eqs. (8.2) we must take $c_3 \neq 0$ and $d_3 = 0$. Similarly, if we take $c_1 = 0$, we must take $c_3 = 0$. Again the two possible solutions for T_1 and T_3 correspond to the two possible orientations of the spin of the electron. We shall restrict ourselves to the case $d_1 = d_3 = 0$, and show how c_1 and c_3 must be taken so that

$$\int J^0 dV = 2(|T_1|^2 + |T_3|^2) = 1. \tag{8.9}$$

Eq. (8.9) will be satisfied if

$$c_1 = \frac{h}{W}\frac{1}{\sqrt{2}}\frac{\Gamma(iW/h)}{\Gamma(2iW/H+1)}e^{-\pi W/2h}, \tag{8.10}$$

$$c_3 = \frac{h}{W}\frac{1}{\sqrt{2}}\frac{\Gamma(iW/h)}{\Gamma(2iW/h+1)}e^{\pi W/2h}. \tag{8.11}$$

Hence we have as solutions of the Dirac equation for this type of space

$$\begin{aligned} \varphi_1 &= T_1\Phi_1(i\alpha, \beta, \varphi), \quad \varphi_3 = T_3\Phi_3(i\alpha, \beta, \varphi), \\ \varphi_2 &= T_1\Phi_2(i\alpha, \beta, \varphi), \quad \varphi_4 = T_3\Phi_4(i\alpha, \beta, \varphi), \end{aligned} \tag{8.12}$$

where the functions T_1 and T_3 are given by Eqs. (8.5) to (8.8), and the functions Φ are defined in Eqs. (6.5). Since there are two sets of solutions of Eqs. (8.2) for every value of W and since W may either be positive or negative, we see that for any set of quantum numbers n, k, m, there are four possible solutions of the Dirac equation.

As before

$$W^2 = \frac{h^2}{\rho^2}\left(n + \frac{2k+1}{2}\right)^2. \tag{8.13}$$

The relation between the constant W and the energy of the electron may be obtained by computing the time-time component of the stress energy tensor given by Fock.[16] It is

$$T_0{}^0 = \frac{h}{2i}\int\left(\varphi^+\gamma^0\frac{\partial\varphi}{\partial t} - \frac{\partial\varphi^+}{\partial t}\gamma^0\varphi\right)dV, \tag{8.14}$$

where φ are the solutions of Eq. (1.3) and $\varphi^+ = \varphi^*\gamma^0$. Therefore

$$T_0{}^0 = mc^2(|T_1|^2 - |T_3|^2) + \frac{iW}{t}(T_1^*T_3 - T_3^*T_1) \tag{8.15}$$

as a consequence of Eqs. (8.2) and the normalization of Φ. We shall evaluate (8.15) for large values of W/h. In this case

$${}_1F_1\left(i\frac{W}{h}, \frac{2iW}{h}+1, -2\mu ct\right) \sim e^{-\mu ct};$$

therefore $T_1{}^{(1)} \sim c_1 e^{-iW \log t/h}$

and similarly $T_3{}^{(1)} \sim c_3 e^{-iW \log t/h}$.

Therefore $T_0{}^0 = WC/t = W/t$,

where C is twice the imaginary part of c_1c_3, and equals one from Eqs. (8.10) and (8.11).

9. Comparison with Dirac's Equation for DeSitter Space[3]

In order to compare the equation used here with the one recently proposed by Professor Dirac for an electron in DeSitter space, we will evaluate our equation for the DeSitter space in a different coordinate system. Since the DeSitter space is a space of constant curvature $1/a^2$, there exists a coordinate system in which the line element takes the form

$$ds^2 = A^{-2}(-(dx^0)^2 + (dx^1)^2 + (dx^2)^2 + (dx^3)^2), \tag{9.1}$$

where $x^0 = ct$, and

$$A = 1 + [-(x_0)^2 + (x^1)^2 + (x^2)^2 + (x^3)^2/4a^2] = (1 + s^2/4a^2). \tag{9.2}$$

A solution of the equations

$$\tfrac{1}{2}(\gamma^\alpha\gamma^\beta + \gamma^\beta\gamma^\alpha) = \tfrac{1}{4}g^{\alpha\beta}\cdot 1$$

in a spin frame in which S_a takes on the form given by Eq. (1.3) is

$$\gamma^0 = \tfrac{1}{2}iA\sigma^0 \quad \gamma^i = \tfrac{1}{2}A\sigma^i, \tag{9.3}$$

where the matrices σ^α are constant matrices following the relation

$$\tfrac{1}{2}(\sigma^\alpha\sigma^\beta+\sigma^\beta\sigma^\alpha)=\delta^{\alpha\beta}. \tag{9.4}$$

By a calculation similar to that given in section one we find

$$\gamma^\alpha S_\alpha=\gamma^\alpha\left(\frac{1}{2}\frac{\partial \log\sqrt{-g}}{\partial x^\alpha}+\frac{1}{4}g_{\alpha\mu}\frac{1}{\sqrt{-g}}\frac{\partial\sqrt{-g}\,g^{\mu\tau}}{\partial x^\tau}+\gamma_\mu\frac{\partial\gamma^\mu}{\partial x^\alpha}\right). \tag{9.5}$$

From the values of the $g_{\mu\nu}$ and the γ_μ given by Eqs. (9.1) and (9.3) we find

$$\gamma^\alpha S_\alpha=-\frac{3}{2}\frac{\partial \log A}{\partial x^\alpha}. \tag{9.6}$$

Thus Eq. (1.1) for a free electron becomes

$$\gamma^\alpha\left(\frac{\partial}{\partial x^\alpha}-\frac{3}{2}\frac{\partial \log A}{\partial x^\alpha}\right)=\mu\psi. \tag{9.7}$$

In order to compare this equation with that proposed by Professor Dirac, we must find a transformation to a flat five space which has the space given by (9.1) as a four-dimensional hypersurface given by the equation

$$(u^1)^2+(u^2)^2+(u^3)^2-(u^0)^2+(u^4)^2=a^2. \tag{9.8}$$

Let us replace x^0 by ix^0 and u^0 by iu^0; then we must find a transformation that carries the space whose metric is given by

$$ds^2=(1+s^2/4a^2)^{-2}((dx^0)^2+(dx^1)^2+(dx^2)^2+(dx^3)^2),\quad s^2=(x^0)^2+(x^1)^2+(x^2)^2+(x^3)^2 \tag{9.9}$$

into the hypersurface

$$(u^0)^2+(u^1)^2+(u^2)^2+(u^3)^2+(u^4)^2=a^2.$$

The transformation needed is

$$u^\beta=x^\beta/A,\quad u^4=a(1-s^2/4a^2)/A,\quad A(u)=2a/u^4+a. \tag{9.10}$$

Therefore
$$\frac{\partial}{\partial x^\alpha}=\frac{\partial u^\beta}{\partial x^\alpha}\frac{\partial}{\partial u^\beta}+\frac{\partial u^4}{\partial x^\alpha}\frac{\partial}{\partial u^4}=\frac{1}{A}\left(\delta_\alpha{}^\beta-\frac{u^\beta u^\alpha}{2a^2}A\right)\frac{\partial}{\partial u^\beta}-\frac{1}{A}\frac{u^\alpha}{a}\frac{\partial}{\partial u^4}.$$

Hence
$$A\sigma^\alpha\frac{\partial}{\partial x^\alpha}=\left(\sigma^\beta-\frac{u^\beta}{a}\left(\frac{\sigma^\alpha u^\alpha}{u^4+a}\right)\right)\frac{\partial}{\partial u^\beta}-\frac{\sigma^\alpha u^\alpha}{a}\frac{\partial}{\partial u^4}=\rho^\beta\frac{\partial}{\partial u^\beta}+\rho^4\frac{\partial}{\partial u^4}, \tag{9.11}$$

where
$$\rho^\beta=\sigma^\beta-\frac{u^\beta}{a}\left(\frac{\sigma^\alpha u^\alpha}{u^4+a}\right),\quad \rho^4=-\frac{\sigma^\alpha u^\alpha}{a}. \tag{9.12}$$

Then we will have

$$\rho^\beta\rho^\alpha+\rho^\alpha\rho^\beta=2\delta^{\alpha\beta}-2u^\alpha u^\beta/a^2,\quad \rho^4\rho^\alpha+\rho^\alpha\rho^4=-2u^\alpha u^4/a. \tag{9.13}$$

Hence five matrices defined by the relations

$$\alpha^\beta=\rho^\beta-\mu^\beta\sigma^4/a,\quad \alpha^4=\rho^4-u^4\sigma^4/a, \tag{9.14}$$

where σ^4 is a matrix which anticommutes with the four matrices σ^α and hence with ρ^β and ρ^4, satisfy

$$\alpha^\sigma\alpha^\rho+\alpha^\rho\alpha^\sigma=2\delta^{\rho\sigma}. \tag{9.15}$$

Eq. (9.11) may now be written as

$$A\sigma^{\alpha}\frac{\partial}{\partial x^{\alpha}}=\alpha^{\rho}\frac{\partial}{\partial u^{\rho}}+\sigma^{4}\frac{u^{\rho}}{a}\frac{\partial}{\partial u^{\rho}}. \tag{9.16}$$

The matrices α^{ρ} are a set of five anticommuting matrices which we will want to identify with those used by Dirac. However, since they are not constant matrices we will first perform a spin-transformation on Eq. (9.7). Setting $\psi=T\varphi$, we have

$$A\sigma^{\alpha *}\frac{\partial\varphi}{\partial x^{\alpha}}+A\sigma^{\alpha *}T^{-1}\frac{\partial T}{\partial x^{\alpha}}-\tfrac{3}{2}\sigma^{\alpha *}\frac{\partial A}{\partial x^{\alpha}}\varphi=2u\varphi, \tag{9.17}$$

where
$$\sigma^{\alpha *}=T^{-1}\sigma^{\alpha}T,\quad \sigma^{4*}=T^{-1}\sigma^{4}T. \tag{9.18}$$

Let

$$T=\frac{1}{A^{\frac{1}{2}}}\left(\sigma^{4}+\frac{x^{\beta}\sigma^{\beta}}{2a}\right)=\left(\frac{u^{4}+a}{2a}\right)^{\frac{1}{2}}\left(\sigma^{4}+\frac{u^{\beta}\sigma^{\beta}}{u^{4}+a}\right). \tag{9.19}$$

Then since $T^{2}=1$, $T=T^{-1}$ and

$$\sigma^{\alpha *}=-\sigma^{\alpha}+(u^{\alpha}/a)(\sigma^{4}+u^{\beta}\sigma^{\beta}/(u^{4}+a)),\quad \sigma^{4*}=(1/a)(u^{4}\sigma^{4}+u^{\beta}\sigma^{\beta}). \tag{9.20}$$

It is readily verified that

$$\alpha^{\alpha}=\sigma^{\alpha *}-(\sigma^{4*}+u^{\beta}\sigma^{\beta *}/(u^{4}+a))u^{\alpha}/a=-\sigma^{\alpha},\quad \alpha^{4}=-(1/a)(\sigma^{\alpha *}u^{\alpha}+\sigma^{4*}u^{4})=-\sigma^{4}, \tag{9.21}$$

and hence are constants.

From Eq. (9.9) it follows that

$$A\sigma^{*\alpha}T^{-1}\frac{\partial T}{\partial x^{\alpha}}-\tfrac{3}{2}\sigma^{*\alpha}\frac{\partial A}{\partial x^{\alpha}}=\frac{2}{a}\frac{\sigma^{4}}{A}\left(1-\frac{s^{2}}{4a^{2}}\right)+\frac{x^{\beta}\sigma^{\beta}}{a^{2}}\left(\frac{1-s^{2}/4a^{2}}{A}+1\right)=\frac{2}{a^{2}}(\sigma^{4}u^{4}+u^{\alpha}\sigma^{\alpha}). \tag{9.22}$$

Thus as a consequence of Eqs. (9.16), (9.21) and (9.22) Eq. (9.17) becomes

$$\left[-\sigma^{\rho}\frac{\partial}{\partial u^{\rho}}+\frac{\sigma^{\rho}u^{\rho}}{a^{2}}u^{\sigma}\frac{\partial}{\partial u^{\sigma}}+\frac{2}{a^{2}}\sigma^{\rho}u^{\rho}\right]\psi=2\mu\psi.$$

Multiplying by $-h/i$, we have

$$\left[\sigma^{\rho}p_{\rho}-\left(\frac{\sigma^{\rho}u^{\rho}}{a^{2}}\right)\left(u^{\sigma}p_{\sigma}+\frac{2ih}{a^{2}}\right)\right]\psi=-mc\psi. \tag{9.23}$$

The equation proposed by Dirac,[17] when evaluated on the DeSitter space, may be written in the form

$$(\sigma^{\rho}p_{\rho}-\sigma^{\rho}u^{\rho}u^{\sigma}p\sigma/a^{2})\psi=(\sigma^{\rho}u^{\rho}/a)(mc-2ih/a), \tag{9.24}$$

where m is real and the term $-2ih/a$ is introduced in order that Eq. (9.24) be Hermitian. It is interpreted as the imaginary part of a complex mass.

From Eq. (9.23) we see that this term arises from the choice of spin coordinate system used and hence is purely a geometrical term and has no physical significance. Eq. (9.23) is exactly the same as Eq. (9.24) if in the former we replace $-m$ by $m\sigma^{\rho}u^{\rho}/a$.

[17] Dirac, reference 4, p. 664.

If instead of Eq. (9.7) we had used the equation

$$A\sigma^{\alpha}\left(\frac{\partial}{\partial x^{\alpha}}-\frac{3}{2}\frac{\partial \log A}{\partial x^{\alpha}}\right)\psi=i\sigma^{4}\mu\psi, \tag{9.25}$$

which is obtained from (9.7) by a constant spin transformation with $T=1/\sqrt{2}(1+i\sigma^{4})$, we would have obtained instead of Eq. (9.23) the equation

$$\left[\sigma^{\rho}p_{\rho}-\frac{\sigma^{\rho}u^{\rho}}{a}u^{\sigma}p\sigma+\frac{2ih}{a^{2}}u^{\rho}\sigma^{\rho}\right]\psi=i\left(\frac{\sigma^{\rho}u^{\rho}}{a}\right)mc\psi. \tag{9.26}$$

This is Eq. (9.24) except that m is replaced by im.

In conclusion I wish to thank Professor H. P. Robertson for his valuable aid and inspiring advice.

MARCH 15, 1937 PHYSICAL REVIEW VOLUME 51

Stable Isobars

D. R. INGLIS
University of Pittsburgh, Pittsburgh, Pennsylvania
and
L. A. YOUNG
Carnegie Institute of Technology, Pittsburgh, Pennsylvania

(Received February 3, 1937)

RECENTLY Wigner[1] has derived some interesting results relating the lowest values of the mass number A having a certain isotopic number $A-2Z$. We have found it possible to derive all of those results in a much simpler manner, and have extended the calculations to include the more general interaction

$$V=\Sigma J(r_{ij})O_{ij}$$
$$O_{ij}=g_{q}P_{ij}{}^{q}+gP_{ij}+g_{1}1_{ij}+g_{\sigma}P_{ij}{}^{\sigma}, \tag{1}$$
$$g_{q}+g+g_{1}+g_{\sigma}=1.$$

In Eq. (1) the sum is to be taken over all pairs of particles in the nucleus, P^{q} is the space-interchange operator, P is the space-spin operator and P^{σ} the spin operator. Wigner carried through calculations only for the special case $g=g_{1}=g_{\sigma}=0$.

We approximate the wave function ψ of a nucleus containing Z protons, π, and $A-Z$ neutrons, ν, by a sum, antisymmetric in like particles, of products of single-particle wave functions:

$$\psi=<\Sigma_{\alpha}u_{1}{}^{+}u_{1}{}^{-}u_{2}{}^{+}u_{2}{}^{-}\cdots>_{\pi}$$
$$\times<\Sigma_{\alpha}u_{1}{}^{+}u_{1}{}^{-}u_{2}{}^{+}u_{2}{}^{-}\cdots>_{\nu}.$$

Single particle states $u_1, u_2 \cdots$ are each filled with four particles (two protons and two neutrons) so long as there are enough particles to fill them. Such a filled state may be called an α group. In evaluating $(0|U|0)=\int\psi^{*}U\psi d\tau$ we may omit the antisymmetry in ψ^{*} (making the normalization factor unity). Since the interaction involves pairs of particles only, we need retain only those terms in ψ arising from single interchanges P of like particles. We follow Wigner and approximate $(0|U|0)$ by its high density limit $(0|U_{0}|0)$ obtained from $(0|U|0)$ by replacing $J(r)$ by $J(o)$:

$$(0|U_{0}|0)=J(o)(0|\Sigma O_{ij}|0)$$
$$=J(o)\{g_{q}(0|\Sigma P_{ij}{}^{q}|0)+g(0|\Sigma P_{ij}|0)$$
$$+g_{1}(0|\Sigma 1_{ij}|0)+g_{\sigma}(0|P_{ij}{}^{\sigma}|0)\}.$$

We therefore have to compute expressions of the form

$$(0|\Sigma P^{q}|0)=\int<u_{1}{}^{+}u_{1}{}^{-}u_{2}{}^{+}u_{2}{}^{-}\cdots>_{\pi}{}^{*}$$
$$<u_{1}{}^{+}u_{1}{}^{-}u_{2}{}^{+}u_{2}{}^{-}\cdots>_{\nu}{}^{*}(\Sigma P^{q})$$
$$<(1-\Sigma P)u_{1}{}^{+}u_{1}{}^{-}u_{2}{}^{+}u_{2}{}^{-}\cdots>_{\pi}$$
$$<(1-\Sigma P)u_{1}{}^{+}u_{1}{}^{-}u_{2}{}^{+}u_{2}{}^{-}\cdots>_{\nu}d\tau.$$

[1] E. Wigner, Phys. Rev. **51**, 106 (1937).

These are easy to evaluate:

$$\begin{aligned}
(0|\Sigma P^q|0) &= (\text{number of bonds})-(\text{number of like-particle, like-spin pairs}),\\
(0|\Sigma P|0) &= (\text{number of like-spin bonds})-(\text{number of like-particle pairs}),\\
(0|\Sigma 1|0) &= (\text{number of pairs}),\\
(0|\Sigma P^r|0) &= (\text{number of like-spin pairs})-(\text{number of like-particle bonds}).
\end{aligned} \tag{2}$$

By "bond" we mean pair of particles in the same space state.

In using these formulas to determine the change in binding energy when a proton in state i becomes a neutron in state j, its interaction with an α group $k(k\neq i,j)$ is unchanged. This conforms with Wigner's division of all nuclei into types $A=4n$, $4n+1$, $4n+2$, $4n+3$.

Still adhering to Wigner's assumptions we write for the change in binding energy in an isobaric transition

$$\begin{aligned}
\Delta W &= \Delta(0|U_0|0)+\Delta C\\
&= \{J(o)\Delta(0|\Sigma O_{ij}|0)/\Delta Z+\Delta C/\Delta Z\}\Delta Z,
\end{aligned}$$

where C is the Coulomb energy. Any such transition may be described by indicating in parentheses the types of particles in the same space state before and after the transition (omitting an arbitrary number of α groups, if desired). If there are m paired-neutron groups these are indicated by $(\nu\nu)^m$. All transitions leading to stable isobars may be divided into the following three types

$$(\pi\nu\nu)(\nu\nu)^m \longrightarrow (\nu\nu)^{m+1}\nu, \tag{3.1}$$

$$(\pi\pi\nu\nu)(\nu\nu)^m \longrightarrow (\nu\nu)^{m+2}, \tag{3.2}$$

$$(\pi\pi\nu\nu)(\nu\nu)^m\nu \longrightarrow (\pi\nu\nu)(\nu\nu)^{m+1}. \tag{3.3}$$

For all such transitions we find

$$\Delta(0|\Sigma O_{ij}|0)/\Delta Z=(m+3)g_q+(2m+3)g. \tag{4}$$

The quantity $\Delta C/\Delta Z$ increases with Z (approximately as $Z^{\frac{1}{3}}$), so the transitions (3.1), (3.2), (3.3) should, for $m=0$ begin to yield stable isobars at about the same value of Z. Indeed they do, Ca^{43}, A^{40}, and Cl^{37} being the lightest products of these transitions. Similarly for transitions with $m=1$, whose lightest products are V^{51}, Ti^{50} and Ti^{49}. For $g>-\frac{1}{2}g_q$, Eq. (4) says that $\Delta(0|\Sigma O_{ij}|0)/\Delta Z$ increases with increasing m, i.e., the isobaric number is an increasing function of Z. This result is, however, to be expected from any sensible theory. To facilitate comparison with Wigner's paper, one may note that the ratio 3/4 of the critical slopes which he discusses on p. 118 is just the ratio of the coefficients of g_q in (4) for $m=0$ and $m=1$.

Further, it is possible to derive the general empirical rule that *odd* Z does not occur with *even* A; a rule which has no exceptions for $A>2Z$. We simply compare the value (4) of $\Delta(0|\Sigma O_{ij}|0)/\Delta Z$ for transition (3.2) with the value

$$\Delta(0|\Sigma O_{ij}|0)/\Delta Z=(m+4)g_q+(2m+2)g$$

for the competing transition

$$(\pi\pi\nu\nu)(\nu\nu)^m\longrightarrow(\pi\nu\nu)(\nu\nu)^m\nu$$

to see that the latter does not lead to stable nuclei (if only $g_q>g$).

Thus far the results seem very satisfactory but, as Wigner has remarked, this may be partially fortuitous. Indeed, if we consider the transitions of Eqs. (3) for general m we find that they first occur at

$$Z_m\sim[(m+3)g_q+(2m+3)g]^{\frac{1}{2}}J(o)^{\frac{1}{2}}\sim m^{\frac{1}{2}},$$

whereas empirically $Z_m\sim m^{3/5}$. This disagreement may perhaps be ascribed to the high density approximation, rather than to the type of interaction used. Surely we should, however, consider as remarkable any success of a theory in which differences of binding energies of isobars are computed from theoretical binding energies which have even the wrong sign, as is the case here for any simple choice of the coefficients g. It seems that the successes which have followed the use of interactions of the type (1) are very insensitive to the precise form of the interaction, and could be achieved in other ways.

LETTERS TO THE EDITOR

Prompt publication of brief reports of important discoveries in physics may be secured by addressing them to this department. Closing dates for this department are, for the first issue of the month, the eighteenth of the preceding month, for the second issue, the third of the month. Because of the late closing dates for the section no proof can be shown to authors. The Board of Editors does not hold itself responsible for the opinions expressed by the correspondents.

Communications should not in general exceed 600 words in length.

Gamma-Radiation from Fluorine Bombarded with Protons

In our recent work[1] on the gamma-radiation from Li^7+H^1 we have shown that the pairs ejected from thin lead foils in a Wilson cloud chamber gave a more accurate determination of the energy of very high energy gamma-radiation than do the recoil electrons. The observed distribution in energy of the pairs showed considerable asymmetry and we concluded from this that the radiation consisted of more than one line since a single line would be expected to give rise to a nearly symmetrical distribution in energy of the pairs.

We have verified this observation in the case of $F^{19}+H^1$. The distributions in energy of pairs and single electrons and positrons are shown in Fig. 1. It is seen that the pairs are very nearly symmetrically distributed and they indicate a single line at 6.0 ± 0.2 Mev. The distribution of recoil electrons is consistent with this and considerably broader as is to be expected from the angular distribution of Compton electrons as given by the Klein-Nishina formula and from the greater uncertainties in the measurement of tracks of large radius of curvature. The energy losses in the scatterers although approximately twice as great for pairs as for single particles are small compared to the uncertainty in measurement.

Some of the data were obtained with lead foil as scatterer and the remainder with aluminum foil. Alternate pictures were taken with 1 cm lead absorber in and out of the beam. Table I gives the number of pairs and single electrons observed in each case.

From this we find

$$\mu_{Pb}=0.4\pm0.1\ \text{cm}^{-1},$$
$$(\sigma/\pi)_{Pb}\approx0.8 \quad \text{and} \quad (\sigma/\pi)_{Al}\approx3.0.$$

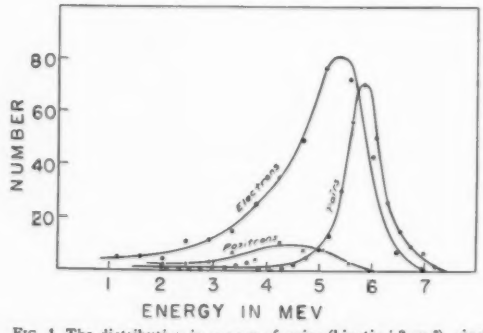

FIG. 1. The distribution in energy of pairs (kinetic $+2\ mc^2$), single electrons (kinetic) and single positrons (kinetic) ejected by the gamma-radiation from $F^{19}+H^1$ from thin scatterers of aluminum (0.10 cm) and lead (0.013 cm). The number of secondaries from each scatterer is given in Table I.

TABLE I. *Number of pairs and single electrons observed.*

	Pairs >4.5 Mev	Pairs <4.5 Mev	Single Electrons	Single Positrons	Recoil Electrons (Electrons-Positrons)
Scatterer					
0.10 cm Al (350 kv)	45	0	197	12	185
.013 cm Pb (160 kv)	98	10	167	38	129
Absorber					
None	87	4	221	28	193
1 cm Pb	56	6	143	22	121

The corresponding theoretical values for 6 Mev radiation are

$$\mu_{Pb}=0.5\ \text{cm}^{-1},$$
$$(\sigma/\pi)_{Pb}=0.72,$$
$$(\sigma/\pi)_{Al}=4.5.$$

The differences are probably not significant since the accuracy is not very great.

The gamma-radiation from $F^{19}+H^1$ was first observed by McMillan[2] by means of an ionization chamber. Tuve[3] and his collaborators have shown that the radiation is produced at several resonance energies, namely; 0.328, 0.892 and 0.942 Mev. The measurements here presented were made with a thick target bombarded with 0.75 Mev protons and we are therefore concerned only with the resonance level at 0.328 Mev. The reaction $F^{19}+H^1\rightarrow Ne^{20}$ is exothermic by 13.3 Mev but no gamma-radiation corresponding to this energy has been observed and we must assume therefore that this transition is forbidden by some rigid selection rule. Because of the sharpness of the resonance level, it seems unlikely that it can disintegrate with appreciable probability to $O^{16}+He^4$, and we should like to ascribe the gamma-radiation not to O^{16}, but to Ne^{20}:

$$F^{19}+H^1\rightarrow(Ne^{20})'\xrightarrow{\gamma}(Ne^{20})''\rightarrow O^{16}+He^4.$$

Alpha-particles with approximately 2 Mev energy should be produced but these have not yet been observed. Perhaps the total energy of the reaction $F^{19}+H^1\rightarrow Ne^{20}$ may be emitted as gamma-radiation from one of the higher resonance levels.

L. A. DELSASSO
W. A. FOWLER
C. C. LAURITSEN

California Institute of Technology,
Pasadena, California,
February 12, 1937.

[1] L. A. Delsasso, W. A. Fowler and C. C. Lauritsen, Phys. Rev. **51**, 391 (1937).
[2] E. McMillan, Phys. Rev. **46**, 325 (1934).
[3] L. R. Hafstad, N. P. Heydenburg and M. A. Tuve, Phys. Rev. **50**, 504 (1936).

On the Ionization of Gases by High Energy Beta-Particles

It has been customary to express the experimentally determined relation between the number (I) of ions of a gas (at STP) formed by a β-particle in a centimeter length of its path, by an equation of the form

$$I = B'\beta^{-C'}, \tag{1}$$

where β is the ratio of the velocity of the β-particle to the velocity of light, and where B' and C' are suitable constants for a given gas; B' and C', of course, change from gas to gas. A more precise representation of the experimental results is an equation of the form

$$I = A + B\beta^{-C}, \tag{2}$$

where A is another constant (which also changes from gas to gas). For almost all calculations based on these experimental results, equations of the form of Eq. (2) are fully as easy to use as equations of the form of Eq. (1). In Table I

TABLE I. *Values of the constants of Eq. (2) for various gases.*

GAS	A	B	C	β RANGE OF VALIDITY
H_2	4.14	1.46	2.87	0.454–0.950
N_2	6.72	12.20	1.64	0.874–0.980
O_2	14.08	8.65	1.95	0.538–0.972
Ne	4.95	7.70	2.01	0.836–0.980

are given the values of A, B and C (as determined by the method of least squares)[1] for the four gases for which I is well known as a function of β; in the last column are the ranges of β for which each trio of constants is known to be valid (i.e., the ranges of β for which I has been determined experimentally).

The data used in getting A, B and C are those of Williams and Terroux[2] on H_2 and O_2 and of Skramstad and Loughridge[3] on N_2 and Ne. In each of the four cases at hand, the sum of the squares of the residuals got by using Eq. (2) is (on the average) only 0.4 of the sum of the squares of the residuals got by using Eq. (1).

F. T. ROGERS, JR.

The Rice Institute,
Houston, Texas,
February 23, 1937.

[1] See, e.g., the Sokolnikoffs, *Higher Mathematics for Physicists and Engineers* (McGraw-Hill, 1934), pp. 407–409.
[2] Williams and Terroux, Proc. Roy. Soc. **A126**, 289 (1930).
[3] Skramstad and Loughridge, Phys. Rev. **50**, 677 (1936).

The Magnetic Anisotropy of $Cs_2[CoCl_4]$

Several salts of cobalt and nickel, chiefly hydrated sulphates, selenates, etc., have recently been studied for their magnetic anisotropy. It is found that while the cobalt salts are strongly anisotropic, $\Delta\chi/\chi$ being of the order of 20 percent to 40 percent, the nickel salts are only feebly so, their $\Delta\chi/\chi$ ranging from 2 percent to 4 percent. This somewhat unexpected difference in the behavior of the two ions, which are both in the F state (d^7 ^4F and d^8 ^3F, respectively) and are adjacent in the periodic table, has been explained elegantly by Van Vleck[1] in the following manner. For a given crystalline electric field which is predominantly cubic in symmetry and has also a feeble rhombic component, the Stark patterns of Co^{++} and Ni^{++} are very similar, except that they are mutually inverted. Since one extreme level in the pattern is a singlet, and the other is a triplet, the inversion naturally makes a great difference to the magnetic anisotropy, which depends on the multiplicity of the lowest level. With the type of cubic crystalline field that obtains in the hydrated sulphates, selenates, etc , the singlet level is lowest for Ni^{++}, which will accordingly be almost isotropic, while for Co^{++} the triplet level is lowest, and will lead to a large anisotropy.

The type of cubic field referred to above as obtaining in the hydrated sulphates corresponds to an octohedral arrangement of 6 negative charges (of the water molecules) around the paramagnetic ion. This arrangement is the usual one. If on the other hand the Co^{++} (or Ni^{++}) ion in a crystal is surrounded by 4 negative charges at the corners of a tetrahedron, or 8 at the corners of a cube, then the terms in the expression for the potential of the field which refer to its cubic part change sign, as has been pointed out by Gorter,[2] and the dispositions of the Stark patterns will be the reverse of those obtaining with the octohedral distribution. The result will be that for Co^{++} the singlet level, and not the triplet level, will now be the lowest, and the crystal will have very little anisotropy.

The tetrahedral type of distribution may be expected to occur in salts in which the Co^{++} ion has a coordination number 4, instead of the usual 6. The blue double chlorides of cobalt with the alkali metals are good examples, and indeed the x-ray analyses of some of these crystals by Powell and Wells[3] show that the Co^{++} ion is closely associated with a group of 4 chlorines, which form a tetrahedron about the Co^{++} at the center.

We have studied the magnetic anisotropy of one such compound, *viz.*, $Cs_2[CoCl_4]$. It forms deep blue crystals, which are orthorhombic. Rough goniometric measurements gave for the axial ratios $a : b : c = 0.38 : 1 : 0.65$. The results of the magnetic measurements are given below. Denoting the gram molecular susceptibilities of the crystal along the "a," "b" and "c" axes by χ_a, χ_b and χ_c, respectively, we find that

$$\chi_a - \chi_b = 143,$$
$$\chi_a - \chi_c = 397,$$
$$\chi = \tfrac{1}{3}(\chi_a + \chi_b + \chi_c) = 8150$$

at 24°C. The χ's are expressed in the usual unit, 10^{-6} c.g.s. e.m.u.

As will be seen from the above data, the anisotropy of the crystal is very feeble, its maximum value 397/8150 being less than 5 percent. This result is strikingly in accord with the prediction from Van Vleck's theory.

It is further significant that the mean susceptibility of the crystal is much less than that of the hydrated sulphates and selenates of cobalt, and is correspondingly nearer to the "spin-only" value; which also is predicted by Van Vleck's theory.

K. S. KRISHNAN
ASUTOSH MOOKHERJI

Indian Association for the Cultivation of Science,
210, Bowbazar Street,
Calcutta, India.
February 8, 1937.

[1] Van Vleck, Phys. Rev. **41**, 208 (1932).
[2] Gorter, Phys. Rev. **42**, 437 (1932).
[3] Powell and Wells, J. Chem. Soc. **359**, (1935).

Quantum Limit of the Continuous Spectrum

In the current number of the *Physical Review* DuMond and Bollman have presented an account of a performance of the Duane-Hunt experiment. They have discovered a feature new to continuous spectrum isochromats in the knee K_2 within 20 volts of the presumed quantum limit, and indeed within the oppositely curving instrumental foot of the isochromat. In discussing this feature DuMond and Bollman assert that this knee was present, though unnoticed, in the data obtained by the writers of this letter in the course of a similar research.[1] As evidence our Fig. 2 is cited.

Prompted by this comment we have carefully inspected not only the single curve which was published in our paper but also ten others which were used in obtaining our conclusions. It was found that although the published curve contained the suggestion of a knee in a position corresponding to those found by DuMond and Bollman our data taken as a whole do not seem to furnish any evidence in support of such a feature.

Since the use of such curves for the determination of fundamental constants is vitally affected by the treatment of this knee it is important to discover the conditions which control its appearance. The most suggestive differences between the experimental conditions of DuMond and Bollman and those of Kirkpatrick and Ross were with respect to the wave-lengths investigated and the nature of the target employed. As to wave-length we notice that in the curves of DuMond and Bollman the knee becomes less conspicuous as the wave-length under observation decreases from 1.28A to 0.62A. Our work was performed with the still shorter wave-length 0.558A, so we might expect some further reduction in visibility, but complete extinction would require a rather abrupt wave-length threshold for which there seems to be no *a priori* likelihood. In the matter of targets there appears a possibly significant difference between DuMond and Bollman's evaporated tungsten on molybdenum and our solid tungsten block. In the lack of a plausible theory of the knee effect this suggestion remains only a hypothesis to be tested by further experiment.

Preoccupied with the relation of their work to the determination of h/e DuMond and Bollman have not displayed a comparison of their results with prior determinations of the Duane-Hunt limit. Such comparisons may be presented in a form free from ambiguity and dependence upon auxiliary constants by stating values of $V' \sin\theta$, where V' is the minimum energy potential in international volts of electrons capable of producing continuous spectrum x-rays reflectible from calcite (cleavage planes) at 18°C at a Bragg angle θ. We have the following table of values of $V' \sin\theta$.

Duane, Palmer, Yeh (adjusted)[1]	2034.6
Feder	2036.0
Kirkpatrick and Ross	2035.3
Schaitberger	2037.7
DuMond and Bollman	2036.8

Another reason for concern over the characteristics of the general radiation near the quantum limit may be mentioned. High resolving power x-ray spectroscopy now awaits the development of means of interpreting the curves of spectrometers in terms of real spectral shapes. Neither the theory of crystals nor any manipulation of multicrystal apparatus has as yet availed to deduce with precision the transmission pattern of a spectrometer in any single case. By observing a spectrum line of accurately known shape the characteristics of any given spectrometer could be obtained, but for the determination of a line shape a standardized calibrated spectrometer is needed, so the proposal ends in circular futility. But instead of a line any other spectral feature of dependably known form might be used. Absorption limits are no better than lines, but the cut-off point of a continuous spectrum offers definite promise, provided one may feel confident about the adjacent spectral form. In short, it is proposed to turn the isochromat foot, or fillet, that long-standing blemish, into a tool for the calibration of spectrometers. First, however, it will be necessary to dispose of doubts as to the real shape of the curve near the limit.

Thanks are due to Dr. DuMond and Dr. Bollman for discussions of their results prior to publication.

PAUL KIRKPATRICK
P. A. ROSS

Department of Physics,
Stanford University,
California,
January 18, 1937.

[1] P. Kirkpatrick and P. A. Ross, Phys. Rev. **45**, 454 (1934).

Raman Effect of Gaseous Methyl- and Dimethylacetylenes

We have investigated the Raman effect of gaseous methyl- and dimethylacetylenes. The experimental procedure employed was that described by us in an earlier paper.[1] The methylacetylene was contained in a Raman tube of about 300 cm³ capacity at a pressure of about $2\frac{3}{4}$ atmospheres. The dimethylacetylene was contained in a similar tube at its vapor pressure which is 1 atmosphere at 25°C. The exposure times were five days for methylacetylene and one week for the dimethyl compound.

Three Raman lines were observed for methylacetylene and one line for dimethylacetylene. More lines could scarcely be expected for the latter because of the low pressure of the sample. All of the lines save the lowest one for methylacetylene were found excited by both Hg 4358 and Hg 4047. On the short wave-length side of the acetylene bond frequency for methylacetylene which lies in the

TABLE I. *Raman effect in gaseous methyl- and dimethylacetylene.*

No. of Plates Measured	Exciting Line Hg	$\Delta\nu$ cm^{-1}	Intensity	$\Delta\nu$ (mean) cm^{-1}
Methylacetylene				
3	4358	930.0	5	930
2	4047	2129.2	1	
1	4358	2125.0	1	2128
2	4047	2135.4	1	
2	4358	2133.4	1	2134
4	4047	2143.0	10	
4	4358	2141.5	10	2142
4	4047	2941.7	10	
4	4358	2940.6	10	2941
Dimethylacetylene				
4	4047	2938.1	3	
4	4358	2937.6	3	2938

TABLE II. *Comparison of Raman frequencies in gases and liquids.*

LIQUID		GAS	
Obs.	Calc.	Obs.	Calc.
Methylacetylene			
929.5	(929.5)	930	(930)
2123.5	2178	2142	2179
2926.2	(2926.2)	2941	2939
Dimethylacetylene			
2920	2926	2938	2938

neighborhood of 2100 cm^{-1} there were observed two faint companions. We first believed they were due to rotation effects but calculations showed that the separations corresponded to no reasonable moment of inertia. The results are given in Table I.

In Table II there appears a comparison of the gas frequencies with those for the liquids.[2] As is generally the case, the gas frequencies are higher than those of the liquids. We have carried out the normal coordinate treatment for the vibrations which are symmetric with respect to the threefold axes of these molecules. Certain of the force constants involved were taken from data on methane and acetylene. Details of the calculations which were extended over a series of compounds will appear later. The calculated values in Table II comprise a portion of our calculated results. The agreement is fairly good although the results indicate that the C≡C force constant is greater in acetylene itself than in the substituted compounds.

GEORGE GLOCKLER
F. T. WALL

University of Minnesota,
Minneapolis, Minnesota,
February 15, 1937.

[1] George Glockler and F. T. Wall, J. Phys. Chem. **41**, 143 (1937).
[2] George Glockler and H. M. Davis, J. Chem. Phys. **2**, 881 (1934).

The Reemission of Visible Light and the Coloration by Ultraviolet Light of Certain Crystals

A new electronic effect in crystals of the type exemplified by magnesium oxide has been observed by the writer. When some large crystals of magnesium oxide are irradiated by ultraviolet light, in particular the 2536A mercury line, they become tinted a deep purple. On removal from the source of radiation a spontaneous decolorization process begins immediately. This process is initially very rapid, but the rate decreases as a function of time. This is shown in Fig. 1. There is a simultaneous emission of light throughout not only the whole visible spectrum but extending to the near infrared. The original magnesium oxide crystals show little absorption, if any, in the ultraviolet.

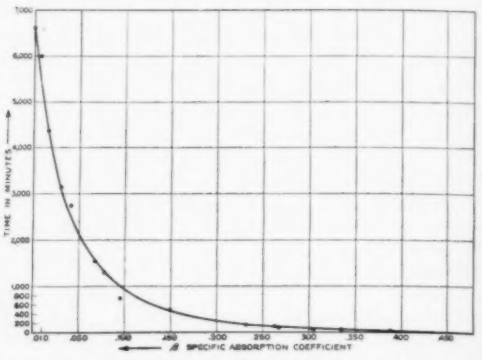

FIG. 1. The decrease in absorption of artificially colored magnesium oxide as a function of time.

It is presumed that this effect owes its origin to a type of electron migration and the reemission is attributed to a recombination. It is similar to the already noted behavior of the alkali halides. Since all crystals of magnesium oxide do not behave in an identical fashion the absorption and reemission may be the result of the accumulation of traces of impurities in specific portions of the magnesium oxide lattice.

It is of interest to note that the rate of reemission of energy as determined by the rate of decolorization is markedly increased by elevating the temperature. At 25°C complete decolorization takes several weeks but is accomplished in three minutes at 1000°C. Furthermore, irradiation of the colored material with the 4358A mercury line will cause decolorization in not more than thirty minutes. Because of the antagonistic effects of the 2536 and 4358A mercury lines, the high pressure silica mercury lamps are not suitable as a source of incident energy to bring about coloration. On the other hand the low pressure discharge type will produce admirable results. A further study of this effect is being made.

JAMES H. HIBBEN

Geophysical Laboratory,
Carnegie Institution of Washington,
February 17, 1937.